DESIGN AND OPTIMIZATION OF SANDWICH PANEL UNDER POST YIELD STRESS

BY
Hussein Zaal Mohammad Maaitah

Supervisor
Dr. Salih Akour

Submitted in Partial Fulfillment of the Requirements for the Degree of Doctor of Philosophy in Mechanical Engineering

Faculty of Graduate Studies
University of Jordan

August, 2008

COMMITTEE DECISION

This Dissertation (Design and Optimization of Sandwich Panel under Post Yield Stress) was Successfully Defended and Approved on **August 4, 2008.**

Examination Committee	Signature
Dr. Salih N. Akour, (Supervisor) Assoc. Prof. of Mechanical Engineering	----------------------------------
Dr. Mohammad H. F. Daddo (Member) Professor of Mechanical Engineering	----------------------------------
Dr. Nazzal S. Armouti (Member) Assoc. Prof. of Civil Engineering	----------------------------------
Dr. Mohammad I. Kilani (Member) Assoc. Prof. of Mechanical Engineering	----------------------------------
Dr. Jamal F. Nayfeh (Member) Professor of Mechanical Engineering (University of Central Florida, USA)	----------------------------------

تعتمد كلية الدراسات العليا
هذه النسخة من الرسالة
التوقيع .... التاريخ ....

ACKNOWLEDGEMENT

First of all, thanks to ***ALLAH*** for completing and finishing the requirements of the degree of PhD.

I would like to express my deepest appreciation to my supervisor Dr. Salih Akour for his support, motivation, and experience that make great contribution to the successful completion of my doctoral studies.

My deep appreciation is also extended to all my committee members Dr. Jamal Nayfeh, Dr. Mohammad H Daddo, Dr. Nazzal Armouti, and Dr. Mohammad Kilani. Their advice, effort, and time through out the course of the study are greatly appreciated.

My warm greetings go to my parents, wife, children, brothers and sisters for their devoted and dedicated support. I am indebted to all of them for their love and support.

TABLE OF CONTENTS

CHAPTER THREE

CHAPTER FOUR

CHAPTER FIVE

CHAPTER SIX

LIST OF FIGURES

LIST OF TABLES

APPENDICES

NOMENCLATURE

a	Length of the panel between the supports
b	Width of the panel between the support
c	Sandwich panel core thickness
h	Sandwich panel overall thickness
m,n	Number of terms in double Fourier series
$p(x,y)$	Pressure in x y-plane expressed in double Fourier series
p_{mn}	Unknown coefficient for pressure
r_{mn}	Unknown coefficient for shear deflection before core yielding
t	Thickness of the panel face sheet
u	In-plane displacement of the panel parallel to x-axis
w	Out-of-plane displacement of the panel parallel to z-axis
w_b	Panel deflection due bending before core yielding
W_s	Panel deflection due shear before core yielding
A_{eff}	Effective contact area with the panel
E	Modulus of elasticity
G	Shear modulus of elasticity
G_{c0}	Shear modulus of core before yielding
P	Total load applied in four point bending
P_b	Measured pressure
S	Shear stiffness
$Rc_{(yg)}$	Total resultant force in global Y-axis in core

$R_{BF(Yg)}$	Total resultant force in global Y-axis in bottom face sheet
$R_{TF(Yg)}$	Total resultant force in global Y-axis in top face sheet
$R_{TOT(Yg)}$	Total resultant force in global Y-axis for sandwich panel
Y_G	Global Y-axis in "I-DEAS"
α , β	Constants used in the double Fourier series
ε_x , ε_y	In-plane stains before core yielding
ϕ	Width of the unloaded panel region
γ_{xzc}	Core shear strain component
ν	Poison's ratio
τ_{xy}	In-plane shear stress
τ_{xz} , τ_{xz}	Shear stress components in sandwich panel
σ_{max}	The maximum Von Misses stress

DESIGN AND OPTIMIZATION OF SANDWICH PANEL UNDER POST YIELD STRESS

By
Hussein Zaal Mohammad Maaitah

Supervisor
Dr. Salih Akour

ABSTRACT

Sandwich panels attracted designer's interest due to its light weight, excellent corrosion characteristics and rapid installation capabilities. Sandwich panels have been implemented in many industrial application such as aerospace, marine, architectural and transportation industry. Sandwich panels consist of two face sheets and core. The core is usually made of material softer than the face sheets. Most of the previous work deals with sandwich panel in the elastic range. However the current investigation unveils the behavior of sandwich panel beyond the yield limit of core material. Three main parameters are investigated by applying invariant search optimization technique. These are the core thickness, the modulus of elasticity ratio of the core to face – sheet material, and the area size on which the load is being applied. The load has been increased in steps in quasi–static manner till face sheets reach the yield point. The panel modeled using a finite element analysis package. Simply supported boundary conditions are applied on all sides of the panel. The model has been validated against numerical and experimental cases that are available in the literature. In addition, experimental investigation has been carried out to validate the finite element model (FEM) and to verify some selected cases. The FEM shows very good agreement with the previous work and the experimental investigation. It is proved in this study that the load carrying capacity of the panel increases as the core material goes beyond the yield point. Also, the softer the core material is, more load is carried by face sheets. The stiffer the core material is, the sandwich panel behavior gets closer to isotopic plate, i.e., the face sheets are going to yield before the core material. As core thickness increases the load carrying capacity of the panel increases, i.e., delays the occurrence of core yielding. As the load-area-size increases, the load carrying capacity of the panel increases, i.e., the smaller the area on which the load is being applied the closer the response of the panel to concentrated load response.

CHARTER ONE

INTRODUCTION AND LITERTURE REVIEW

1.1 Introduction

Research efforts continuously are looking for new, better and efficient construction materials. The main goal of these researches is to improve the structural efficiency, performance and durability. New materials typically bring new challenges to designer who utilizes these new materials. In the past decades various sandwich panels have been implemented in aerospace, marine, architectural and transportation industry. Light-weight, excellent corrosion characteristics and rapid installation capabilities created tremendous opportunities for these sandwich panels in industry. Sandwich panel normally consists of a low-density core material sandwiched between two high modulus face skins to produce a lightweight panel with exceptional stiffness as shown in Figure 1.1. The face skins act like the flanges of an I-beam to provide the resistance to the separating the face skins and carrying the shear forces. The faces are typically bonded to the core to achieve the composite action and to transfer the forces between the components.

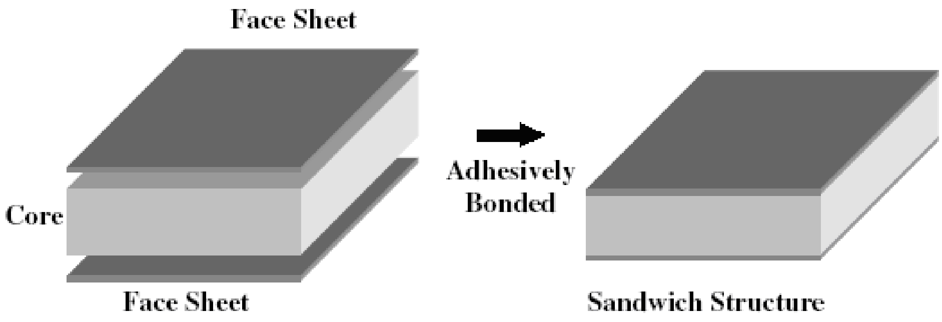

Figure 1.1. Schematic of sandwich construction

1.2 Main Principles of Sandwich Structures

Typical sandwich composite construction consists of three main components as illustrated in Figure 1.1. The sandwich consists of two thin, stiff and strong faces are separated by a thick, light and weaker core. The faces and the core material are bonded together with an adhesive to facilitate the load transfer mechanism between the components, therefore effectively utilize all the materials used. The two faces are placed at a distance from each other to increase the moment of inertia, and consequently the flexural rigidity, about the neutral axis of the structure.

In sandwich structure, typically the core material is not rigid compared to face sheets; therefore, the shear deflection within the core is insignificant in most cases. The shear deflection in the faces can be also neglected. The effect of shear rigidity in the core is shown in Figure 1.2. Figure 1.2 (a) shows an ideal sandwich beam using relatively stiff core, therefore the two faces cooperate without sliding relative to each other. Figure 1.2 (b) shows a sandwich beam using weak core, therefore the faces are no longer coupled together effectively and each face works independently as plates in bending. Use of weak core in shear results in significant loss of the efficiency of the sandwich structures. In a typical sandwich the faces carry the tensile and compressive stresses. The local flexural rigidity of each face is typically small and can be ignored. Materials such as steel, stainless steel, aluminum and fiber reinforced polymer materials are often used as materials for the face. The core has several important functions. It has to be stiff enough to maintain the distance between the two faces constant. It should be also rigid to resist the shear forces and to prevent sliding the faces relative to each other. Rigidity of the core forces the two faces to cooperate with each other in composite action. If these conditions are not fulfilled, the faces behave as two independent beams or panels, and the sandwich effect will be totally lost. Furthermore, rigidity of the core should be sufficient to maintain the faces nearly flat, therefore prevent possibility of buckling of the faces under the influence of compressive stress in their plane. The adhesive between the faces and the core must be able to transfer the shear forces between the face and the core.

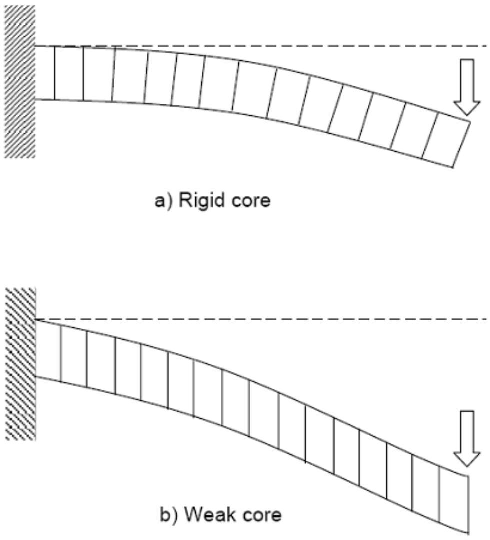

Figure 1.2. Effect of rigid and week core

1.3 Applications

Sandwich construction provides efficient utilization of the materials used for each component to its ultimate limit (Zenkert, 1997). The sandwich structure offers also a very high stiffness-to-weight ratio. It enhances the flexural rigidity of a structure without adding a substantial weight and making it more advantageous as compared to composite materials. Sandwich constructions have superior fatigue strength and exhibit superior acoustical and thermal insulation. Sandwich composites could be used in a wide variety of applications. Aerospace Industry: Sandwich composites are increasingly being used in the aerospace industry because of their bending stiffness-to-weight ratio. Floorboards, composite wing, horizontal stabilizer, composite rudder, landing gear door, speed brake, flap segments, aircraft interior and wingspans are typically made of sandwich composites. Marine Industry: Sandwich composites are ideally suited for the marine industries most advanced designs. The foam cores meet the critical requirements of strength, buoyancy and low water absorption. Applications include the construction of bulkheads, hulls, decks, transoms and furniture.

Transportation Industry: High strength-to-weight ratios of sandwich composites offer great advantages to the transportation industry. The insulating, sound damping properties and low cost properties make them the choice materials for the constructions of walls, floors, doors, panels and roofs for vans, trucks, trailers and trains. Architectural Industry: The foam offers an excellent thermal and acoustical insulation which makes it ideal choice for the architectural industry. Typical applications include structural columns, portable buildings, office partitions, countertops and building facades.

1.4 Literature Review

Work on the theoretical description of sandwich structure behavior began after World War Two. In (Plantema, 1966) published the first book about sandwich structures, followed by books by (Allen, 1969), and more recently (Zenkert, 1995). Although (Triantafillou and Gibson, 1987) developed a method to design for minimum weight, and reported the failure mode map of sandwich construction, without considering the post yield state of the sandwich structure.

The basic sandwich structure theory presented in all these texts is generally called the classical sandwich theory. This theory assumes that :

- The core carries the entire shear load in sandwich beams and plates.
- The face sheets carry the entire bending load.
- Core compression is negligible.

This theory states that the above–mentioned assumptions are true if:

1. The core and face sheets are elastic.
2. The overall length to thickness ratio is high.
3. The face sheet thickness is small compared to the overall thickness.
4. The ratio of mechanical properties between the face sheet and the core is high.

With these assumptions, a sandwich structure is considered to be incapable of acquiring additional load carrying capacity once the core yields.

(Mercado and Sikarskie, 1999) reported that the load carried by sandwich structures continue to increase after core yielding. Knowing that the core could not carry additional load after yield, this increasing load carrying capacity of post yield sandwich structure initiates the postulation that the additional shear load was transferred to the face sheets.

This is particularly true for sandwich structures that have nearly perfectly plastic cores post yield. In their work, it was shown that this load transfer allows the sandwich structures with aluminum face sheets and foam cores to carry an additional 20 ~ 30% of total load after the initiation of core yielding (Mercado, Sikarskie, 1999). To account for the above-mentioned phenomenon, (Mercado et al, 2000) developed a higher order theory by including a bilinear core material module. This theory states that core plasticity, especially for cores that are near perfectly plastic condition after yielding, greatly increase the shear deformation and shear curvature of the sandwich structures. This increased curvature causes face sheet curvature and thus bending resistance about the face sheets' neutral axes. This resistance contributes to the additional load carrying capability by the structure after core yielding. This means that the additional load carrying capacity of sandwich structures after core yielding is due to both additional shear load carried by the face sheets due to shear deformation, as well as the bending resistance of the face sheets against shear curvature caused by yielded core. The additional shear load is assumed to be carried equally by the top and bottom face sheets.

This theory yields a fairly accurate prediction on the deflection of a foam cored sandwich structure in four point bending (Mercado et al, 2000), but the assumed shear distribution within the sandwich structure was not validated. In addition, this theory does not take into account the core compression under localized load, or any geometric non-linearity. The classical sandwich beam theory also assumes that in-plane displacements of the core through its depth are linear. In other words, it was assumed that the core thickness remains constant and cross-sections perpendicular to the neutral axis remain plane after deformation.

This assumption is generally true for traditional core material such as metallic honeycomb (Frostig et al, 1992), (Frostig, and Baruch, 1990). However, this assumption is not suitable for soft, foam-based cores, especially when the sandwich structure is subjected to a concentrated load (Thomsen, 1995). With a much lower rigidity compared to metallic honeycomb, foam-based cored sandwich structures are susceptible to localized failure. Insufficient support to the face sheets due to core compression near the application points of concentrated loads can lead to failures such as face sheet/ core delamination, face sheet buckling, and face sheet yielding. This localized non-linearity is reported by many researchers such as (Thomsen, 1995), (Thomsen, 1997), (Rothschild 1994), (Caprino, 2000), and (Gdoutos et al, 2001) the shear distribution at localized failure points has not been well defined. (Miers, 2001) investigated the effect of localized strengthening inserts on the overall stiffness of a sandwich structure. This localized strengthening increased the rigidity of the sandwich structure, but the addition of high stiffness inserts will complicate the manufacturing process of sandwich structure. Therefore there is a need to investigate the shear distribution at close proximity of concentrated loading and support points in order to avoid unexpected failure caused by core compression. The two most popular theories that include these localized effects are the superposition method (Zenkert 1997) and high order theory (Frostig, 1992) and (Frostig, 1993)

The superposition approach assumes that the bending behavior of the sandwich structures is the result of two components (Zenkert, 1997). One of the components is the shear and bending effects on the structure. The structure in this case is considered to have constant thickness. Another component is the localized crushing of the structure. In this case the structure is assumed to be free of shear stresses.

Usually, the local failure starts in the core and results in core crushing, face–core debonding and (or) residual dentformation and, therefore, in substantial reduction of the structural strength (Shipsha A.,2003) Thus, it is of a practical importance to predict the elastic stress–strain response of sandwich structures subject to localized loads. Besides experimental and finite element analysis,(Shipsha A, 2003, Lolive _EE, Berthelot J-M, 2002, Thomsen OT, 1993), there are two approaches to analytical modeling of sandwich structure local behavior e.g. These approaches are based on different descriptions of core deformation. The simplified approach is based on the assumption that the plate is resting on a continuously distributed set of independent springs, the stiffness of which defines the Winkler foundation modulus and results in dependence of the interface stress only on the deflection at the same point. The main problem of this approach concerns determination of the modulus using characteristics of the sandwich layers. A complete correspondence between the Winkler type foundation and elastic layer can be found only for a thin core; in this case the modulus can be obtained solely. For the case of a thick core determination of the modulus can be fulfilled by various means (for instance, to ensure coincidence of deflection, bending moments or interface stress under a concentrated force in exact and simplified formulations). These two limit cases (very thin and very thick core) are used for solving numerous static problems in (Thomsen OT, 1995, Zenkert D, 1995).

Dynamic analysis approach for the given modulus is performed in (Olsson R, 2002, Slepian LI., 1972). In many cases the Winkler model or the more advanced Winkler–Pasternak model (Thomsen OT., 1995, Pasternak PL, 1954) provides satisfactory agreement with experimental results, but it is not universal for a general case of the sandwich constitution

The core in the localized crushing component is treated as an elastic foundation model, also called Wrinkler's Foundation (Mercado, Sikarskie, 1999). Wrinkler's Foundation idealizes the structure by treating the core as continuously distributed springs that provide support to the face sheets. By adding the effect of these two components the general behavior of the structure can be determined.

However, the superposition method is not as realistic as the high order theory because it only combines the localized effects with the classical theory. This approach does not take the interaction between layers such as shearing stresses in between layers into account. In addition, this theory also assumes small deflection of the sandwich panel and does not take geometric non-linearity after core yielding into account. High order theories take transverse flexibility of the core into account and may produce more accurate results for soft-core sandwich structures. By utilizing a high order theory, (Frostig et al. 1992, 1993) have developed solutions for various cases of a sandwich beam in four-point bending. This includes the research on point loads and support regions (Mercado et al, 2000), edge and inner delamination regions (Frostig, 1992) edge, inner transverse diaphragms and cut-off edge connections (Frostig, 1993). In high order theories, face sheets and core are related through compatibility and equilibrium at their interfaces. (Thomsen and Frostig, 1997) verified their theory by using photoelasticity techniques and (Frostig and Baruch, 1990) further developed this theory for sandwich plate applications to account for the localized load effects in plate bending. (Schwarts-Givli and Frostig ,2000) then attempted to predict the post core yielding behavior of a foam core sandwich beam under three point bending by adopting the bilinear core material model to the high order theory.

These researches limited their study to the linear behavior of the face sheets and core.

In order to investigate the post core yield load carrying capability of sandwich panels, (Chintala, 2002) extended (Mercado et al, 2000) higher order theory to a sandwich panel under the loading condition of Hydromat Test System (Rau, 1994). Adapted from higher order theory, (Chintala, 2002) attributes the extra load carrying capacity of sandwich panels after core yielding to the bending resistance of the face sheets about their own neutral axes. This study does not take core compression into account, i.e. it assumes the thickness of the core remains constant throughout the loading condition due to the distributed loading nature of the test system.

1.5 Research Objective

To design an efficient sandwich structure, it is vital to understand the load distribution pattern in each layer of the structure. Most of the previous efforts are made by using classical sandwich theory, and higher order theory, where high order theory predicted the sandwich panel behavior fairly well in the linear range. However, these theories could not give an accurate prediction of the shear distribution in each layer after core yielding. Large deflection of sandwich structures due to core yielding could vary the direction of the applied load on the structure. Change in loading direction would obviously change the shear distribution in the sandwich structure. In order to investigate the exact change of shear distribution due to distributed loads, as well as geometric nonlinearity and localized core failure, finite element analysis is used in this research effort. The main objective of this research is to investigate the following:

1. Post yield behavior of sandwich panel.
2. Effect of geometric non-linearity under distributed loads.
3. The effect of the design parameter of the sandwich panel are unveil face sheet thickness to overall thickness ratio, ratio of face sheet Young's modulus to the core Young's modulus ratio and distributed load area. These parameters are the determining factors of significance on geometric non-linearity and core material nonlinearity

The above investigation is done in view of the following points:

1. Localized core yielding occurs mainly through core compression. Therefore, analysis should be done using material properties determined from compression test.
2. For practical purposes, the assumptions that have been made in developing the sandwich panel theory eliminated part of the problem physics.
3. The Finite Element Model (FEM) is extended to include the relative dominance of core shear failure and face sheet yielding.
4. Localized loads are modeled as load on small partitioned area to better simulate the actual loading condition.
5. Experimental verification is conducted for selected cases.

1.6 Scope and Content

Simply supported sandwich panel is investigated and baseline data has been generated to help designers make better design for sandwich panel. This study covers the design in elastic range as well as the post yielding rang.

A simply supported plate from all sides is tested using uniaxial testing machine by applying distributed loads acting on different sizes of area within the plate. This scenario is modeled using a finite element analysis tool called 'I-DEAS'. The selection of this scenario is due to the availability of experimental data for validation purposes. The shear distribution in each layer of the sandwich panel is obtained from the finite element analysis results. Materials and geometric non-linearities are considered in the simulation.

This dissertation consists of six chapters a brief description of each one is below.

Chapter two (Physical Model): This chapter presents the physical model of the sandwich panel, which includes geometry, assumptions, boundary panel conditions and loading.

Chapter three (Finite Element Model): This chapter presents the development of finite element model for sandwich plate and utilization of the pre and post processing modules ' I-DEAS ' software.

Chapter four (Model Verification): In this chapter the FEM model is tested against previous experimental and FEM model to assure model accuracy and integrity. Also experimental verification is carried out for selected cases to provide confidence of the results.

Chapter five (Results and Discussion): In this chapter effect of material nonlinearity and geometric non-linearity are unveiled. The effects of distributed loading are included in chapter five. Conclusions and recommendations are provided in **Chapter six.**

CHAPTER TWO

PHYSICAL MODEL

This chapter presents the physical model of the sandwich panel, which includes geometry, boundary conditions as well as the materials used in the investigation.

2.1 Sandwich Panel Geometry

The sandwich panel consists of two face sheets made of metal. The thickness of each face is **t**. Soft core of **c** thickness is sandwiched between those face sheets. The core material is made of foam which is soft compared to the face sheets .The panel is square in shape. The side length is designated by **a** Figure 2.1 illustrates the sandwich panel geometry while the dimensions of the sandwich panel are shown in Table 2.1

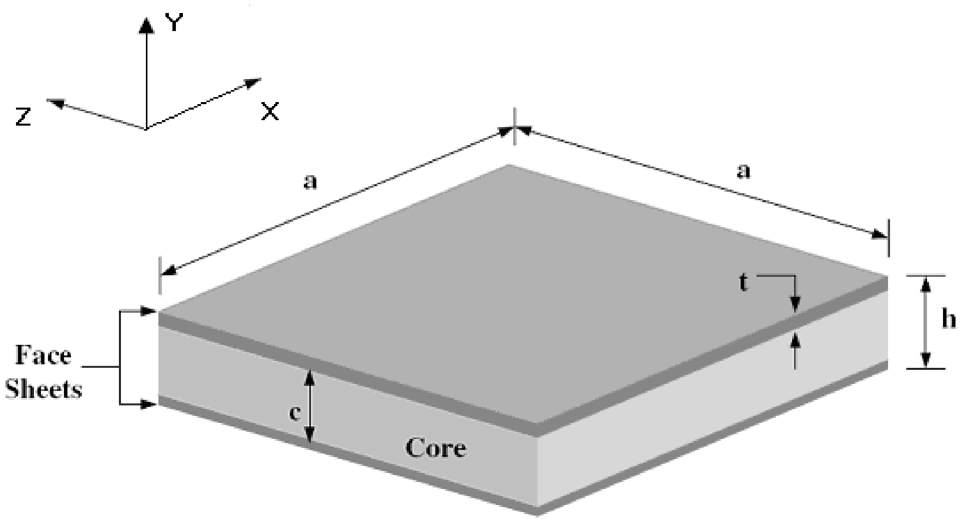

Figure 2.1. Illustration sandwich plate geometry.

Table 2.1. The value of the parameters shown in Figure 2.1

Parameter	Dimension	Note
a	608mm	constant
t	1.0mm	constant
c	15mm-50mm	variable

2.2 Assumptions

This research takes into consideration the geometric non-linearity as will as the material nonlinearity. The following assumptions are made to simplify the model without loosing the physics of problem

1. Face sheets and core are perfectly bonded.

   The FEM model assumes no delamination occur between layers.

2. Face sheets remain elastic at all time.

   Due to the significantly higher yield strength and modulus of elasticity of the face sheets compared to the core, face sheets are assumed to remain elastic throughout the loading for simply supported panel. The analysis stops when the face sheets start to yield.

3. Geometric non-linearity has a significant effect:

   Geometric non-linearity is considered to have significant effect on the load distribution on each layer of the sandwich structure.

2.3 Boundary Condition

Due to the symmetry of the sandwich panel (symmetric over X-axes and symmetric over Z-axes), only quarter of it is being modeled. Such symmetric boundary conditions are applied of the X-axes and Z-axes. The two planes of symmetry of the panel have symmetric boundary conditions, (see Figure 2.2 and 2.3). A simply supported boundary condition is applied to strip area of the quarter panel as shown in Figure 2.2 and 2.3. This simulates the simply supported condition of the panel. The loading area is square in shape, its side length varies in steps from a 100,200,400and 600mm for full panel dimension. But when we are dealing with quarter of the panel the side length will be 50, 100, 200, and 300mm

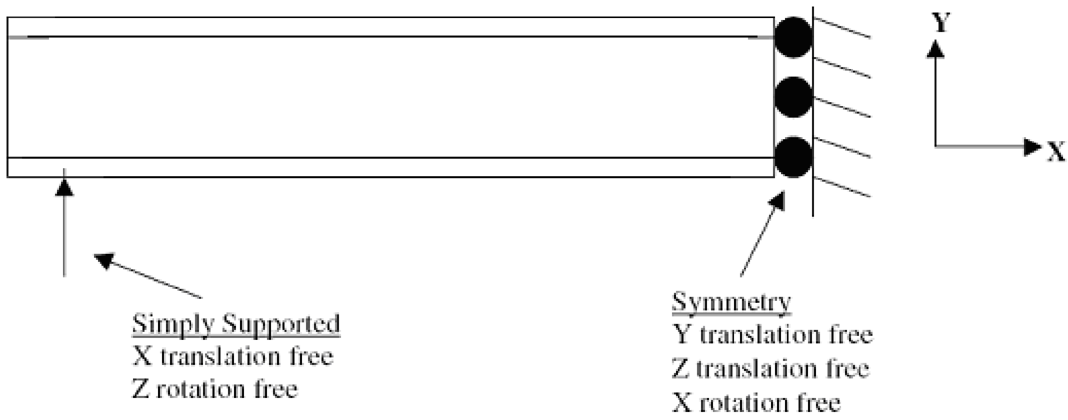

Figure 2.2. Sandwich panel boundary condition, X-Y plane.

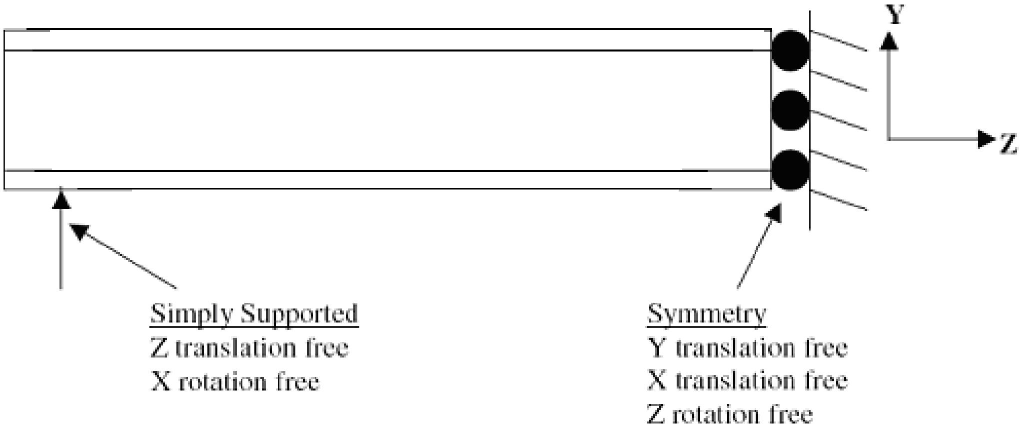

Figure 2.3. Sandwich panel boundary condition, Y-Z plane.

2.4 Study Parameters

The main parameters that have influence on the performance of the sandwich plate are, loading step area on which the load is distributed, the core thickness, and core material stiffness.

2.4.1 Loading

The load is applied to the sandwich top face sheet as a distributed load which is increased gradually (step by step) till the face sheet stress reaches yield stress

2.4.2 Loading Area

A distributed load is applied on the top surface of the sandwich panel. The area on which the distributed load is applied is shown in Figure 2.4 located at the middle of the top face sheet plate. The loading area at the middle top face of sandwich panel is square area. This area has been varied from 50*50 mm^2 through 100*100 mm^2, 200*200 mm^2, 300*300 mm^2.

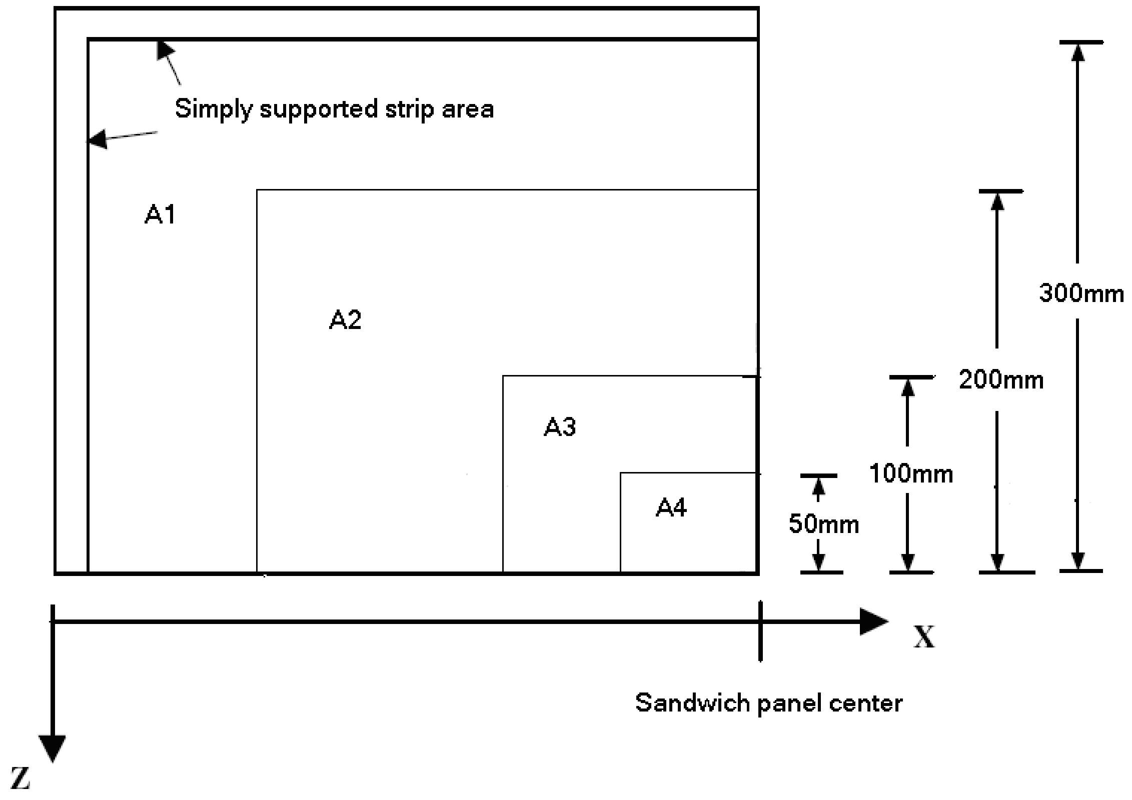

Figure 2.4. panel span overview of quarter sandwich panel for different loading area

2.4.3 Core Thickness

The core thickness plays important role in the performance of the sandwich structure. The core thickness is varied from 15mm, through 20mm, 25mm, 30mm, 40mm, to 50mm.

2.4.4 Core Material

In the current research, different materials are used. Their modulus of elasticity is varying from 37.5 MPa through 138.6 MPa, 180 MPa, and 402.6 MPa

2.5 Material Properties

The core of a sandwich structure is used to separate the two faces, most often identical in material and thickness, which primarily resist the in plane and bending load. The core is mainly subjected to shear so that the core shear strain produces global deformations and core shear stresses. Thus, a core must be chosen such that not to fail under applied transverse load. It should have a shear modulus high enough to give the required stiffness. Furthermore, its young's modulus normal to the faces should be high enough to prevent contraction of the core thickness and therefore a rapid decrease in flexural rigidity. The core should have low density in order to add as little as possible to the total weight of sandwich structure. Because of low density requirement, core materials are very different from face sheet materials. A detailed characterization of their mechanical behavior is essential for their efficient use in structural application. Four types of foam H100, H250, AirexR63.50 and Herex C70.200 are investigated.

2.5.1 Mechanical Properties for Face Sheet

Material properties for the sandwich plate face sheets are taken from (material handbook, 1991) whereas the material properties for the foam core are provided by (Rao, 2002). Aluminum 3003-H14 is a type of aluminum alloy that has high resistance to corrosion and is easy to weld. The 3003-aluminum family is normally used in the production of cooking utensils, chemical equipment, and pressure vessels. The face sheets are assumed to remain elastic at all times. Therefore only elastic material properties are required for the face sheets and they are presented in Table 2.1**.**

2.5.2 Mechanical Properties for Core

This subsection presents the core material properties used to model the simply supported panel. In all cases, face sheets of the sandwich structures are assumed to remain elastic throughout the analyses. Therefore, only core materials require a good post yield behavior descriptions. The core materials undergo plastic deformation; hence there is a need to obtain a full description of the core materials' behavior upon yield initiation.

Airex R63.50 has high fatigue strength, high three-dimensional formability, and high resistance to dynamic loads. Materials in Airex R63 family are widely used in the production of marine hulls and lightweight cars due to the appreciation of their low density and high strength and stiffness to weight ratio. Airex R63.50 is presented in Table 2.2.

Material properties of the HerexC70.200 foam core is obtained from (Rao, 2002) work. Herex C70.200 is an isotropic and stiff foam material with high stiffness and strength to weight ratios. The materials in Herex C70 family have excellent chemical resistance and low thermal conductivity and water absorption. The appreciation of these inherent properties of Herex C70 materials makes this material a popular choice for the core materials of structural sandwich structures in marine and railway applications. The stress strain curve of this material is presented in Figure 2.5.

In this research a first-order idealized core material property module suggested by (Mercado, Sikarskie, 1999) is used. This first-order idealized model, also called the bi-linear model, describes the material properties of the core with the stress strain curve as shown on Figure 2.5 and Figure 2.7.

The other material used in this research is linked PVC close called cellular foam (divinycell) the type of divinycell, H100, H250 with densities of 100 and 250 kg/m^3 and the mechanical properties are stated in Table 2.2 and stress strain curve is shown in Figure 2.6 and Figure 2.8 respectively.

Table 2.2. Compression of sandwich panel material properties

Material	Property source	Young's modulus (MPa)	Poisson's ratio	Shear modulus(Mpa)	Shear strength(Mpa)	0.2% offset yield strength(Mpa)	Strain at yield point(mm/mm)
Face sheet Aluminum 3003-H14	Material Handbook 1991	69,000	0.33	25,000	120	145	Not available
AirexR63.50 core A	Rao,2002	37.5	0.335	14.05	0.45	0.637	0.019
H100 core B	Kuang,2001	138.6	0.35	47.574	1.2	1.5	0.0108225
Herex C70.200 core C	Rao,2002	180	0.37	65.69	1.6	2.554	0.0162
H250 Core D	Kuang,2001	402.6	0.35	117.2	4.5	5	0.014

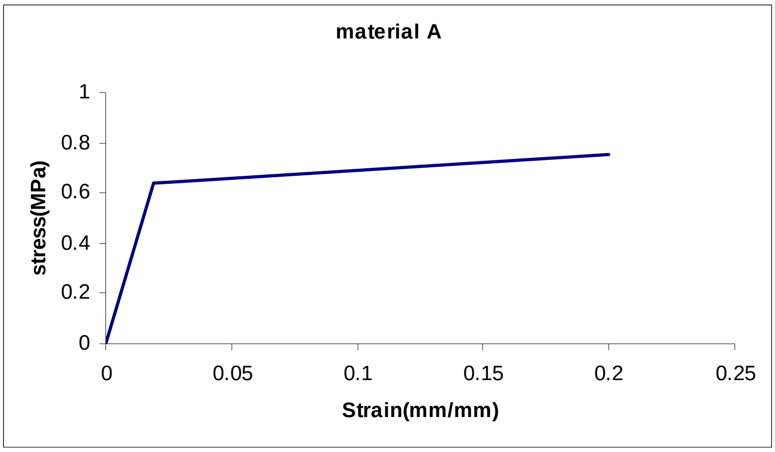

Figure 2.5. Stress strain curve for material A (AirexR63.50) (Rao, 2002)

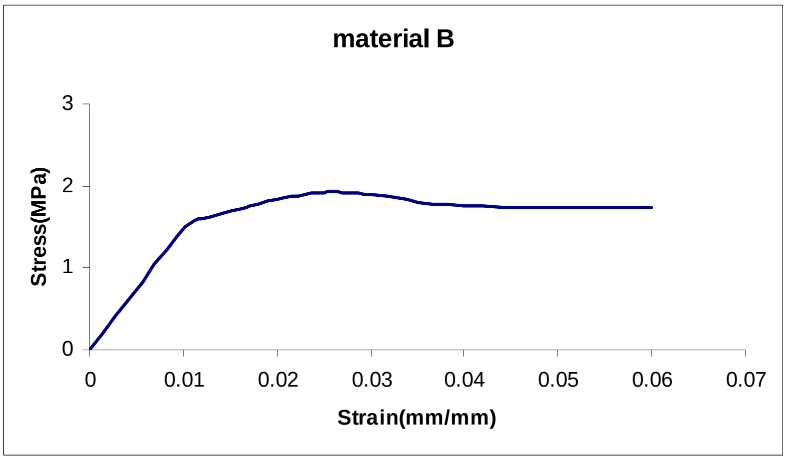

Figure 2.6. Stress strain curve for material B (H100) (Kuang, 2001)

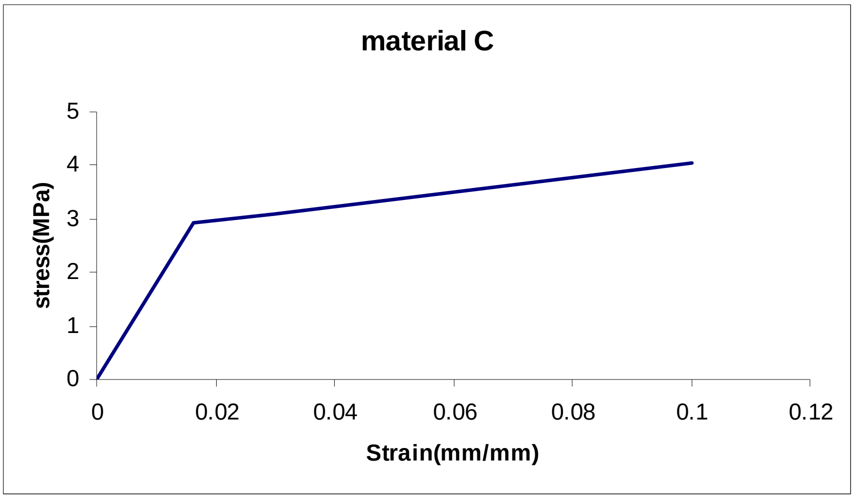

Figure 2.7. Stress strain curve for material C (Herex C70.200) (Rao, 2002)

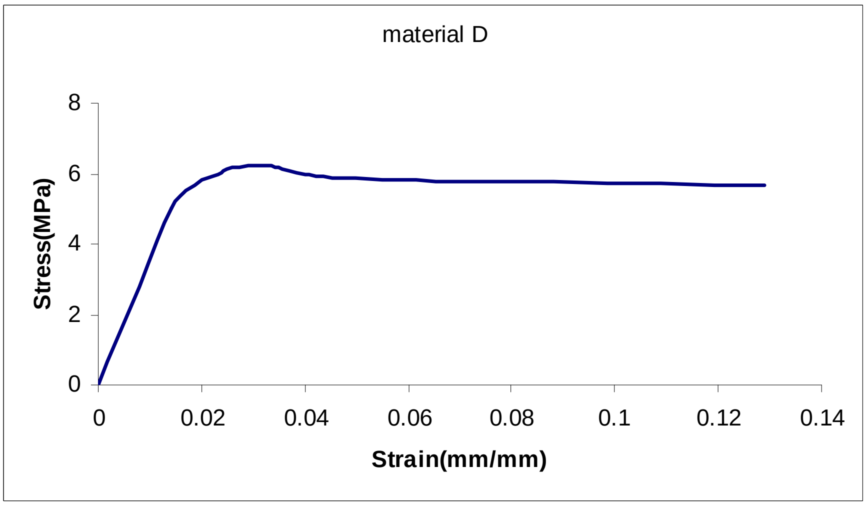

Figure 2.8. Stress strain curve for material D (H250) (Kuang, 2001)

CHAPTER THREE

FINITE ELEMENT MODEL

This chapter presents the development of finite element models for simply supported sandwich panel. Detailed descriptions of the boundary conditions, element types, and the loading are presented in this chapter. The finite element software used in the development of the finite models is (I-DEAS Master Series 10 1999). The relatively robust and user-friendly solid modeling and finite element meshing interface are the main advantages of this solid modeling/ finite element software.

3.1 Model Assumptions

All the finite element model analyses done in this research involves the use of non-linear analysis capability of I-DEAS, which includes geometric non-linearity and material nonlinearity. With geometric non-linearity, the software takes the effect of geometry changes into account while calculating the solution. Using material non-linearity option the non-linear behavior of the material response (i.e. post yield material properties) is taken into account.

Below are the assumptions made for the numerical model.

1. Face sheets and core are perfectly bonded

The numerical model assumes no delamination occur between layers. This assumption is applied by utilizing the partitioning option in the preprocessing module of the software. This option allows the analyst to deal with the whole volume of the structure as one unit also it allows the analyst to assign different material for each partitioned volume.

2. Face sheets remain elastic at all time:

Due to the high yield strength and modulus of elasticity of the face sheets compared to the core, face sheets are assumed to remain elastic throughout the loading for simply supported panel.

3. Load scenarios are quasi-static:

The loading cases considered are modeled quasi-static instead of dynamic. Incremental loadings are applied slowly during the actual experiments (i.e. simulates exactly the real situation). Therefore, the type of analysis done for this research effort is “static, non-linear analysis”.

4. Geometric non-linearity has a significant effect:

Geometric non-linearity is considered to have significant effect on the load distribution on each layer of the sandwich structure. Therefore, all finite element analysis that is done takes into consideration the geometric non-linearity. This is the main difference between the numerical models and the theoretical models. Classical sandwich plate theory and higher order theory do not take shape change of the sandwich structures into account.

5. The panel is simply supported from all sides. It is partitioned into three layers, forming three bonded material layers.

3.2 Boundary Conditions

The symmetric nature of the problem allows only quarter of the whole panel to be meshed. The boundary conditions applied are shown on Figure 3.1.

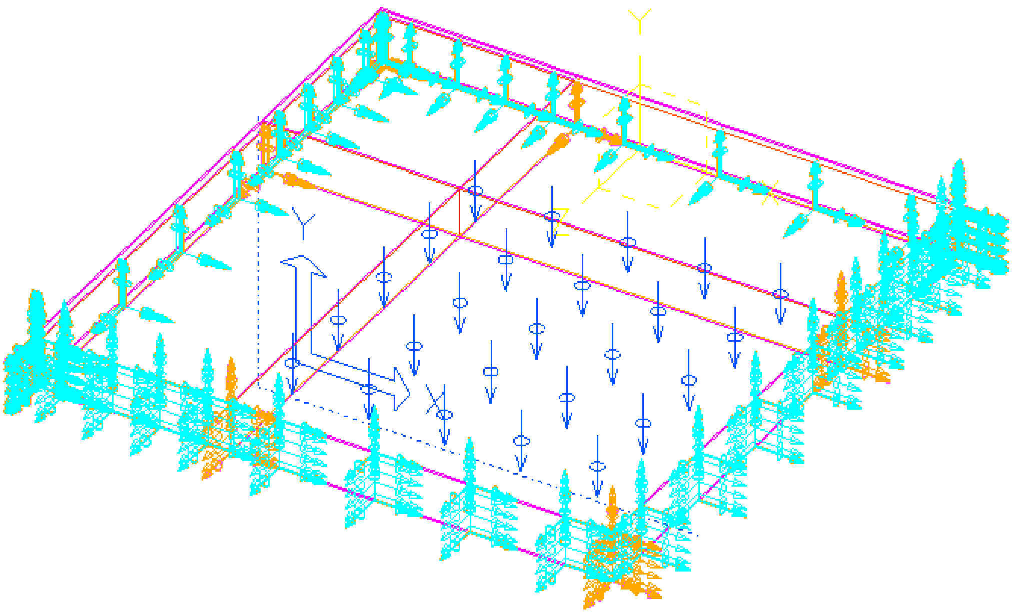

Figure 3.1 Sandwich panel boundary condition and loading

The two planes of symmetry of the panel have symmetric boundary conditions, where in-plane displacements and rotation about an axis respective normal to the symmetry plane is allowed. A simply supported boundary condition is applied to the two other sides of the quarter panel. A distributed load is applied on the top surface of the sandwich panel. The area in which the distributed load is applied is varying as shown in Figures 3.2a, 3.2b, and 3.2c.

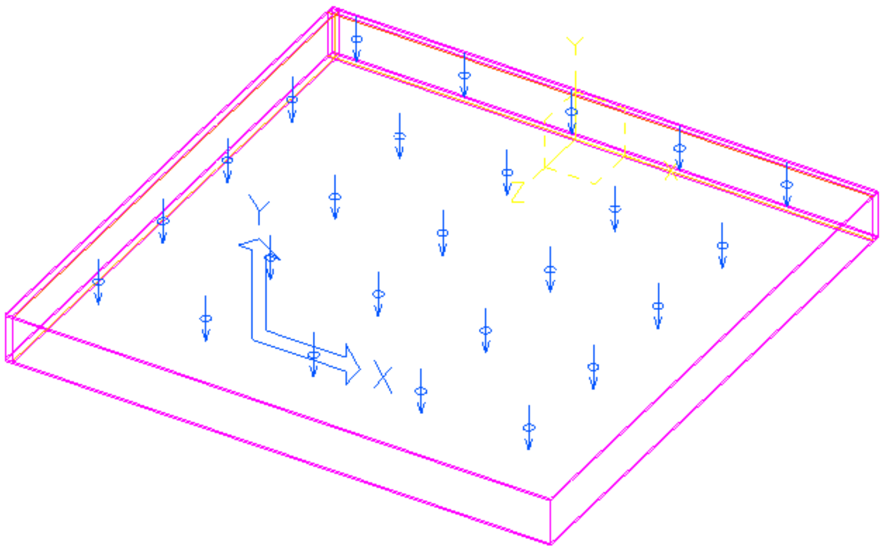

Figure 3.2(a). The loading area with side length 300mm

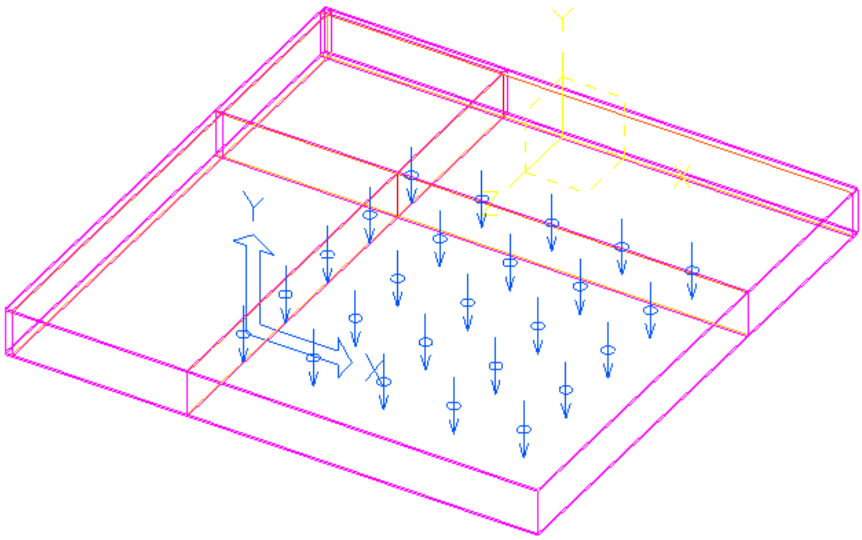

Figure 3.2(b). The loading area with side length 200mm

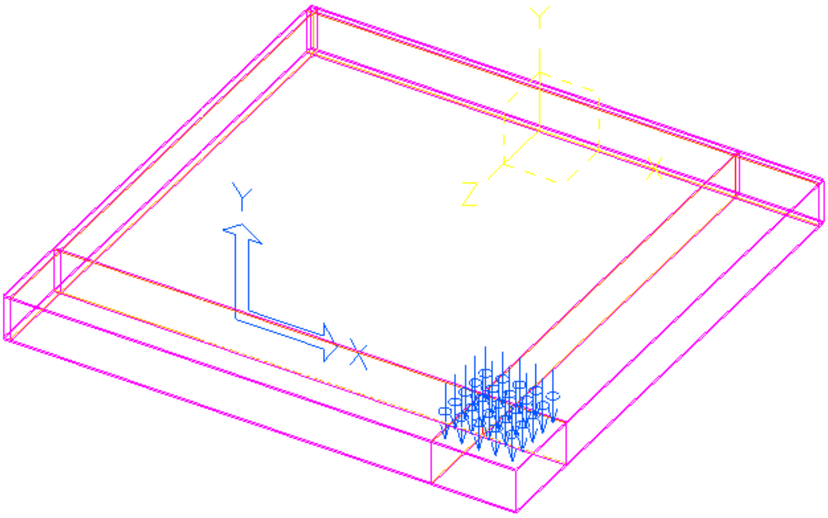

Figure 3.2 (c). The loading area with side length 50mm

The plate is loaded with a set of loads that are varying slowly with time, and the analysis is carried out at each load step. Figure 3.3 shows the load stepping variation form. The column titled by time is the stepping column and the other one titled by magnitude contains the corresponding at load each step.

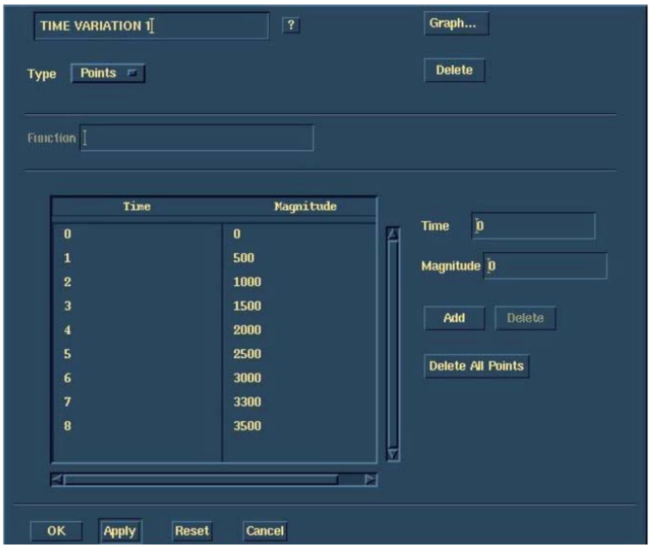

Figure 3.3. Load stepping window of I-DEAS preprocessor

The finite element software is set in such a way to solve the model at each load step as shown in Figure 3.4. This allows all the analysis to be done in a single run of the finite element model. As a result of this model would take up less memory space because one single solid model and finite element model can be used for all load steps.

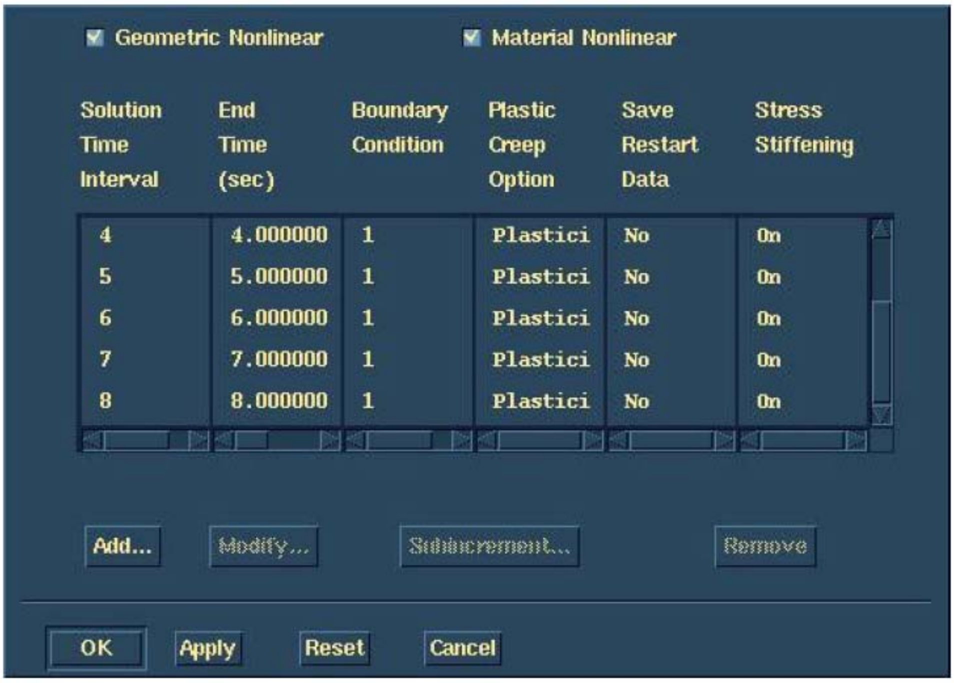

Figure 3.4. Setting multiple solution points on I-DEAS.

The numerical model utilizes the map meshing facility in I-DEAS. By controlling the number of nodes along each edge of the solid model, this function providing full control of the mesh size. The element size is chosen by referring to (Miers, 2001) work in mesh refinement. (Mires, 2001) recommended a core element size of 1.5 mm and face element size of 3 mm in order to achieve convergence in the data obtained. Constant mesh density is ensured with the mapped meshing function. This is important because constant mesh density ensures that data collected from any region of the plate are of the same degree of resolution. Three-dimensional (solid) brick elements are used in this analysis. Second order (parabolic) brick elements are chosen over the first order (linear) brick elements in order to better interpolate the data between nodes. Figure 3.5 shows the FEM mesh model of the sandwich panel.

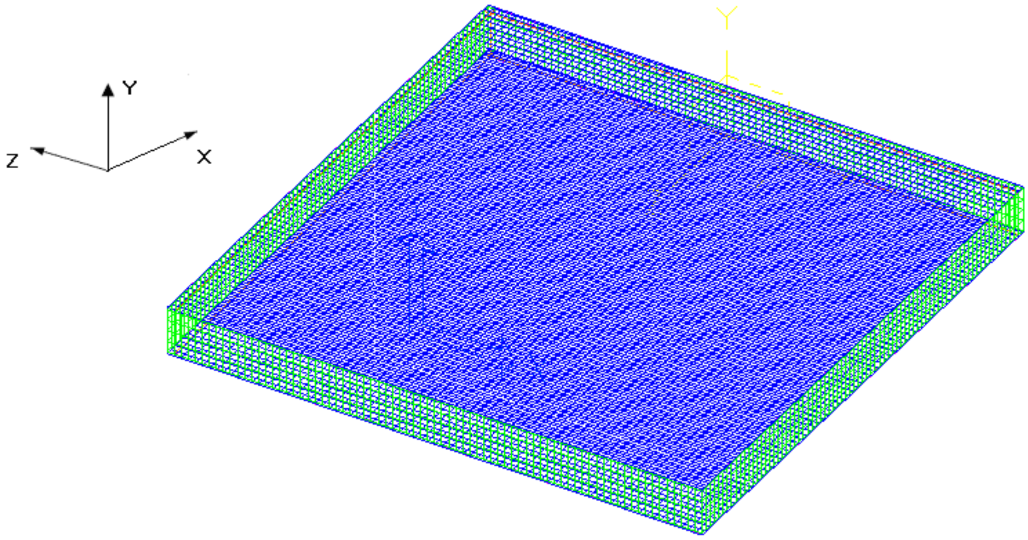

Figure 3.5(a) Meshed quarter sandwich plate

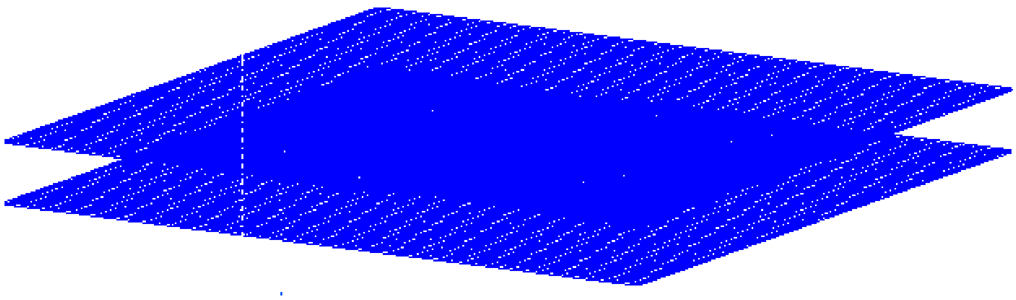

Figure 3.5(b). FEM mesh for top and lower face sheet

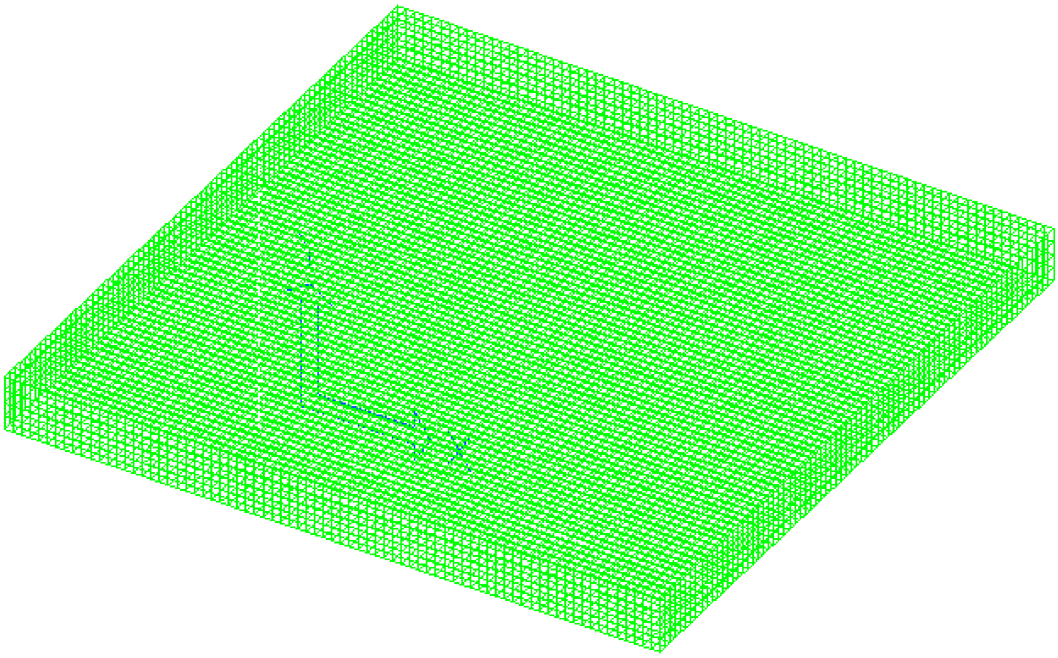

Figure 3.5(C). FEM mesh for core

Since the analysis involves material non-linearity, a yield function or yield criteria needs to be defined for the model. Von Mises yield criteria and its associated flow rule is used in this analysis. Isotropic hardening is also used to describe the change of the yield criterion as a result of plastic straining. Only the core elements are assigned a yield function due to the assumption that only core yielding occurs throughout the loading process. The face sheets are assumed to remain elastic at all time; hence no yield function is assigned to the face sheet elements. However the yield point of the face sheet material is fed to the software to be used as indicator for stopping the analysis.

CHAPTER FOUR

MODEL VERIFICATION

To assure validity and accuracy of FEM model comparison with other researches findings is carried out. The comparison with the previous finite element analysis (FEA) and experimental findings shows excellent agreement. To be more confident of the finite element model and its results, some selected cases are verified experimentally. The experimental results and FEM findings show excellent agreement

4.1 Previous Works.

The previous work (Eyre, 1995), (OOI, 2003) that our model is going to be validated against it is two types, one is experimental and the other is finite element analysis.

4.1.1 Experimental Validations

The experimental work (Eyre, 1995) that we are comparing our model results with it is performed using Hydromat Test System (HTS). Figure 4.1 illustrates a schematic diagram of the test system. The specimen panel used for testing in (HTS) is presented in Figure 4.2, while Table 4.1 presents the dimensions of this specimen. The solid model of sandwich panel subjected to HTS is partitioned into three perfectly bonded layers. The panel is placed in HTS and simply supported from all sides. A brief description of HTS is presented below.

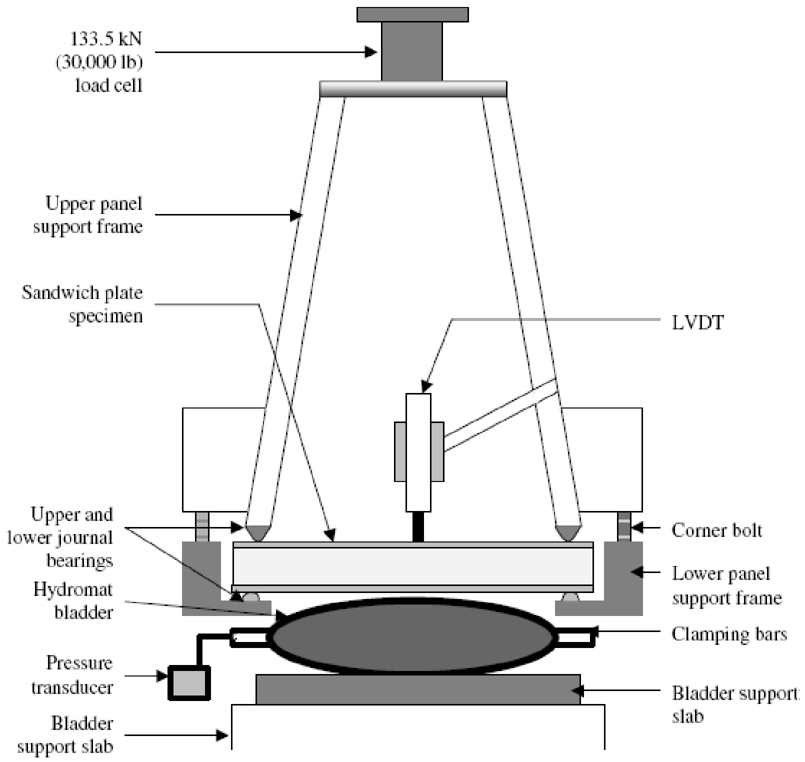

Figure 4.1. Schematics of hydromat test system fixture setup (Eyre, 1995)

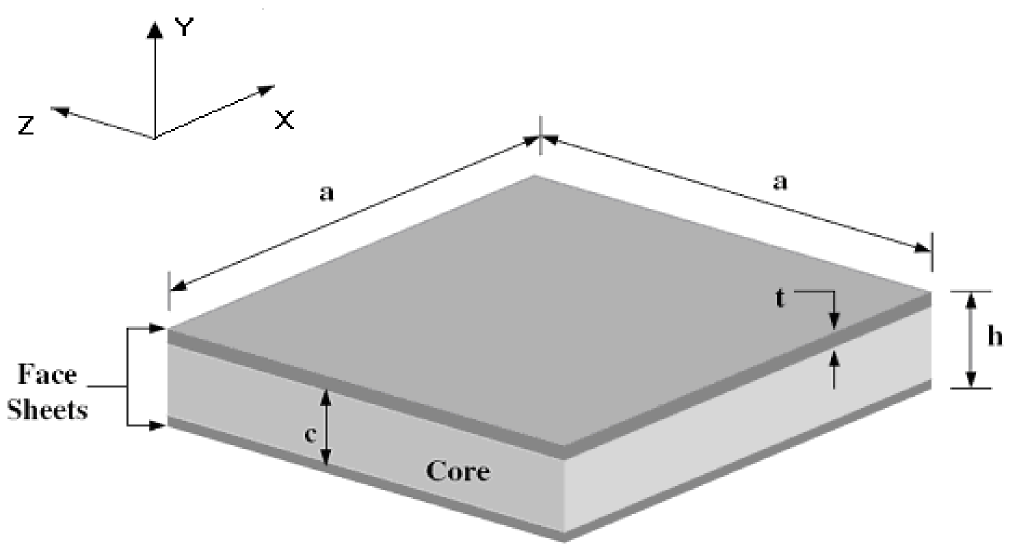

Figure 4.2 Sandwich plate dimension used for HTS

Table 4.1. The value of dimension of sandwich plate Figure 4.2

Dimension	Description	Value
a	Side length of the panel	609.6mm
t	Sheets thickness	0.98mm
c	Core thickness	24.8mm
h	Overall sandwich panel thickness	26.76mm

4.1.1.1 Hydromat Test System Setup

Hydromat test system is divided into three parts: the upper panel support frame, lower panel support frame and the hydromat bladder. The schematic of the hydromat test system fixture is shown in Figure 4.1. The upper panel support is made of fiberglass covered Douglas fir laminate and has a shape of tetrahedron. This upper panel support frame was originally designed by Gougeon Brothers Inc. of Bay City and then fabricated by (Rau, 1991). The upper support frame is attached to a 133.5 kN (30,000 lb) load cell, which is mounted to a crosshead load frame. The lower support frame is made of steel and offers support from the bottom of the sandwich panel specimen.

Corner bolts are used to fasten the upper and the lower panel support frame. As the corner bolts are tightened, the upper and lower support frames move closer to each other. This pushes the upper and lower journal bearings closer to the sandwich plate and eventually providing simply supported boundary condition to the specimen. The four pairs of aluminum journal bearings are situated at the four edges of the base of the tetrahedron, at top and bottom of the sandwich specimen. These pairs of bearing, with appropriate tightening of the corner bolts, will constrain the edges of the panel in a simply supported state during the test. This “forced” simply supported edge constraint is a better emulation of the actual marine hull condition in water. It also enabled the use of the same simply supported boundary condition in all the HTS numerical simulations.

The downward movement of the crosshead that holds the load cell pushes the test specimen against the hydromat bladder. This movement thus applies a distributed load on the lower surface of the specimen. The skin of hydromat bladder is made of two pieces of reinforced vinyl conveyer belt material. The two pieces of skins are clamped at its four edges by four pairs of steel clamping bars. Filled with approximately 17 Liters (4.5 gallon) of pressurized water, the hydromat has a flexible loading surface that can conform to the shape change of the sandwich panel specimen, hence providing normal distributed load to the specimen at all times.

Table 4. HTS loading details

Pressure (kPa)	Area (m^3)	Total Applied Load(kN)
17.2	0.180	3.10
34.5	0.189	6.52
51.7	0.196	10.14
68.9	0.201	13.83
86.2	0.205	17.63
103.4	0.208	21.55

The sandwich panel is partitioned into ten different regions that are labeled from Region 1 to Region 10 respectively). Distributed loads are applied beginning from is assumed to be a perfectly square shape, therefore the aspect ratio between the length and width of the effective contact area is set as one. This uniform aspect ratio ensures the symmetry nature of the loading scenario and allows analysis done on only a quarter of the plate.

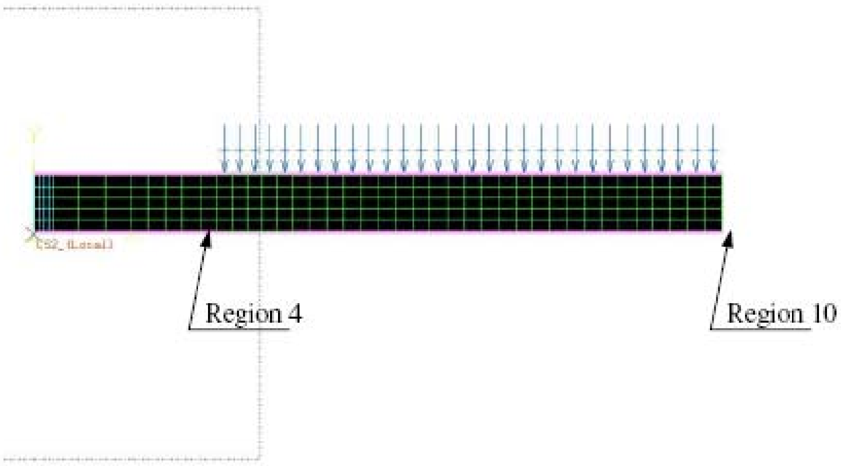

Figure 4.3. Distributed load applied on the panel top surface.

Similar to the four-point bend test model, the elements used in this simulation are three dimensional, parabolic, brick elements. Again the element sizes were chosen according to the recommendation made in (Miers , 2001) work, where a core element size of 1.5 mm and face element size of 3 mm are used. The solid model is meshed using the mapped meshing capability of I-DEAS. The core is assumed to be the only material that undergoes plastic deformation. The core elements use the Von Mises plastic yield function and undergo isotropic hardening.

4.1.1.2 Comparison of Results:

The loading applied to the specimen is presented in Table 4.2. The results obtained from current model are plotted against those produced by Eyers 1995. Figure 4.4 present the verification of the panel center point deflection versus the loading for both our FEM results and the previous experimental results is obtained by Eyers 1995. As it may be seen from Figure 4.3 that our results are in good agreement with Eyers results.

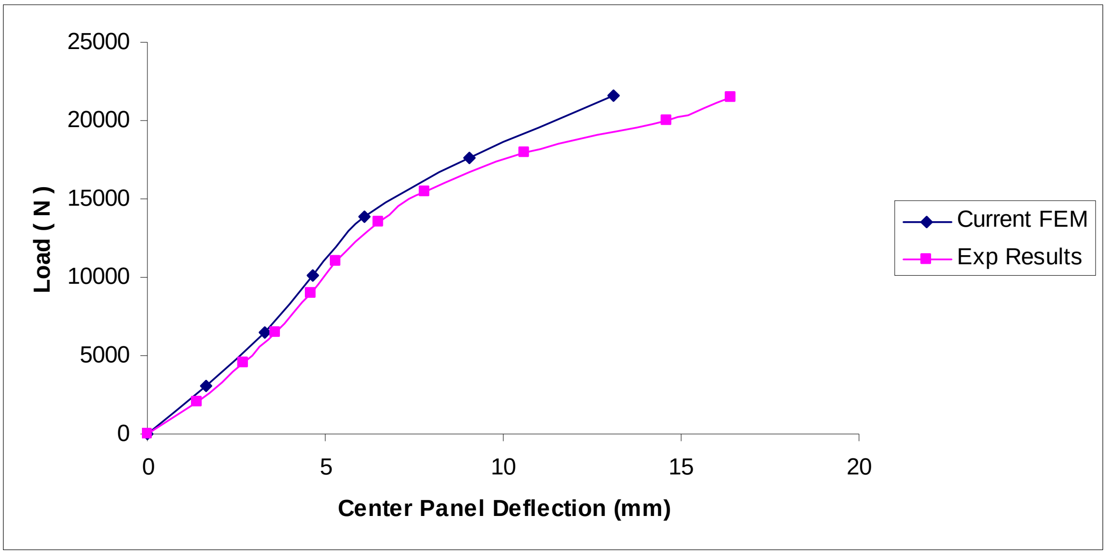

Figure 4.4. comparison of load versus center deflection panel deflection.

4.1.2 Finite Element Validation

In this section the results of current model are compared with the results obtained by (OOI, 2003) for simply supported panel from all sides. The panel has the same characteristics and properties of that shown in experimental validation section. Here the comparison is carried out over the shear load distribution on the top face sheet, bottom face sheet and the core. Collecting the shear load over model goes through many steps. Here is a summary of how to collect their by using 'I-DEAS'.

4.1.2.1 Shear Load Collection Procedure

In order to calculate the amount of load carried by each layer of the sandwich Panel at several locations along the panel's length, the panel is partitioned into ten different portions. Each portion consists of top face sheet, core, and bottom face sheet, thus there are thirty volumes altogether. By utilizing the grouping capability of I-DEAS, specific volumes and finite element entities of interest can be grouped together and analyzed. The grouped model then functions as free body diagrams, allowing to find out the load distribution on the regions of interest.

By only showing this group of entities, the cross section of Region 5 can be exposed. The element force, stress and strain contour can be analyzed on that specific surface. In order to see the cross sections of all the thirty volumes of the panel model thirty groups were created. The groups were labeled as Core Region 1-10, Top Face Sheet Region 1-10 and Bottom Face Sheet Region 1-10. The groupings are like making a cut on a free body diagram. The Region 1 cut would consist of the volume prior to Region 1, Region 2 cut would include all the volumes before the Region 2 cross section, and so on. In order to find out the actual load carried by a particular layer (core, top face sheet or bottom face sheet) at any surface of interest, the load carried by each node on that surface needs to be calculated. To achieve this there are three challenges that need to be overcome:

1. Data search from the data pool: The element force data associated with each node can be stored in a specific data file using I-DEAS. However, there is a need to extract the element force data that corresponds only to the nodes on the surface of interest.

2. Nodes of interest identification:

I-DEAS labels each node with a unique node number in order to make each node identifiable. Therefore each node that is on the surface of interest has a unique node number. There is a need to obtain the list of node numbers that corresponds to the nodes on the surface of interest.

3. Distinguish nodes on different material layer surfaces:

In the list of node numbers of interest collected, the nodes that correspond to each layer (core, top face sheet, or bottom face sheet) needs to be distinguished.

The first step to overcome the above-mentioned problems is to collect the node numbers of the nodes on the surface of interest. In order to do this we used the“info” function of I-DEAS to list the info of all the nodes on a specific surface. I-DEAS allows its users to limit the entity selection. In this case, we made nodes the only pickable entity. I-DEAS also allows a user to pick entities that are related to certain geometry. Therefore if the surface of interest is the cross section of the top face sheet users can set the options as “pick only nodes” and “related to surface”, and then pick the cross section of the top face sheet. I-DEAS will then list the information about the nodes that are on that selected surface on the I-DEAS List screen (Figure 4.5).

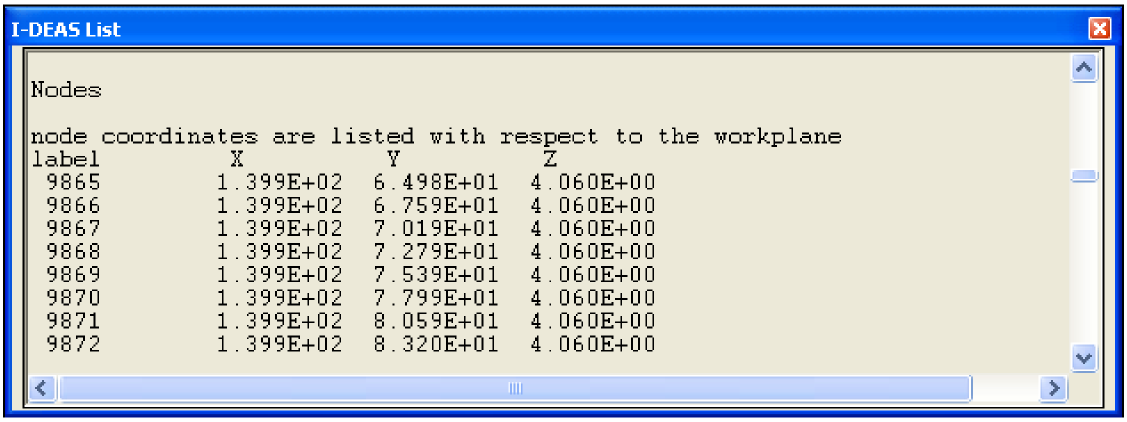

Figure 4.5. Node information on I-DEAS list window

The information listed including node numbers and their x, y, z-coordinate positions. This list of node information can be copied, pasted and saved on a text editor. Same process would be repeated for the cross section of each layers of each of the ten regions along the panel, resulting in a total of thirty sets of node numbers and locations. The next step is to extract the element force data. Element force data is extracted from the thirty volume groups. Thus there are thirty corresponding element force data files for the sixty groups of the beam. By using the “Report Writer” function of I-DEAS (Figure 4.6), the element force data can be generated and stored as **.dat** format.

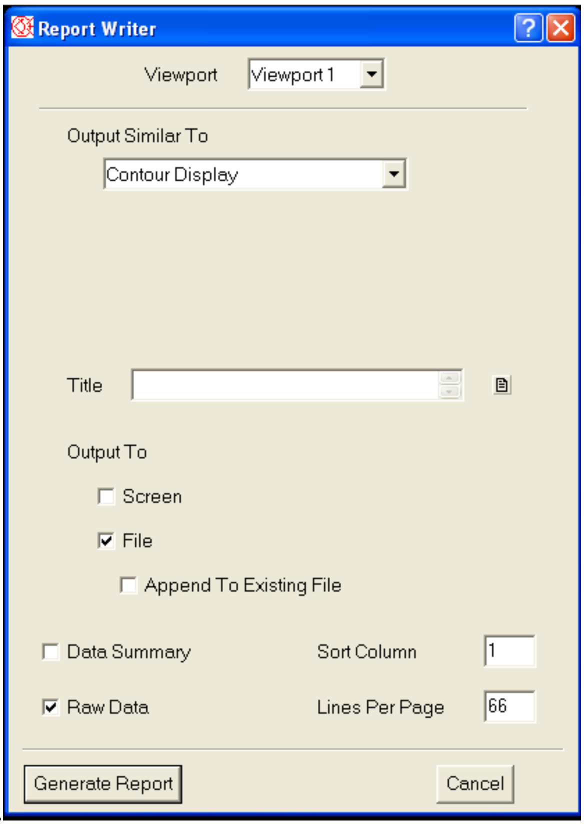

Figure 4.6. Report writer window

Figure 4.7 shows an example of the element force data file for the region one core, opened using an 'I-DEAS' list. The node numbers and element forces are then loaded and saved in an Excel file. The information listed on the element force data file are the node numbers, element forces in x, y, and z directions, and moments about x, y, and z-axes. It should be noted that this coordinate system is with respect to the global coordinate system. At this point the element force data from the sets of free body diagram cuts and the node number sets on the surfaces of interest has been obtained.

I-DEAS List

```
I-DEAS 10 NX Series :    Simulation                          12-Jul-08   18:05:53
F:\EDS\plate\103m2.mf1

Group ID            : None
Result Set          : 4 -  B.C. 1,TIME =  1.0,ELEMENT FORCE_4
Report Type         : Contour                      Units          : MM
Result Type         : ELEMENT FORCE
Frame of Reference: Part                           Data Component: Y-Component
```

Node	Elemen-X	Elemen-Y	Elemen-Z	Elemen-RX	Elemen-RY	Elemen-RZ
9856	1.110E+03	1.719E+03	5.468E+02	0.000E+00	0.000E+00	0.000E+00
9857	1.569E+03	-2.112E+03	-7.294E+02	0.000E+00	0.000E+00	0.000E+00
9858	1.405E+03	-1.669E+03	-5.060E+02	0.000E+00	0.000E+00	0.000E+00
9859	1.235E+03	-1.670E+03	-3.412E+02	0.000E+00	0.000E+00	0.000E+00
9860	9.755E+02	-1.548E+03	-2.117E+02	0.000E+00	0.000E+00	0.000E+00
9861	6.670E+02	-1.541E+03	-1.411E+02	0.000E+00	0.000E+00	0.000E+00
9862	3.245E+02	-1.465E+03	-1.159E+02	0.000E+00	0.000E+00	0.000E+00
9863	-4.256E+01	-1.406E+03	4.838E+01	0.000E+00	0.000E+00	0.000E+00
9864	-1.412E+02	8.638E+01	-3.638E+02	0.000E+00	0.000E+00	0.000E+00
9865	-1.118E+02	3.543E+03	1.115E+03	0.000E+00	0.000E+00	0.000E+00
9866	6.899E+00	-3.993E+03	-1.437E+03	0.000E+00	0.000E+00	0.000E+00
9867	5.417E+00	-3.103E+03	-1.005E+03	0.000E+00	0.000E+00	0.000E+00
9868	6.809E+00	-3.108E+03	-6.796E+02	0.000E+00	0.000E+00	0.000E+00
9869	7.200E+00	-2.870E+03	-4.221E+02	0.000E+00	0.000E+00	0.000E+00

Figure 4.7. Element force data file on' I-DEAS' list

The final procedure would be to match the node numbers on the surfaces of interest with the element force data files of each group of free body diagram cuts. To surface and extract the corresponding element force values from the corresponding set of element force data. All node forces can then be summed and the resulting load in the x, y, and z directions of a particular surface is obtained.

4.1.2.2 Results of Verifications HTS.

Comparison of the current model results with OOI model results for core - shear - distribution -ratio and face sheet-shear- distribution- ratio are presented in following sections

4.1.2.3 Core Shear Distribution

Both classical sandwich plate theory and higher order theory assume that the core carries the entire shear load in the linear range. In order to investigate the validity of this assumption a ratio between the core global Y load, $R_{C\,(Yg)}$, and the total global Y load, $R_{TOT\,(Yg)}$) in the sandwich structure was examined. This shear ratio was calculated at the partitioned regions along the plate span. The cross section at 190.5 mm from the left edge is selected to see the changes of the shear ratio with the progression of core yielding. Figure 4.8 depicts the shear ratio change at 190.5 mm plate span for different applied load step the results show that at any location, the core takes up about 94% or higher load of the structure in the linear range. This confirms the validity of the classical assumptions that the core carries majority of the shear load. Geometric non-linearity in this case does not affect the load carrying method of the sandwich panel significantly because the deformation is small relative to the core thickness. The low modulus of elasticity prevents the axial load components of the core to contribute significantly to $R_{TOT\,(Yg)}$. In Figure 4.8, it can be seen that the initiation of core yielding has caused the shear ratio of the core to drop. Figure 4.8 shows that shear ratio at X = 190.5 mm drops from more than 98% in the linear range to about 91% at 86.2 kPa and 72% at 103.4 kPa. This shows that once the core begins to have significant plasticity, there is a load transfer from the core to the face sheets. The face sheets carry a significant amount of shear load once core starts to yield

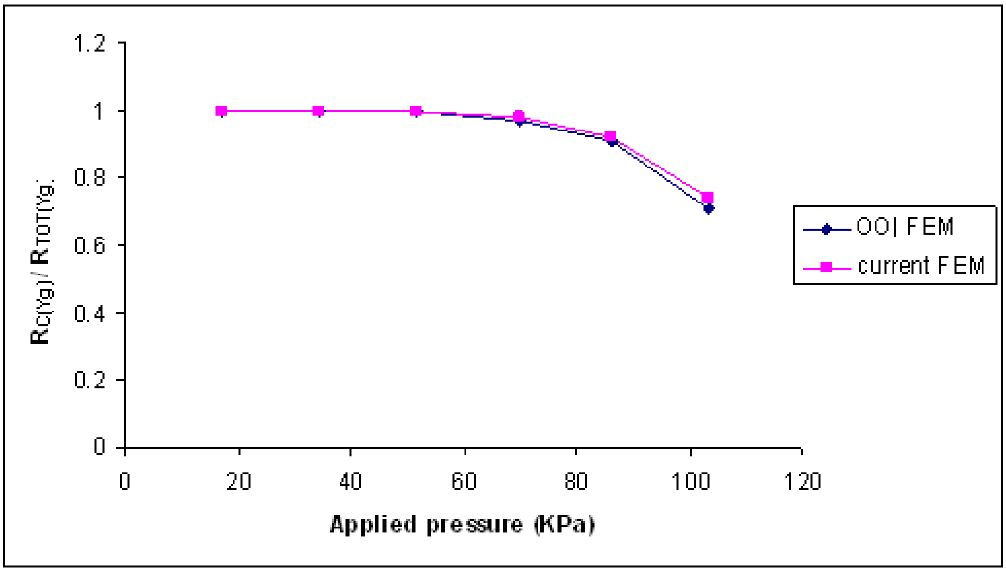

Figure 4.8. Core shear ratio at X = 190.5 mm for various load steps.

4.1.2.4 Top Face Sheet Shear Distribution

When geometric nonlinearity comes into play, the resultant shear within the top face sheet turns out to be positive. In order to analyze the effect of material non-linearity on the top face sheet's shear distribution, the shear ratio between the top face sheet and the whole structure is analyzed. Figure 4.9 shows the shear ratio of the top face sheet along the X-axis plate span at various load steps.

Since the top face sheet shear resultant, $R_{TF\,(Yg)}$, is in a direct opposite to the total shear resultant, $R_{TOT\,(Yg)}$, a negative ratio is obtained. The ratio becomes increasingly negative as the load increases. This increase is consistent with the sandwich beam shear distribution for four point bend test. At 103.4 kPa the shear ratio falls out of the pattern and shows a drastic drop. This could be due to the sudden increase in core plasticity that reduces the top face sheet's slope. In other words, due to large core plasticity, the center of the top face sheet becomes more flat than the previous load step. This argument is supported by the apparent sudden drop in the ratio negativity at the loaded region (about 76.2 mm plate span onwards).

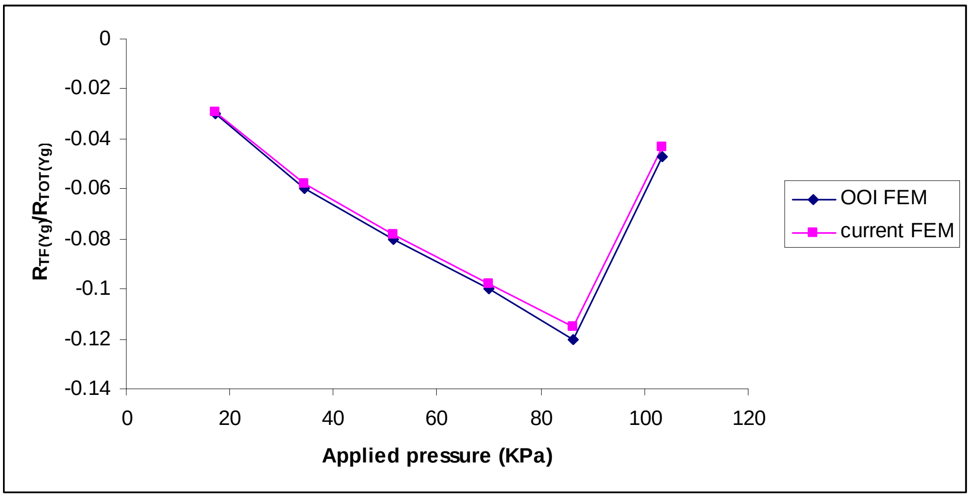

Figure 4.9. Top face sheet and total shear ratio at X = 190.5 mm for Various load steps

Figure 4.9 shows the top face sheet shear ratio change at 190.5 mm from the left edge for various load steps. As expected, the ratio becomes increasingly negative as the load increases, showing a more apparent sign of membrane effect. The negativity of the ratio decreases at 103.4 kPa due to large core plasticity.

In order to visualize the membrane effect in the top face sheet, it is useful to know the strain conditions in the top face sheet. The membrane effect in this two dimensional case is much more complicated because now membrane effects occur along both X and Z-axes. Figure 4.10 shows the schematic view of the resultant membrane effect on an element of the top face sheet.

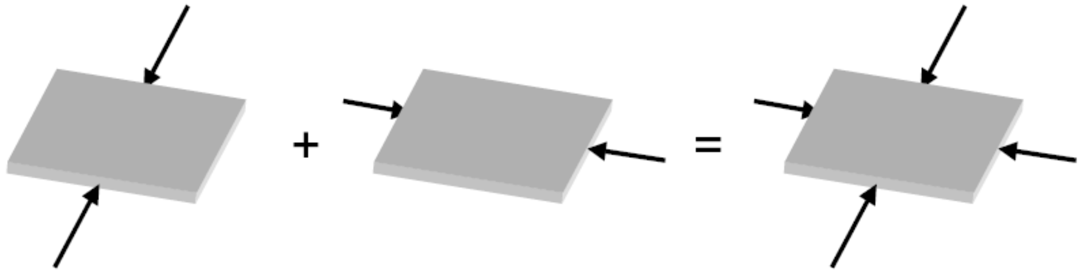

Figure 4.10. Resultant membrane effects on an element on the top face sheet

4.1.2.5 Bottom Face Sheet Shear Distribution

The bottom face sheet of the plate is in tension. Therefore with geometric nonlinearity, the resultant global Y force of bottom face sheet, $R_{BF\ (Yg)}$, becomes increasingly in negative.

The shear ratio for bottom face sheet has a positive value. The ratio increases at locations closer to the center of the plate. This is because the bottom face sheet increases in tension as it moves closer to the center of the plate. However it is important to note that there is no deflection angle at the plate mid-plane (X = 304.8 mm) and therefore there is no membrane contribution to the global Y resultant of the bottom face sheet, $R_{BF\ (Yg)}$ at that location. Membrane effect becomes more significant as the applied load increases. A sudden increase in shear ratio for the 86.2 kPa and 103.4 kPa load steps is observed. This is mainly due to the initiation of core yielding that has caused the load transfer from the core to the face sheets. The bottom face sheet carries this additional load through membrane forces.

The core used in this analysis is Airex 63.50, one that is qualified as a “soft core”. The core could have experienced a change of thickness near the top face sheet region and hence caused the flattening of the region.

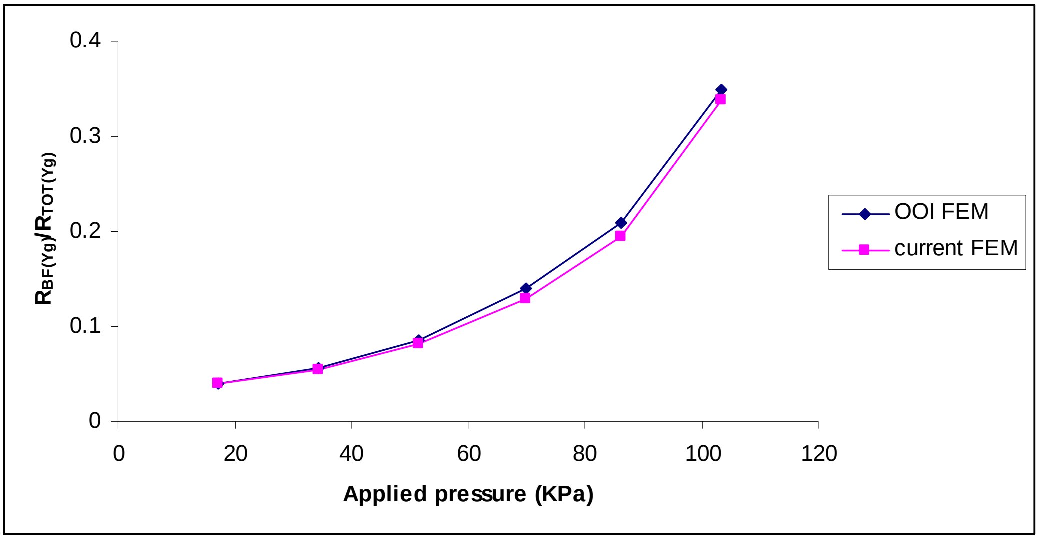

Figure 4.11. Bottom face sheet shear ratio at X = 190.5 mm for various load Steps.

Further conclusions can be made from the shear ratio plots of the bottom face sheet at a fixed location for various load steps. This type of shear ratio change is shown in Figure 4.11. The ratio shows a gradual increase throughout with increased changes for the 86.2 kPa and 103.4 kPa load steps. The load transfer to the face sheets due to core plasticity and the geometric non-linearity are the main causes of these increases in the shear ratio. Figures 4.12and 4.13 show the propagation of yielded region with increasing load steps from 86.2 kPa to 103.4 kPa .Note that scale of plastic strain color bands has been manually set so that two load steps have same scale. The usage of standardized scale allows better comparisons to be made between the two plastic strain contours. Core yielding initiation has occurred at 86.2 kPa, the yielded region is not large and does not affect the shear distribution significantly. The plastic yielding region expanded tremendously at 103.4 kPa.

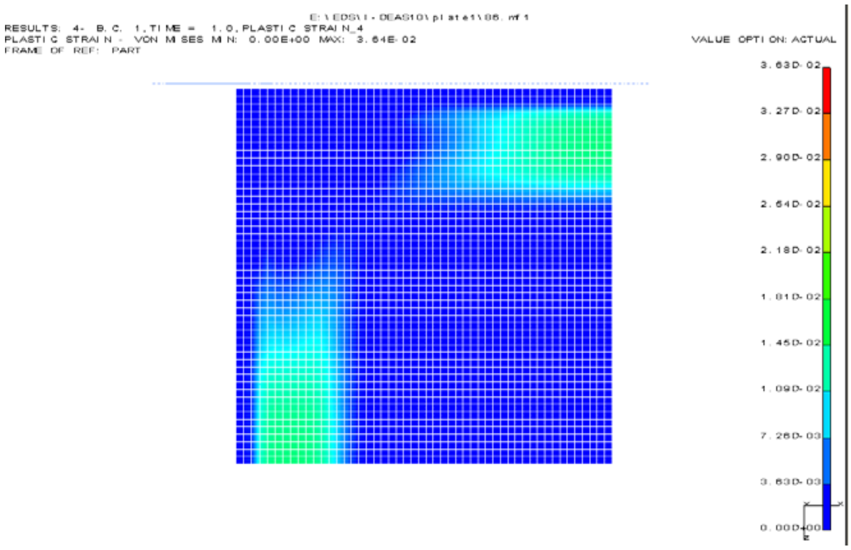

Figure 4.12. Plastic strain contours in sandwich core at 86.2.4 kPa (top view)

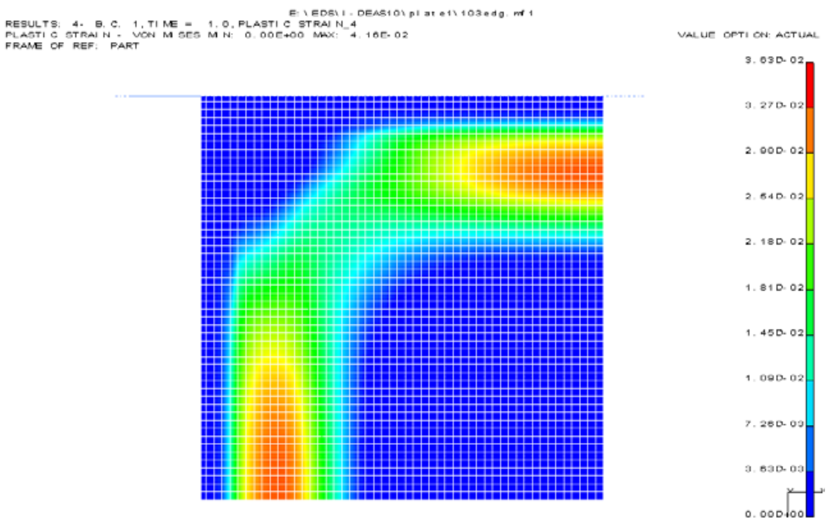

Figure 4.13 Plastic strain contours in sandwich core at 103.4 kPa (top view)

4.1.3 Analytical Verification

Classical sandwich theory has been utilized to obtain close form solution (Zenkret, 1995, Ooi, 2003). The equations that are derived are programmed using Matlab Software. The comparison between the numerical and theoretical models in the linear rang are presented in Appendix C. Figure 4.14 is a sample of the comparison that carried out. The Figure shows very good agreement between theoretical and numerical solution.

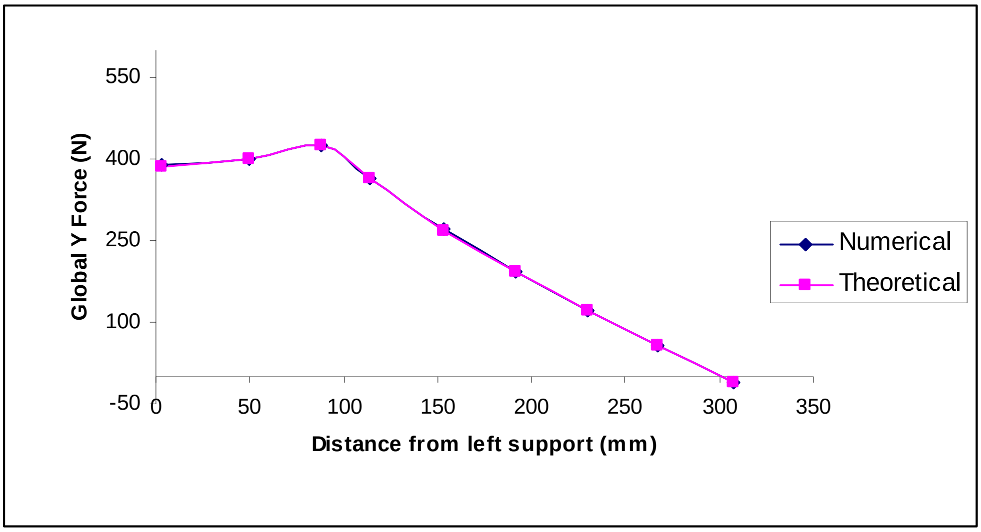

Figure 4.14. Total plate shear distribution comparison along X-axis at 17.2 kPa

4.2 Experimental Verification

To assure accuracy and validity of the results some selected cases are investigated. Experimental results obtained from the FEM are compared against those obtained experimentally where both results show excellent agreement.

4.2.1 Test Setup

Here is a description of the experimental setup used in the study and consists of the following:

1. The Specimens have been manufactured by ' Maani Prefab Company '. Core of the sandwich panel is made of polyurethane foam. Top and bottom sheets of the sandwich panel are made of steel. The dimensions of panel used for verification is shown in Figure 4.15. Table 4.3 presents the thicknesses used in the investigation Mechanical properties of the sheet metal are obtained experimentally.

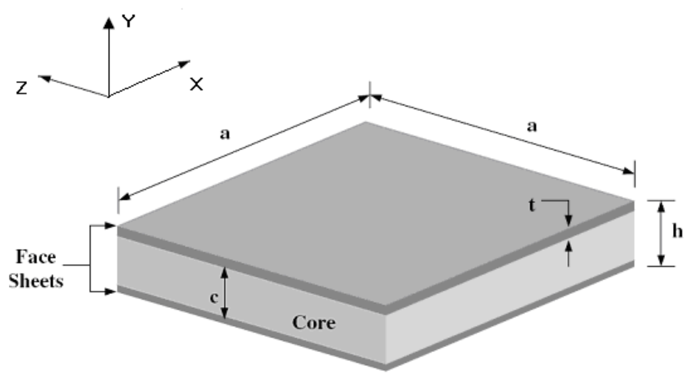

Figure 4.15. Sandwich plate dimensions

Table 4.3. Dimensions of the Parameter shown in Figure 2.1

Parameter	Dimension	Note
a	250mm	constant
t	0.5mm-1mm	variable
c	15mm-50mm	variable

2. Fixture for applying simply supported boundary condition is produced. Figures 4.16 a and b show different views of the fixture

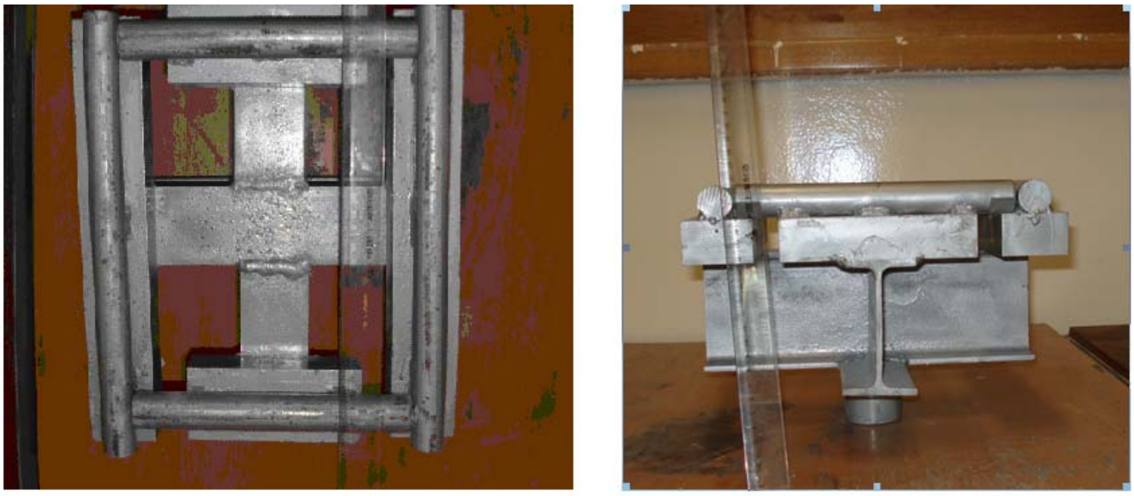

Figure 4.16. Fixture that is produced for applying simply supported boundary condition (different views)

3. The test is performed on a uniaxial testing machine that is shown in Figure 4.17.

   Figure 4.18 is a schematic presentation of the full test set up

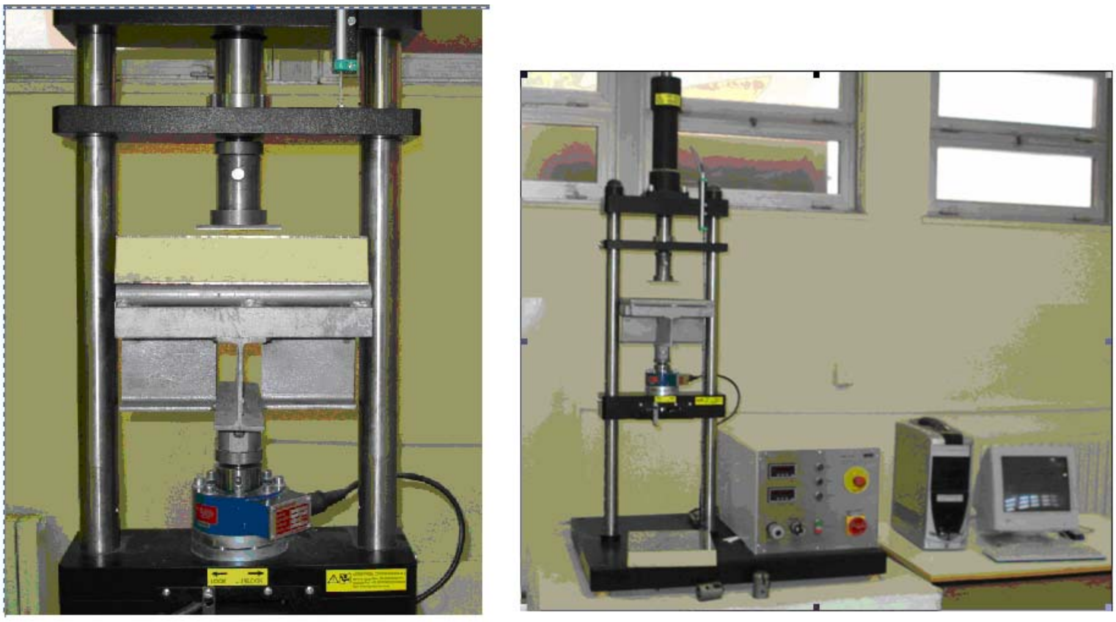

Figure 4.17. Uniaxial testing machine with and without specimen

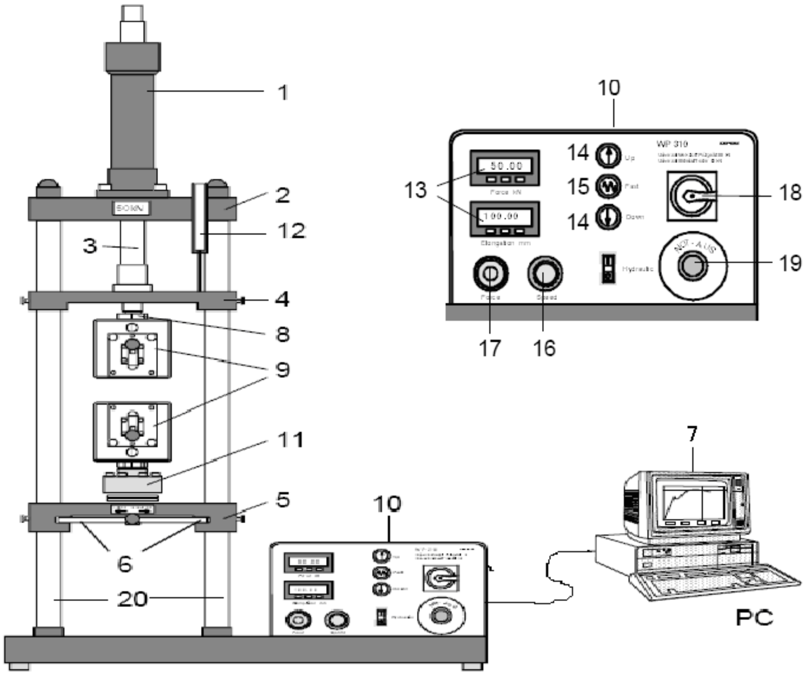

Figure 4.18. Schematic of simply supported from all sides test fixture setup

The system is a vertical column-tester, hydraulically driven, and with direct display of the force. The maximum testing force is 50 kN. In the working space, tensile force as well as compressive force can be applied. The double-action hydraulic cylinder (1) is mounted on top of the stationary crosshead (2). The piston rod (3) acts on the upper traverse (4). The height of the lower traverse (5) can be changed in coarse steps. It is fixed on both columns (20) by means of interlock and grooves (6). The working space, where the test is conducted, is located between the upper and lower traverses. The cylindrical receptacle (8) on the traverses allows for easy interchange of various chucks, e.g. specimen grips. The displays of force and displacement, the hydraulic unit and the control of the system are found in the cabinet (10). The force is measured via a force sensor (11) in the lower traverse. The displacement is measured by displacement sensor (position transducer) (12) located on the upper traverse. Both force and displacement measurements are shown on digital displays (13), and can be transferred to a computer via a serial interface for data evaluation (7). The displacement of the upper traverse can be controlled by a push button (4). For fast movement in both directions, a switch (15) is available. Displacement speed (16) and maximum force (17) can be infinitely adjusted. Besides the main switch (18), the system has an emergency switch (19).

4. Distributed load is applied to the specimen by adaptors manufactured for this purpose. Figure 4.19 illustrates the adapters used in experimental setup.

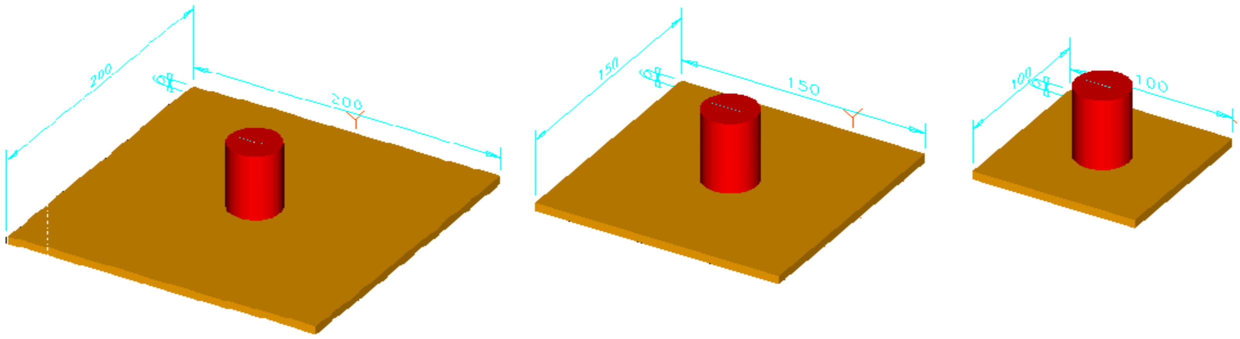

Figure 4.19. The adapters used in the experiments for applying distributed load on specimen. (All dimensions shown in mm)

4.2.2 Mechanical Properties of the Specimen

The sandwich panel is made of polyurethane foam and steel sheets Table 4.4 present the mechanical properties that are obtained experimentally for both the sheets and the core. ASTM Designation: C 365 – 00 used for testing the core material while ASTM Designation D 638 – 00 for testing sheets. The results of those specimens shown in Figure 4.20 for core material force- deformation curve while the Figure 4.21 presents the sheet material force – deformation curve

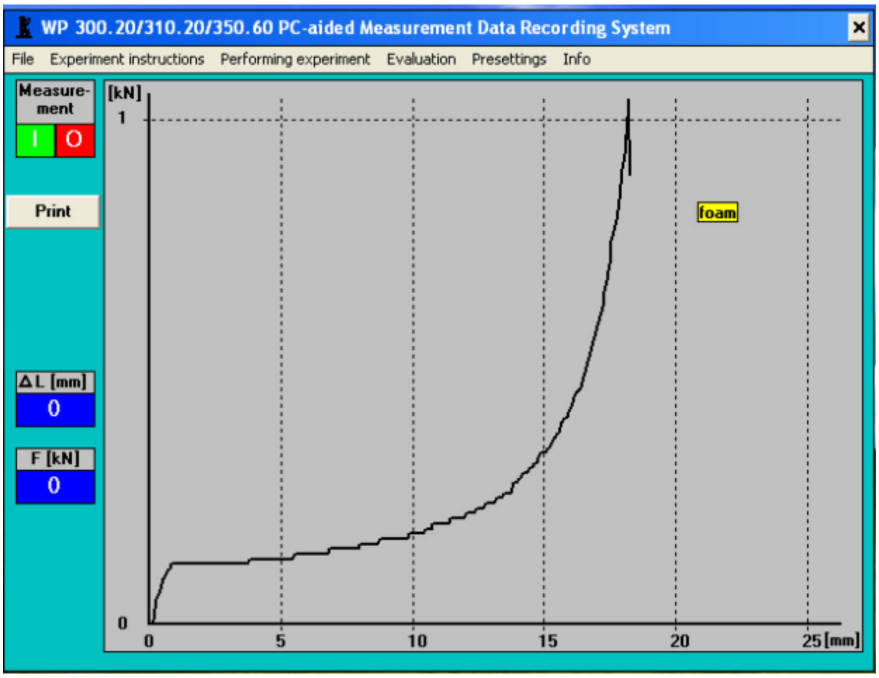

Figure 4.20. Force deflection curve for specimen sandwich panel core material

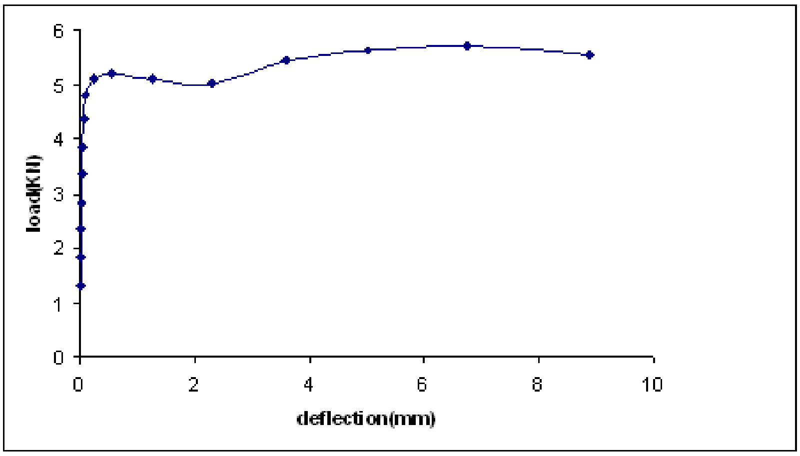

Figure 4.21. Force deflection curve for specimen face sheet material

4.2.3 Analysis

The experiments are carried out and sample result is shown in Figure 4.22 for specimen of 49 mm core thickness and 0.5 mm sheet thickness.

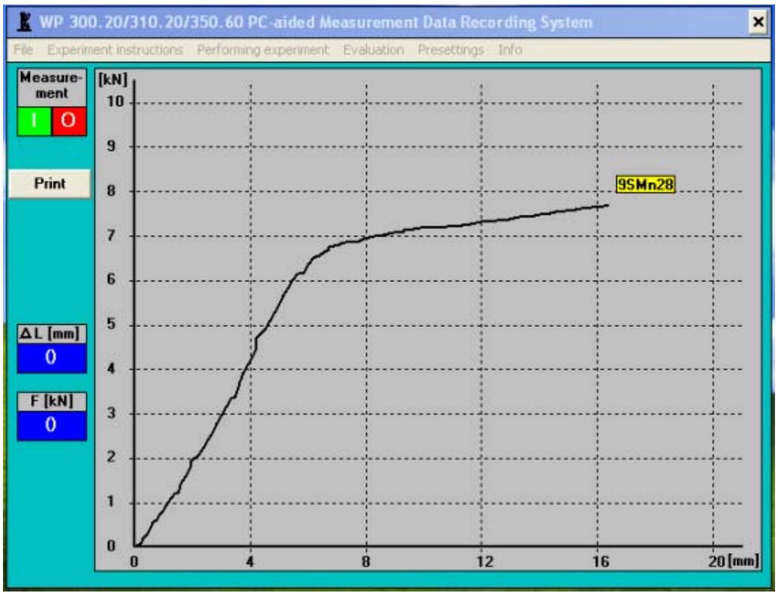

Figure 4.22. Experimental Force deflection curve for the sandwich panel of 49 mm core thickness and 0.5 mm sheet thickness.

The relation between the applied load and the deflection of the specimen center point are shown in that Figures 4.23 and Figure 4.24 presented a comparison between the experimental results and FEM results. It may be seen that the results are in very good agreement.

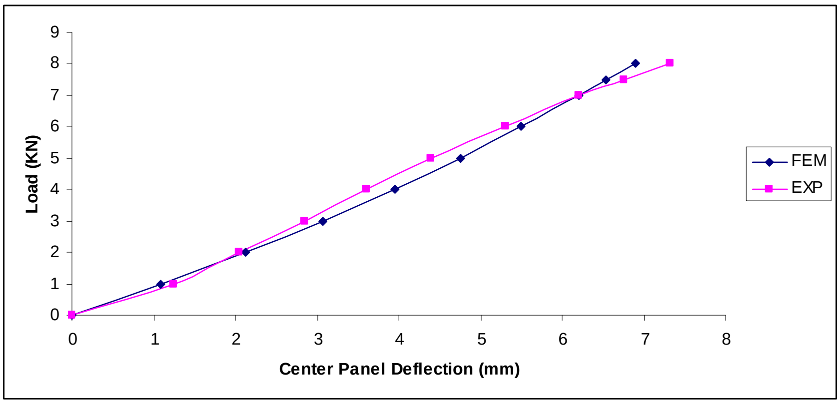

Figure 4.23. Comparison of load versus center deflection for core thickness = 49 mm, Sheet Thickness = 0.5 mm, applied load area = 200 mm*200 mm

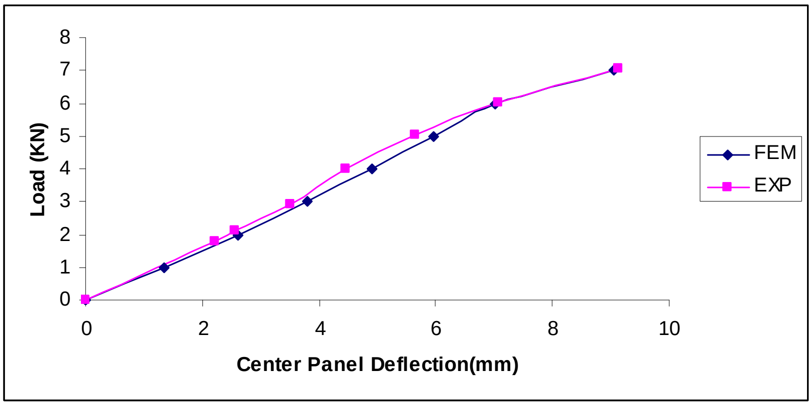

Figure 4.24. Comparison of load versus center deflection for core thickness=71 mm, sheet Thickness = 0.5 mm, applied load area = 150 mm*150 mm

To assure accuracy of the experimental results, the experiment is performed many times and the average values are plotted. The variation in the experimental results dose not exceeds 7% of the average value.

CHAPTER FIVE

RESULTS AND DISCUSSION

5.1 Results

The Finite Element Analysis (FEA) full results are presented in graphical format in Appendix A.The whole results are presented in tabulation format in appendix B. Three main parameters are investigated, the sandwich panel thickness, the core material (different materials with different modulus of elasticity) and the area on which the load is being applied. Baseline data for designing sandwich panel has been generated and tabulated in Appendix B. For designing any sandwich panel within the parameter range these tables could be used. These results are very beneficial for design engineers to obtain (to select) the optimum parameters that fit their design. The main advantage of this result over the sandwich panel theory is that both geometric and material nonlinearities are considered without approximation. Usually these approximations eliminate part of the problem physics. By utilizing “I-DEAS’ post processing module, stress and it is all components, strain and it is all components including the plastic strain, and deformations are obtained. Figure 5.1a and Figure 5.1b show the results selection window for partial of results.

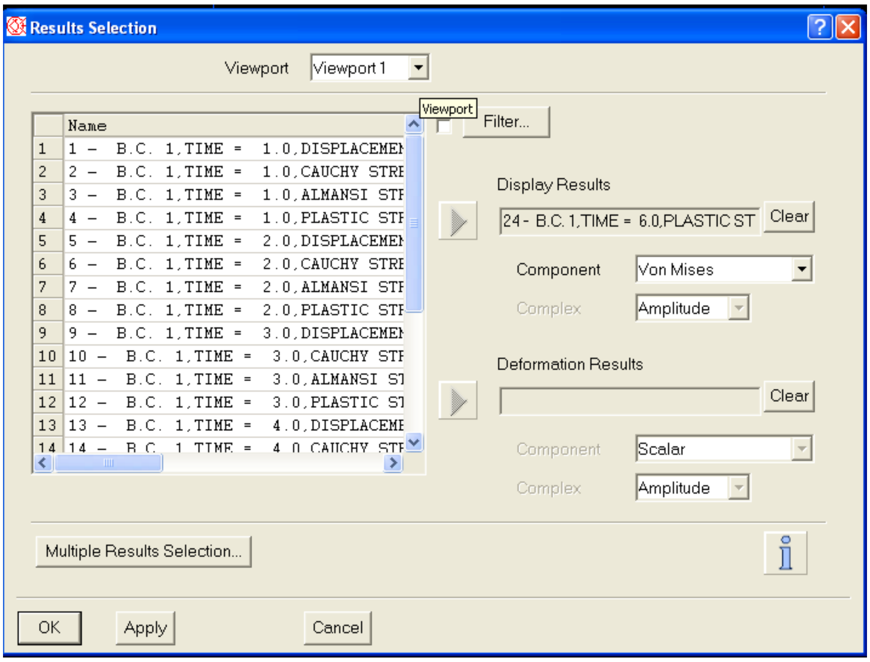

Figure 5.1(a). Snap- shot of results selection window showing partial list of the results generated.

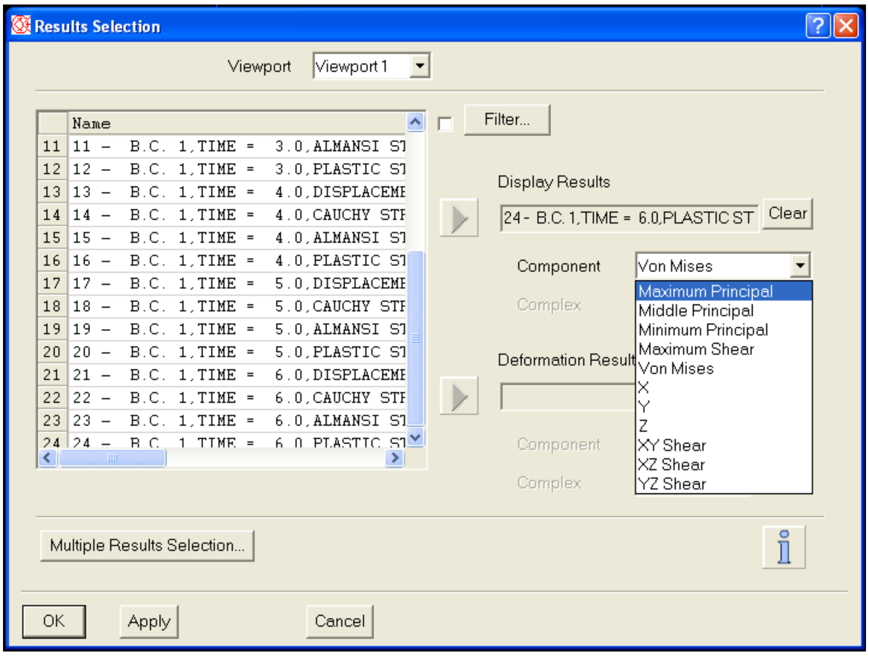

Figure 5.1(b. Snap-shot of 'I-DEAS' results selection window showing the partial list results and the stress results components that could be obtained

Figures 5.2, 5.3 and 5.4 present stress contours of Von Mises stress contour for both the panel and the core, deformation contour for both panel and core, and plastic strain for both panel and core respectively

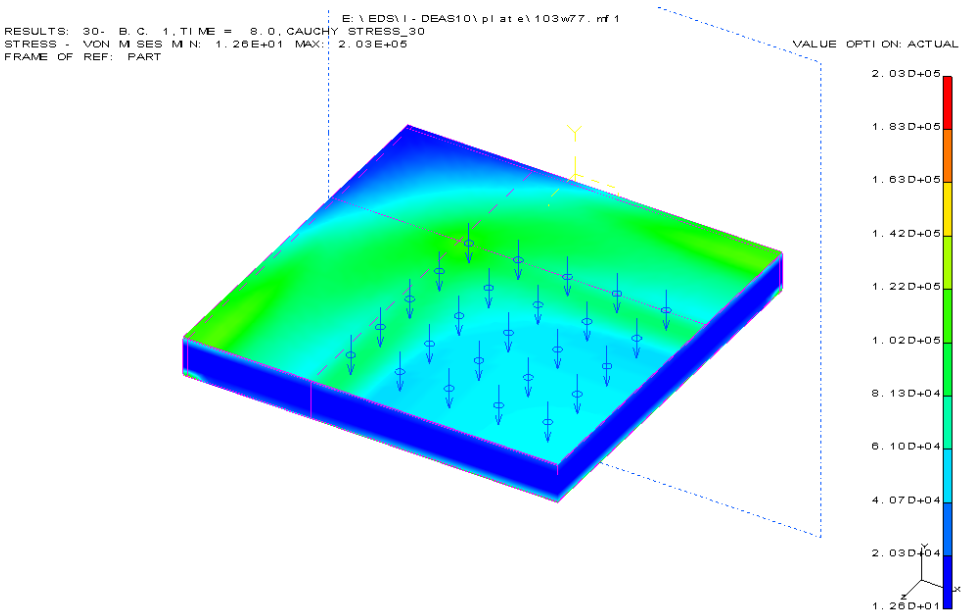

Figure 5.2(a). Von Mises stress contour (in MPa) for panel 0.66A30 at load step 145 kPa.

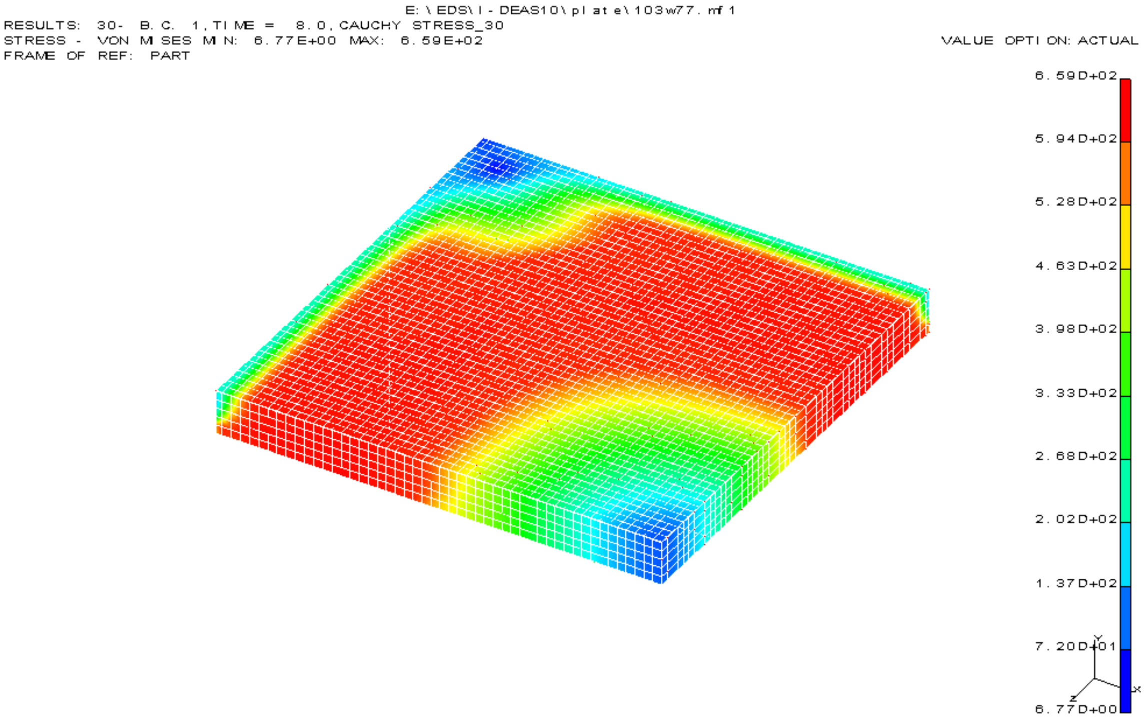

Figure 5.2(b). Von Mises stress contour (in MPa) for core 0.66A30 at load step 145 kPa

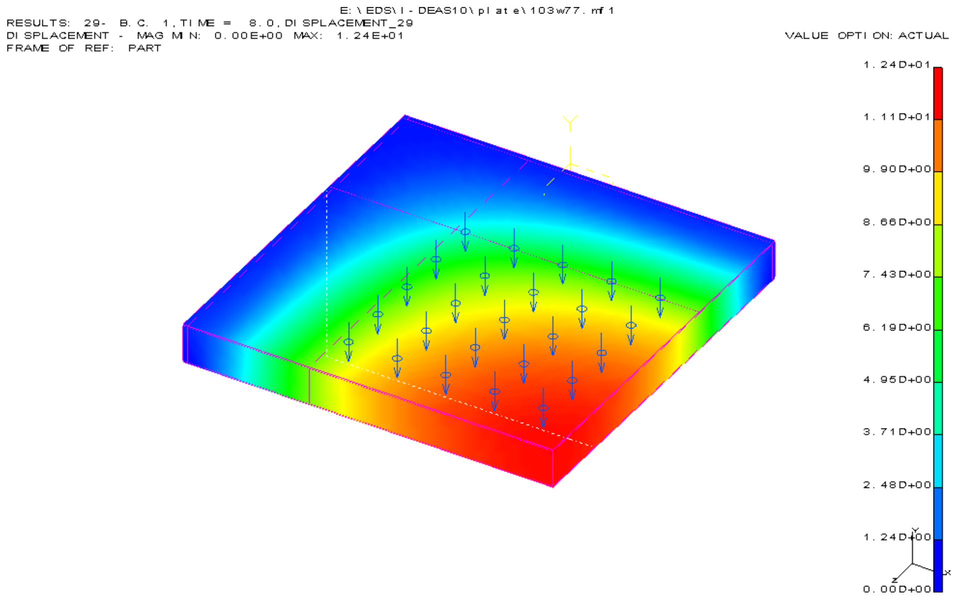

Figure 5.3(a) Illustration of the panel deformations contour for 0.66A 30 at load step 145 kPa

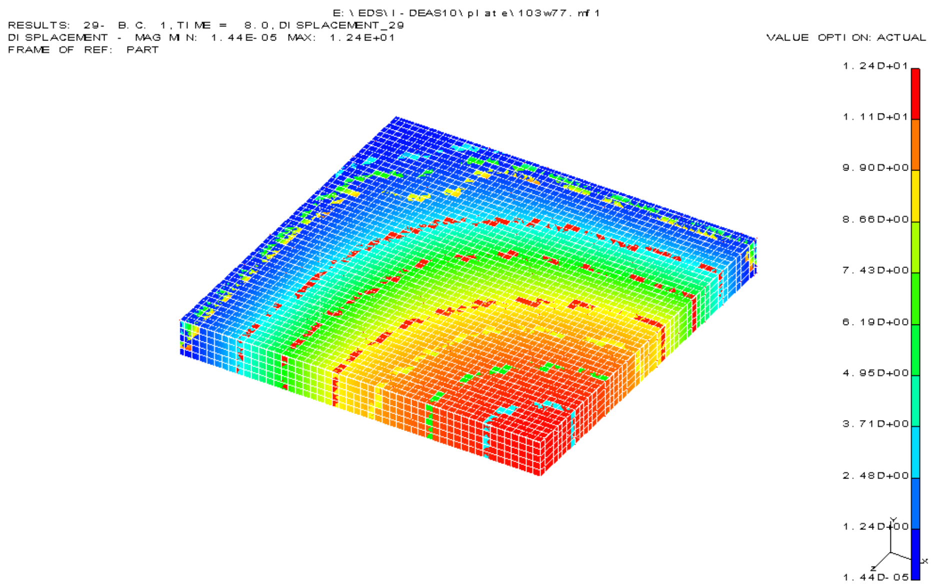

Figure 5.3(b). Illustration of the core deformations contour for 0.66A 30 at load step 145 kPa

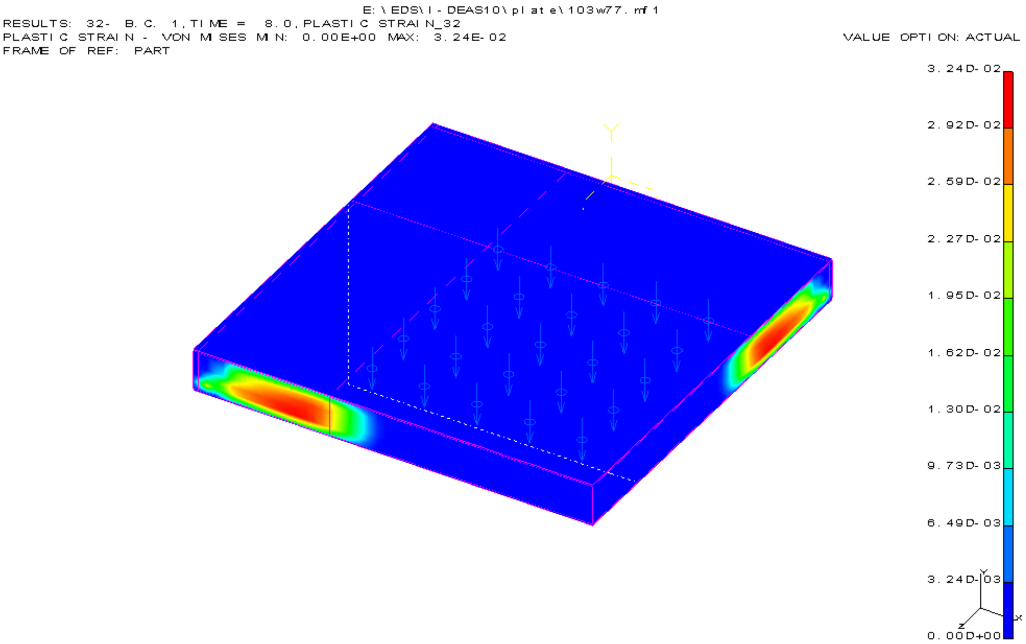

Figure 5.4(a). Demonstration of the plastic deformations contour for panel 0.66A 30 at load step 145 kPa

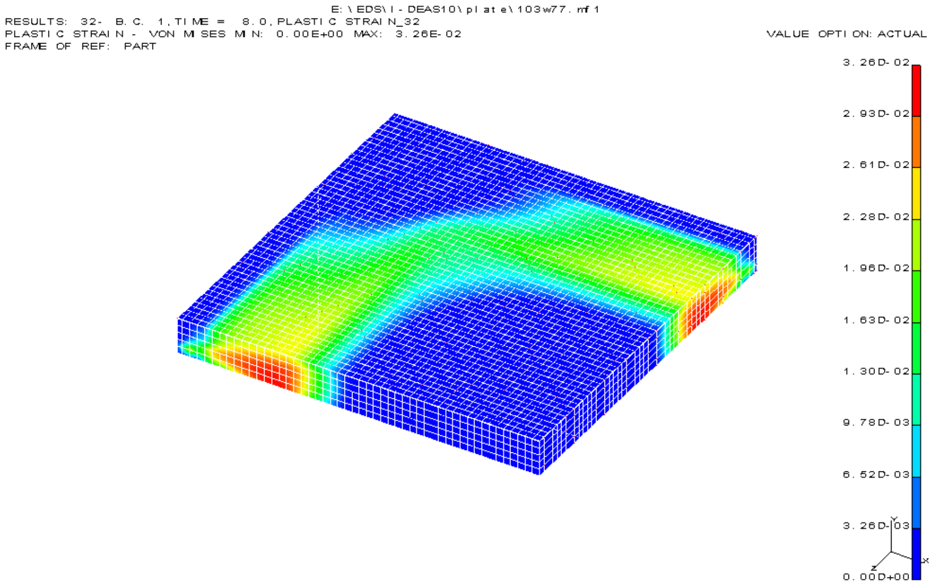

Figure 5.4(b). Demonstration of the core plastic deformations contour for panel 0.66A 30 at load step 145 KPa

Figure 5.5 presents the code (FEM identification) used in appendices and Figures 5.3 through 5.15 the letter in the code represent the material; the materials are ordered in ascending manner i.e. A has the lowest modulus of elasticity while D has the highest modulus of elasticity.

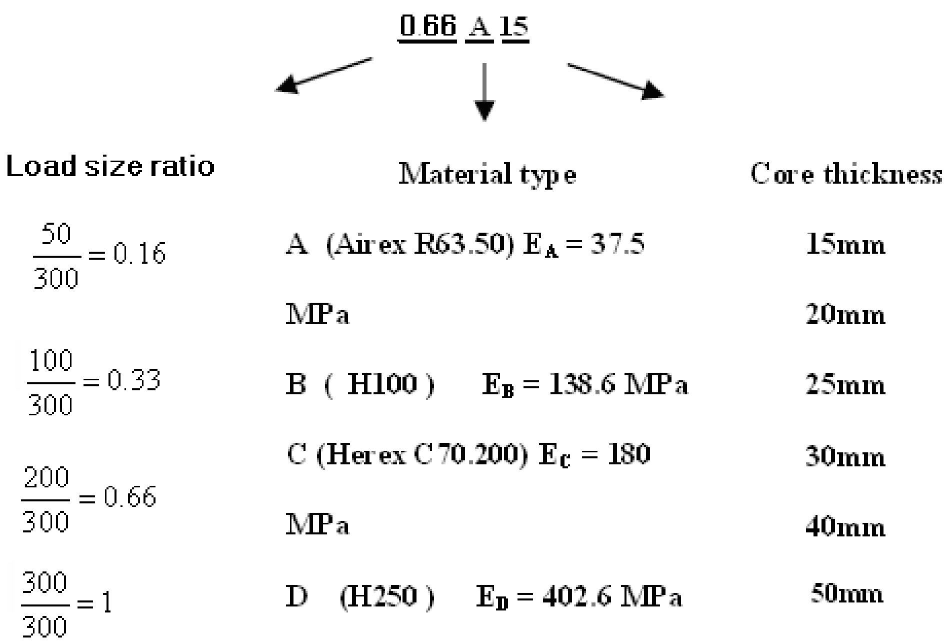

Figure 5.5. Definition of panel code used in all figures and appendices

It may be seen that each figure of Figures 5.2 through 5.5, is no more than one entry to Tables presented in Appendix B. It is clear from Figure 5.4 (a) and 5.4 (b) that the plastic deformation occurs close to the panel support (close to the area where boundary conditions are applied). Sample results will be presented to illustrate the behavior of the sandwich panel with respect to each parameter.

The criterion that is adopted by this investigation at what load step the FEM should stop, when any of face sheets starts to yield. This criterion fulfills the need of the designer; in general design engineer tries to avoid panel permanent distortion. As soon as the face sheet metal starts to yield, this means that permanent deformation is taking place. So all results produced do not exceed the loading that could cause face - sheet yielding.

5.2 Parametric Study

Three main parameters are investigated, the sandwich panel thickness, the core material (different materials with different modulus of elasticity) and the area on which the load is being applied. The following subsections present the effect of each parameter.

5.2.1 Core Thickness

Figures 5.6 and 5.7 represent the effect of core thickness of material A on both core and bottom sheet maximum shear stress. It may be seen from Figure 5.6 as the core thickness increases the load carrying capacity of the panel increases. Figure 5.7 presents the effect of panel - core - thickness on the bottom – face - sheet rather than the top – face - sheet. The reason behind this is, in all results it is found that the bottom - face - sheet starts to yield before the top one.

Since the failure of core material is due to shear stress, all graphical results are showing shear stresses not Von Misis stress.

As the core starts to yield, its maximum stress stay constant (see Figure 5.6) while the bottom - face - sheet, its stress keeps increasing as the load increases, this means that the load is being transferred to the face sheet metal. This is the main advantage of increasing the load beyond the yield point of the core material.

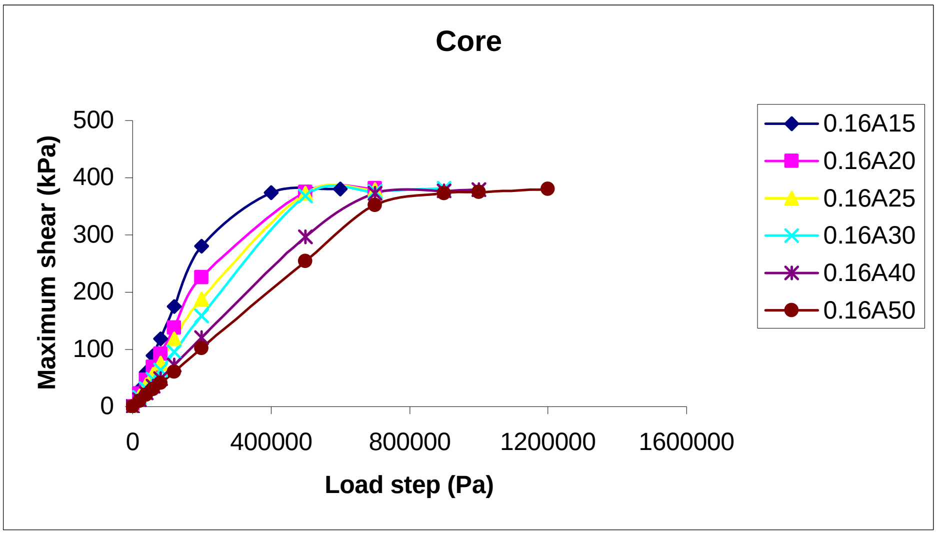

Figure 5.6. the variation of maximum shear of the core material A with load step for different values of core thickness at load size ratio 0.16

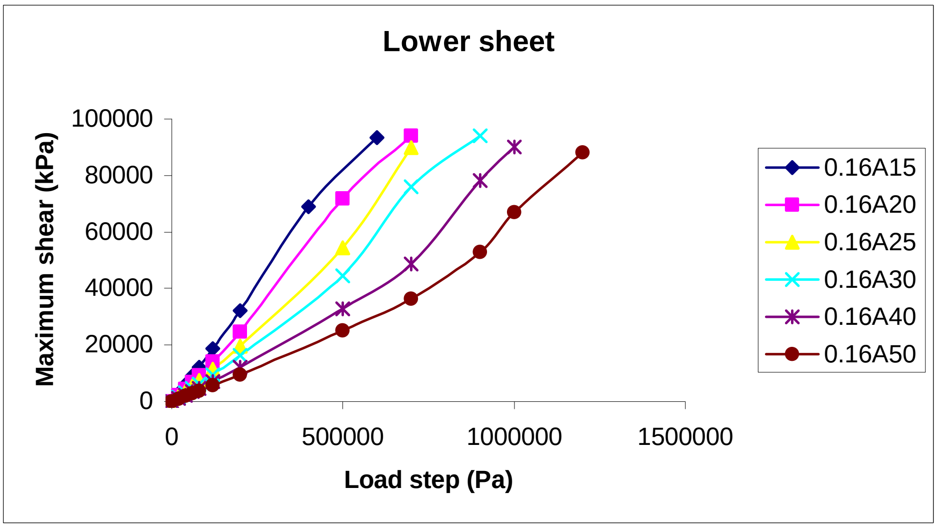

Figure 5.7. the variation of maximum shear of the bottom sheet with load step of the core material A for different values of core thickness at load size ratio 0.16

5.2.2 Material Stiffness

Figure 5.8 and 5.9 demonstrate the effect of material stiffness. Since the modulus of elasticity $E_A < E_B < E_C < E_D$, it can be seen that the softer material is, the more load is transferred from core material to the sheet metal as the core starts to yield.

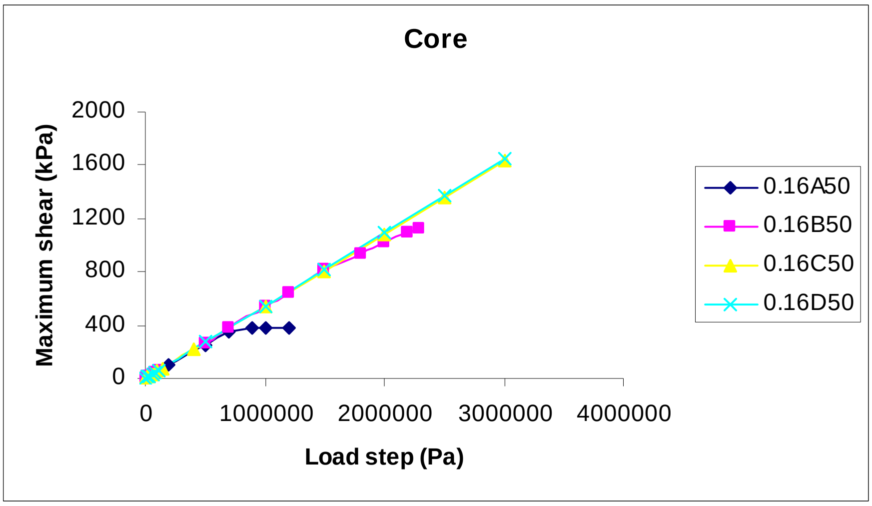

Figure 5.8. Maximum core shear versus load with variation material at thickness 50mm and load size ratio 0.16

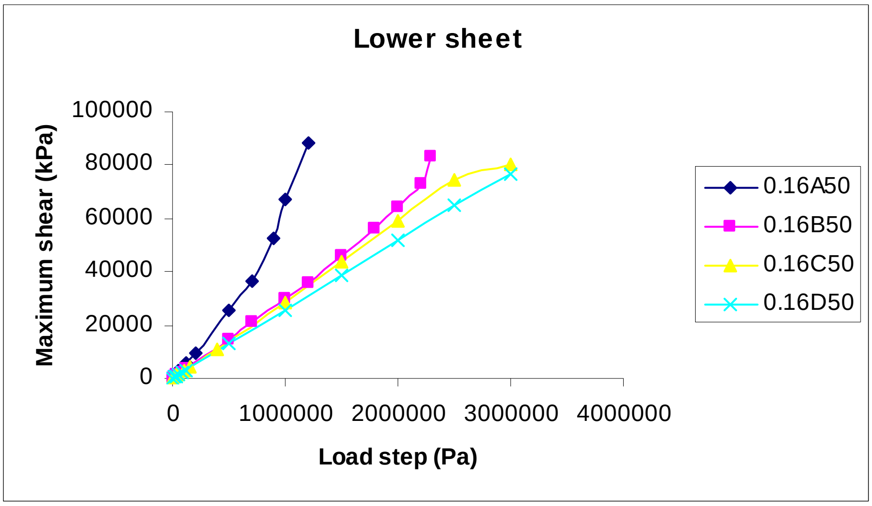

Figure 5.9. Maximum lower sheet shear versus load with variation material at thickness 50 mm and load size ratio 0.16

It is obvious that the load carrying capacity of the panel increases as its core material is stiffer. It may be seen that in Figure 5.8 the core material is still within the elastic range for 0.16A50 and 0.16D50, however in Figure 5.9 in the bottom face sheet l starts to yield (entering the plastic region).

By comparing Figures 5.10 and 5.11 with Figures 5.12 and 5.13 respectively, it can be seen that materials B, C and D in Figures 5.10 and 5.11 are almost coincident, for thickness of 20 mm.

However for Figures 5.12 and 5.13 they are not coincident. It can be seen that as the thickness increase the curves of material B, C and D spreads more.

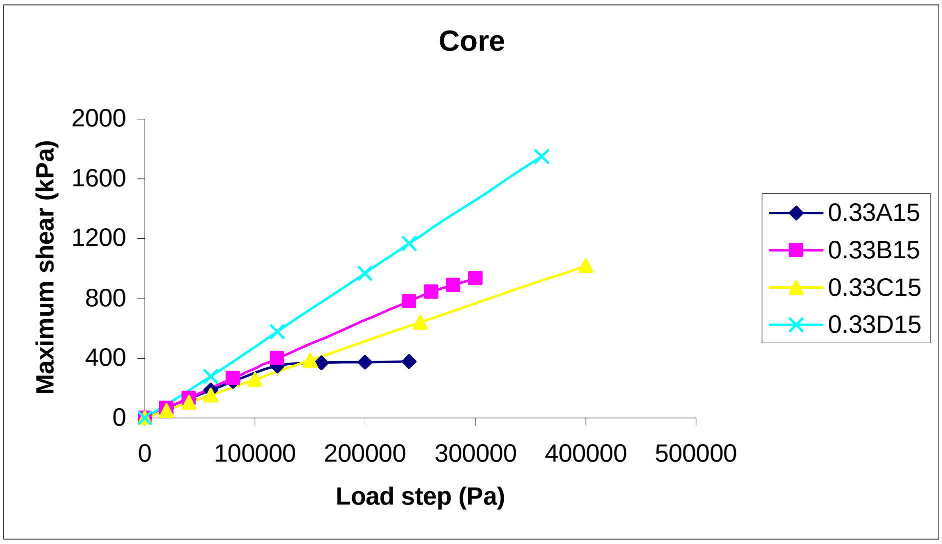

Figure 5.10. Maximum core shear versus load with variation material at thickness 20 mm and load size ratio 0.33

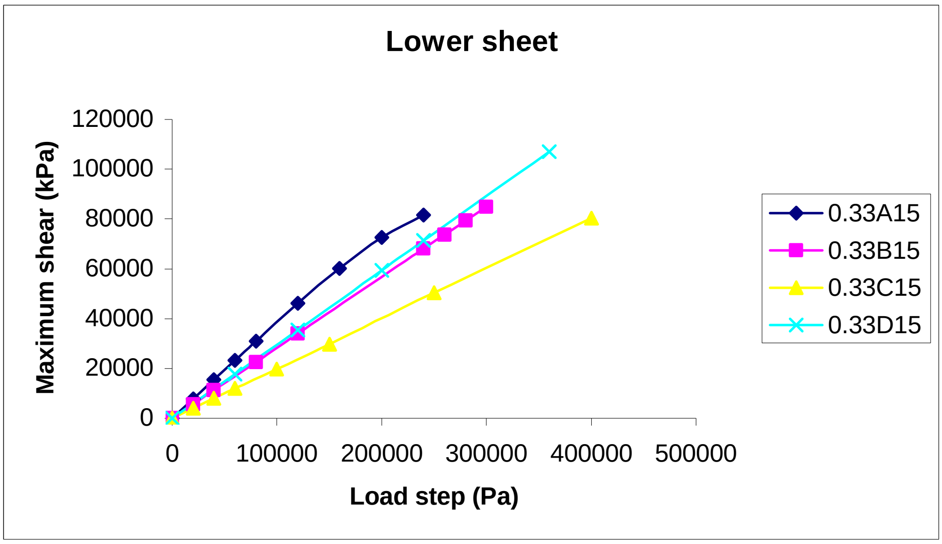

Figure 5.11. Maximum lower sheet shear versus load with variation material at thickness 20 mm and load size ratio 0.33

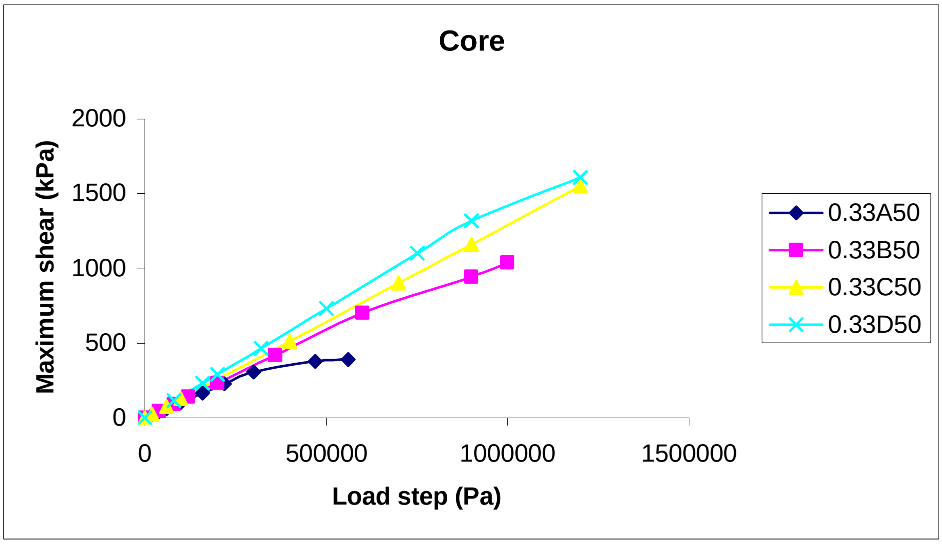

Figure 5.12. Maximum core shear versus load with variation material at thickness 50 mm and load size ratio 0.33

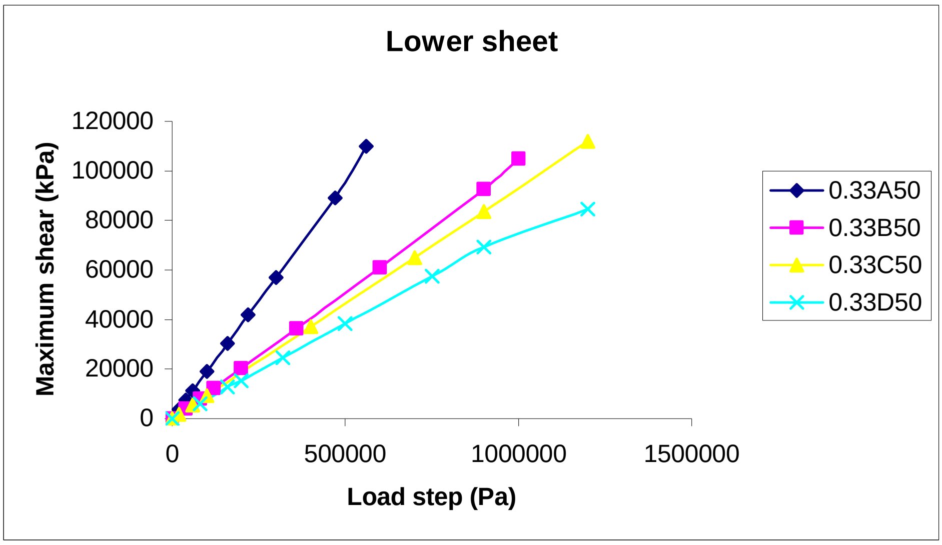

Figure 5.13. Maximum lower sheet shear versus load with variation material at thickness 50 mm and load size ratio 0.33

5.2.3 Load Size

Figures 5.14 and 5.15 present the effect of load size (area on which the load is applied).

For core material A as the loading area increases the stress decreases for the same amount of loading. Same thing can be said for the bottom face sheet in Figure 5.15. The core material (Figure 5.14) reaches yield at low loads when the loading area is small.

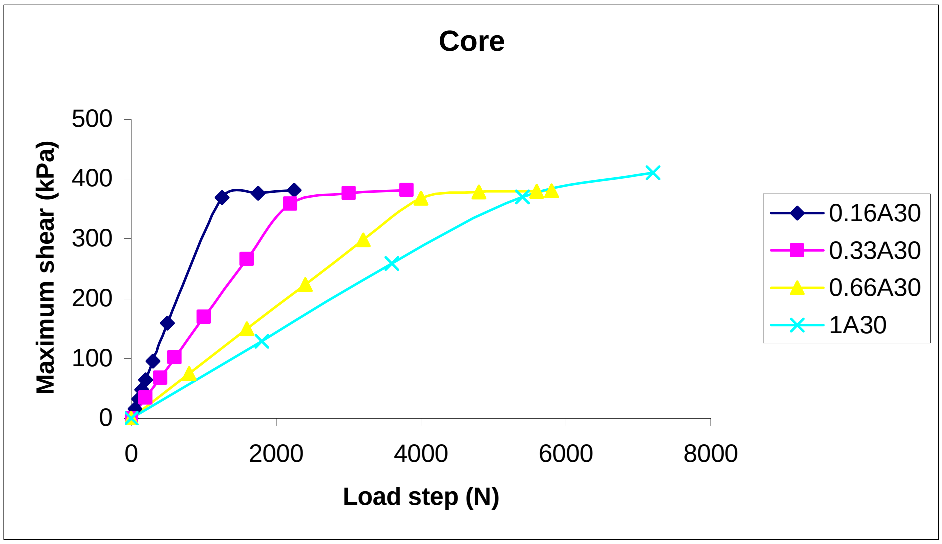

Figure 5.14. Maximum core shear versus load with variation of load size ratio at thickness 30mm and material A

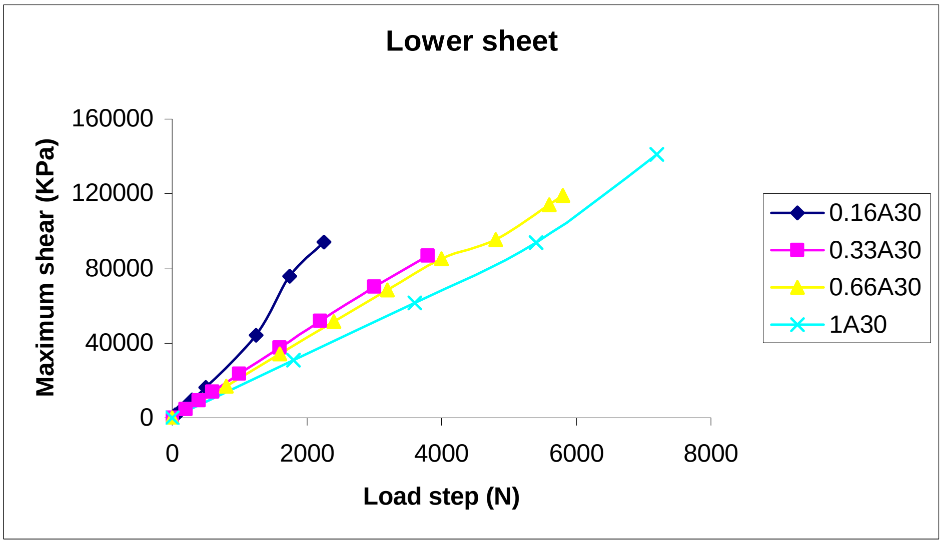

Figure 5.15. Maximum lower sheet shear versus load with variation of load size ratio at thickness 30mm and material A

5.2 Discussion

It is demonstrated in Figures 5.6 and 5.7 that as the thickness of core material increases the load carrying capacity of panel increases. This is justifiable because the increase in thickness increases the second moment of the cross-section area of the panel. Also the shear stress in the core decreases for same mount of loading because the shear load distributed over larger area as the thickness increases .When the core material reaches the yield point, the shear stress stays constant while the load is being increased

In yield range the core material keeps deforming while stress is constant (see Figure 5.16). This deformation works as a mechanism of transferring the excess load to the face sheets.

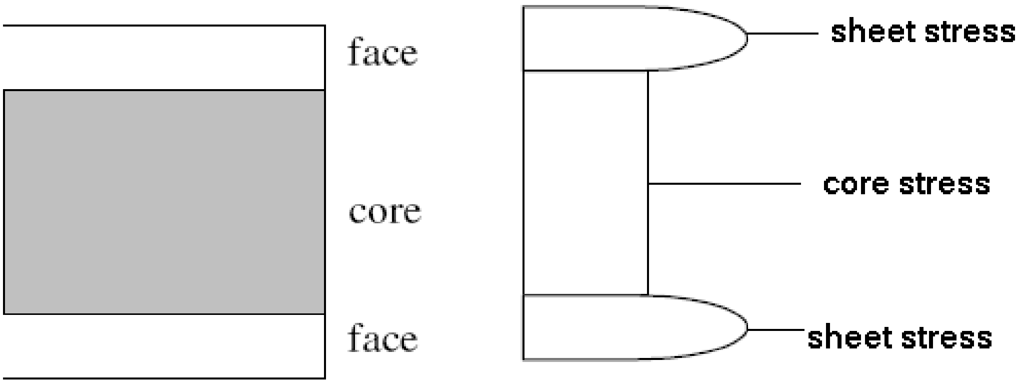

Figure 5.16. Schematic drawing of the shear stress for both face sheets and the core within plastic range

For example panel 0.16A50 in Figures 5.6 and 5.7 the core reaches yield point at 800kPa load and it is stress stays constant while the bottom sheet stress keeps increasing.

As illustrated in Figure 5.4, the metal material starts to yield (entering the plastic range) close to the support (where the boundary conditions are applied). This is physically true, the distributed load over the loading area becomes reaction force concentrated on the strip area on which the boundary conditions (simply supported boundary condition) are applied, and i.e. distributed load is converted to concentrated load. So the area where the boundary conditions are applied reaches the yield stress range before any other part of the panel. The correspondent tables for Figure 5.8 and 5.9 are in Tables in appendix B

These tables show that sheet materials of C and D have reached the yield point before the core material. This can be referred to the high stiffness at their core materials, i.e. the panel gets closer in its behavior to isotropic plate. This mean that the relative shear deformation between the top face sheet and the bottom face sheet is reduced. These results in increase on the sheet material stress.

Comparing Figures 5.10 and 5.11 with Figures 5.12 and 5.13 it is obvious that the curve of panels B, C and D in Figures 5.10 and 5.11 are coincident while they are spreading in Figures 5.12 and 5.13. The core material thickness in case of coincidences is 20mm**.** However in case of spreading the thickness is 50 mm. To explain this behavior let us look at the plate from one dimension (along one axis). The panel along one axis could be shrunk into a beam.

To replace the core material with same material of the top and bottom sheets its width should be shrunk according to the ratio of the modulus of elasticity of the core to that of the metal. The materials B, C and D are relatively stiff in comparison with A.

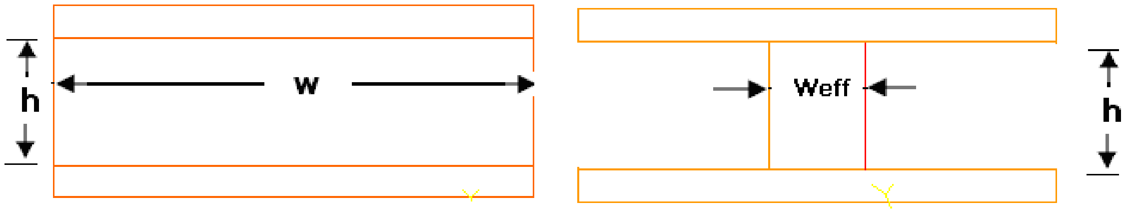

Figure 5.17. Equivalent cross-section of core material with have the same height

Equivalent cross-section of core material (see Figure 5.17 have the same high for all cases and the width is increasing according to the modulus of elasticity ratios. For a rectangle the second moment of area ($wh^3/12$) is varying linearly with the width (equivalent width) the effect of the difference between the materials B, C, and D is relatively small. So the stress curves for these panels are close to each other and the differences are small. However when the core thickness increases the amount of the second moment of area increases significantly and the differences increase also.

As the load area decreases the load is getting closer to the concentrated load, this is why in Figure 5.15 and 5.16. Panel 0.16A30 reaches the yield (plastic range) at lower load, than the other panels presented in the figures. Increasing the area of loading increases the load carrying capacity of the panel. The results of this work are generated according to the univariate search optimization technique (Chapra and Canal, 2006). Based on this numerical optimization technique. the tables in Appendix B are produced using 'I-DEAS' software. The tables contain all the information that design engineer needs to design his panel.

5.3 Example

To show the benefit of the baseline data that are presented in Appendix B, here is an example of how to use them.

Assume that a design engineer is intended to design a sandwich panel with the following constrains:

- The distributed load covers 2/3 size ratio of the panel.
- The sandwich panel total thickness should not exceed 25mm.
- The sandwich panel needs to carry a load of 100 kPa.

Since the panel should not exceed as total 25mm the search for optimum design in the appendix B is within tables of thicknesses 15mm and 20mm of load size ratio 2/3=0.66

From table B-1.9

At thickness 15mm and load 100 kPa (0.66A15)

$\frac{\tau_c}{\tau_{yc}} = 0.853$ $\frac{\tau_s}{\tau_{ys}} = 1$

At thickness 20mm and load 100 kPa (0.66A20)

$\frac{\tau_c}{\tau_{yc}} = 0.84$ $\frac{\tau_s}{\tau_{ys}} = 0.83$

From table B-1.10

At thickness 15mm and load 100 kPa (0.66B15)

$\frac{\tau_c}{\tau_{yc}} = 0.475$ $\frac{\tau_s}{\tau_{ys}} = 0.748$

At thickness 20mm and load 100 kPa (0.66B20)

$\frac{\tau_c}{\tau_{yc}} = 0.375625$ $\frac{\tau_s}{\tau_{ys}} = 0.583$

From table B-1.11 interpolate to get the values for 100kPa

At thickness 15mm and load 100 kPa (0.66C15)

$\frac{\tau_c}{\tau_{yc}} = 0.375$ $\frac{\tau_s}{\tau_{ys}} = 0.79$

At thickness 20mm and load 100 kPa (0.66C20)

$\frac{\tau_c}{\tau_{yc}} = 0.315$ $\frac{\tau_s}{\tau_{ys}} = 0.51$

From table B-1.12 interpolate to get the values for 100kPa

At thickness 15mm and load 100 kPa (0.66D15)

$\frac{\tau_c}{\tau_{yc}} = 0.225$ $\frac{\tau_s}{\tau_{ys}} = 0.81$

At thickness 20mm and load 100 kPa (0.66D20)

$\frac{\tau_c}{\tau_{yc}} = 0.19$ $\frac{\tau_s}{\tau_{ys}} = 0.5$

Note that for thickness 15mm the sheet metal in all cases is very close to yield point. So thickness 15mm is excluded. For thickness 20mm material A is not good because the sheet metal is very close to yield. You may see that the best choice is material B where the maximum shear to shear strength ratio is 0.375 for core and for sheet is 0.58 i.e. the core is carrying good amount of the load compared to other materials.

CHAPTER SIX

CONCLOSIONS AND RECOMINDATIONS

6.1 Conclusions

- Investigation of sandwich panel behavior beyond core material yield is carried out. The investigation is accomplished in sight of the core material nonlinearity and the geometric nonlinearity of the whole panel. Highly technology software 'I-DEAS' (Integrated Design Engineer Analysis software) is utilized to carryout the investigation.
- Finite element model is generated using 'I-DEAS' software. This model is validated against experimental and numerical cases available in the literature. To assure model accuracy experimental investigation for selected cases is carried out and compared with FEM. The model shows very good agreement with the previous work as well as the experimental one.
- Base line data has been produced to help design engineer in selecting the panel that fits his application best. The effects of main parameters that are necessary in designing sandwich panels are unveiled.
- It is proved that the load carrying capacity of sandwich panel can be improved by loading the panel beyond the yield limit of the core. This load is going to be transmitted to the face sheet.
- Increasing the stiffness of the core material to a certain extent leads to face sheet yielding before the core material. It is proved that increasing core thickness increases the load carrying capacity of the sandwich panel.

6.2 Recommendations:

- This work can be extended to investigate the effect of boundary conditions other than simple supports from all sides of the panel.
- In–plane type of loading could be investigated as well as moment application.
- Core other than foam can be investigated like honeycomb core, etc.
- Replacing face sheets by fiber reinforced composite material in sight of this investigation is of great benefit.
- Dimensional analysis could be carried out to find similarity variables for the sandwich panel behavior in the post yield region.

REFERENCES

"Airex R63 (2008), Typical Mechanical Properties", Baltek Corporation, **www.baltek.com,**.

Allen, H.G (1969), **Analysis and Design of Structural Sandwich Panels**, Pergamon Press, Oxford,.

Chapra and Canale(2005), **Numerical Methods for Engineers,** fifth edition pp.358, McGraw-Hill.

Caprino, G., Langelan, A (2000), "**Study of 3 pt. Bending Specimen for Shear Characterization of Sandwich Cores**", Journal of Composite Materials, Vol. 34, No. 9, , pp. 791-814.

Chintala, S. (2002)., "**Analytical and Experimental Study of Sandwich Panels**", Master of Science Thesis, Michigan Technological University.

"**C 393-94 Standard Test Method for Flexural Properties of Sandwich Constructions"**, (1995). Annual Book of ASTM Standards, Vol. 15, No. 3.

"**D 6419-99 Standard Test Method for Two-Dimensional Flexural Properties of Simply Supported Composite Sandwich Plates Subjected to a Distributed Load"**, (1999),Annual Book of ASTM Standards, Vol. 15, No. 3.

Eyre, M.W (1999)., “**Verification of the Hydromat Test System for Sandwich Panels”, Master of Science Thesis**, Michigan Technological University.

Frostig, Y., Baruch, M., Vilnai, O., Sheinman, I(1992)., “**Higher-Order Theory for Sandwich Beam Behavior with Transversely Flexible Core**”, Journal of Engineering Mechanics, Vol. 118 No. 5,

Frostig, Y., Baruch, M (1990), “**Higher Order Buckling Analysis of Sandwich Beams with Transversely Flexible Cores”**, AIAA Journal, Vol. 28 No. 3.

Frostig, Y. (1992), “**Behavior of Delaminated Sandwich Beams with Transversely Flexible Core High-Order Theory**”, Composite Structures, 20, pp. 1-16.

Frostig, Y(1999), “**High-Order Behavior of Sandwich Beams with Flexible Core and Transverse Diaphragms**”, Journal of Engineering Mechanics, Vol. 119, No. 5, , pp. 955-972.

Frostig, Y. (1993), “**On Stress Concentration in the Bending of Sandwich Beams with Transversely Flexible Core**”, Composite Structures, 24, pp. 161-169.

Gdoutos, E.E., Daniel, I.M., Wang, K.-A., Abot, J.L (2001), “**Non-linear Behavior of Composite Sandwich Beams in Three-point Bending**”, Experimental Mechanics, Vol. 41, No. 2, , pp. 182–189.

Kuang-An,W (2001), "**Failure Analysis of Sandwich Beams'', Doctor of Philosophy Dissertation,** Northwestern University, Lovile E, Berthrlot J-M (2002), Non-linear behavior of foam cores and sandwich materials, Part 2: **indentation and three-point bending. J Sandwich Struct Mater**; 4(October):297–352.

Meyer-Piening and D. Zenkert (Eds.) (2000), EMAS, , pp. 141-153.

Mercado, L.L., Sikarskie, D.L(1999), "**On Response of a Sandwich Panel with a Bilinear Core**", Mechanics of Composite Materials and Structures –6, , pp.57–67.

"Metals Handbook" (1991), **American Society for Metals, H.E. Boyer and T.L. Gall** (Eds.),.

Miers, S.A. (2001), "**Analysis and Design of Edge Inserts in Sandwich Beams**", Master of Science Thesis, Michigan Technological University,.

Olsson R. (2002) **Engineering method for prediction of impact response and damage in sandwich panels**. J Sandwich Struct Mater; 4(1):3–29.

Ooi, P.H, (2003) " **Analysis of Post Yield Shear Distribution within Sandwich Beam and Panel''** Master of Science Thesis, Michigan Technological University,.

Plantema, F.J(1966), **Sandwich Construction, John Wiley and Sons**, New York,.

Photoelastic Investigation versus High Order Sandwich Theory Results", (1997) Composite Structures, , 37, No. 1, pp. 97-108.

Pasternak PL (1954) [in Russian]. **Fundamentals of a new method of analyzing structures on an elastic foundation by means of two foundation modul**i. Moscow–Leningrad: Stroigiz;

Rao, T.(2002), "**Study of Core Compression Using Digital Image Correlation (DIC)**", Master of Science Thesis, Michigan Technological University,.

Rau, C.S(1994)., "**Evaluation of the Hydromat Distributed Loading Panel Testing Method**", Master of Science Thesis, Michigan Technological University,.

Shipsha A, Hallstrom S, Zenkert D (2003). **Failure mechanisms and modeling of impact damage in sandwich beams—A 2D approach**: Part I—Experimental investigation. J Sandwich Struct Mater; 5(1):7–32.

Slepian LI. Nonstationary elastic waves1972 [in Russian]. Leningrad: Sudostroenie;

Thomsen OT(1993). **Analysis of local bending effects in sandwich plates with orthotropic face layers subjected to localized loads**. J Compos. Struct

Thomsen, O.T(1992)., Frostig, Y., "**Localized Bending Effects in Sandwich Panels**.

Thomsen, O.T)1995), "**Theoretical and Experimental Investigation of Local Bending Effects in Sandwich Plates**", Composite Structures, Vol. 30 No. 1,.

Triantafillou, T.C., Gibson. L.J (1987),., "**Minimum Weight of Foam Core Sandwich panels for a Given Strength**", Material Science and Engineering, 95 pp. 55–62.

Zenkert, D.(1995),**An Introduction to Sandwich Construction**, (EMAS), The Chameleon Press Ltd., London,

Zenkert, D1997., **The Handbook of Sandwich Construction, Engineering Materials Advisory Services**, United Kingdom,

APPENDIX A

Graphical Results of Maximum Shear Stress to shear strength ratio Versus Load Step For Sandwich Panel Under Different Parameters (Thickness, Load Size, Material Type)

This Appendix presents the graphical results of finite element model for sandwich panel, showing maximum shear versus loading step for variation of thickness (15mm to 50mm), material (A,B,C,and D), and load size ratio (0.16 to 1).

A-1 Graphical results for maximum shear stress versus load step for core and lower sheet of sandwich panel under variation of thickness

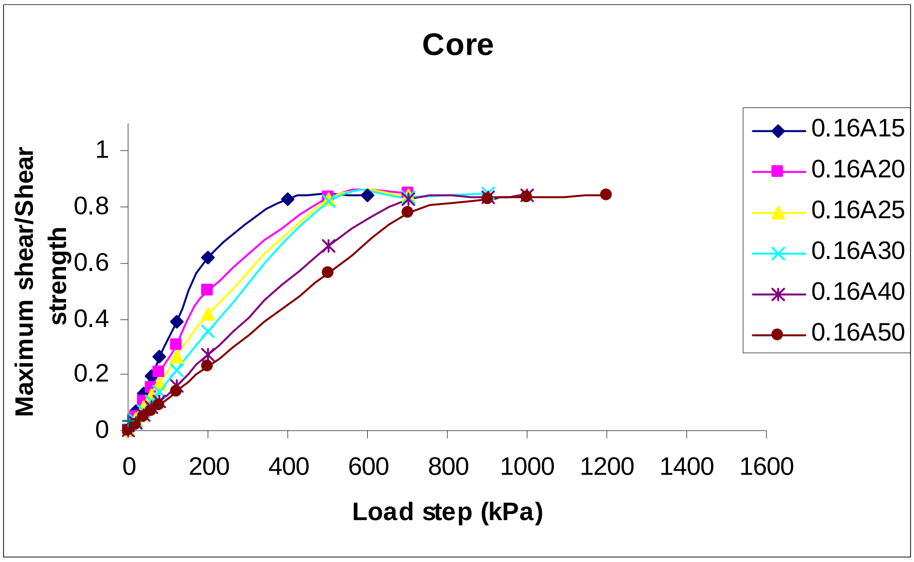

Figure A-1.1 Load step versus maximum shear core to shear strength with variation thickness for material A at load size ratio 0.16

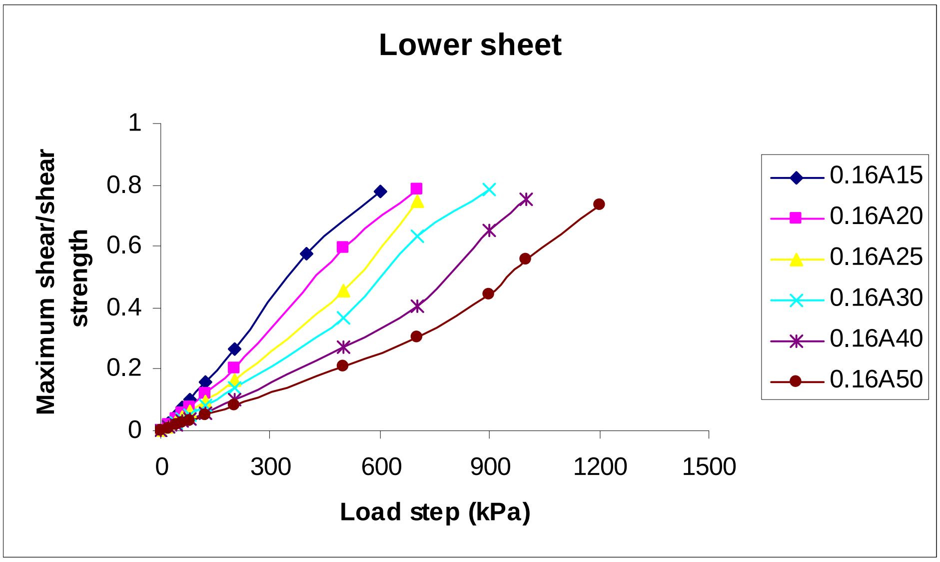

Figure A-1.2 Load step versus maximum lower sheet shear to shear strength with variation thickness for material A at load size 50mm

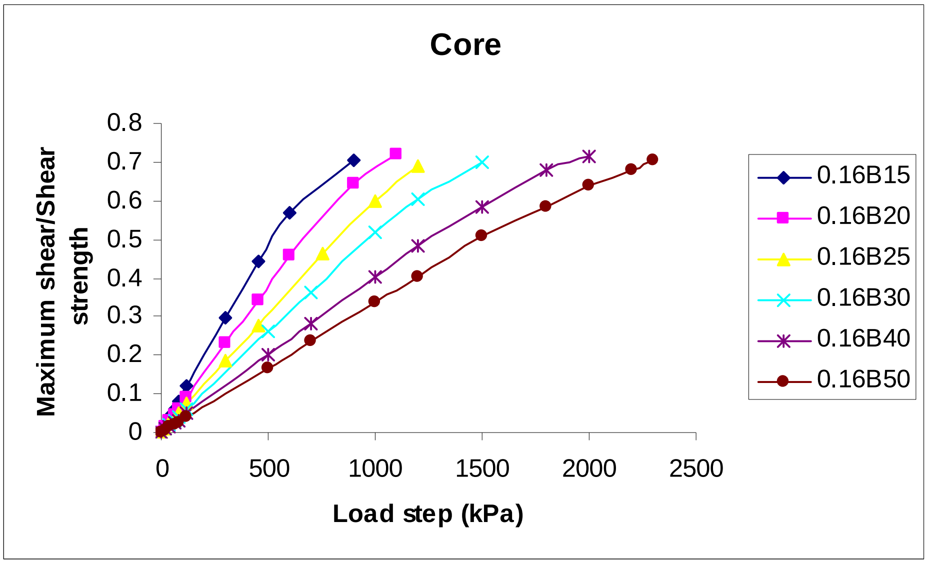

Figure A-1.3 Load step versus maximum core shear to shear strength with variation thickness for material B at load size ratio 0.16

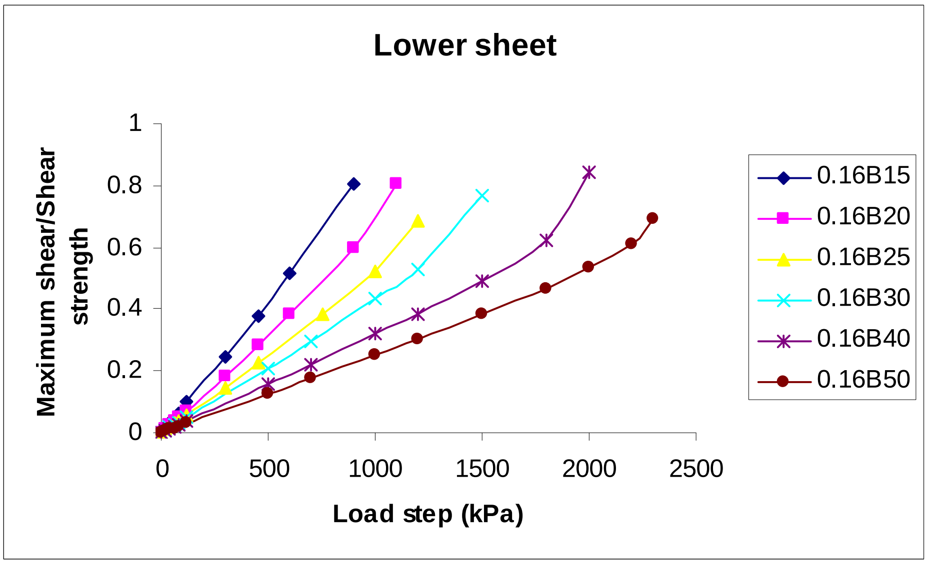

Figure A-1.4 Load step versus maximum lower sheet shear to shear strength with variation thickness for material B at load size ratio 0.16

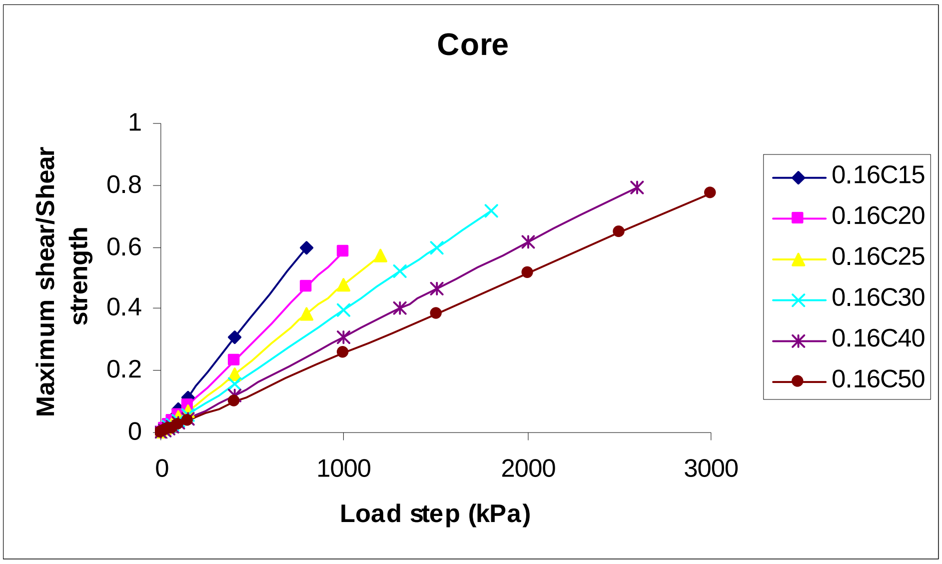

Figure A-1.5 Load step versus maximum core shear to shear strength with variation thickness for material C at load size ratio 0.16

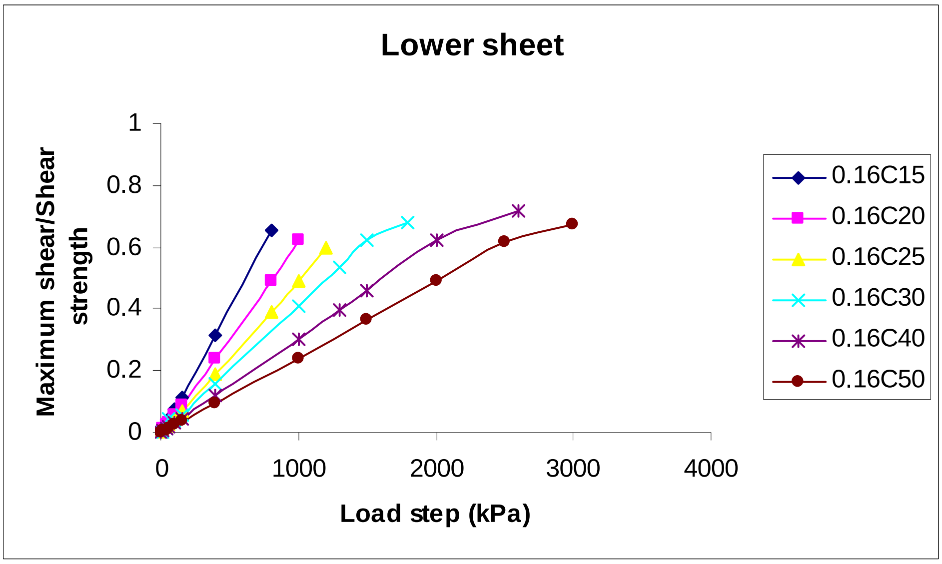

Figure A-1.6 Load step versus maximum lower sheet shear to shear strength with variation thickness for material C at load size ratio 0.16

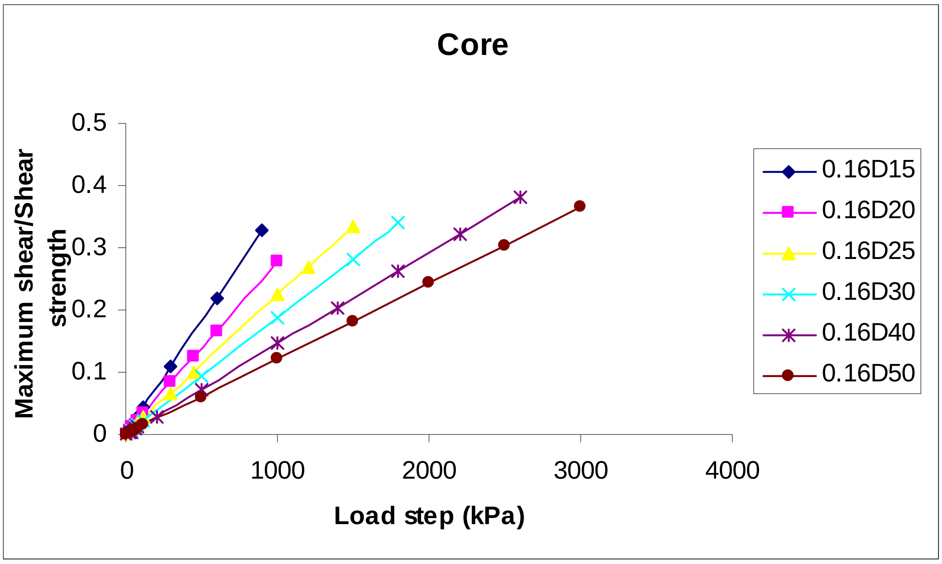

Figure A-1.7 Load step versus maximum core shear to shear strength with variation thickness for material D at size ratio 0.16

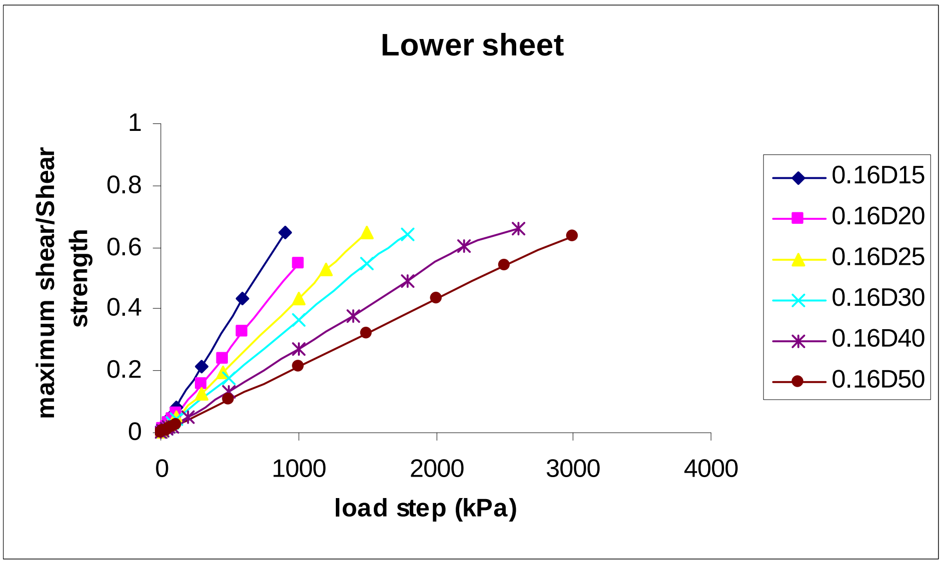

Figure A-1.8 Load step versus maximum lower sheet shear to shear strength with variation thickness for material D at load size ratio 0.16

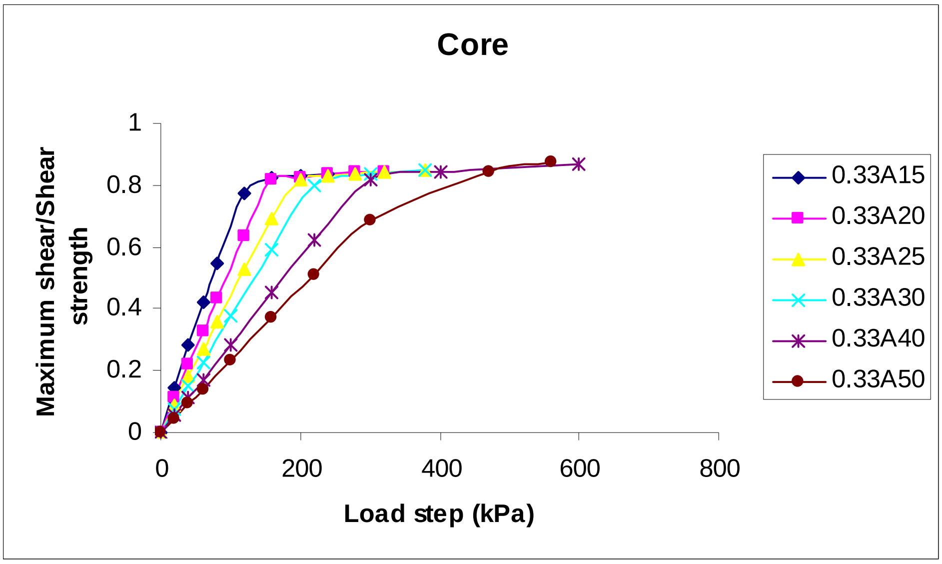

Figure A-1.9 Load step versus maximum core shear to shear strength with variation thickness for material A at load size ratio 0.33

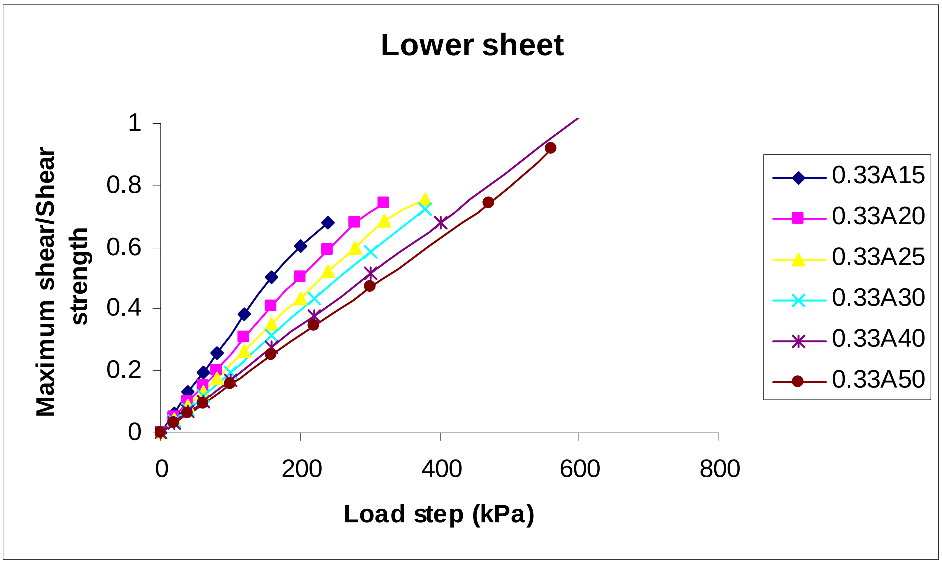

Figure A-1.10 Load step versus maximum lower sheet shear to shear strength with variation thickness for material A at load size ratio 0.33

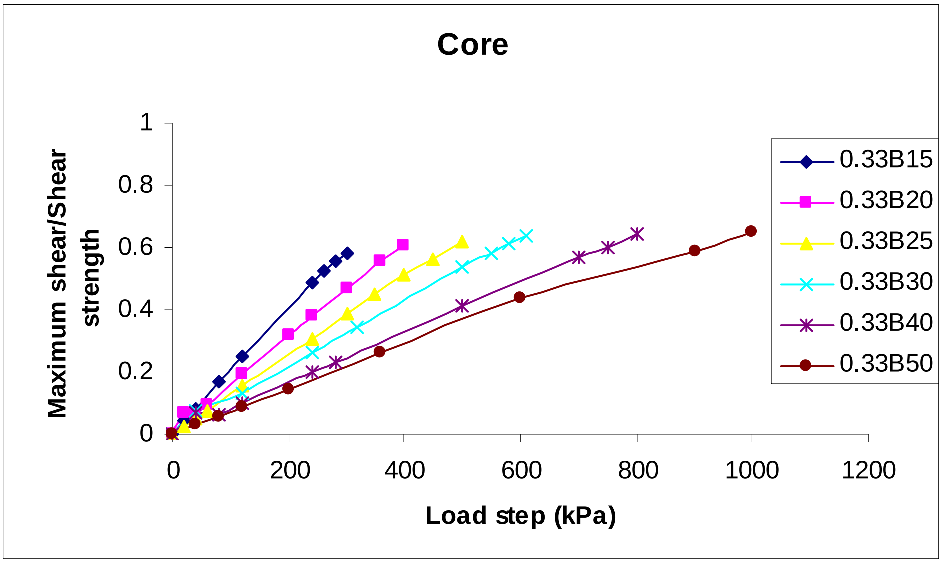

Figure A-1.11 Load step versus maximum core shear to shear strength with variation thickness for material B at load size ratio 0.33

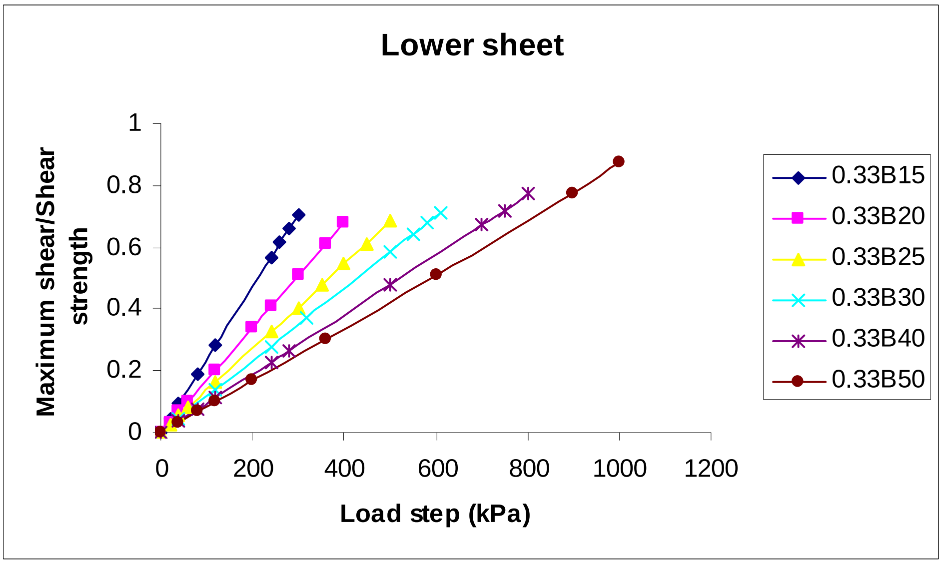

Figure A-1.12 Load step versus maximum lower sheet shear to shear strength with variation thickness for material B at load size ratio 0.33

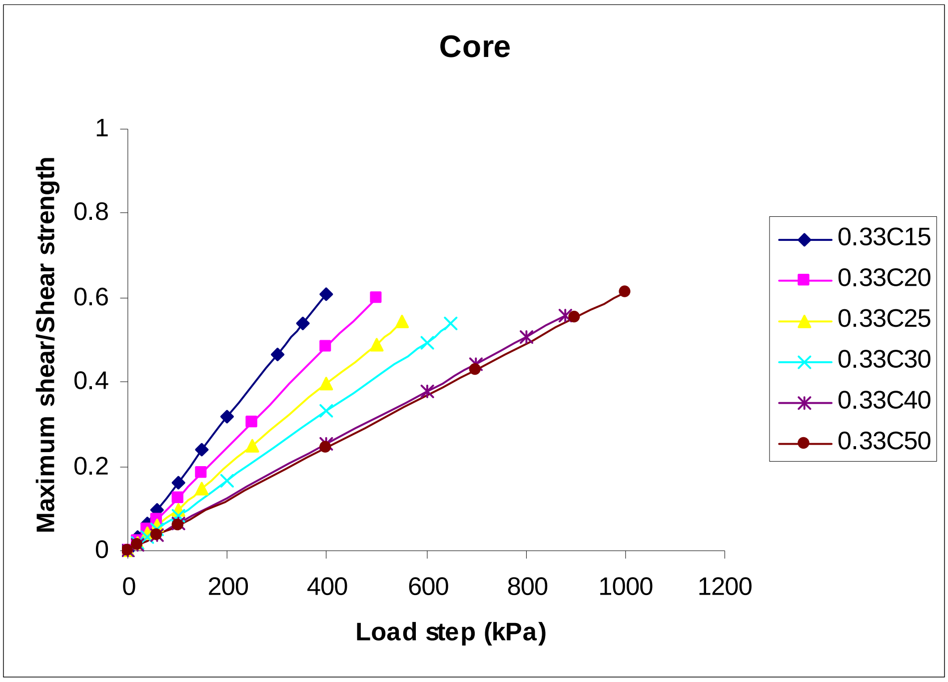

Figure A-1.13 Load step versus maximum core shear to shear strength with variation thickness for material C at load size ratio 0.33

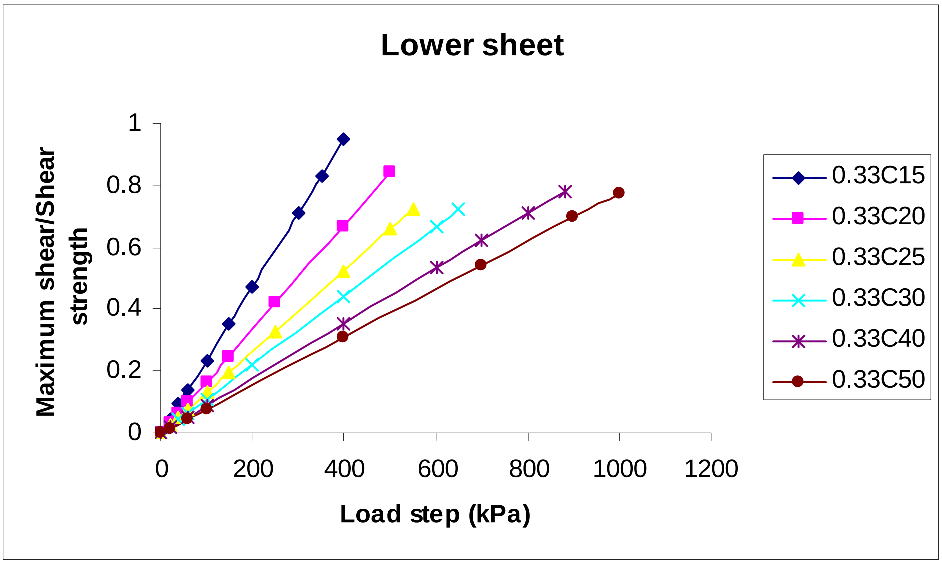

Figure A-1.14 Load step versus maximum lower sheet shear to shear strength with variation thickness for material C at load size ratio 0.33

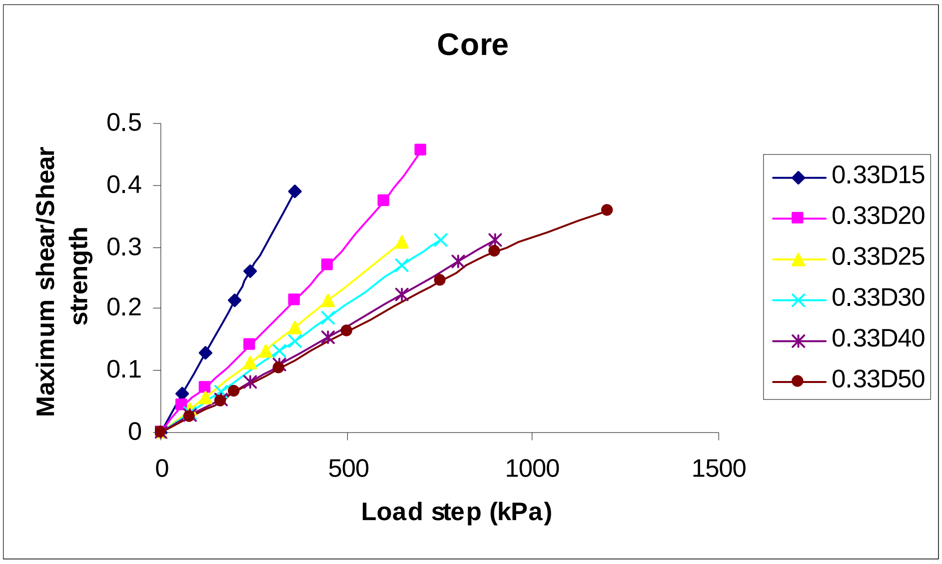

Figure A-1.15 Load step versus maximum core shear to shear strength with variation thickness for material D at load size ratio 0.33

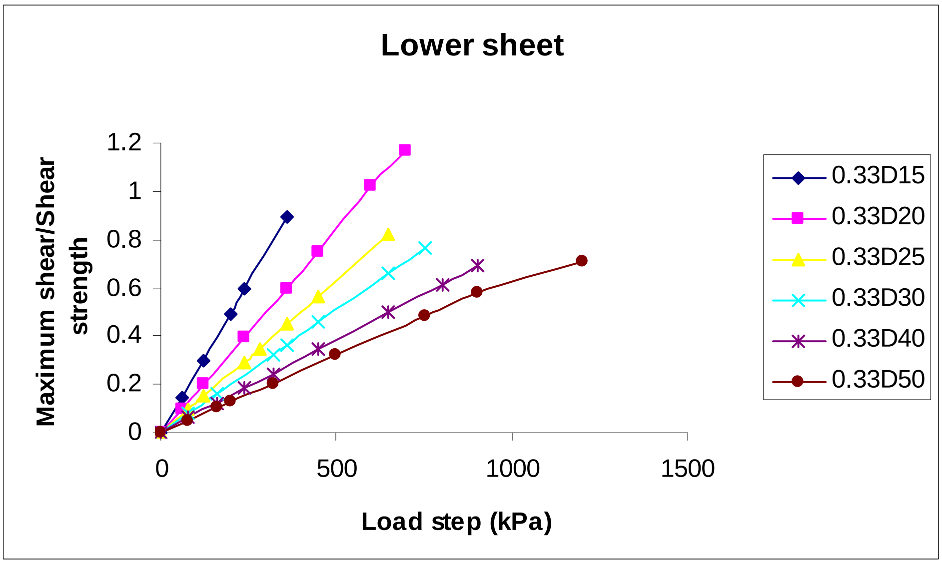

Figure A-1.16 Load step versus maximum lower sheet shear to shear strength with variation thickness for material D at load size ratio 0.33

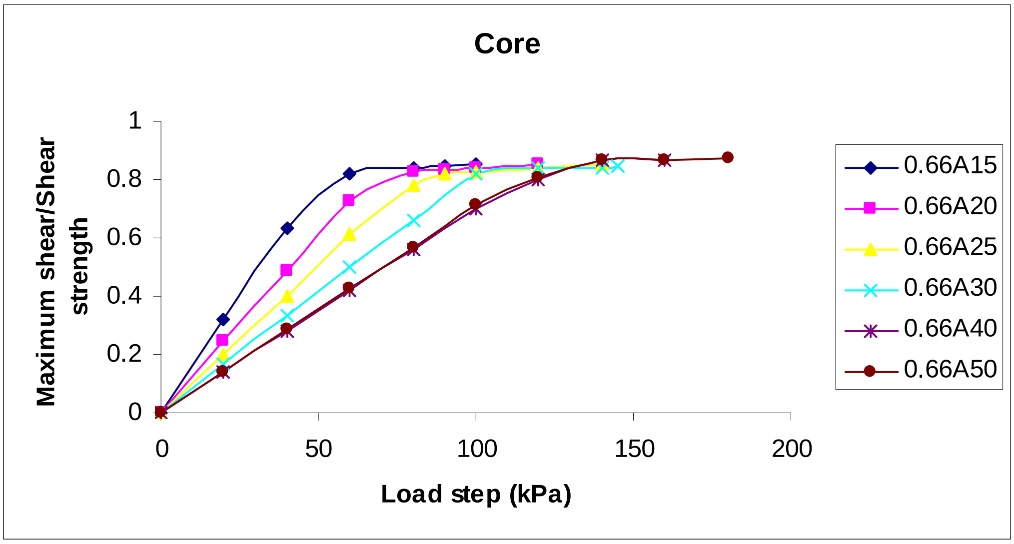

Figure A-1.17 Load step versus maximum core shear to shear strength with variation thickness for material A at load size ratio 0.66

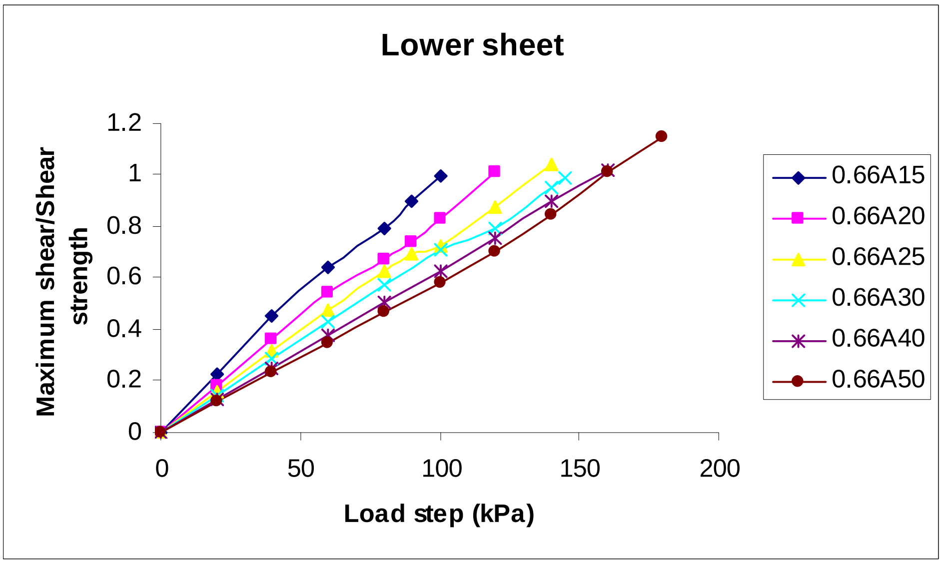

Figure A-1.18 Load step versus maximum lower sheet shear to shear strength with variation thickness for material A at load size ratio 0.66

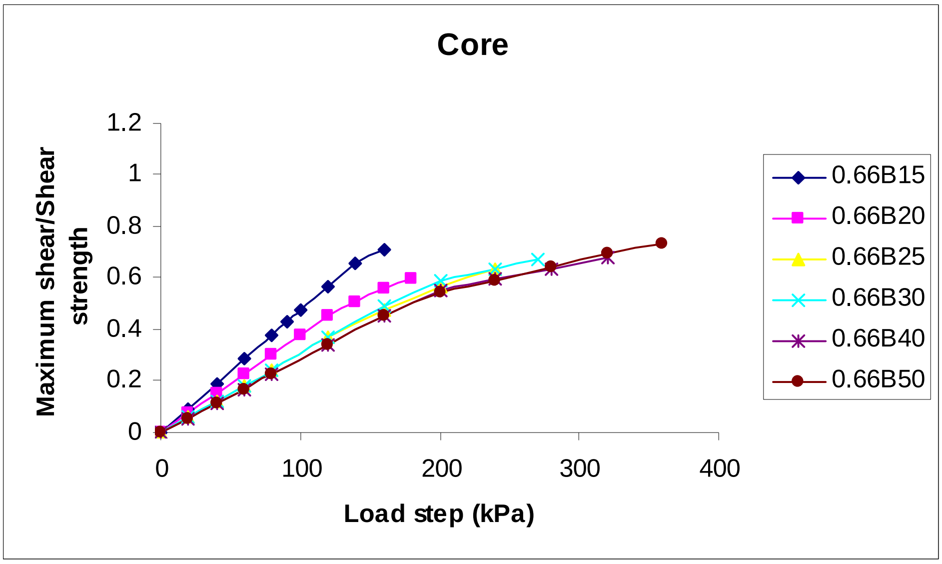

Figure A-1.19 Load step versus maximum core shear to shear strength with variation thickness for material B at load size ratio 0.66

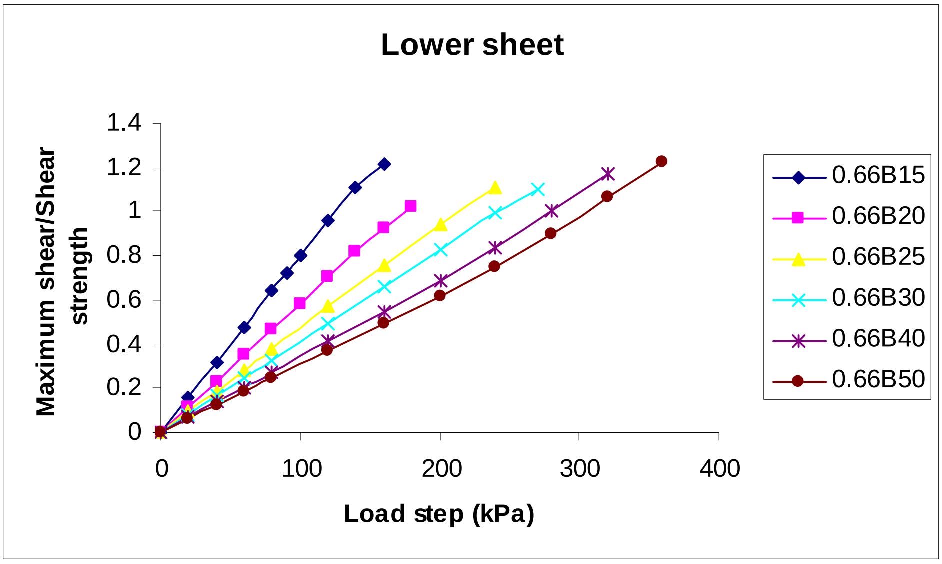

Figure A-1.20 Load step versus maximum lower sheet shear to shear strength with variation thickness for material B at load size ratio 0.66

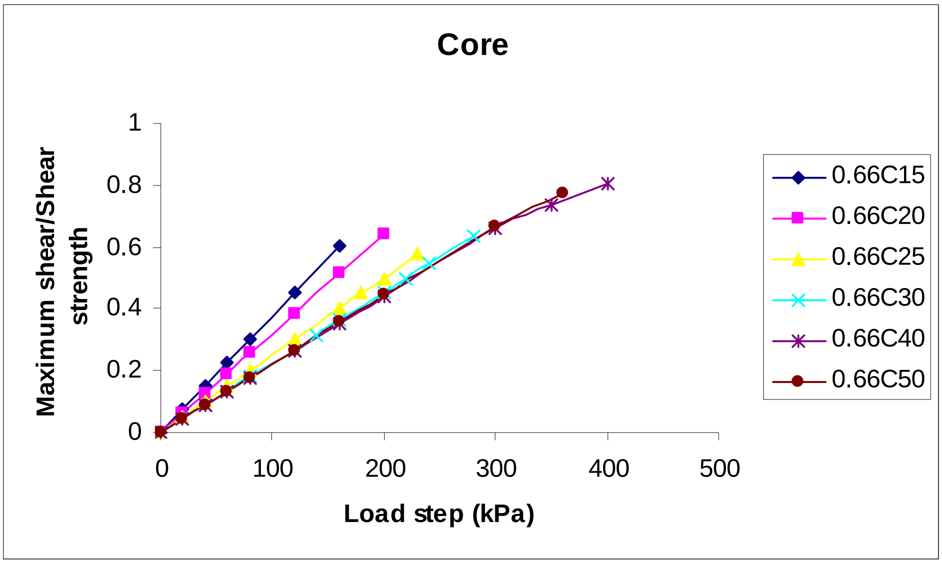

Figure A-1.21 Load step versus maximum core shear to shear strength with variation thickness for material C at load size ratio 0.66

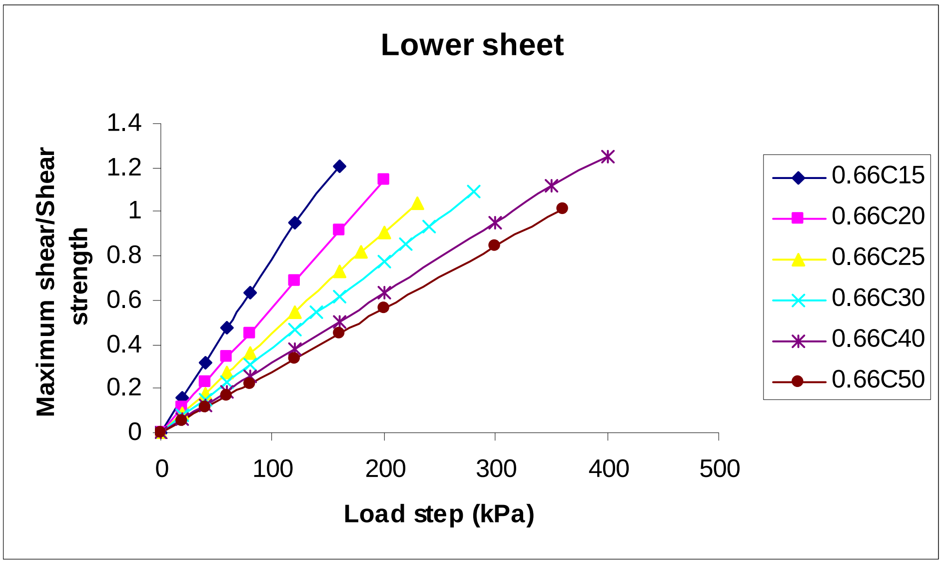

Figure A-1.22 Load step versus maximum lower sheet shear to shear strength with variation thickness for material C at load size ratio 0.66

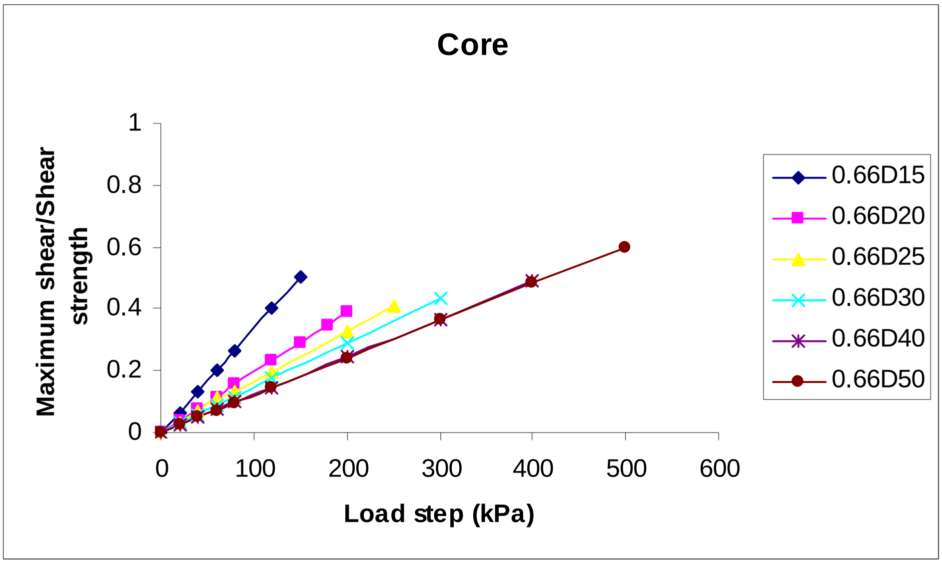

Figure A-1.23 Load step versus maximum core shear to shear strength with variation thickness for material D at load size ratio 0.66

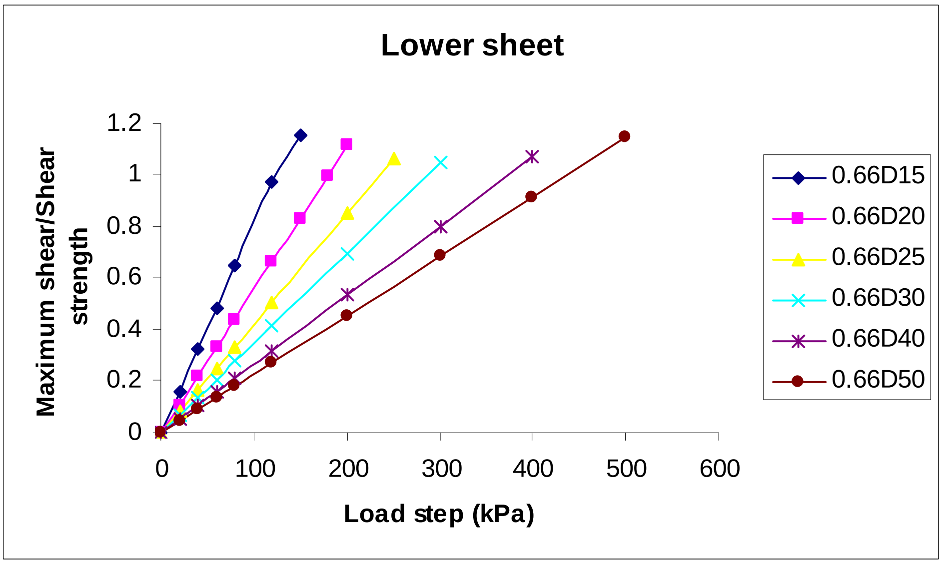

Figure A-1.24 Load step versus maximum lower sheet shear to shear strength with variation thickness for material D at load size ratio 0.66

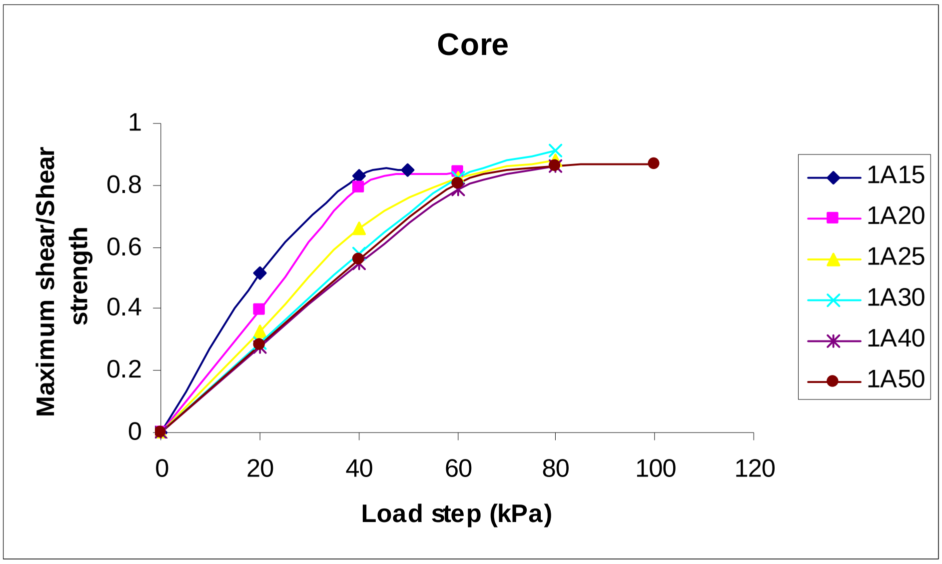

Figure A-1.25 Load step versus maximum core shear to shear strength with variation thickness for material A at load size ratio 1

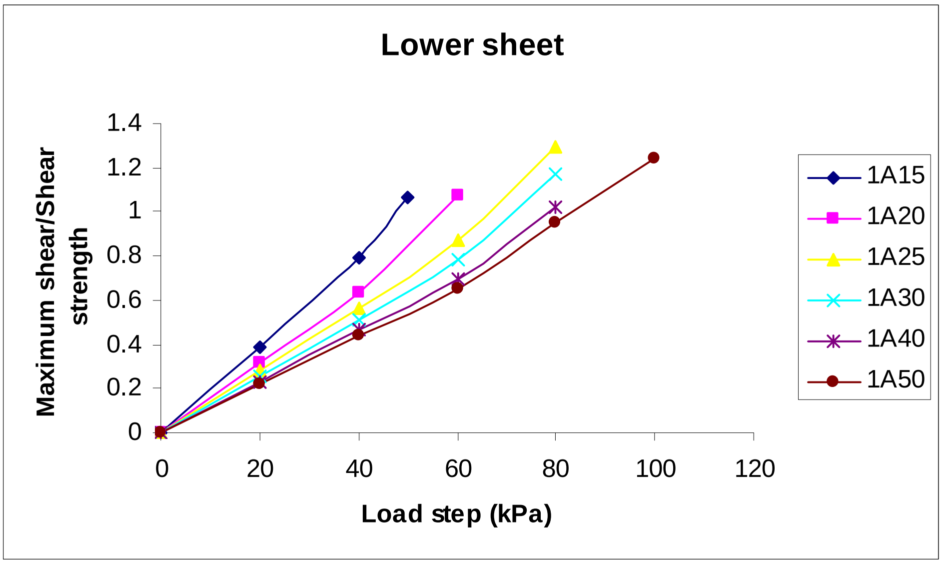

Figure A-1.26 Load step versus maximum lower sheet shear to shear strength with variation thickness for material A at load size 300mm

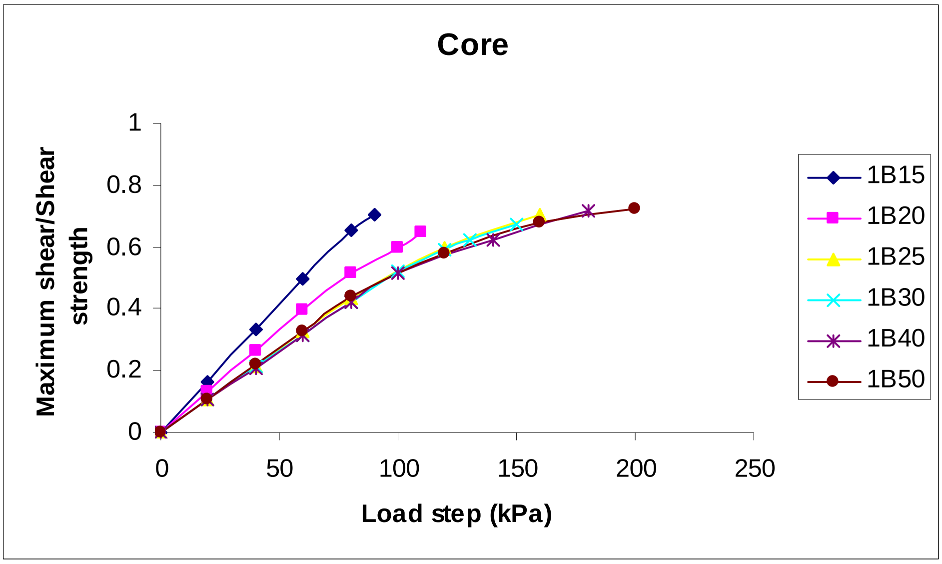

Figure A-1.27 Load step versus maximum core shear to shear strength with variation thickness for material B at load size 300mm

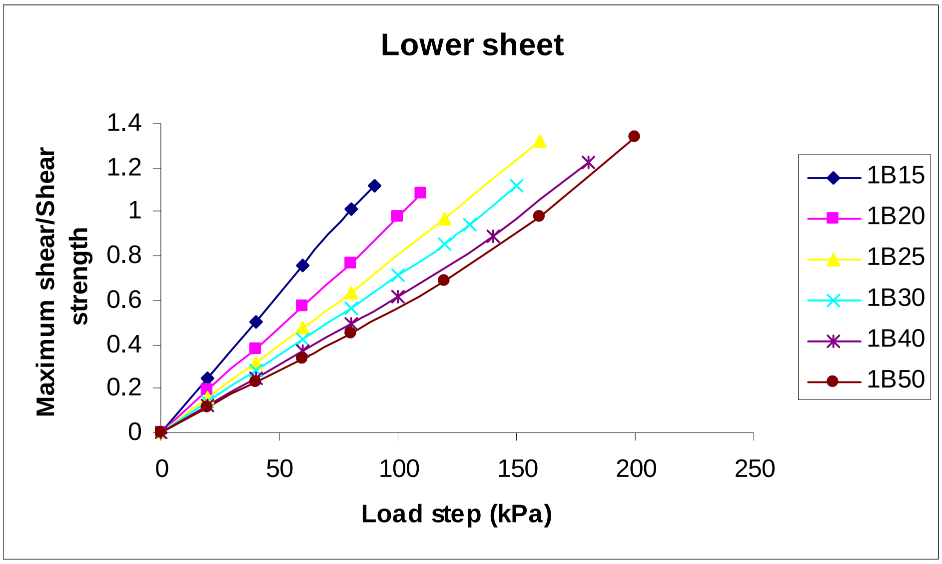

Figure A-1.28 Load step versus maximum lower sheet shear to shear strength with variation thickness for material B at load size ratio 1

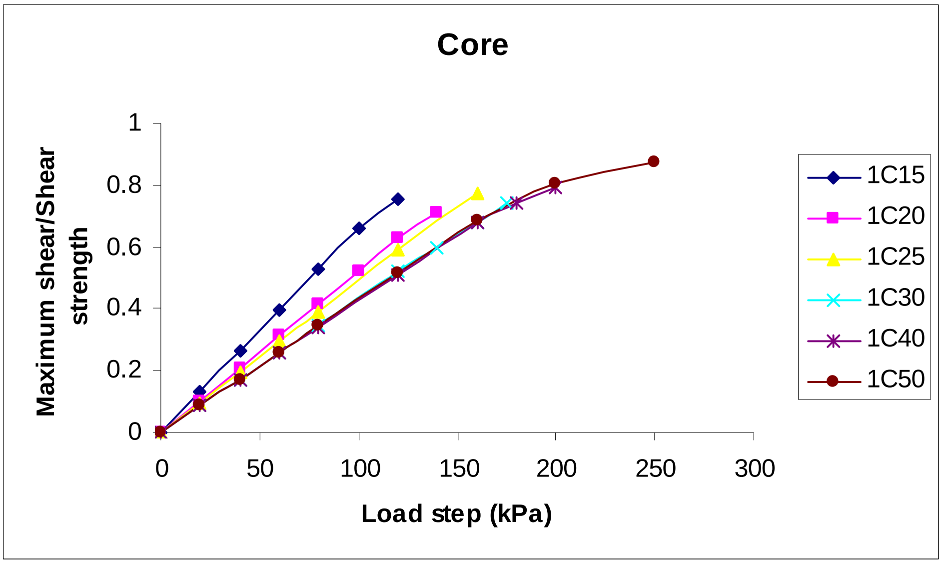

Figure A-1.29 Load step versus maximum core shear to shear strength with variation thickness for material C at load size ratio 1

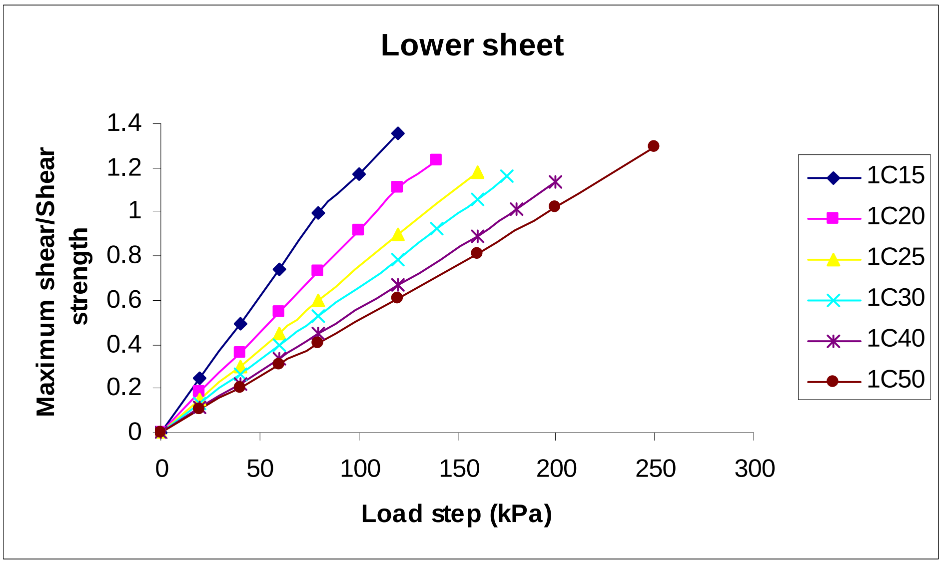

Figure A-1.30 Load step versus maximum lower sheet shear to shear strength with variation thickness for material C at load size 300mm

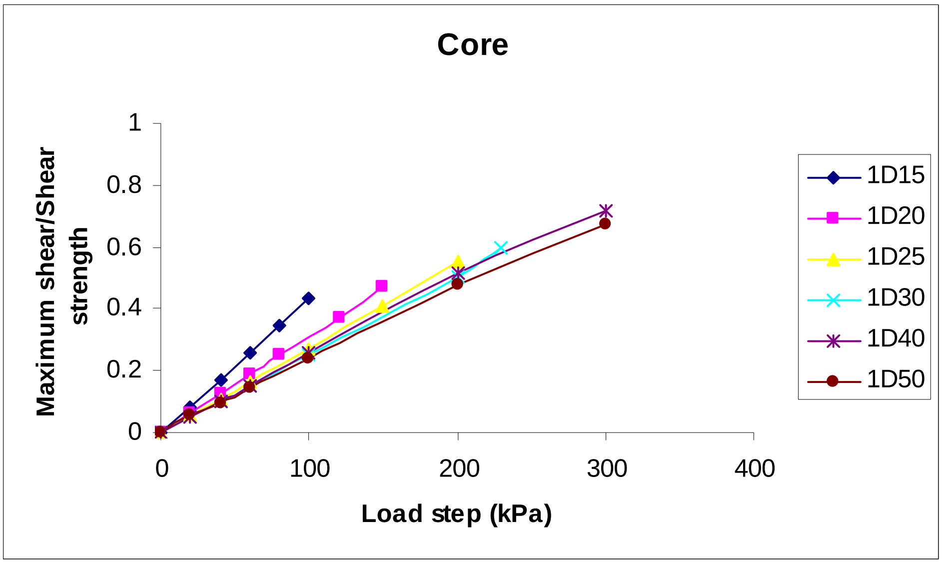

Figure A-1.31 Load step versus maximum core shear to shear strength with variation thickness for material D at load size ratio 1

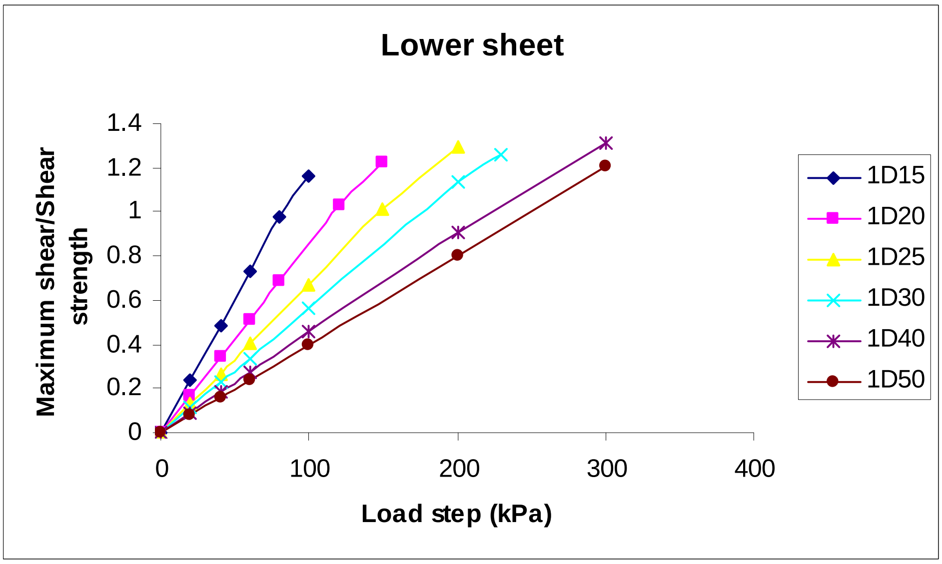

Figure A-1.32 Load step versus maximum lower sheet shear to shear strength with variation thickness for material D at load size ratio 1

A-2 Graphical results for maximum shear stress to shear strength ratio versus load step for core and lower sheet of sandwich panel under variation of material

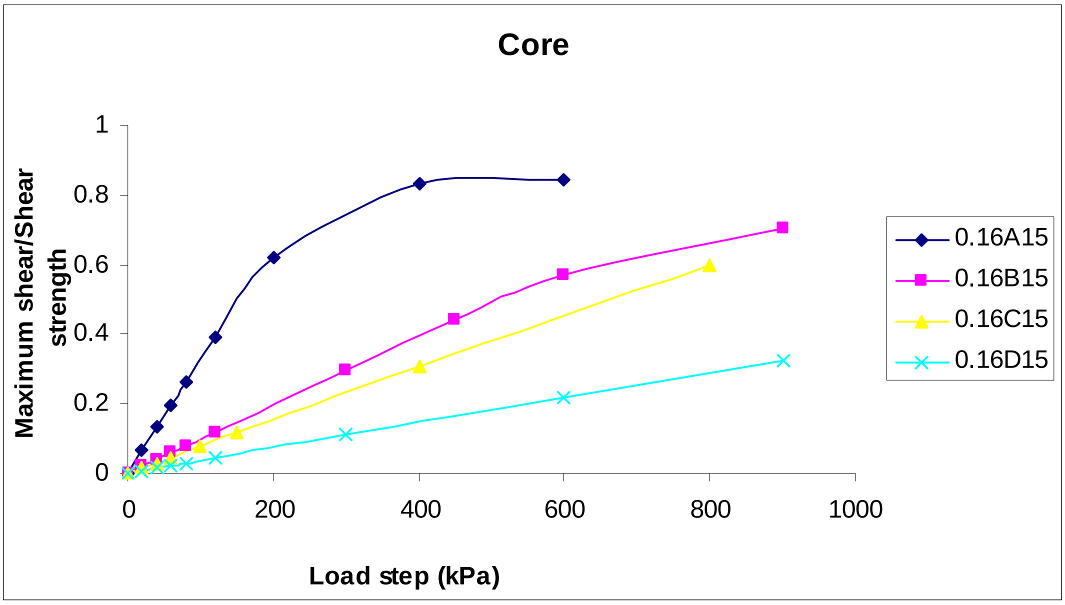

Figure A-2.1 Maximum core shear to shear strength versus load with variation material at thickness 15mm and load size ratio 0.16

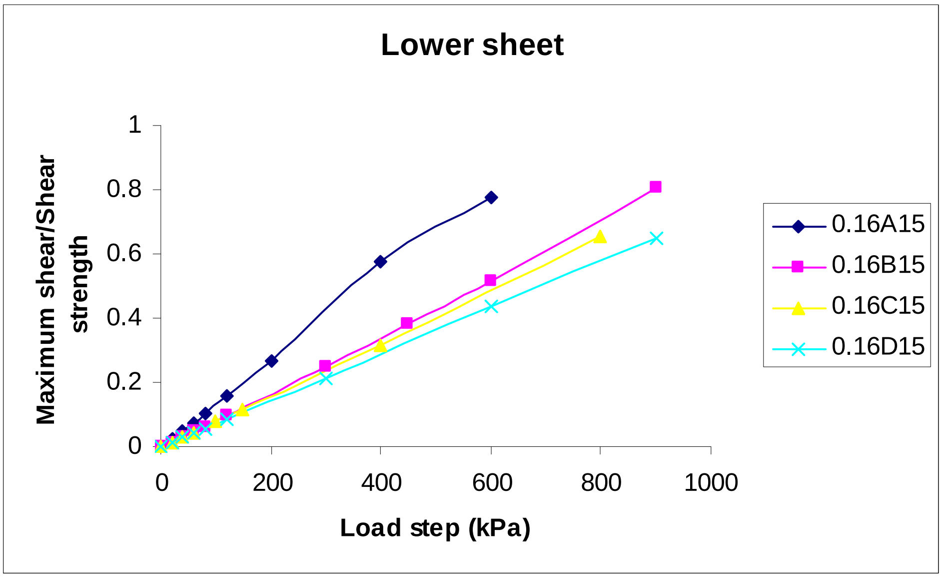

Figure A-2.2 Maximum lower sheet shear to shear strength versus load with variation material at thickness 15mm and load size ratio 0.16

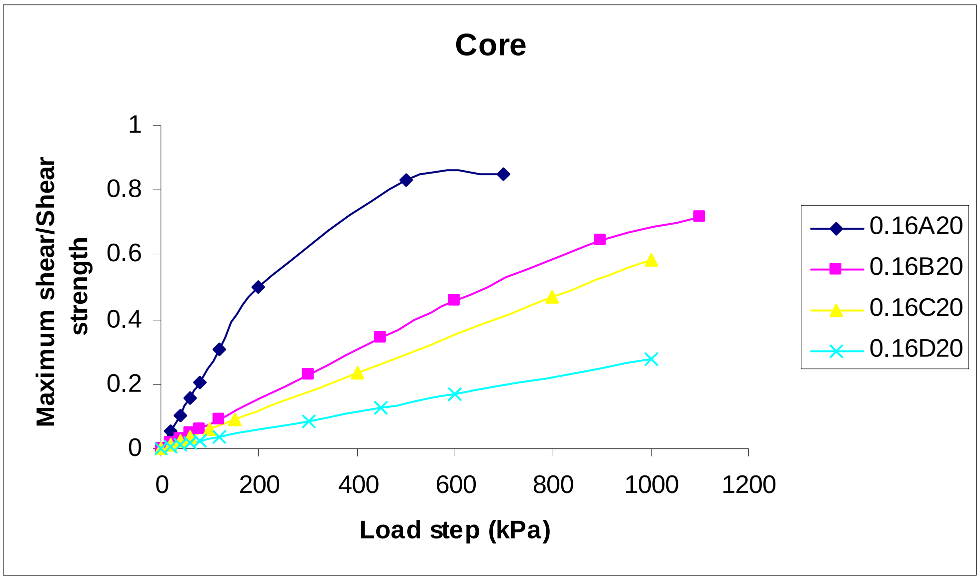

Figure A-2.3 Maximum core shear to shear strength versus load with variation material at thickness 20mm and load size ratio 0.16

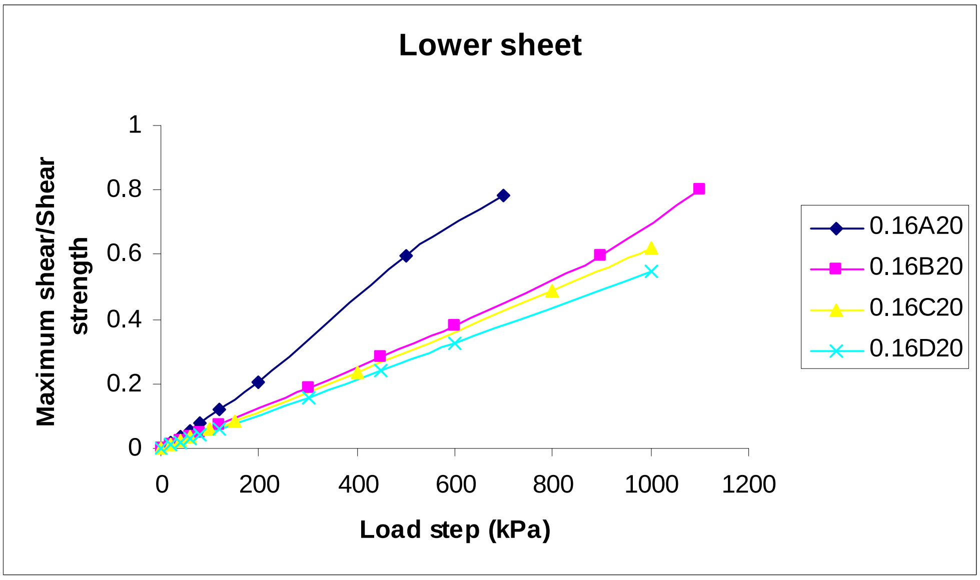

Figure A-2.4 Maximum lower sheet shear to shear strength versus load with variation material at thickness 20mm and load size ratio 0.16

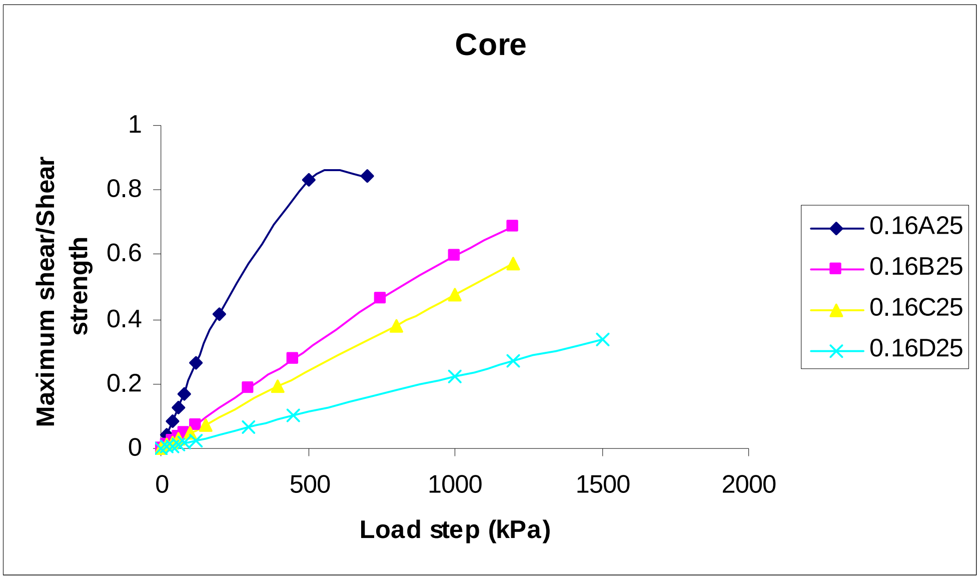

Figure A-2.5 Maximum core shear to shear strength versus load with variation material at thickness 25mm and size ratio 0.16

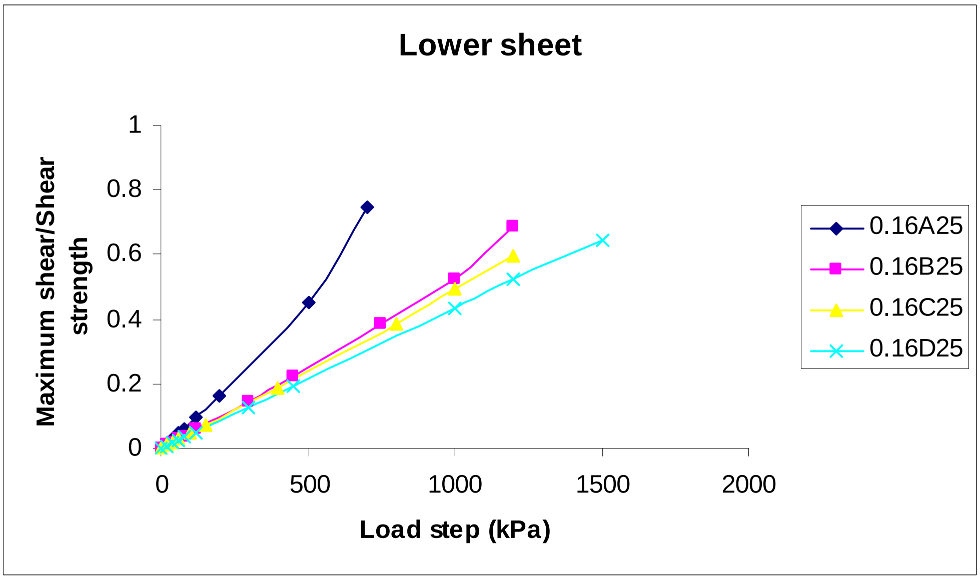

Figure A-2.6 Maximum lower sheet shear to shear strength versus load with variation material at thickness 25mm and load size ratio 0.16

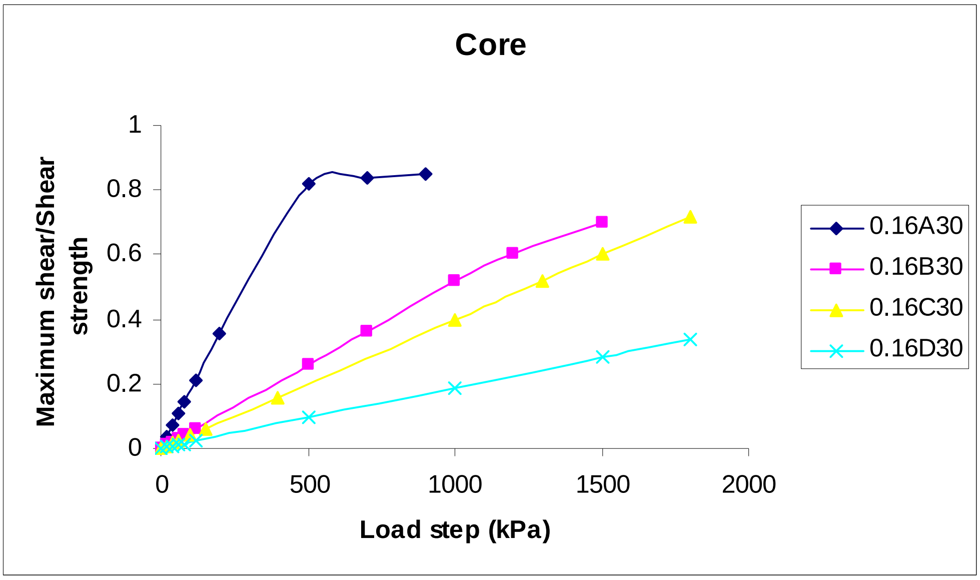

Figure A-2.7 Maximum core shear to shear strength versus load with variation material at thickness 30mm and load size ratio 0.16

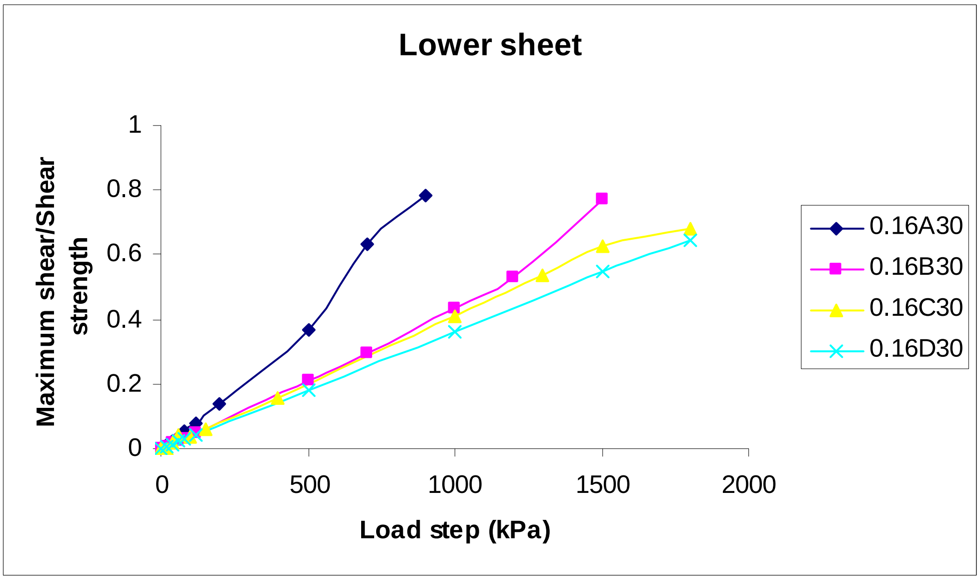

Figure A-2.8 Maximum lower sheet shear to shear strength versus load with variation material at thickness 30mm and load size ratio 0.16

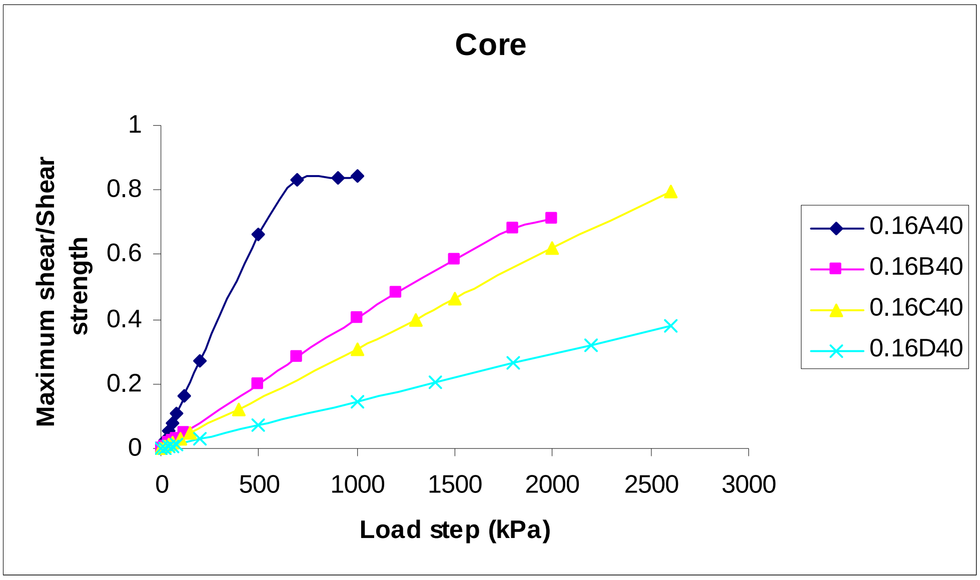

Figure A-2.9 Maximum core shear to shear strength versus load with variation material at thickness 40mm and load size ratio 0.16

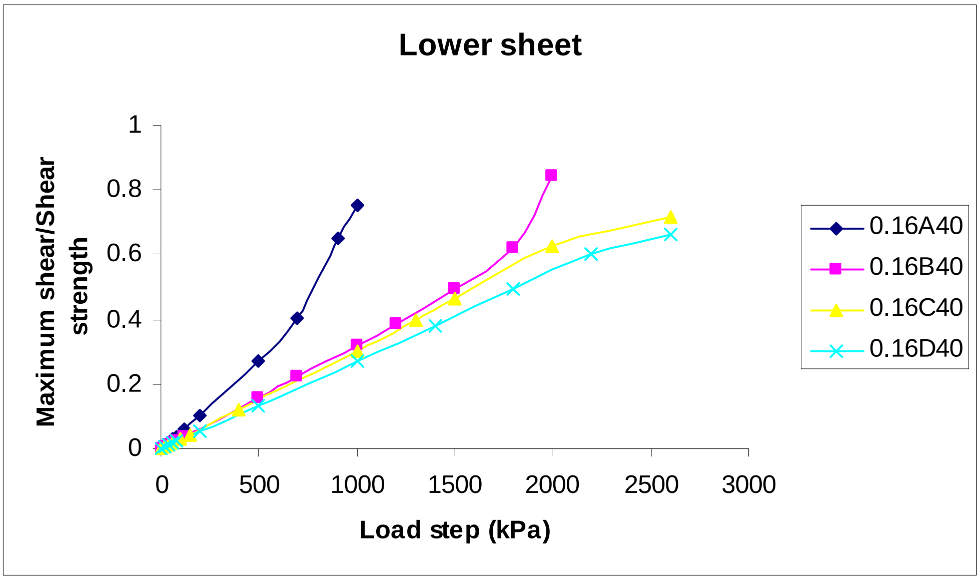

Figure A-2.10 Maximum lower sheet shear to shear strength versus load with variation material at thickness 40mm and load size ratio 0.16

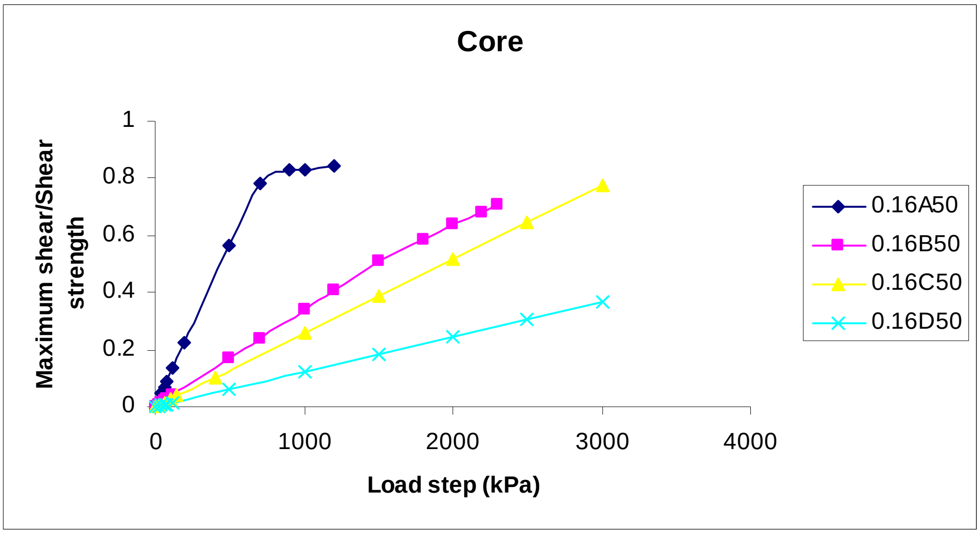

Figure A-2.11 Maximum core shear to shear strength versus load with variation material at thickness 50mm and load size ratio 0.16

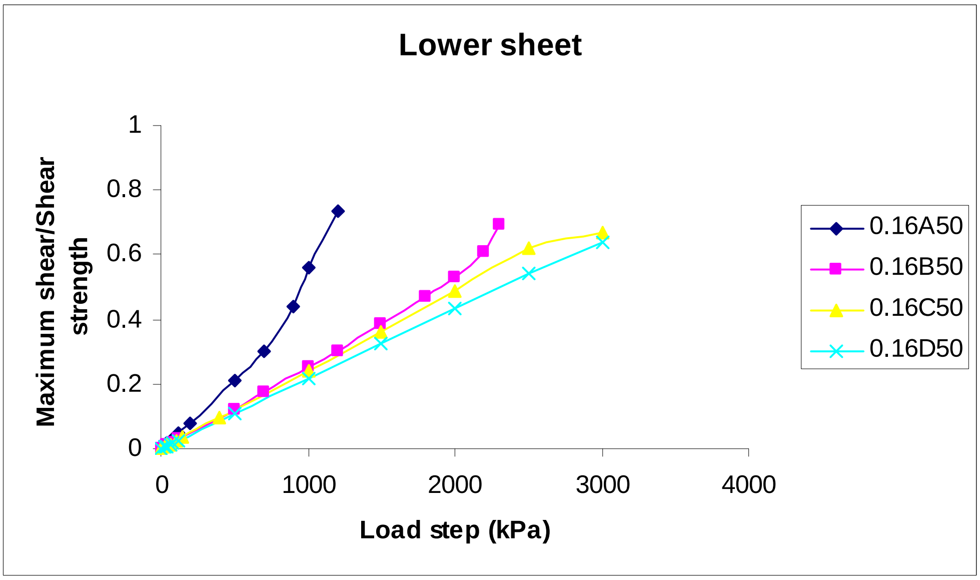

Figure A-2.12 Maximum lower sheet shear to shear strength versus load with variation material at thickness 50mm and load size ratio 0.16

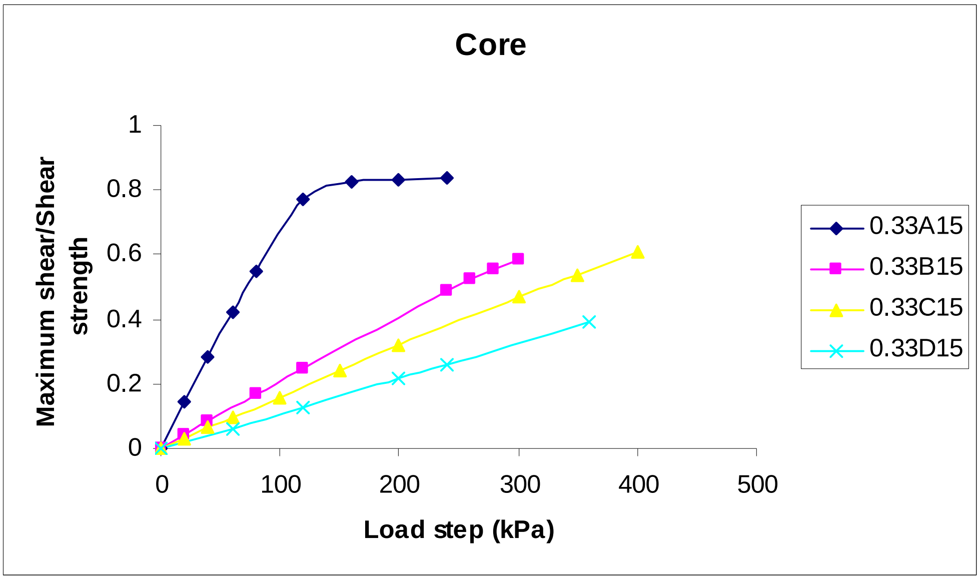

Figure A-2.13 Maximum core shear to shear strength versus load with variation material at thickness 15mm and load size ratio 0.33

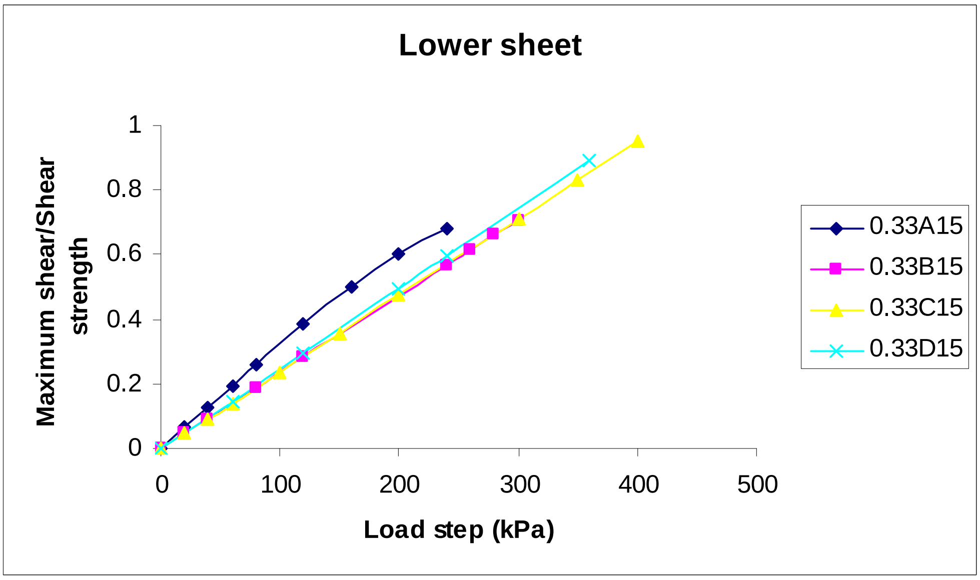

Figure A-2.14 Maximum lower sheet shear to shear strength versus load with variation material at thickness 15mm and load size100mm

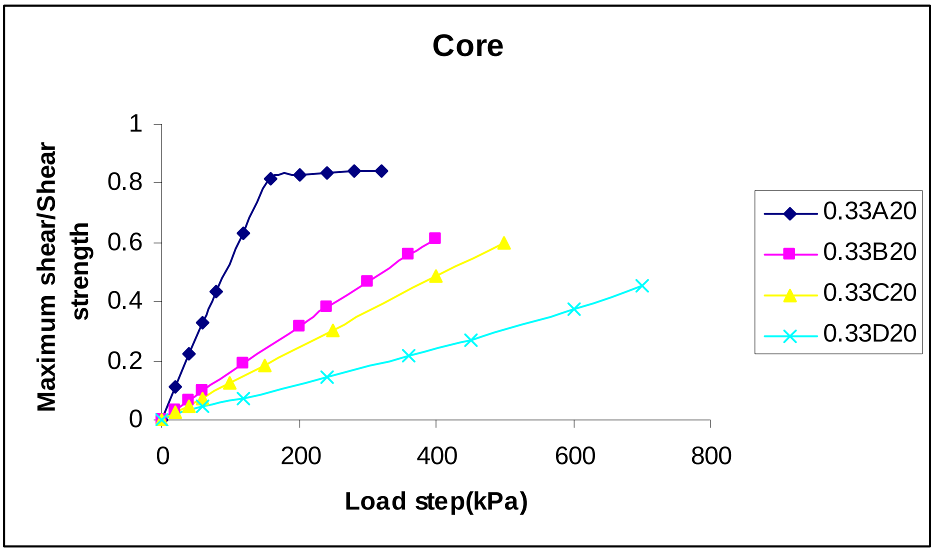

Figure A-2.15 Maximum core shear to shear strength versus load with variation material at thickness 20mm and load size ratio 0.33

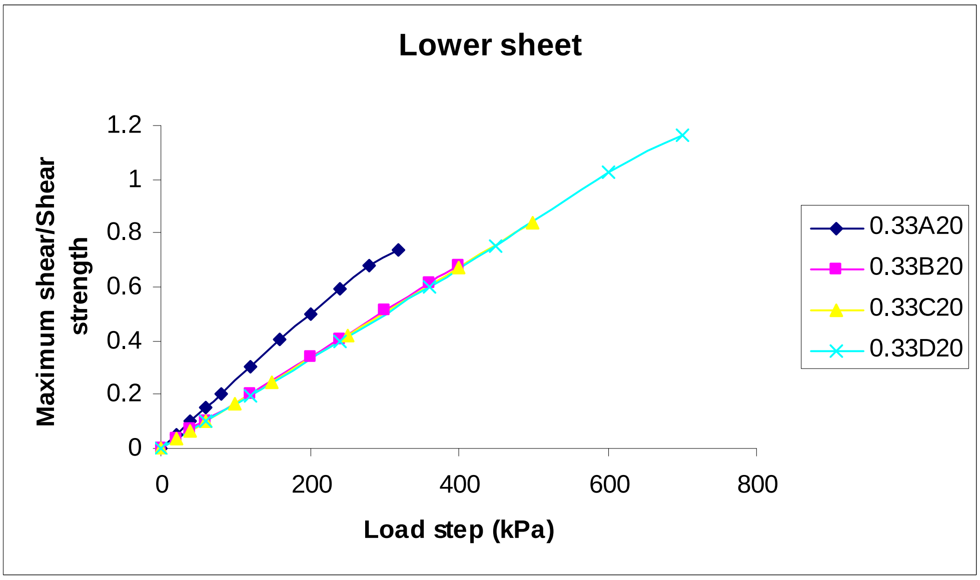

Figure A-2.16 Maximum lower sheet shear to shear strength versus load with variation material at thickness 20mm and load size ratio 0.33

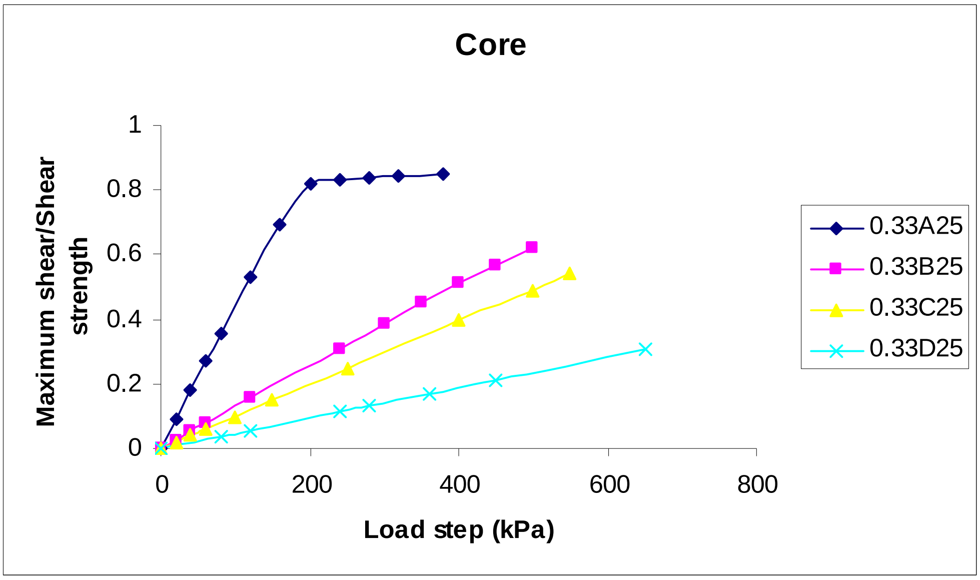

Figure A-2.17 Maximum core shear to shear strength versus load with variation material at thickness 25mm and load size ratio 0.33

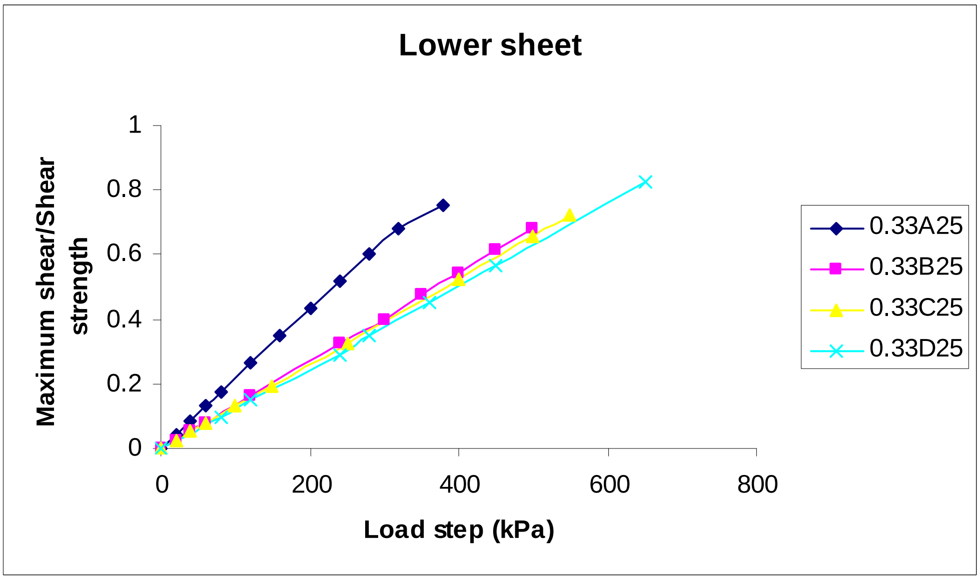

Figure A-2.18 Maximum lower sheet shear to shear strength versus load with variation material at thickness 25mm and load size ratio 0.33

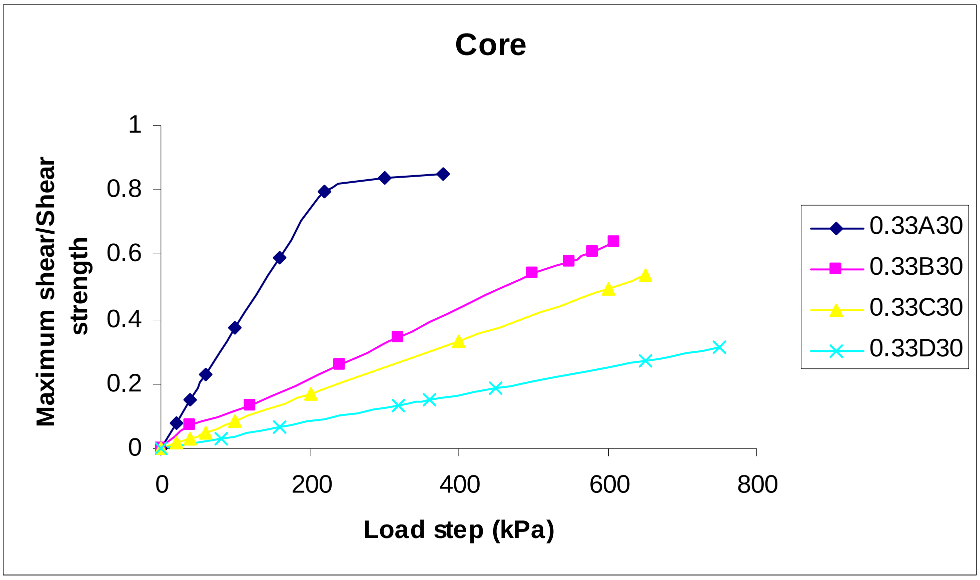

Figure A-2.19 Maximum core shear to shear strength versus load with variation material at thickness 30mm and load size ratio 0.33

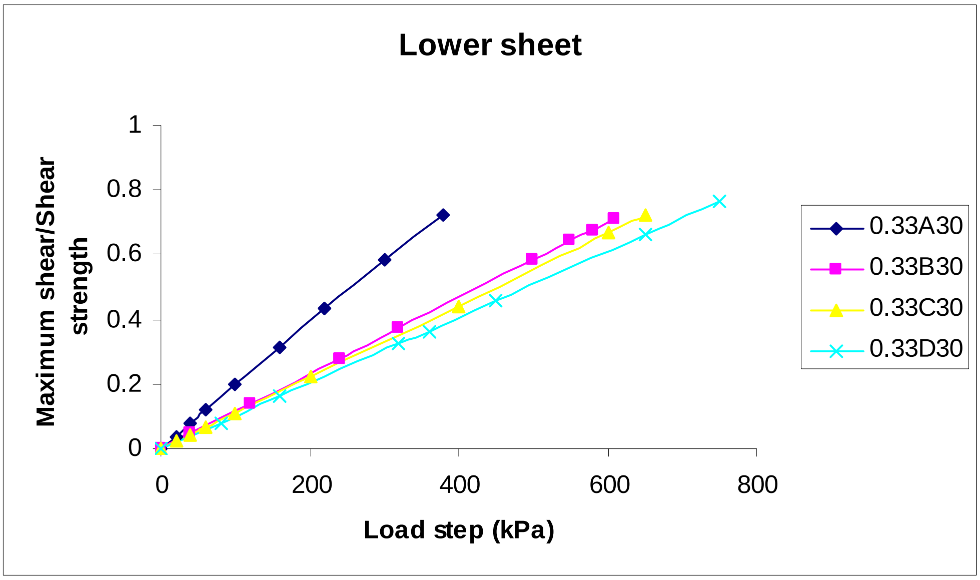

Figure A-2.20 Maximum lower sheet shear to shear strength versus load with variation material at thickness30mm and load size ratio 0.33

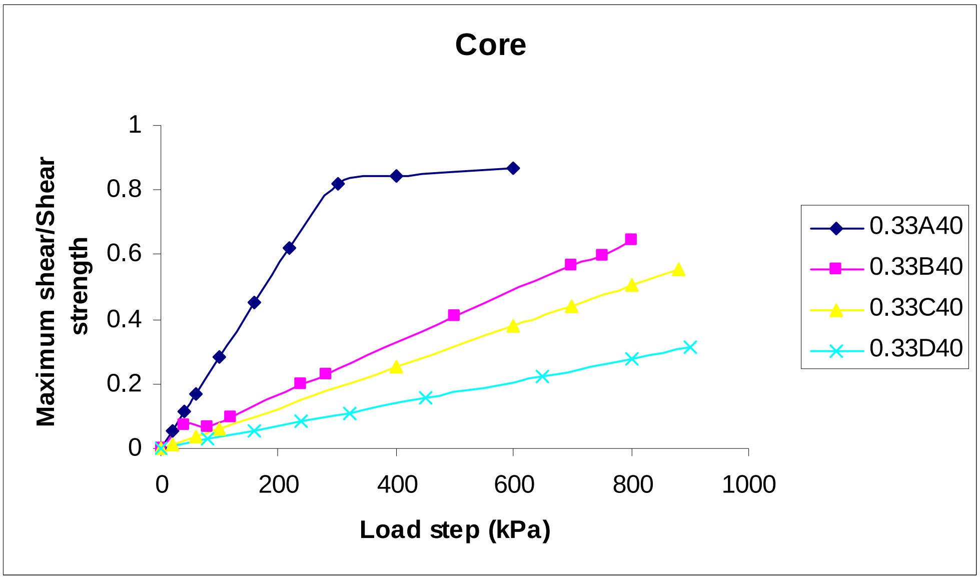

Figure A-2.21 Maximum core shear to shear strength versus load with variation material at thickness 40mm and load size ratio 0.33

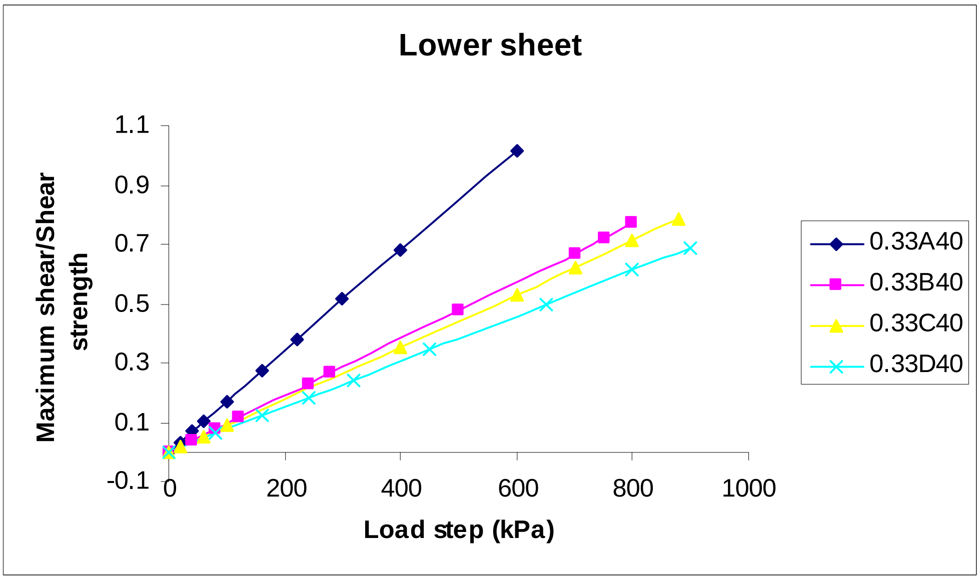

Figure A-2.22 Maximum lower sheet shear to shear strength versus load with variation material at thickness 40mm and load size ratio 0.33

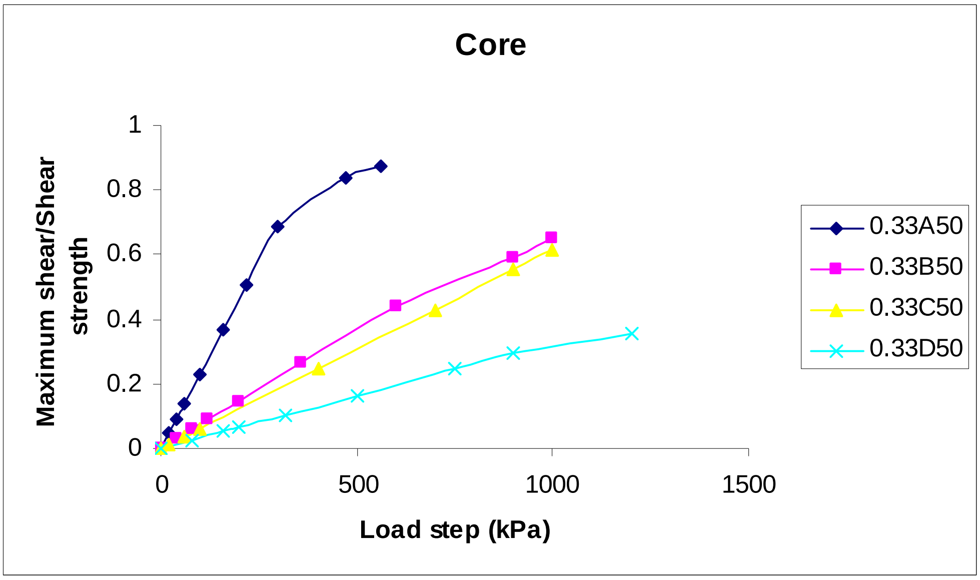

Figure A-2.23 Maximum core shear to shear strength versus load with variation material at thickness 50mm and load size ratio 0.33

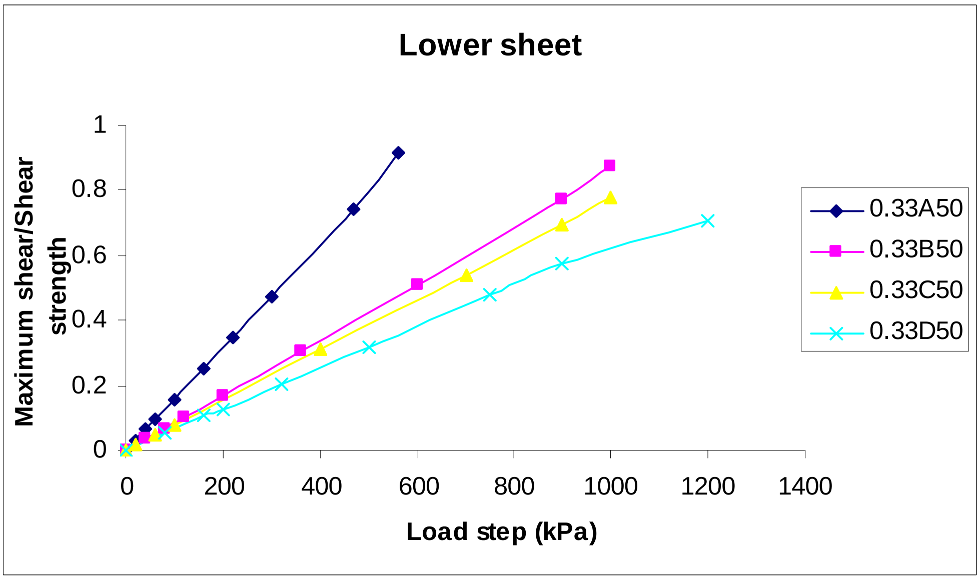

Figure A-2.24 Maximum lower sheet shear to shear strength versus load with variation material at thickness 50mm and load size ratio 0.33

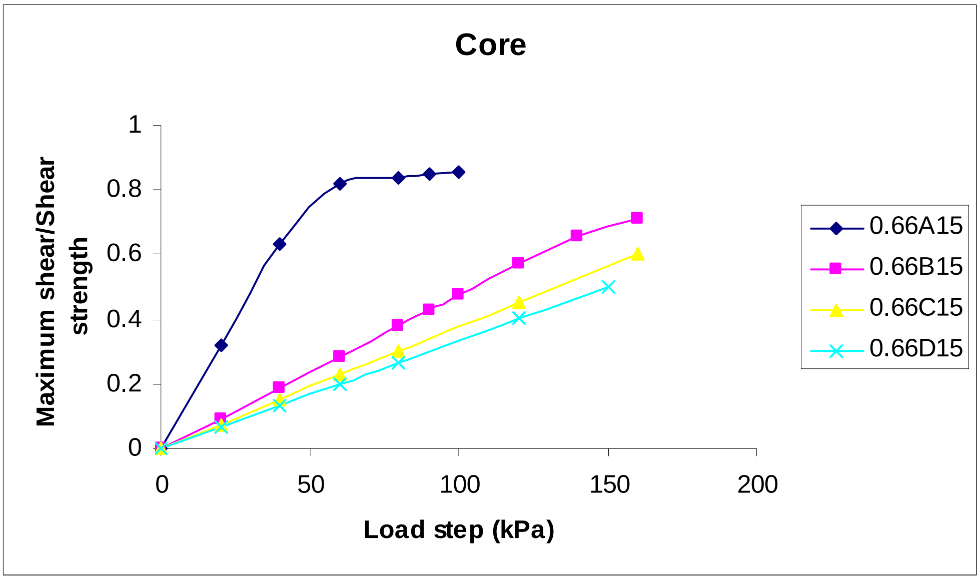

Figure A-2.25 Maximum core shear to shear strength versus load with variation material at thickness 15mm and load size ratio 0.66

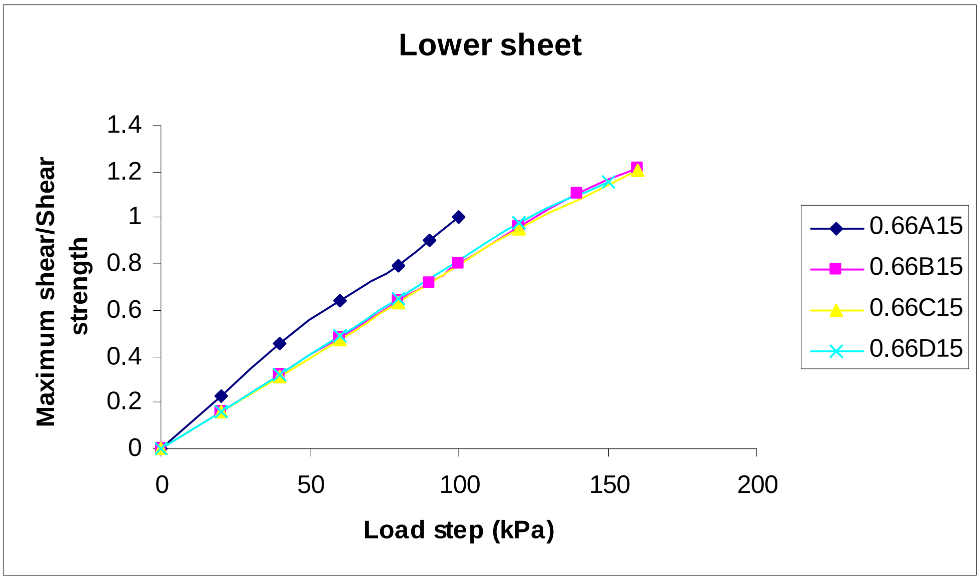

Figure A-2.26 Maximum lower sheet shear to shear strength versus load with variation material at thickness 15mm and load size ratio 0.66

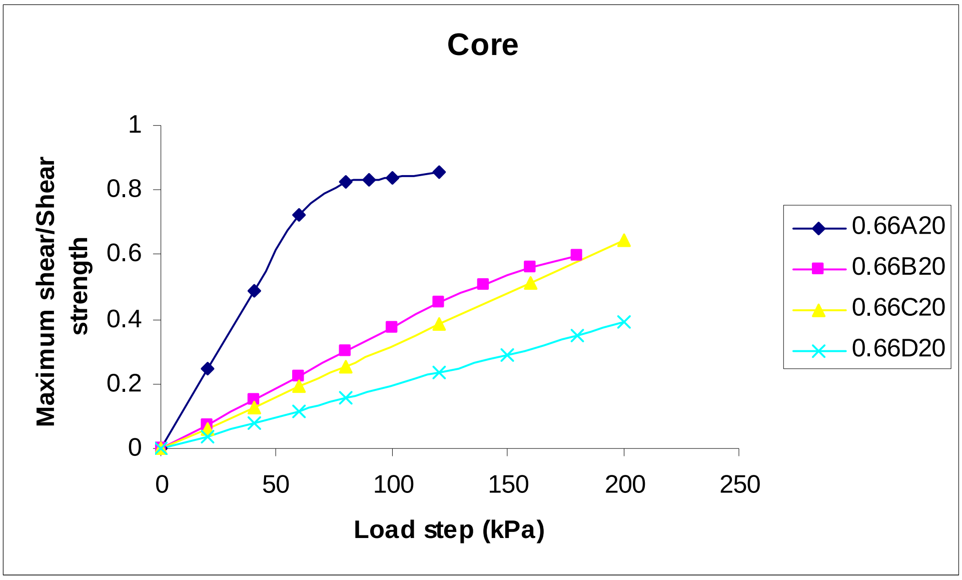

Figure A-2.27 Maximum core shear to shear strength versus load with variation material at thickness 20mm and load size ratio 0.66

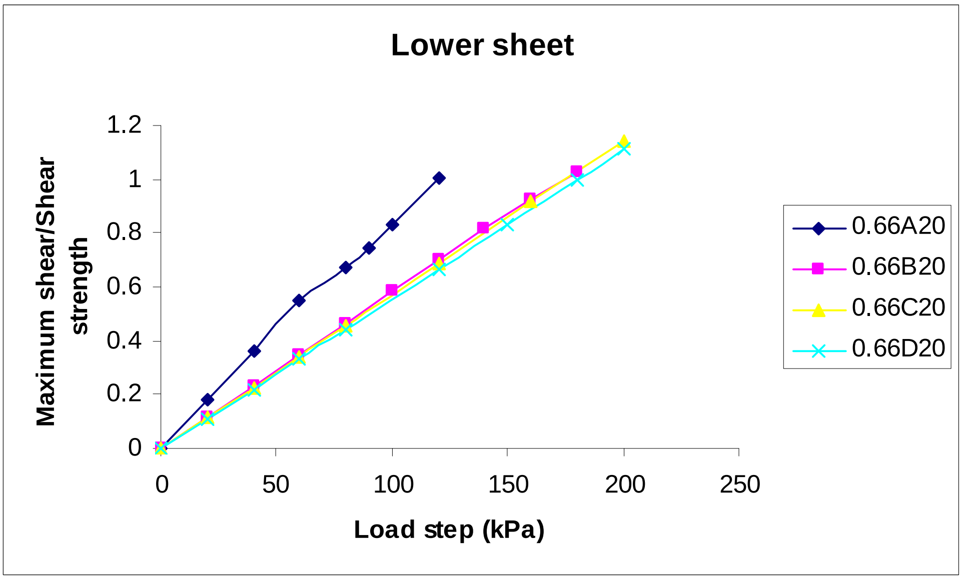

Figure A-2.28 Maximum lower sheet shear to shear strength versus load with variation material at thickness 20mm and load size ratio 0.66

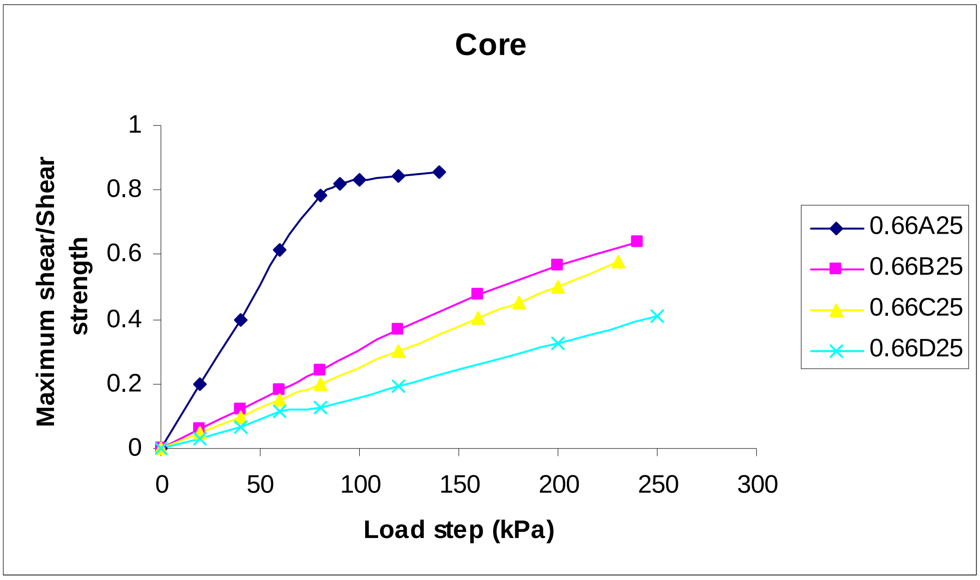

Figure A-2.29 Maximum core shear to shear strength versus load with variation material at thickness 25mm and load size ratio 0.66

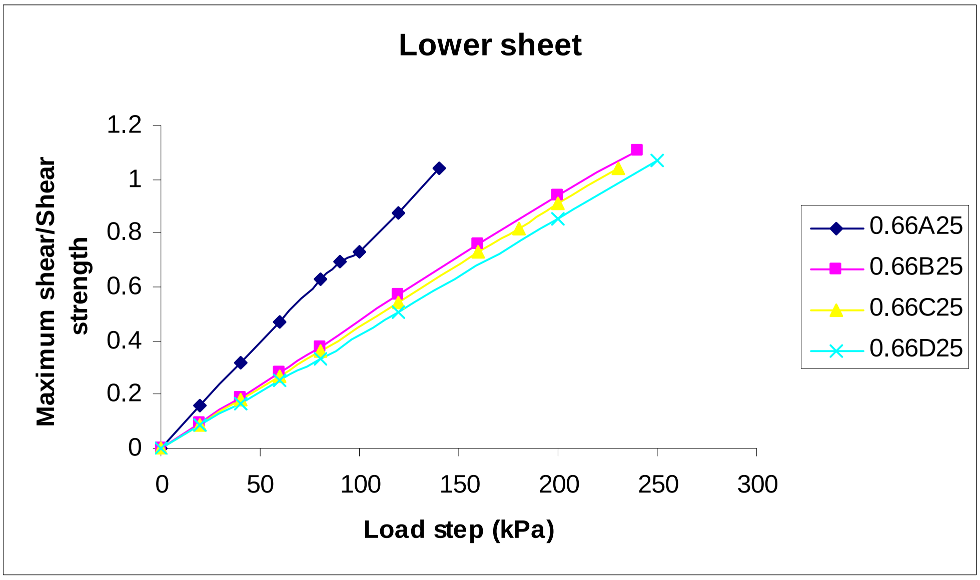

Figure A-2.30 Maximum lower sheet shear to shear strength versus load with variation material at thickness 25mm and load size ratio 0.66

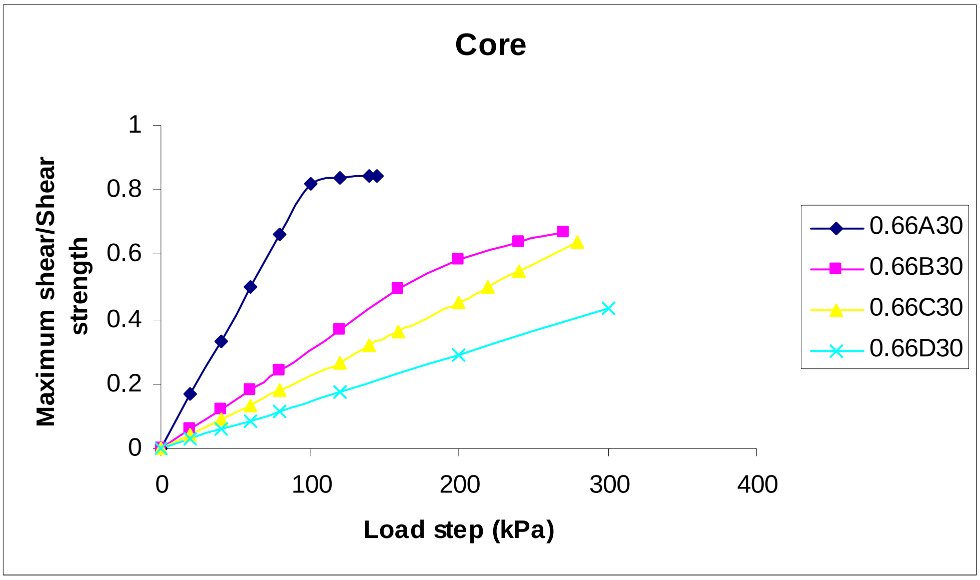

Figure A-2.31 Maximum core shear to shear strength versus load with variation material at thickness 30mm and load size ratio 0.66

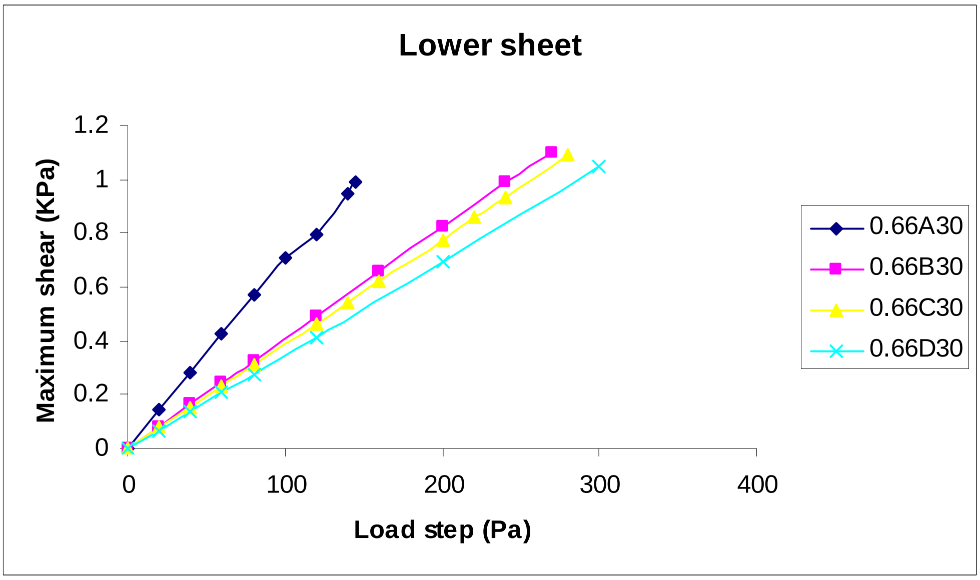

Figure A-2.32 Maximum lower sheet shear to shear strength versus load with variation material at thickness 30mm and load size ratio 0.66

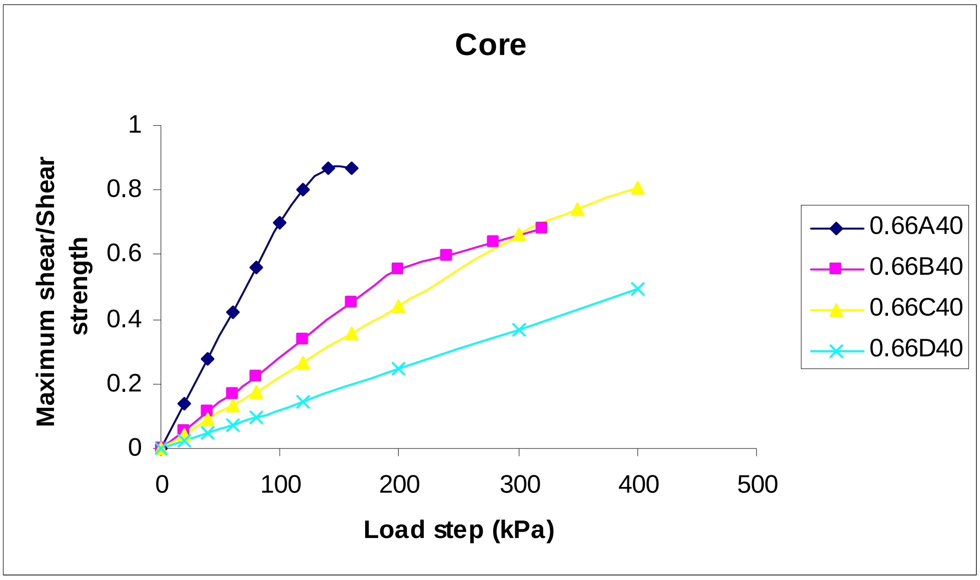

Figure A-2.33 Maximum core shear to shear strength versus load with variation material at thickness 40mm and load size ratio 0.66

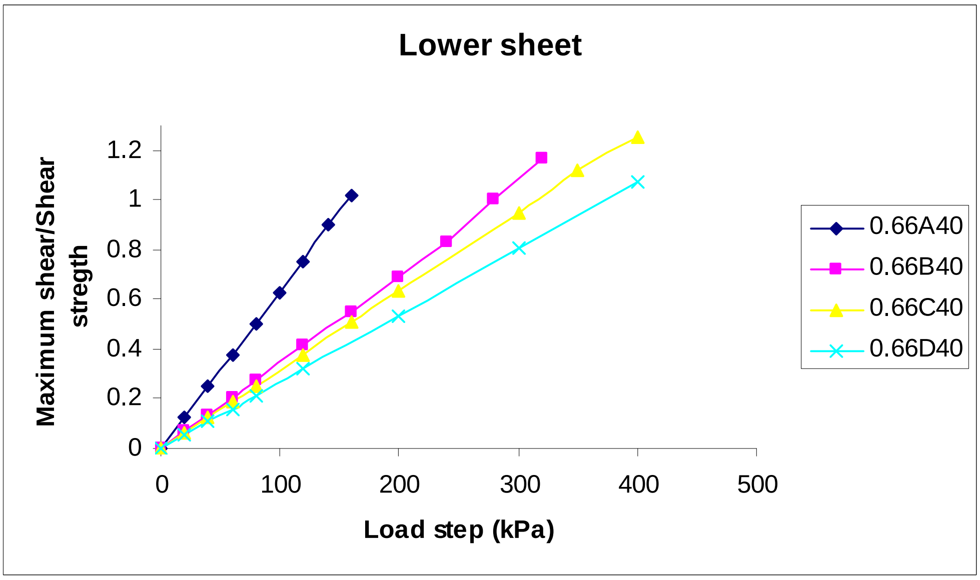

Figure A-2.34 Maximum lower sheet shear to shear strength versus load with variation material at thickness 40mm and load size ratio 0.66

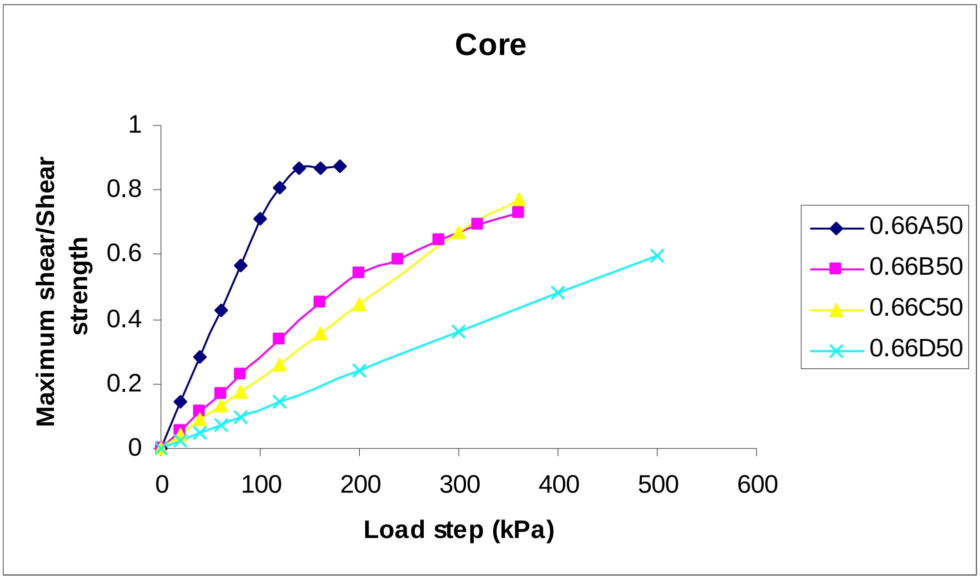

Figure A-2.35 Maximum core shear to shear strength versus load with variation material at thickness 50mm and load size ratio 0.66

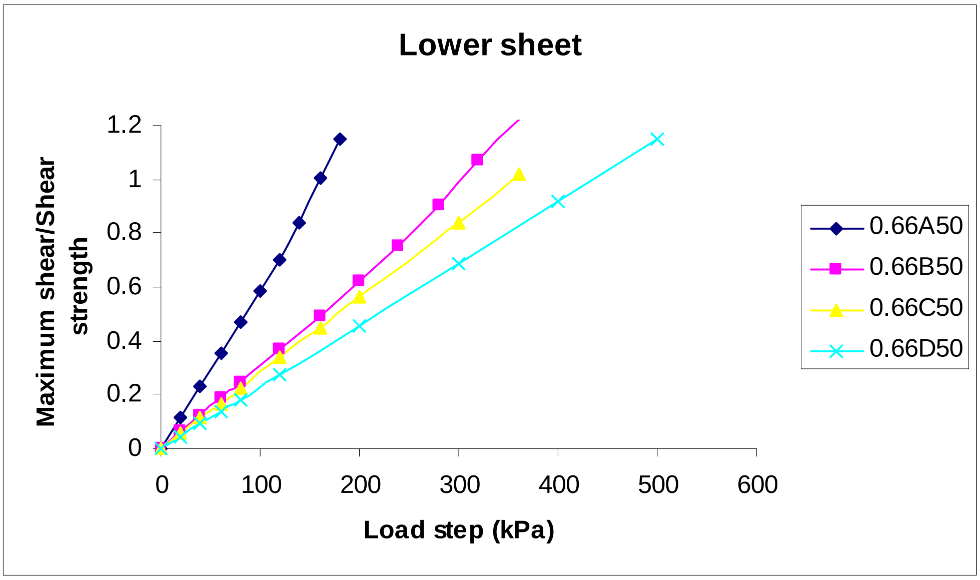

Figure A-2.36 Maximum lower sheet shear to shear strength versus load with variation material at thickness 50mm and load size ratio 0.66

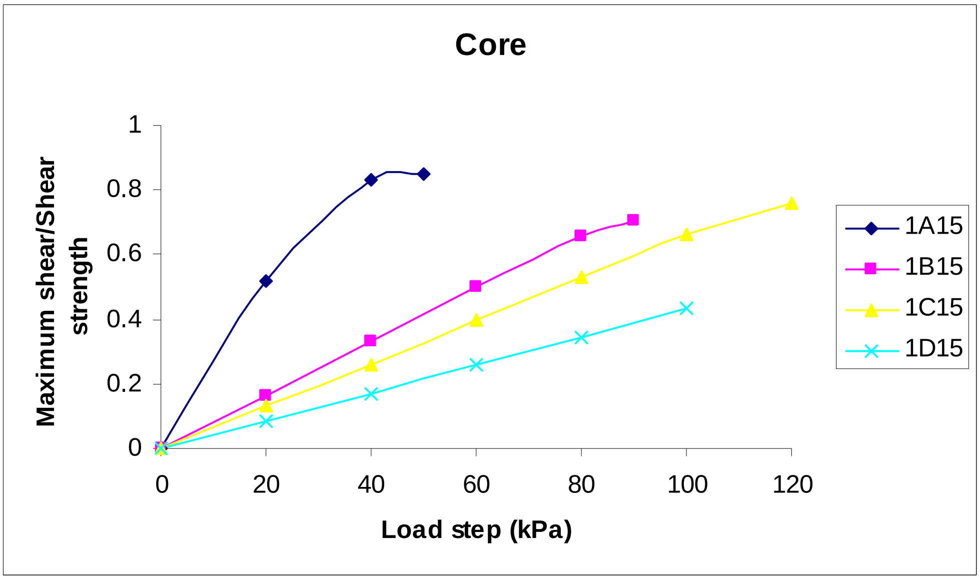

Figure A-2.37 Maximum core shear to shear strength versus load with variation material at thickness 15mm and load size ratio 1

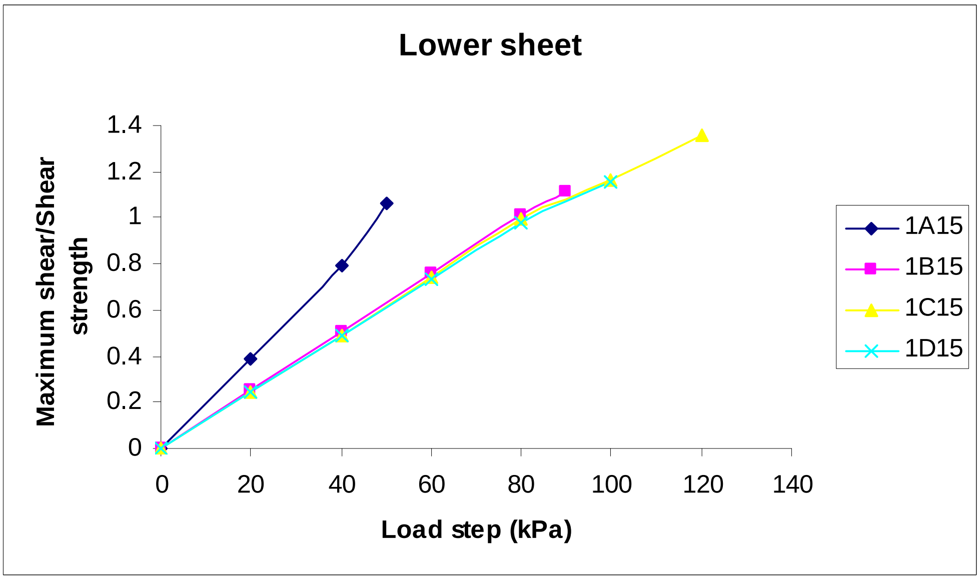

Figure A-2.38 Maximum lower sheet shear to shear strength versus load with variation material at thickness 15mm and load size ratio 1

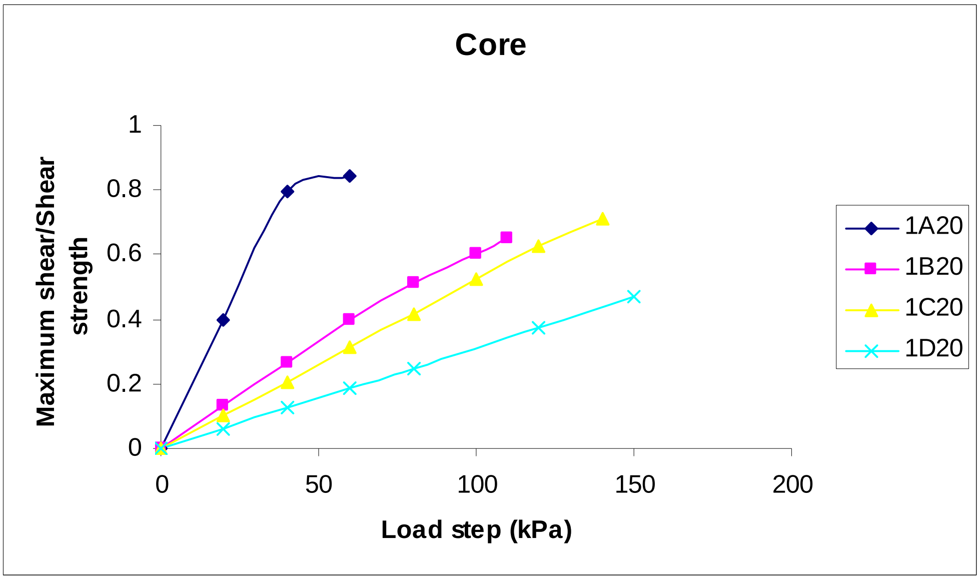

Figure A-2.39 Maximum core shear versus to shear strength load with variation material at thickness 20mm and load size ratio 1

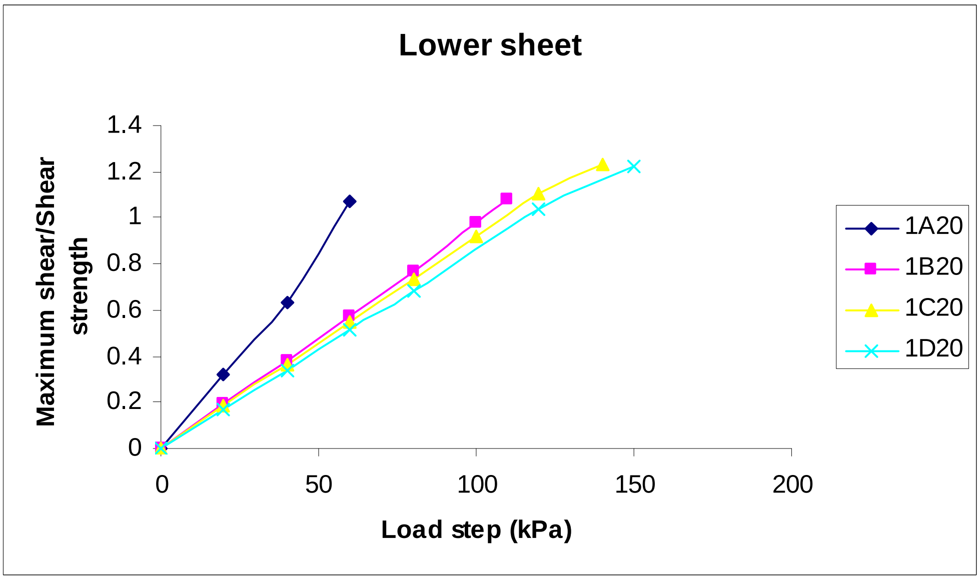

Figure A-2.40 Maximum lower sheet shear to shear strength versus load with variation material at thickness 20mm and load size ratio 1

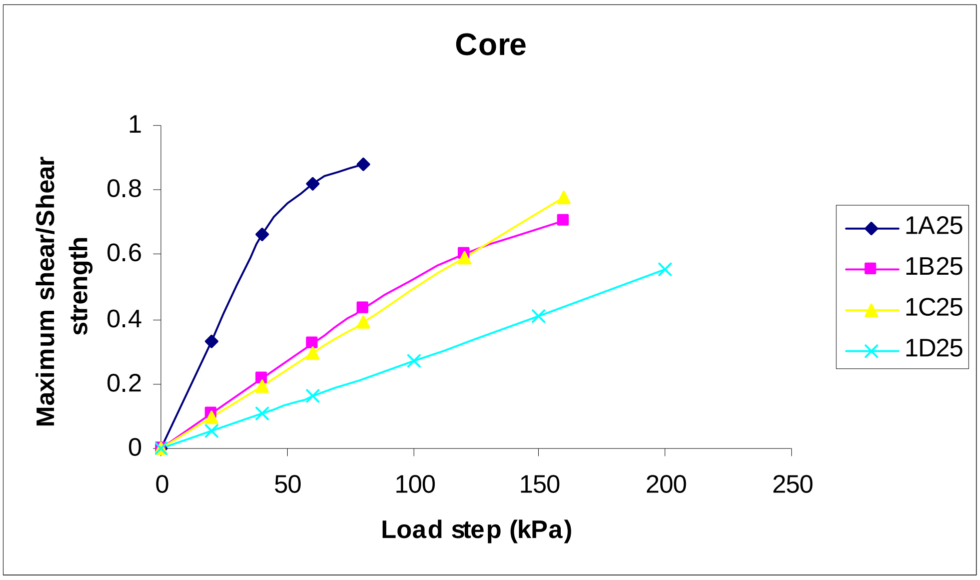

Figure A-2.41 Maximum core shear to shear strength versus load with variation material at thickness 25mm and load size ratio 1

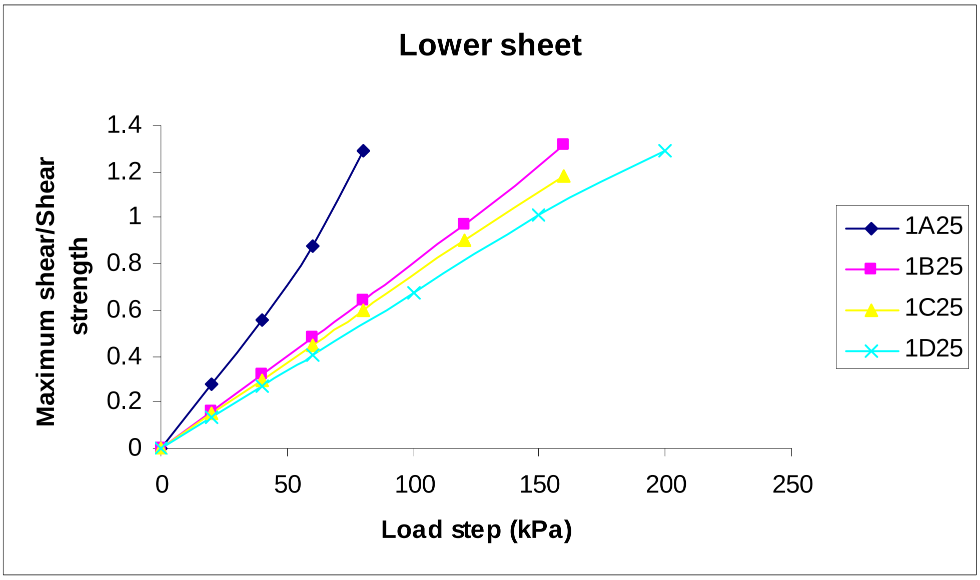

Figure A-2.42 Maximum lower sheet shear to shear strength versus load with variation material at thickness 25mm and load size ratio 1

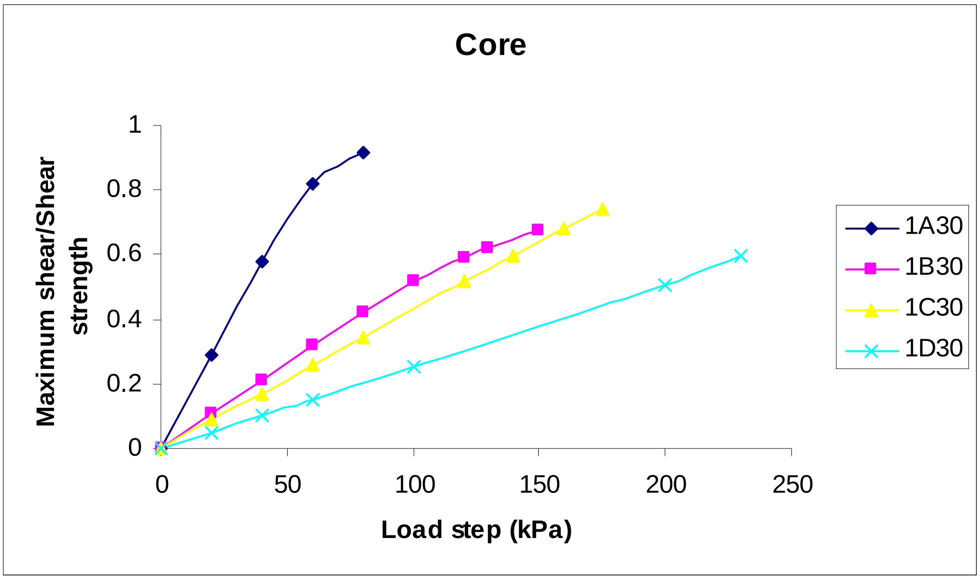

Figure A-2.43 Maximum core shear to shear strength versus load with variation material at thickness 30mm and load size ratio 1

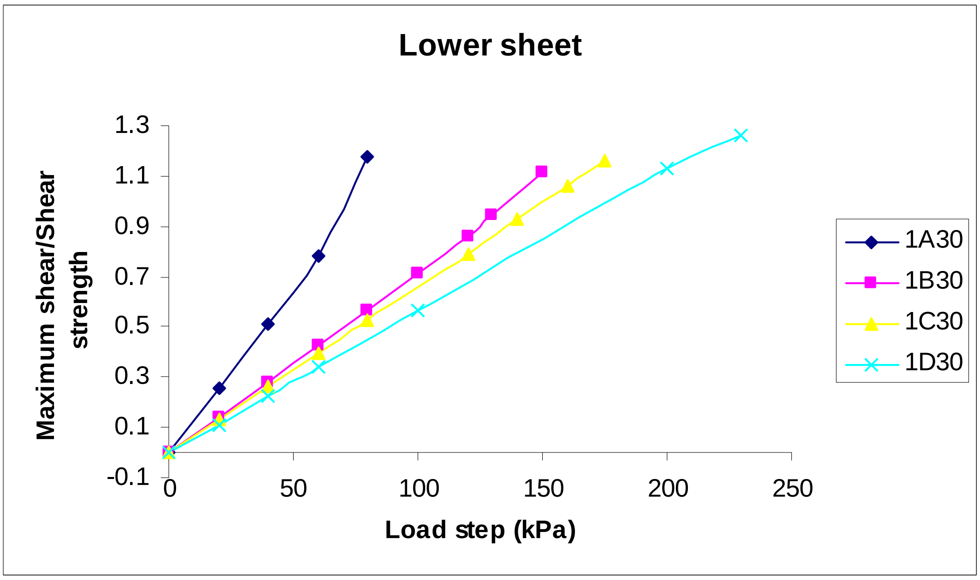

Figure A-2.44 Maximum lower sheet shear to shear strength versus load with variation material at thickness 30mm and load size ratio 1

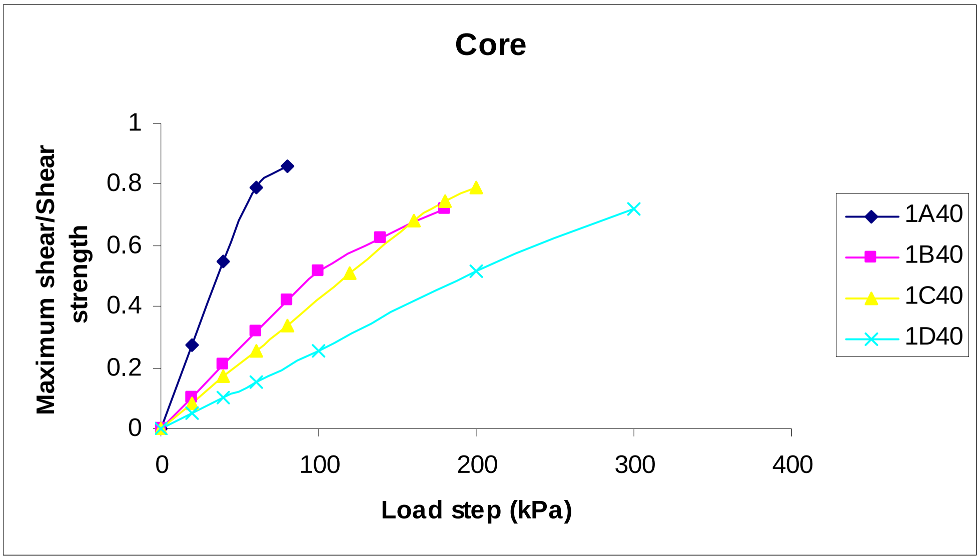

Figure A-2.45 Maximum core shear to shear strength versus load with variation material at thickness 40mm and load size ratio 1

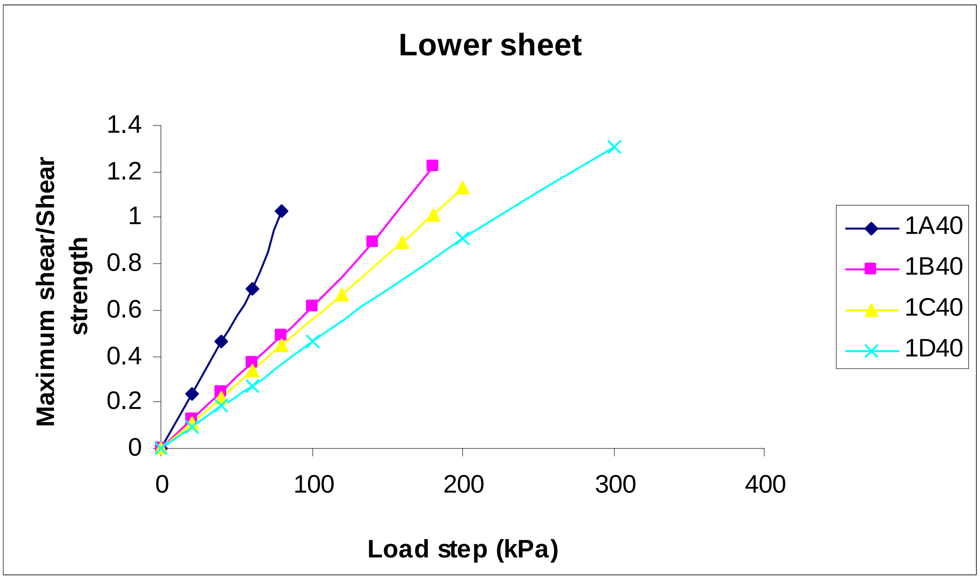

Figure A-2.46 Maximum lower sheet shear to shear strength versus load with variation material at thickness 40mm and load size ratio 1

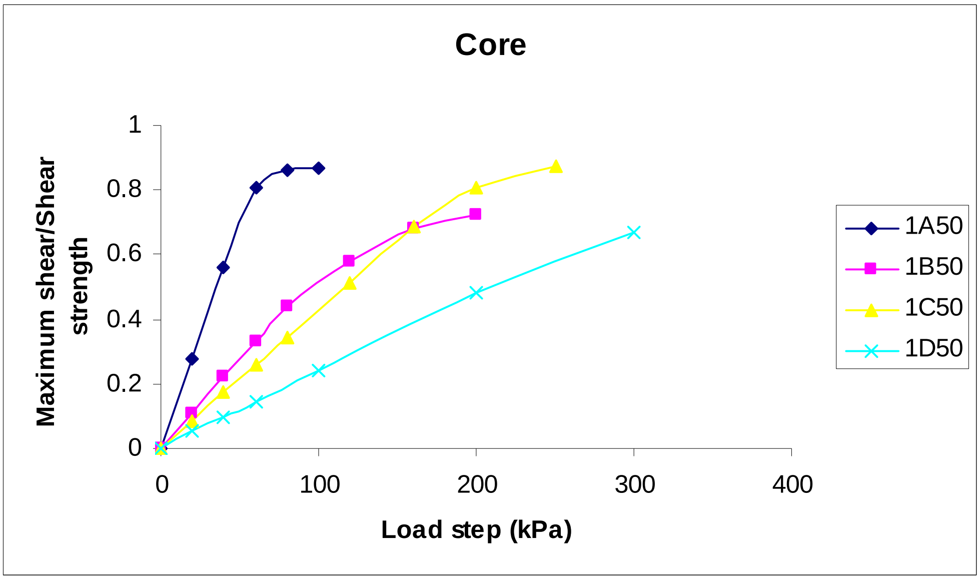

Figure A-2.47 Maximum core shear to shear strength versus load with variation material at thickness 50mm and load size ratio 1

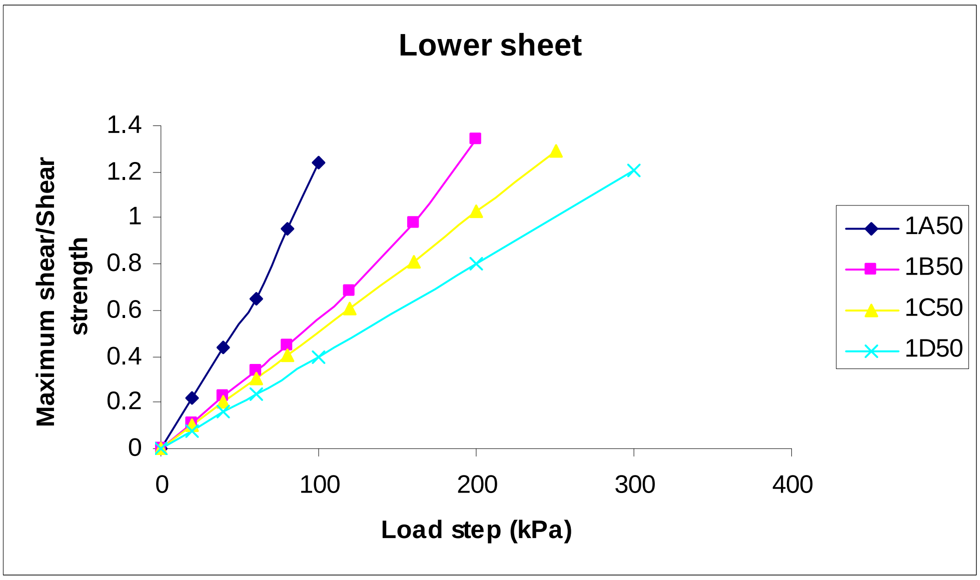

Figure A-2.48 Maximum lower sheet shear to shear strength versus load with variation material at thickness 50mm and load size ratio 1

A-3 Graphical results for maximum shear stress versus load step for core and lower sheet of sandwich panel under variation of load size.

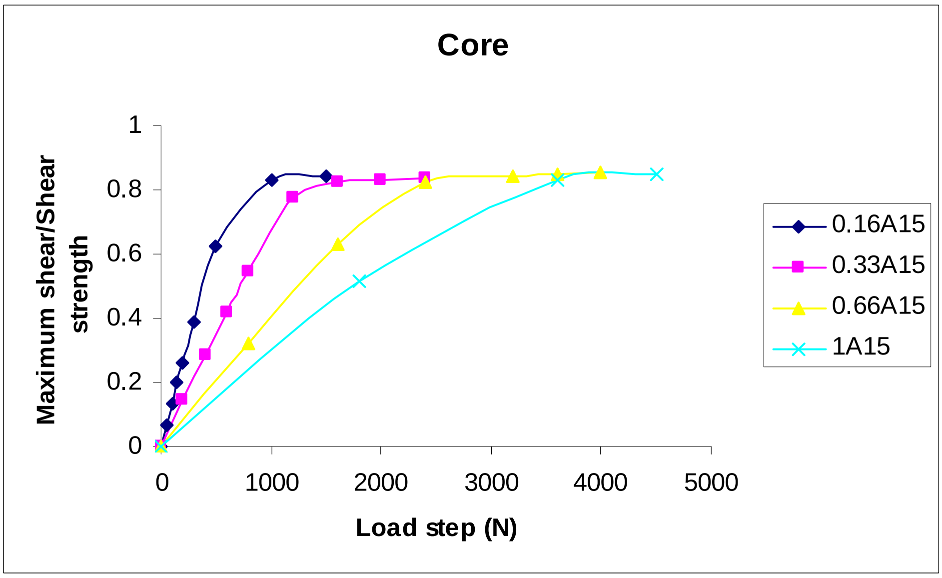

Figure A-3.1 Maximum core shear to shear strength versus load with variation of load size at thickness 15mm and material A

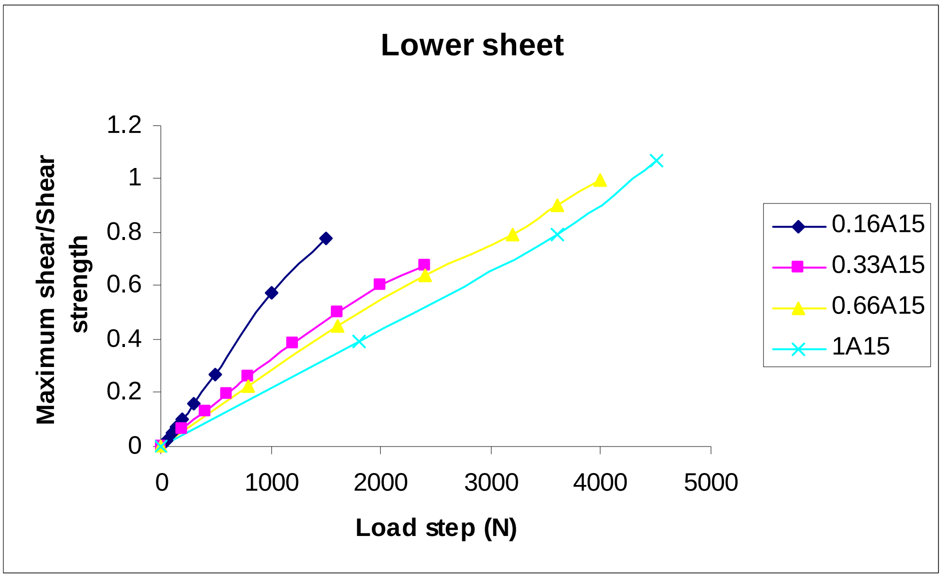

Figure A-3.2 Maximum lower sheet shear to shear strength versus load with variation of load size ratio at thickness 15mm and material A

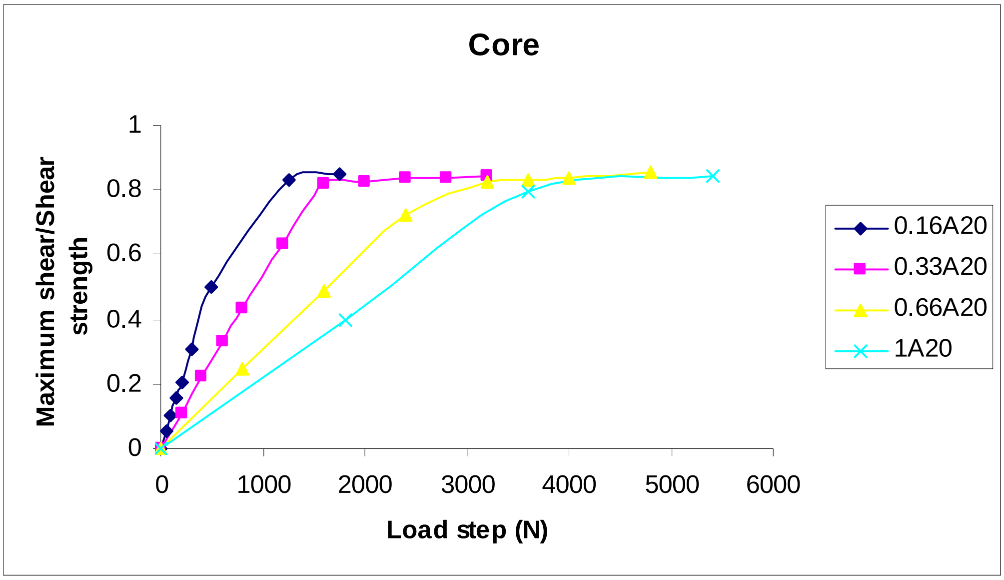

Figure A-3.3 Maximum core shear to shear strength versus load with variation of load size ratio at thickness 20mm and material A

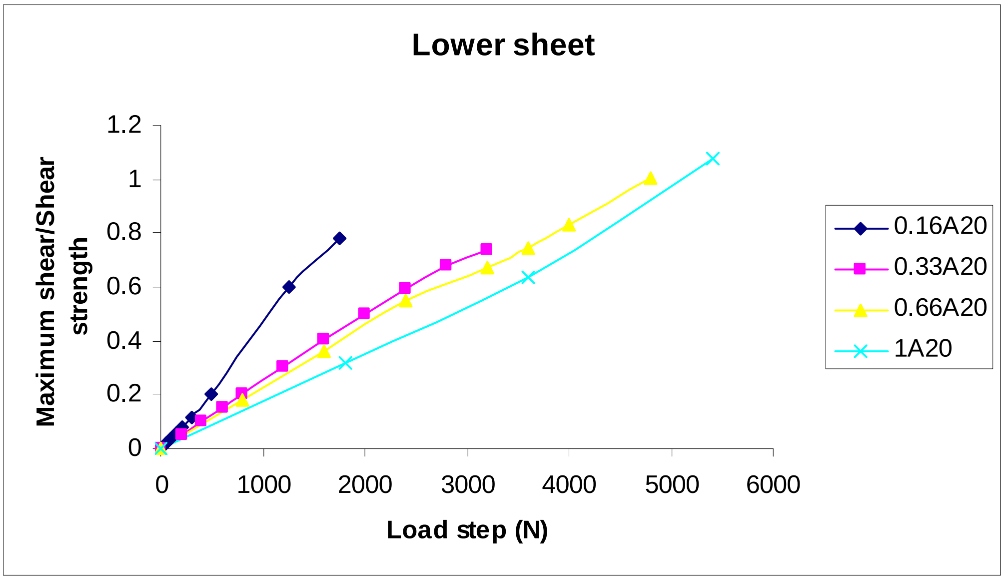

Figure A-3.4Maximum lower sheet shear to shear strength versus load with variation of load size ratio at thickness 20mm and material A

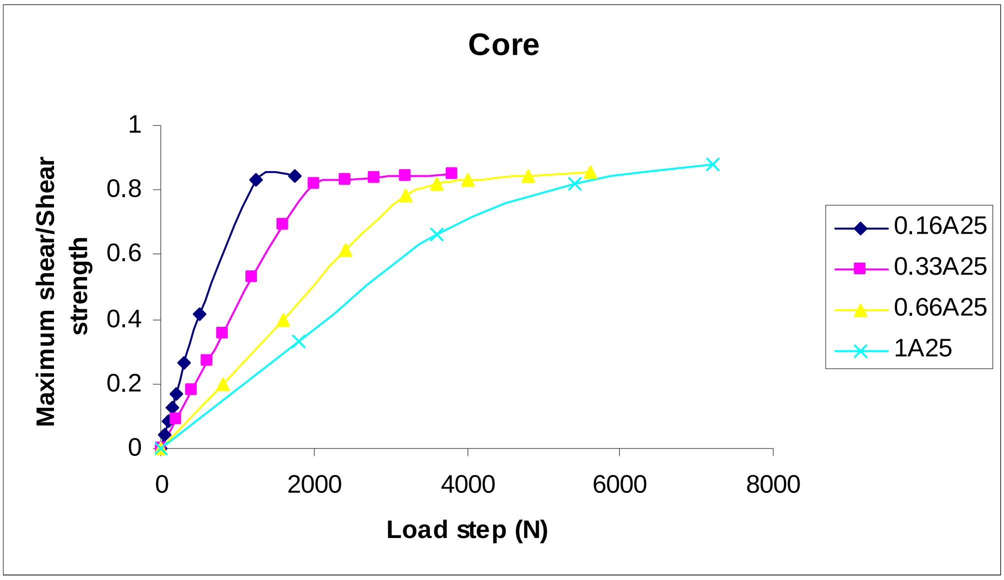

Figure A-3.5 Maximum core shear to shear strength versus load with variation of load size ratio at thickness 25mm and material A

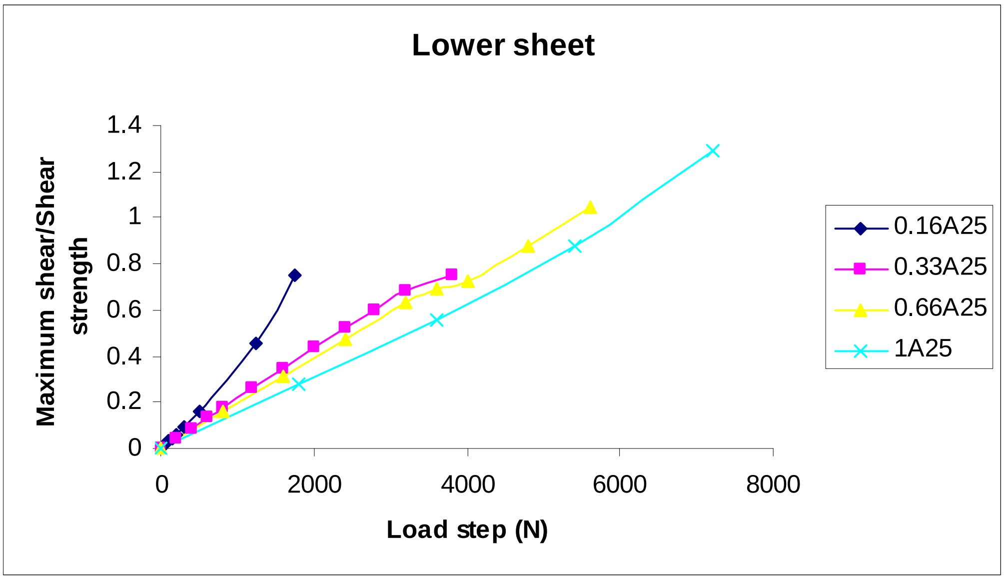

Figure A-3.6 Maximum lower sheet shear to shear strength versus load with variation of load size ratio at thickness 25mm and material A

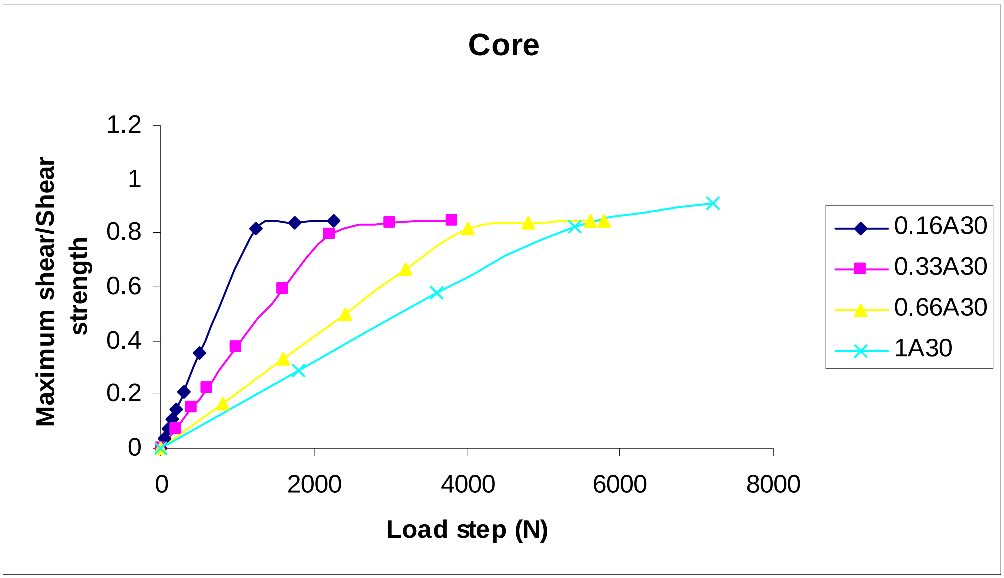

Figure A-3.7 Maximum core shear to shear strength versus load with variation of load size ratio at thickness 30mm and material A

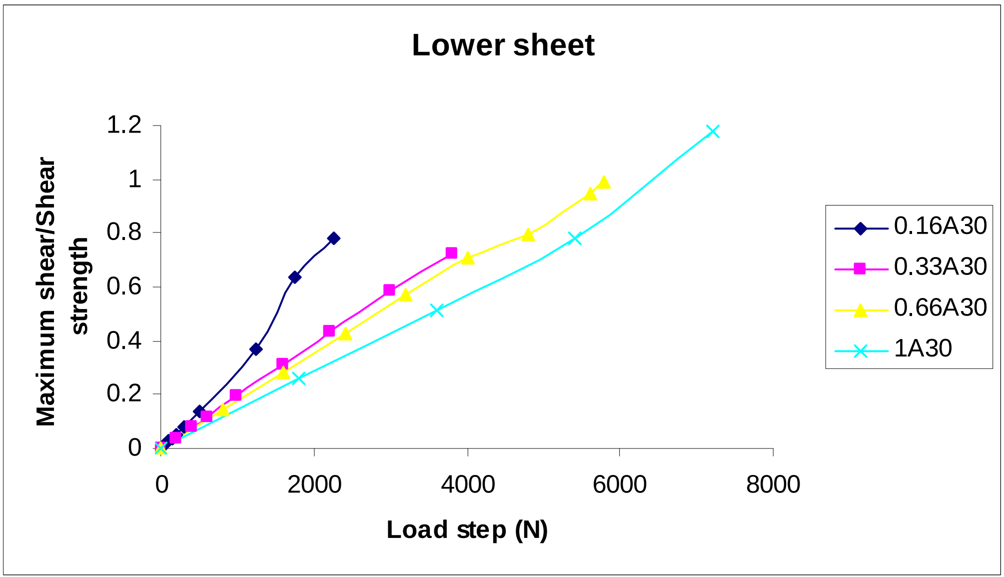

Figure A-3.8 Maximum lower sheet shear to shear strength versus load with variation of load size ratio at thickness 30mm and material A

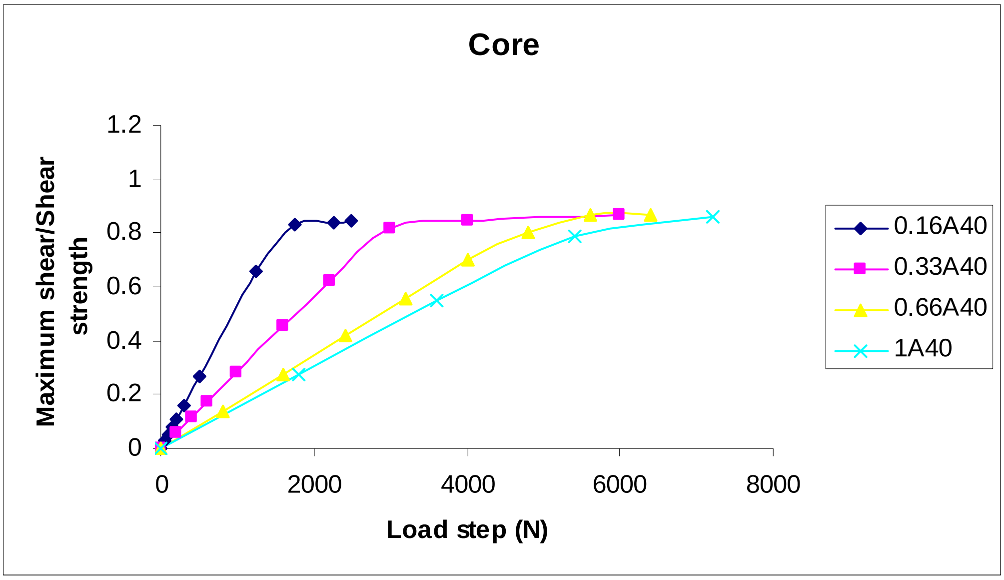

Figure A-3.9 Maximum core shear to shear strength versus load with variation of load size ratio at thickness 40mm and material A

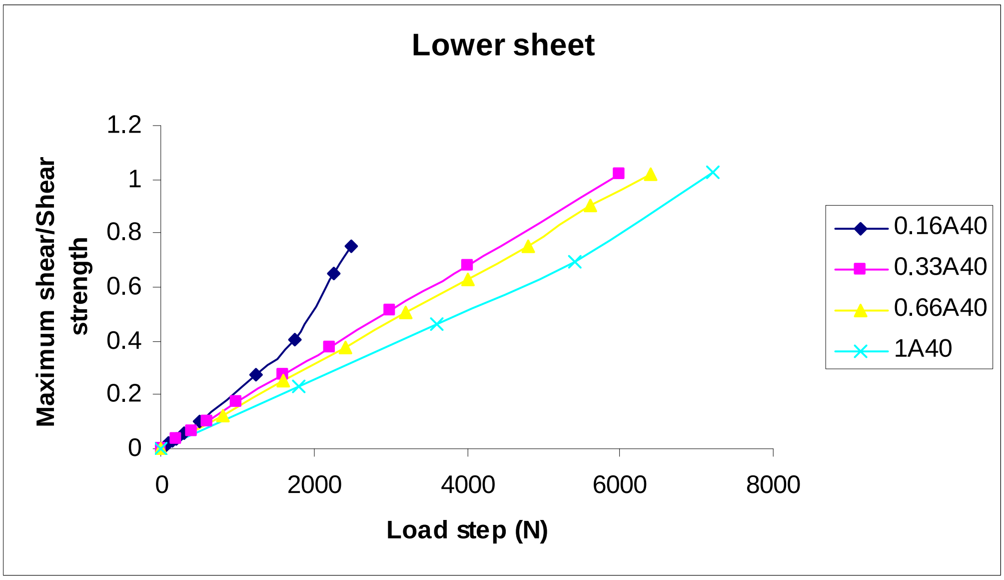

Figure A-3.10 Maximum lower sheet shear to shear strength versus load with variation of load size ratio at thickness 40mm and material A

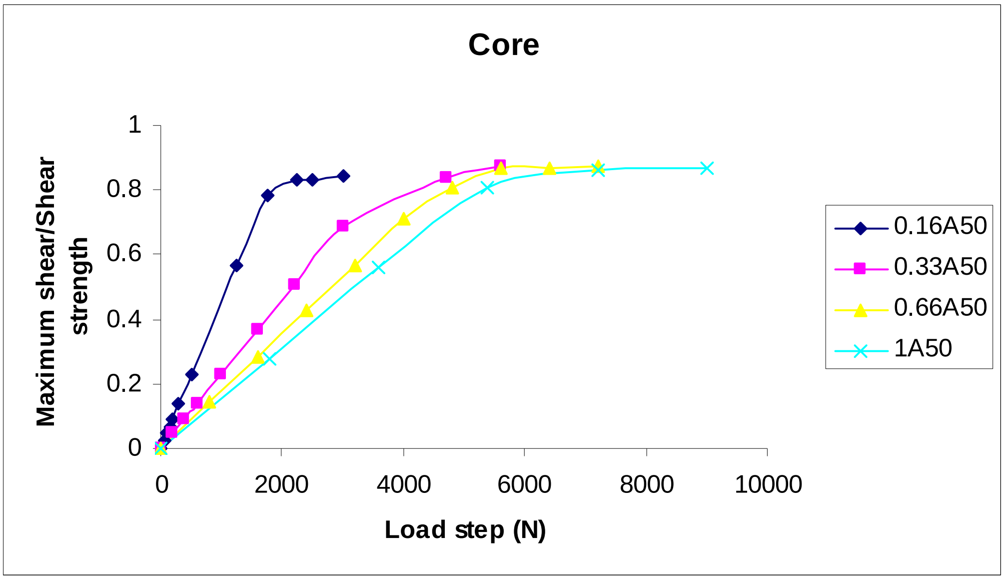

Figure A-3.11 Maximum core shear to shear strength versus load with variation of load size ratio at thickness 50mm and material A

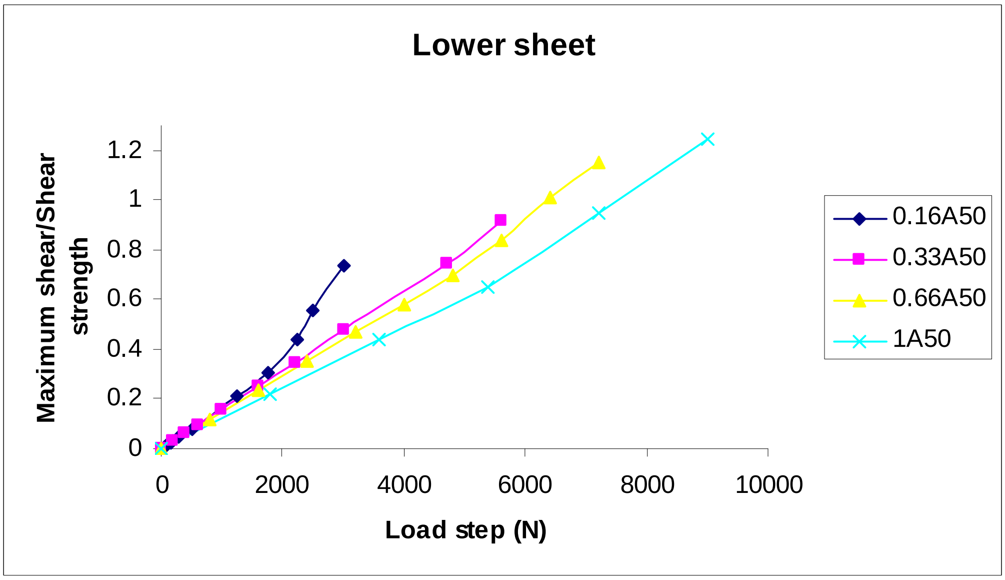

Figure A-3.12 Maximum lower sheet shear to shear strength versus load with variation of load size ratio at thickness 50mm and material A

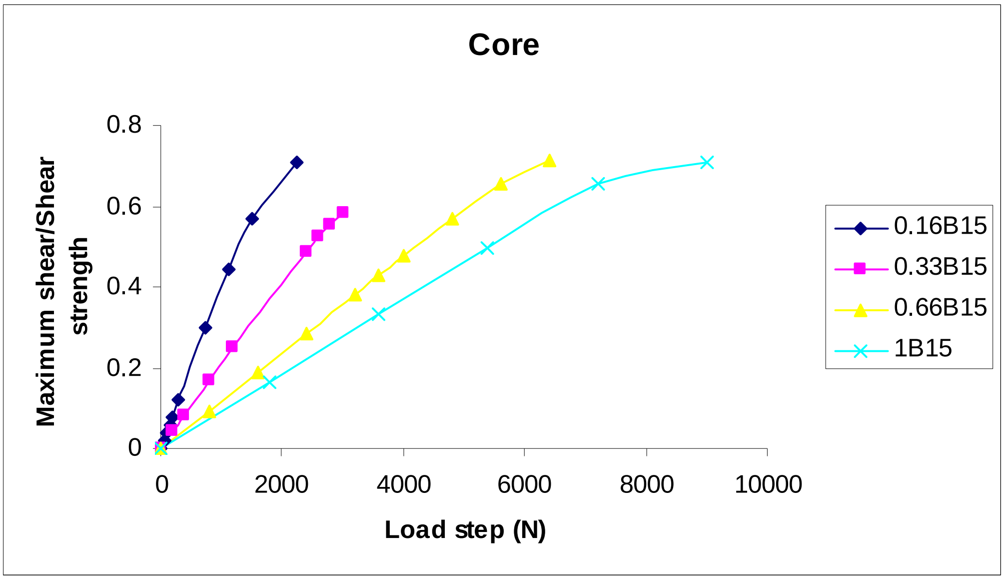

Figure A-3.13 Maximum core shear to shear strength versus load with variation of load size ratio at thickness 15mm and material B

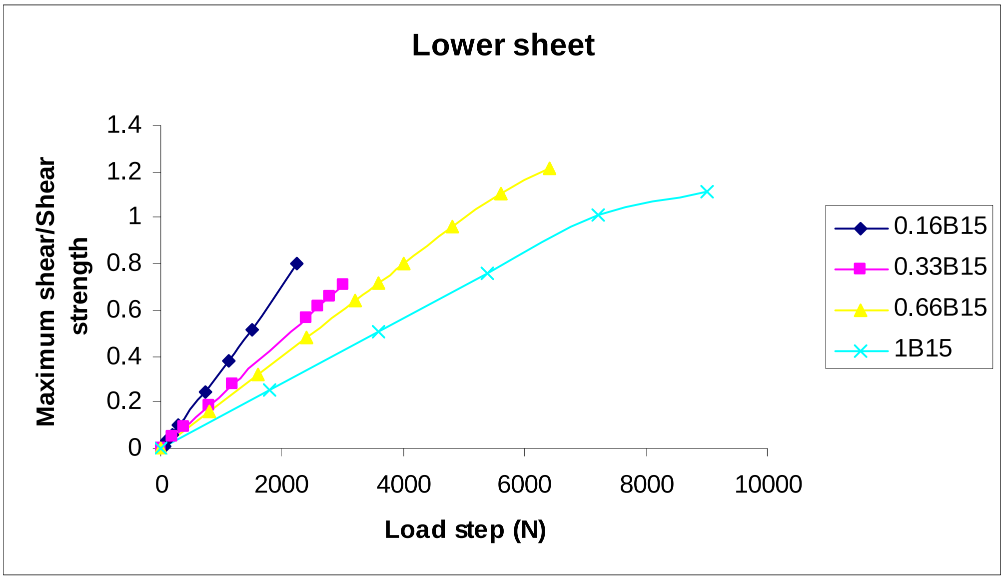

Figure A-3.14 Maximum lower sheet shear to shear strength versus load with variation of load size ratio at thickness 15mm and material B

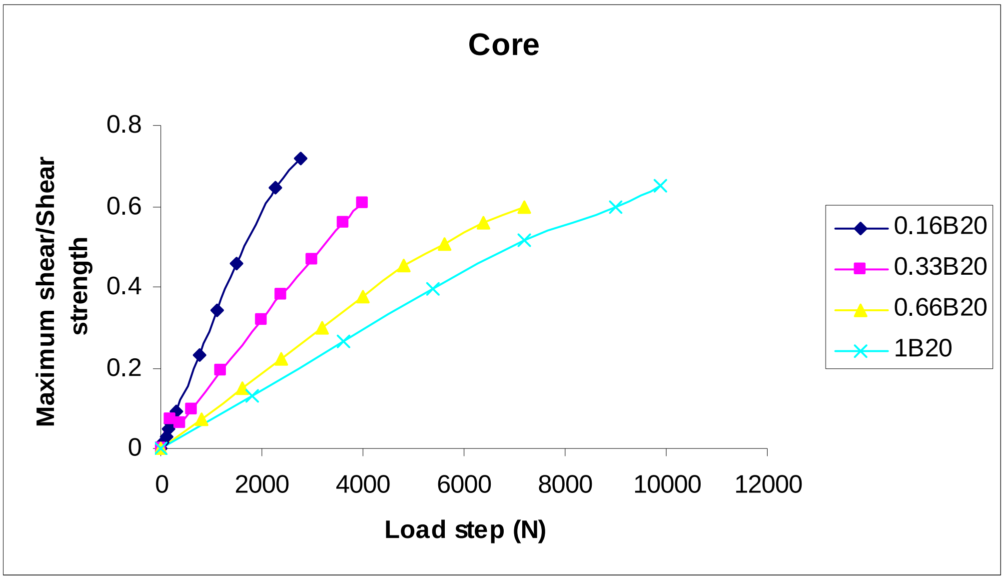

Figure A-3.15 Maximum core shear to shear strength versus load with variation of load size ratio at thickness 20mm and material B

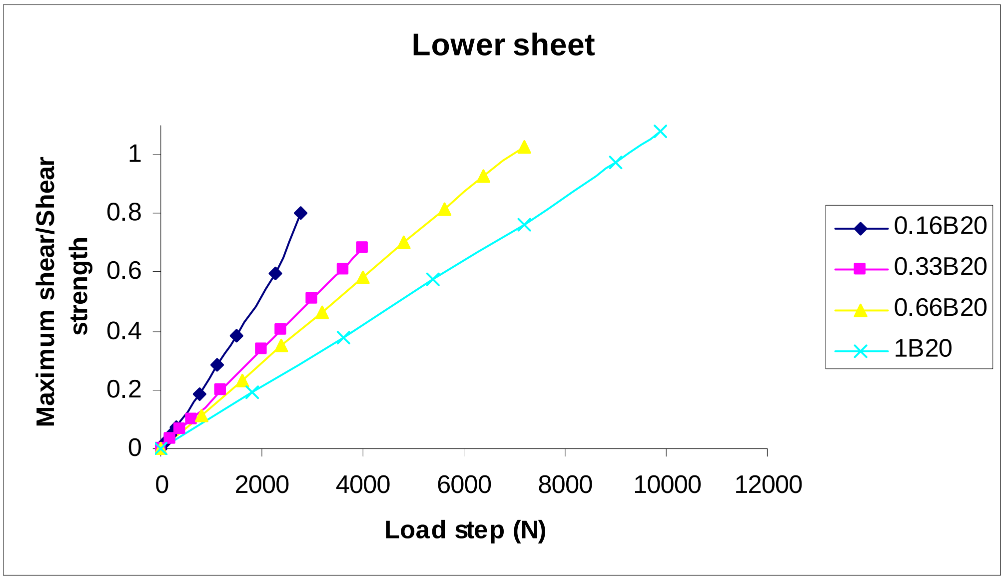

Figure A-3.16 Maximum lower sheet shear to shear strength versus load with variation of load size ratio at thickness 20mm and material B

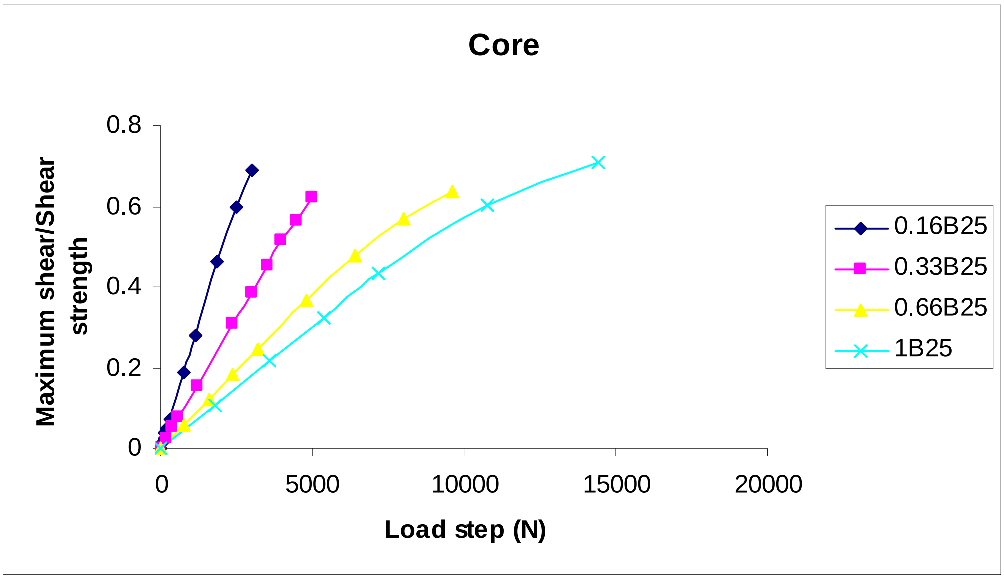

Figure A-3.17 Maximum core shear to shear strength versus load with variation of load size ratio at thickness 25mm and material B

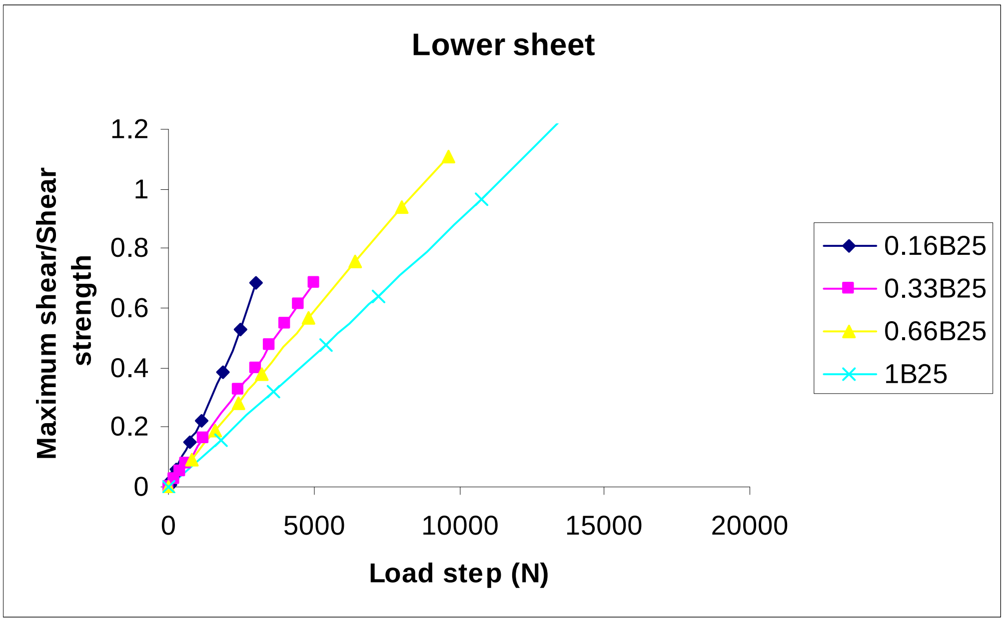

Figure A-3.18 Maximum lower sheet shear to shear strength versus load with variation of load size ratio at thickness 25mm and material B

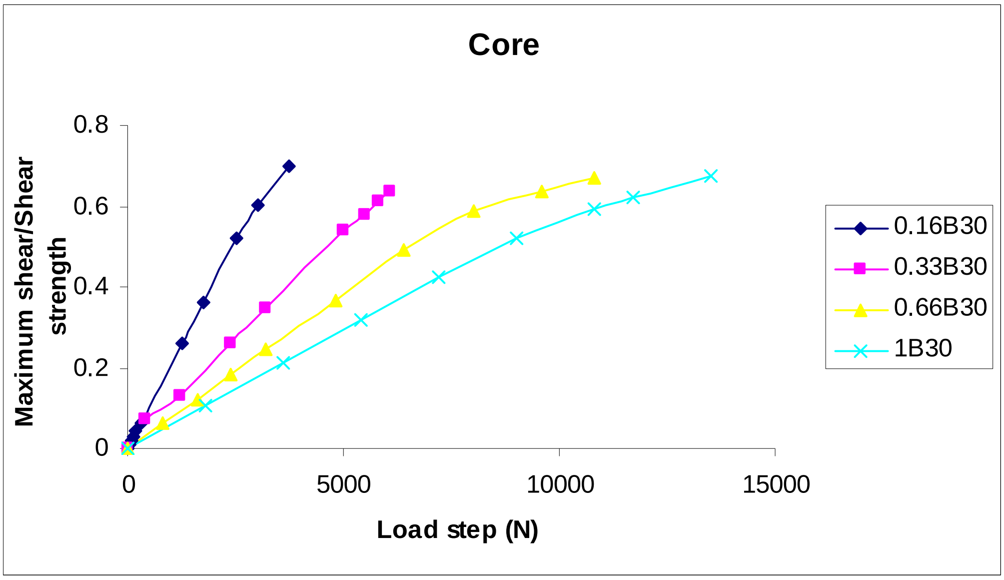

Figure A-3.19 Maximum core shear to shear strength versus load with variation of load size ratio at thickness 30mm and material B

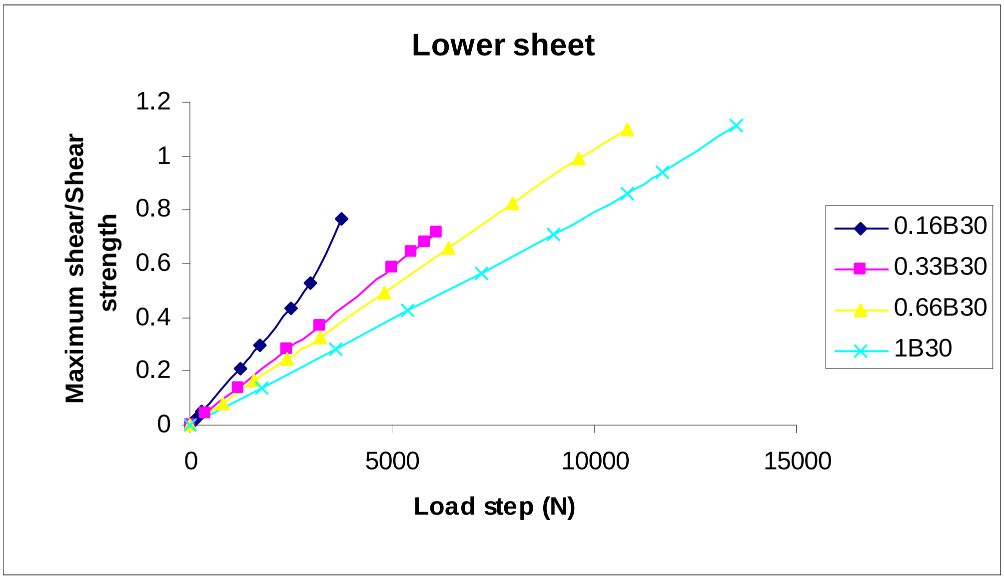

Figure A-3.20 Maximum lower sheet shear to shear strength versus load with variation of load size ratio at thickness 30mm and material

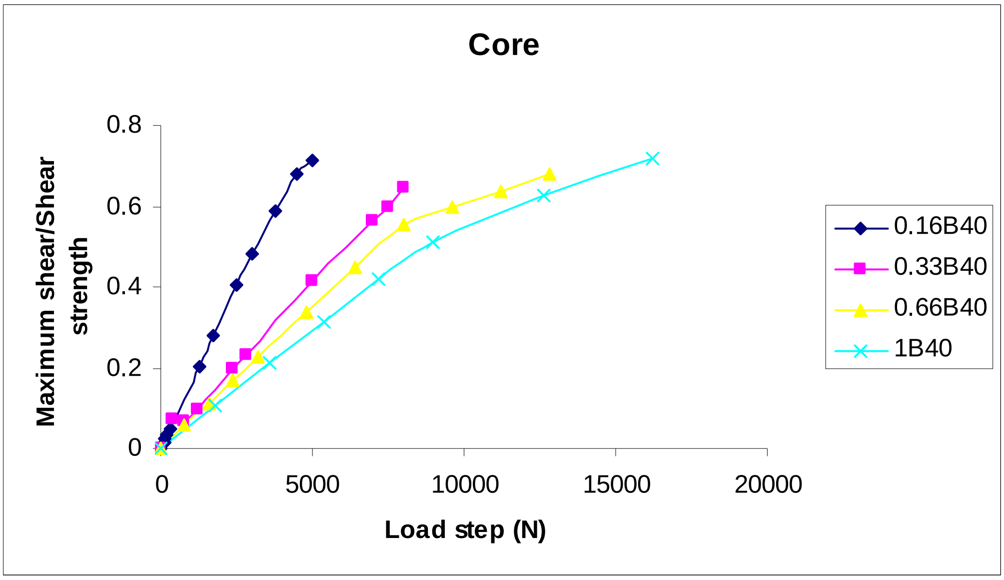

Figure A-3.21 Maximum core shear to shear strength versus load with variation load size ratio at thickness 40mm and material B

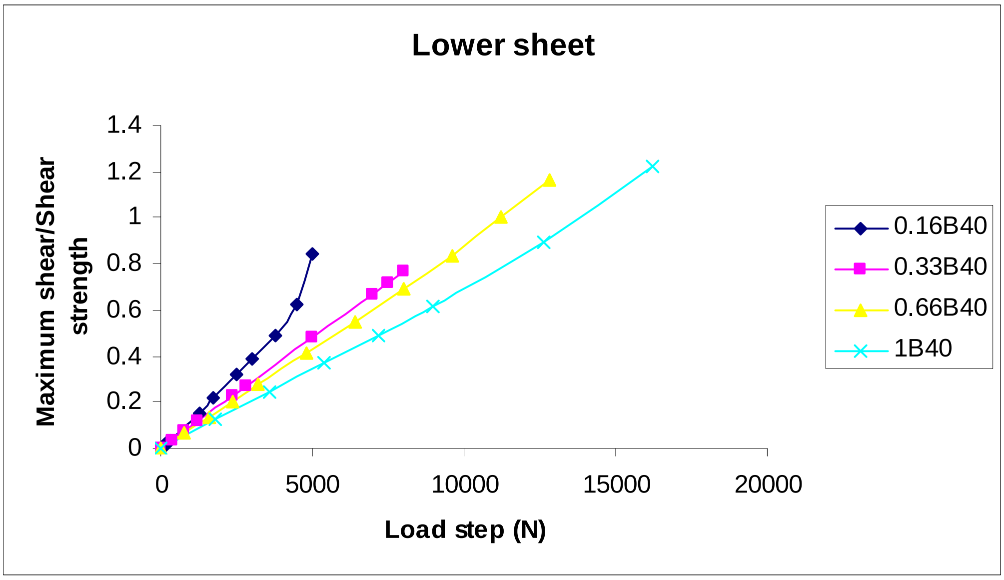

Figure A-3.22 Maximum lower sheet shear versus load with variation of load size ratio at thickness 40mm and material B

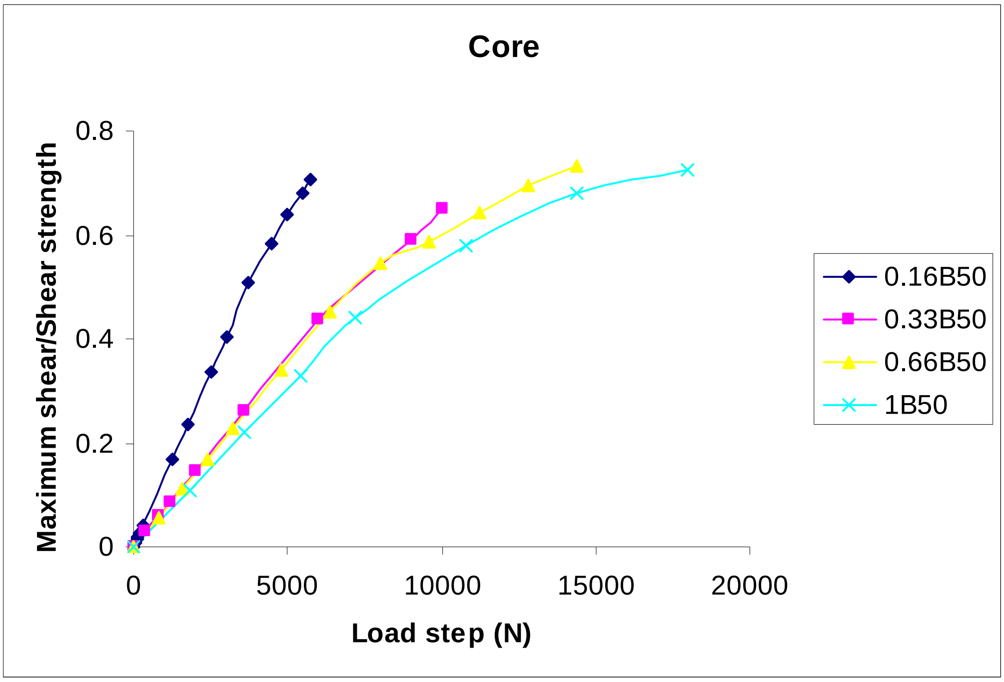

Figure A-3.23 Maximum core shear to shear strength versus load with variation of load size ratio at thickness 50mm and material B

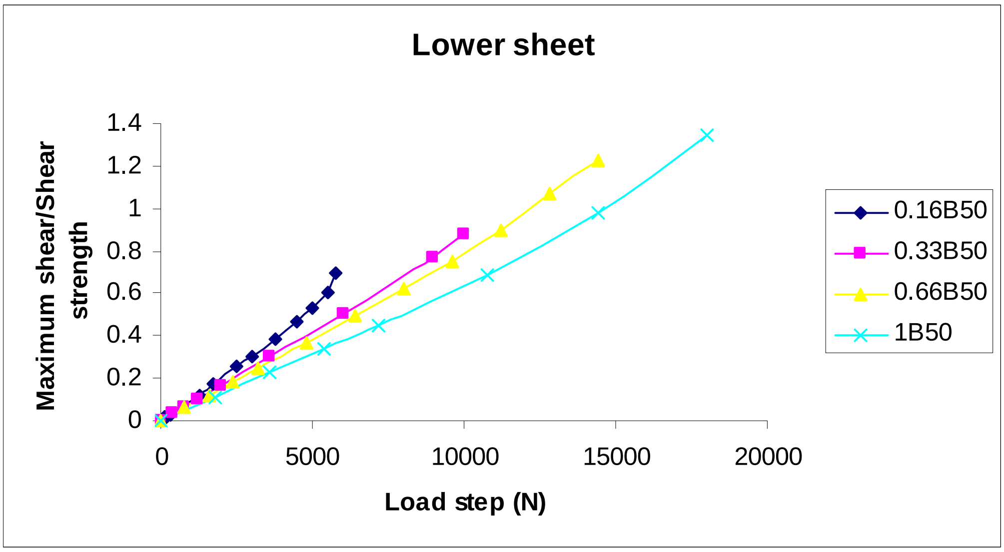

Figure A-3.24 Maximum lower sheet shear to shear strength versus load with variation of load size ratio at thickness 50mm and material B

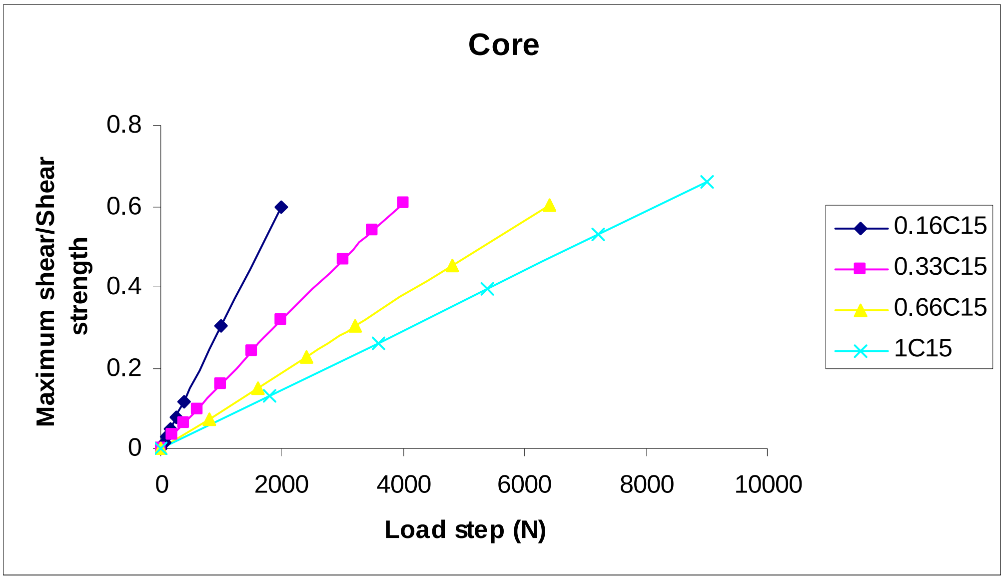

Figure A-3.25 Maximum core shear to shear strength versus load with variation of load size ratio at thickness 15mm and material C

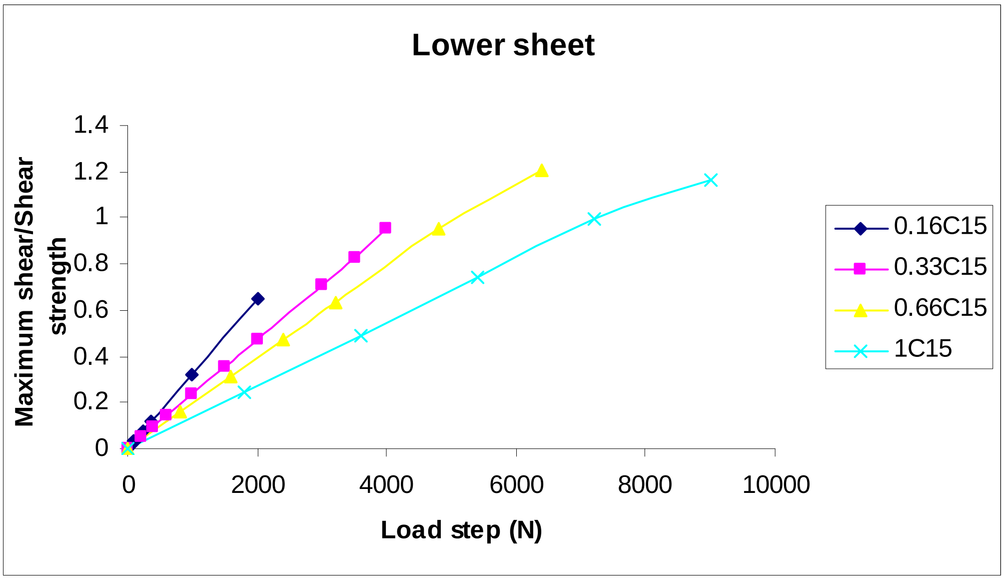

Figure A-3.26 Maximum lower sheet shear to shear strength versus load with variation of load size ratio at thickness 15mm and material C

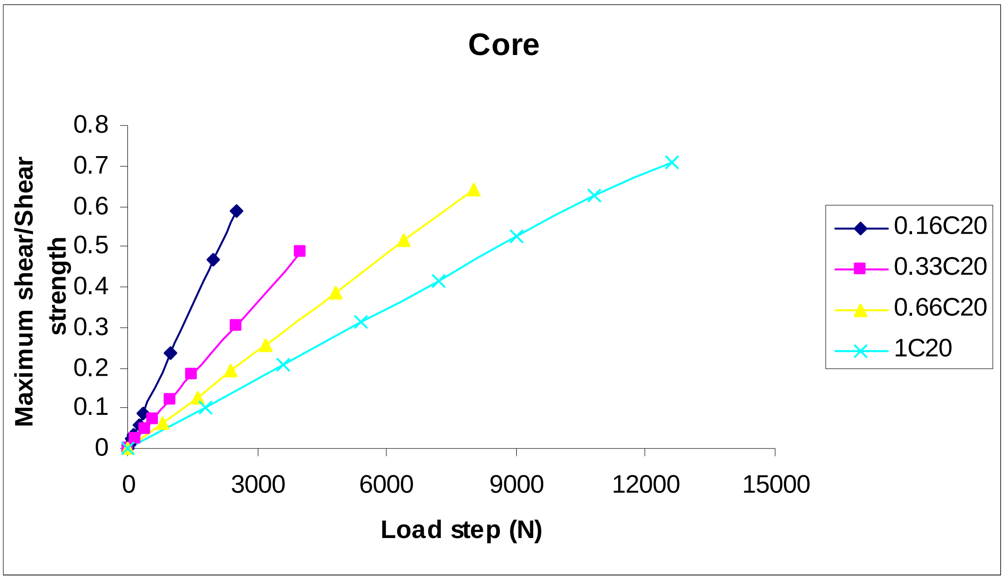

Figure A-3.27 Maximum core shear to shear strength versus load with variation of load size ratio at thickness 20mm and material C

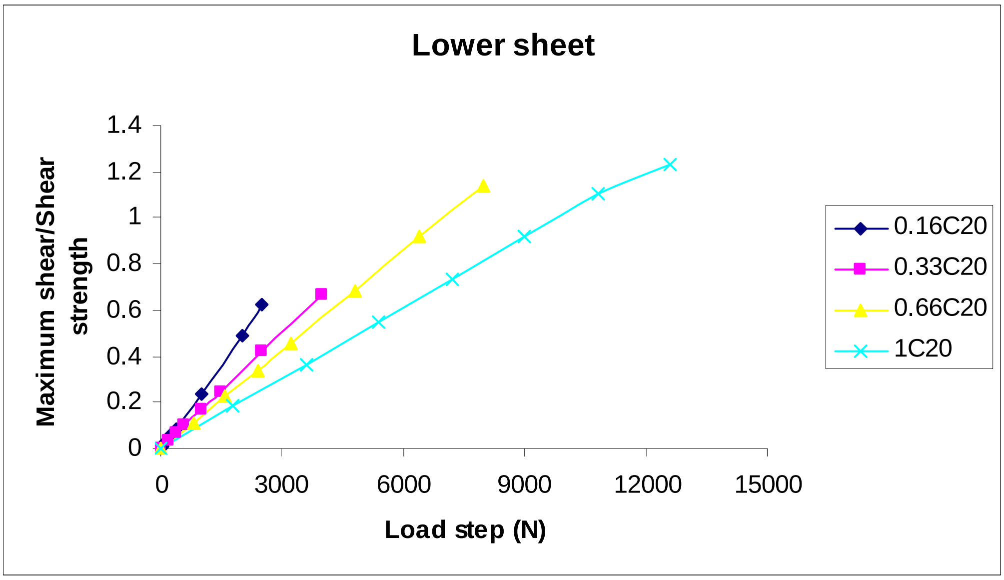

Figure A-3.28 Maximum lower sheet shear to shear strength versus load with variation of load size ratio at thickness 20mm and material C

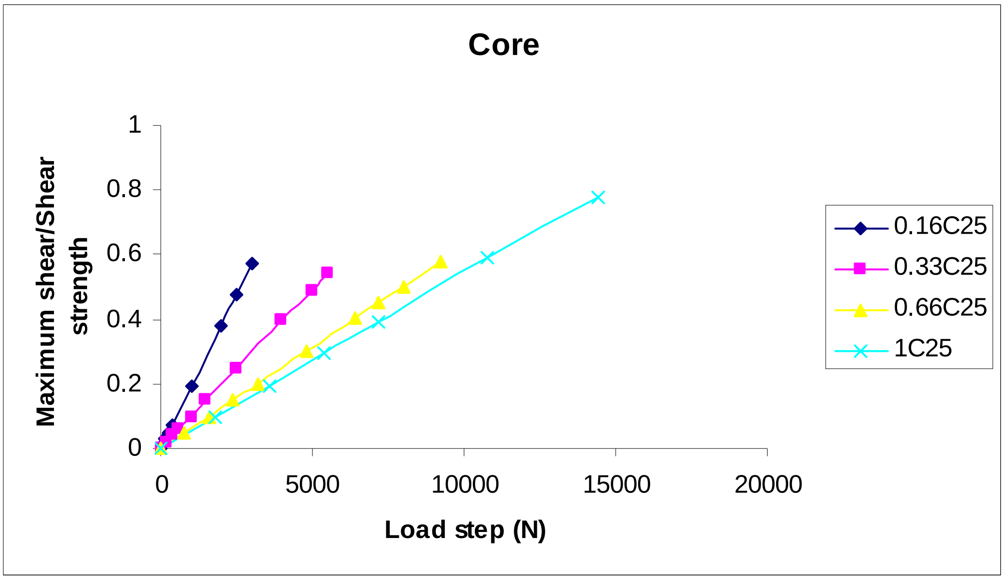

Figure A-3.30 Maximum core shear to shear strength versus load with variation of load size ratio at thickness 25mm and material C

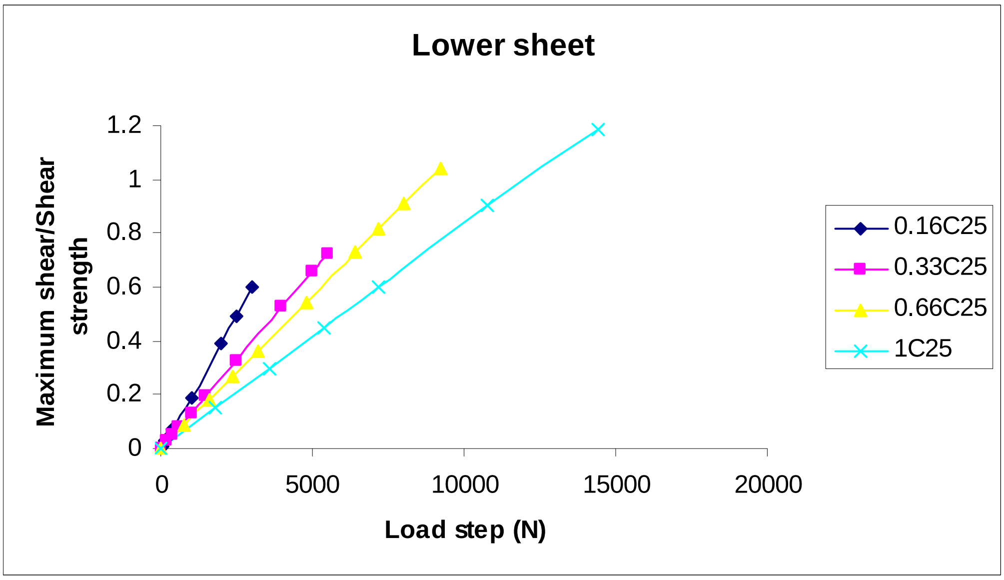

Figure A-3.31 Maximum lower sheet shear to shear strength versus load with variation of load size ratio at thickness 25mm and material C

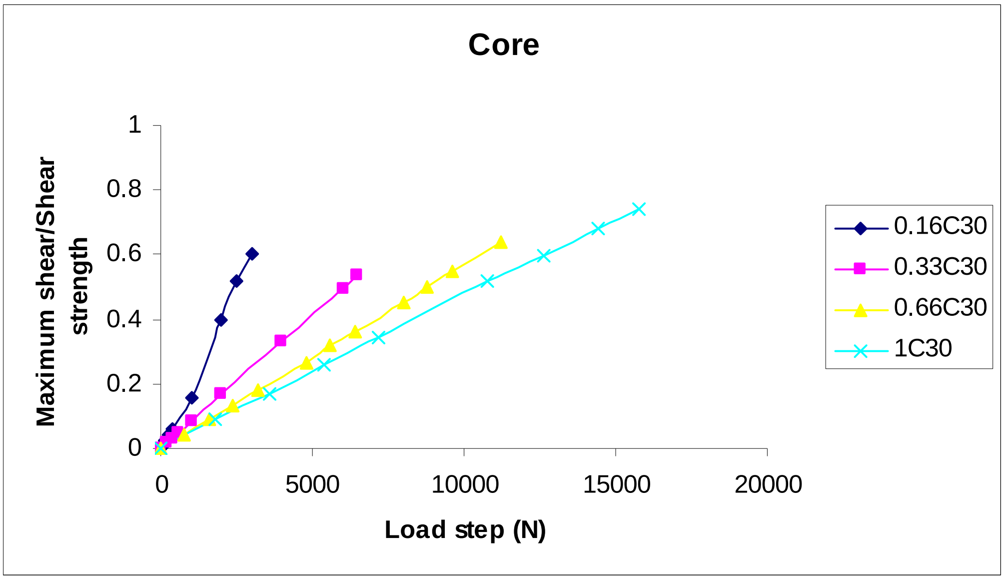

Figure A-3.31 Maximum core shear to shear strength versus load with variation of load size ratio at thickness 30mm and material C

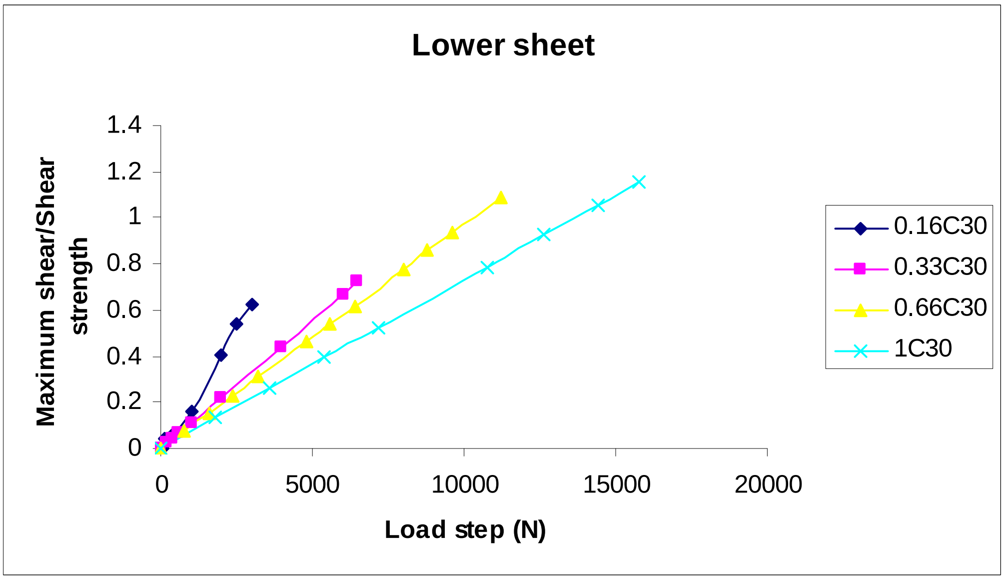

Figure A-3.32 Maximum lower sheet shear to shear strength versus load with variation of load size ratio at thickness 30mm and material C

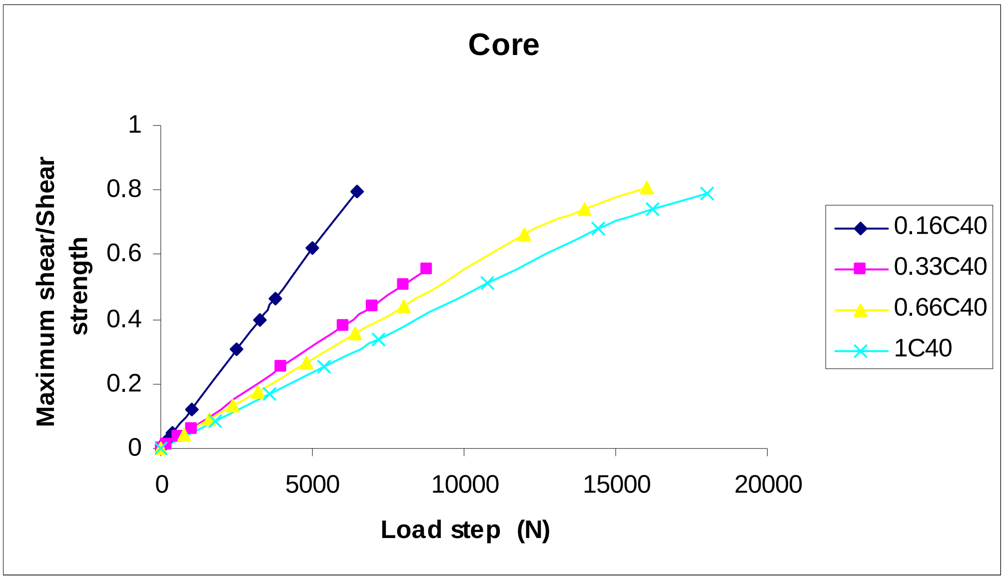

M
Figure A-3.33 Maximum core shear to shear strength versus load with variation of load size ratio at thickness 40mm and material C

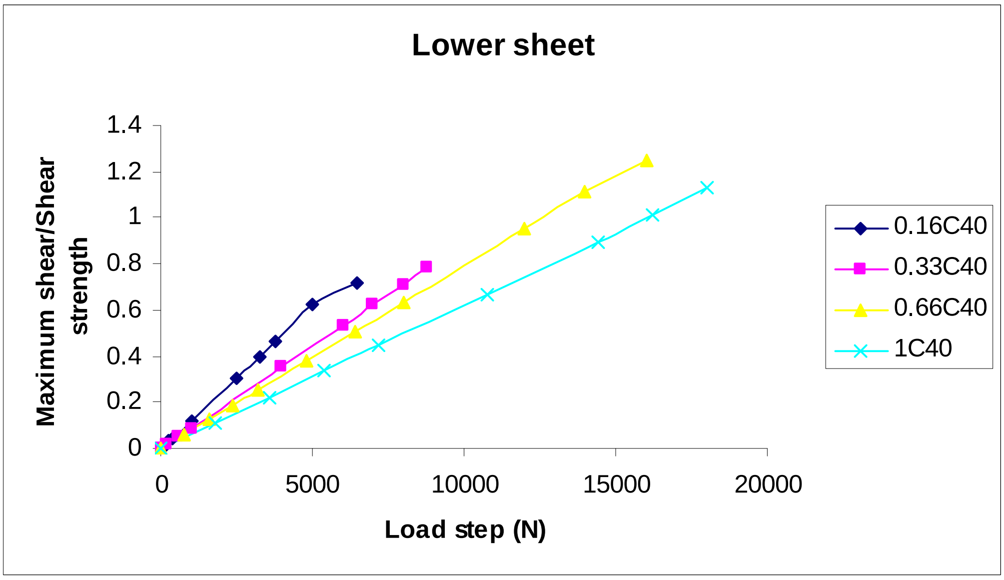

Figure A-3.34 Maximum lower sheet shear to shear strength versus load with variation of load size ratio at thickness 40mm and material C

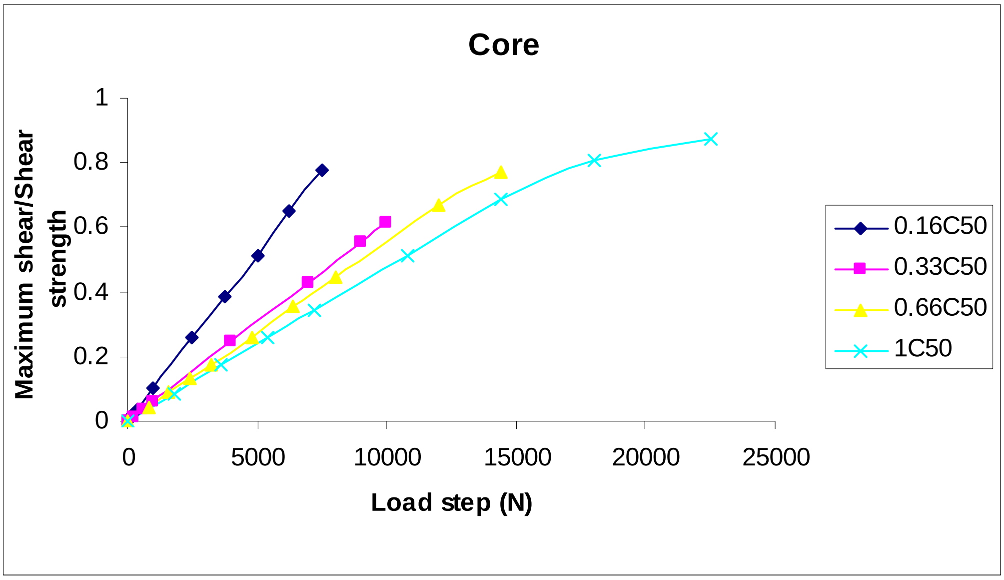

Figure A-3.35 Maximum core shear to shear strength versus load with variation of load size ratio at thickness 50mm and material C

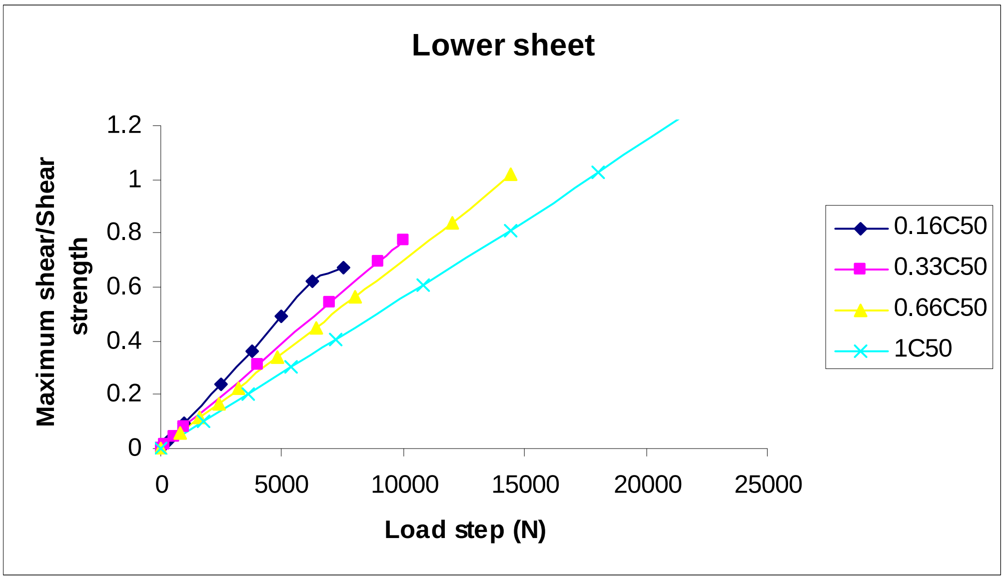

Figure A-3.36 Maximum lower sheet shear to shear strength versus load with variation of load size ratio at thickness 50mm and material

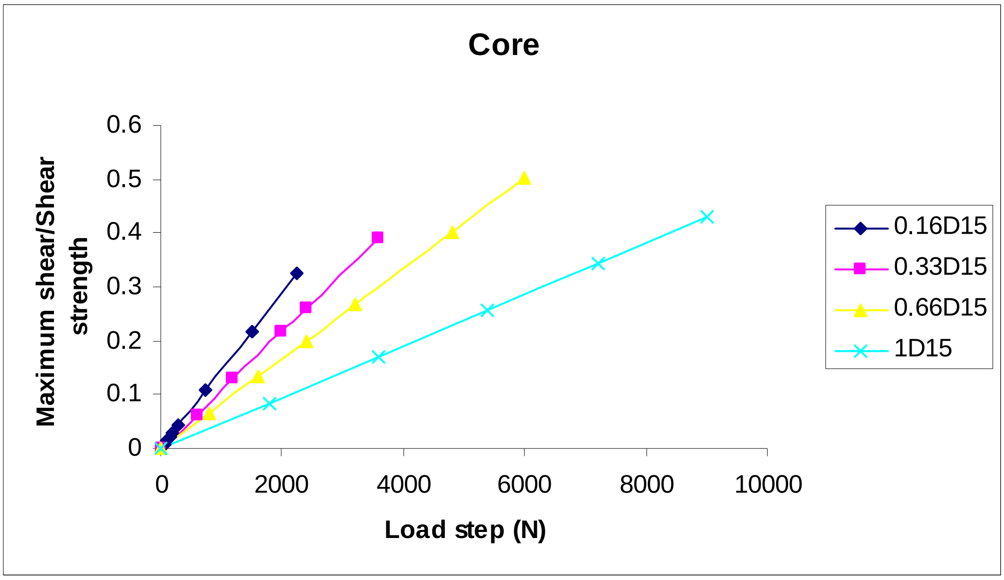

Figure A-3.37 Maximum core shear to shear strength versus load with variation of load size ratio at thickness 15mm and material D

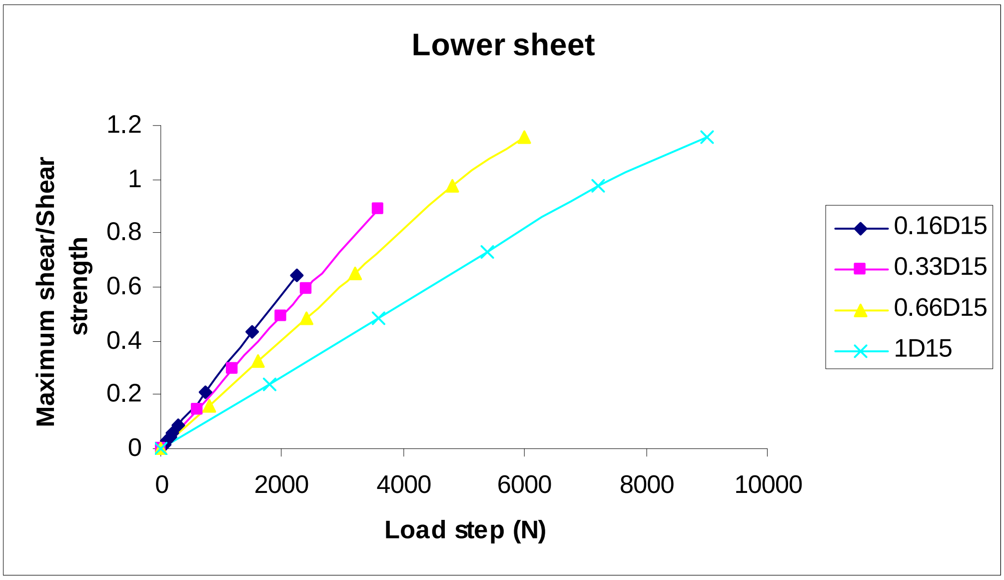

Figure A-3.38 Maximum lower sheet shear to shear strength versus load with variation of load size ratio at thickness 15mm and material D

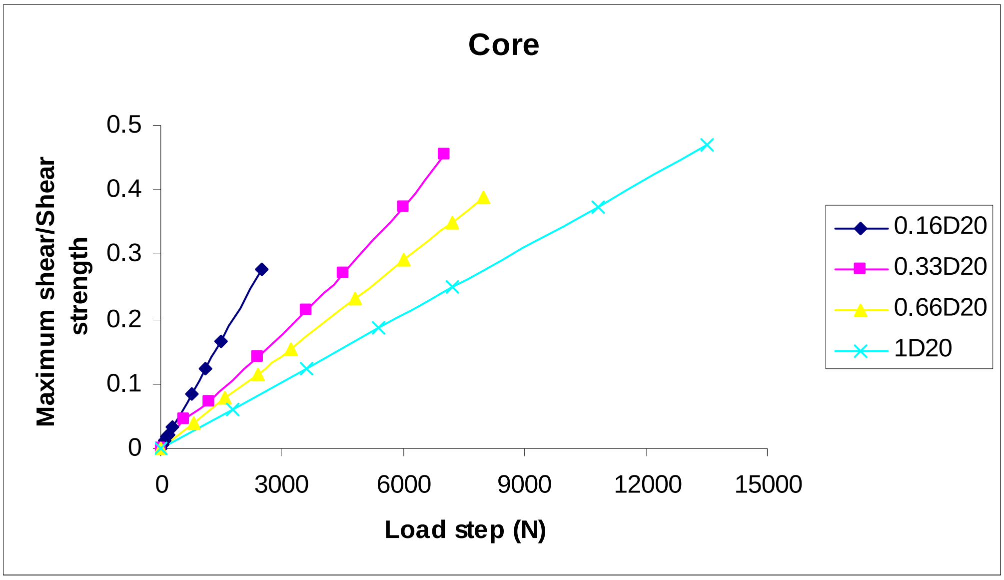

Figure A-3.39 Maximum core shear to shear strength versus load with variation of load size ratio at thickness 20mm and material D

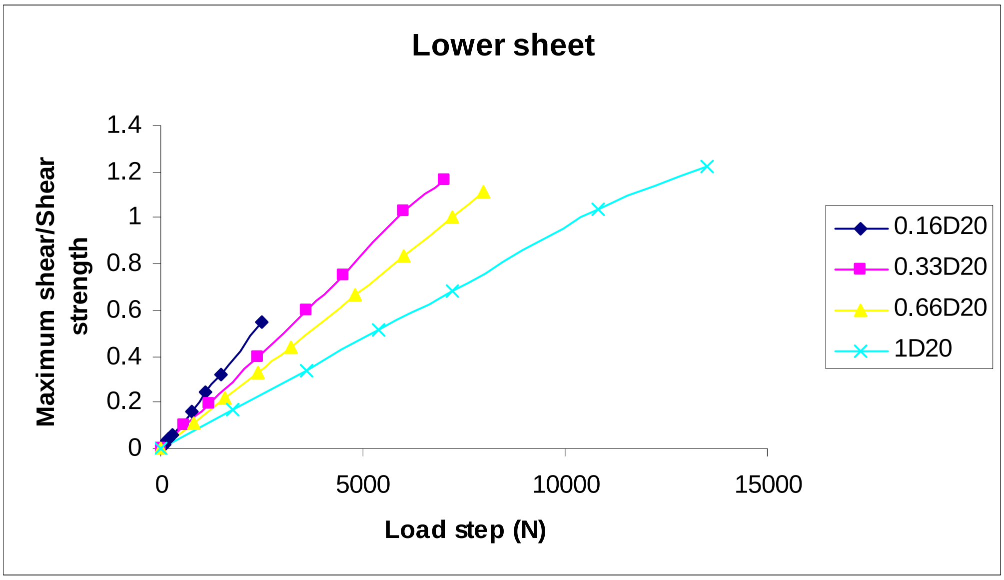

Figure A-3.40 Maximum lower sheet shear to shear strength versus load with variation of load size ratio at thickness 20mm and material D

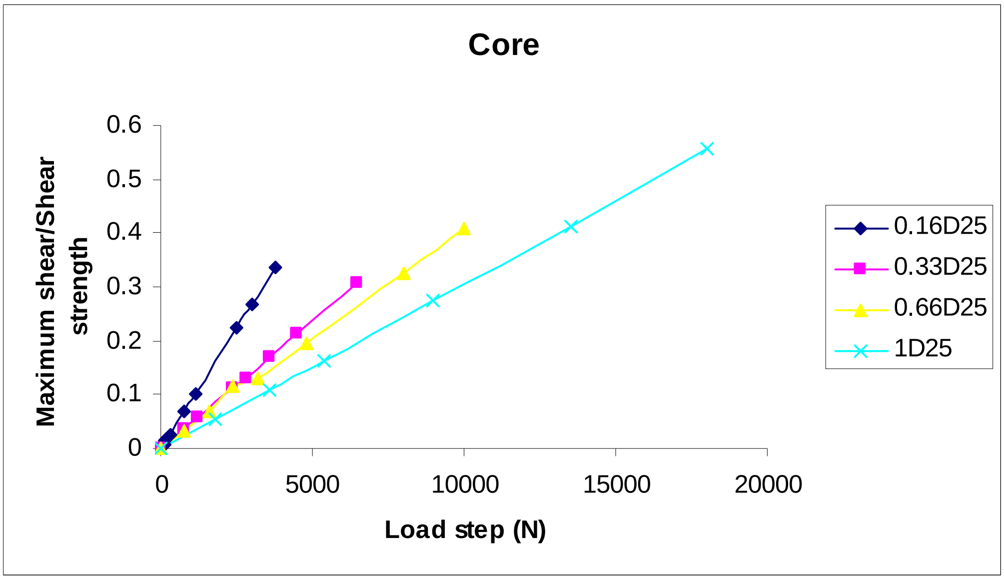

Figure A-3.41 Maximum core shear to shear strength versus load with variation of load size ratio at thickness 25mm and material D

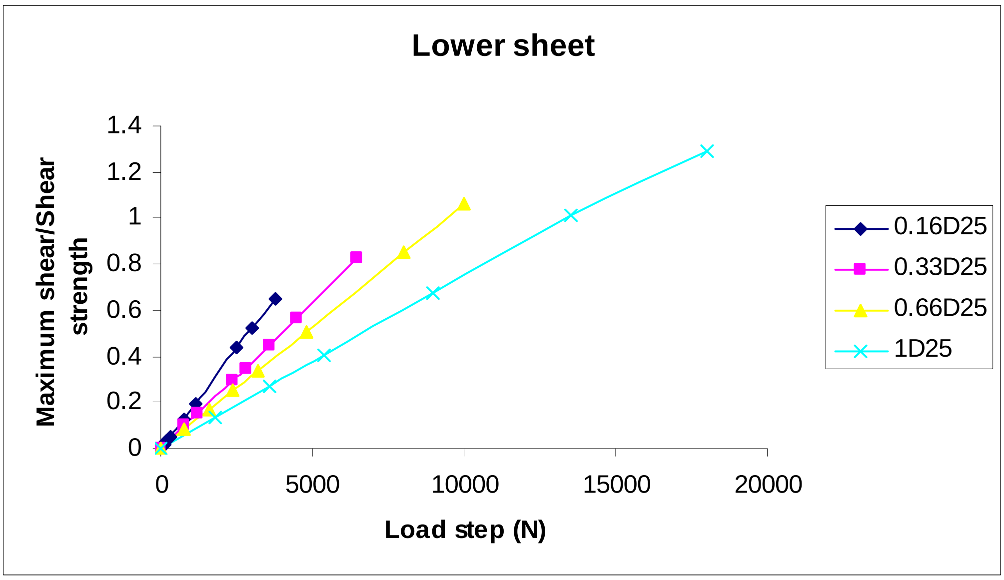

Figure A-3.42 Maximum lower sheet shear to shear strength versus load with variation of load size ratio at thickness 25mm and material D

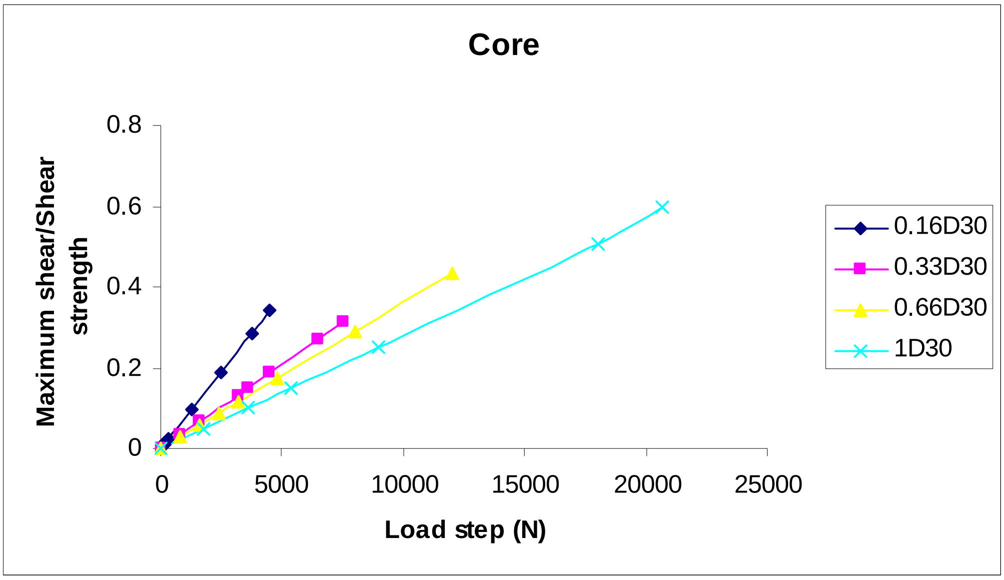

Figure A-3.43 Maximum core shear to shear strength versus load with variation of load size ratio at thickness 30mm and material D

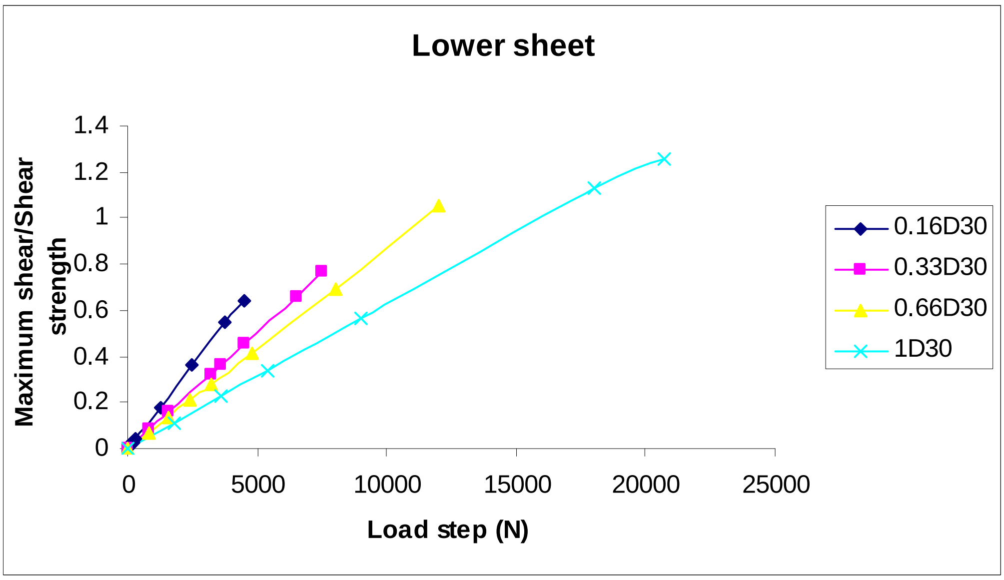

Figure A-3.44 Maximum lower sheet shear to shear strength versus load with variation of load size ratio at thickness 30mm and material D

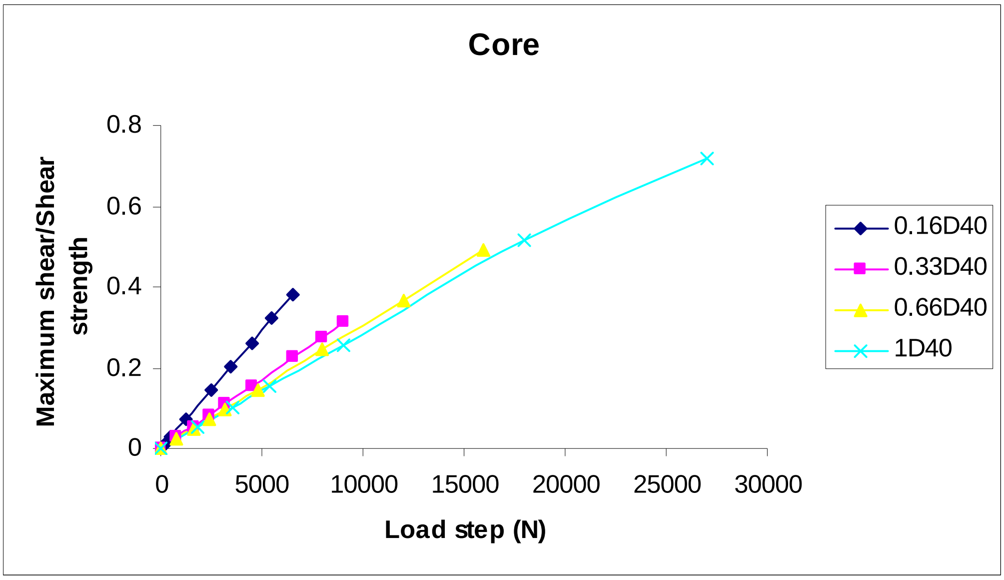

Figure A-3.45 Maximum core shear to shear strength versus load with variation of load size ratio at thickness 40mm and material D

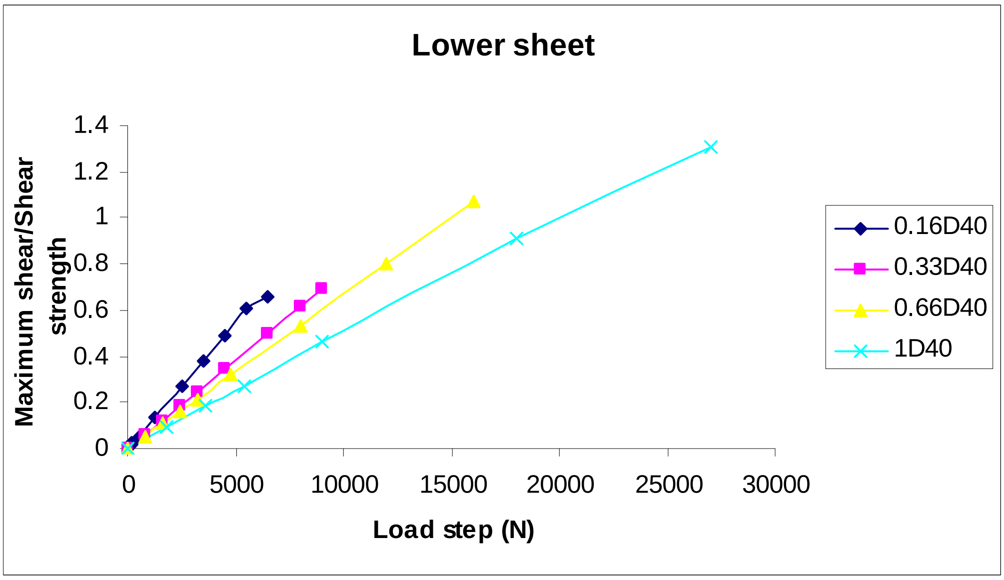

Figure A-3.46 Maximum lower sheet shear to shear strength versus load with variation of load size ratio at thickness 40mm and material D

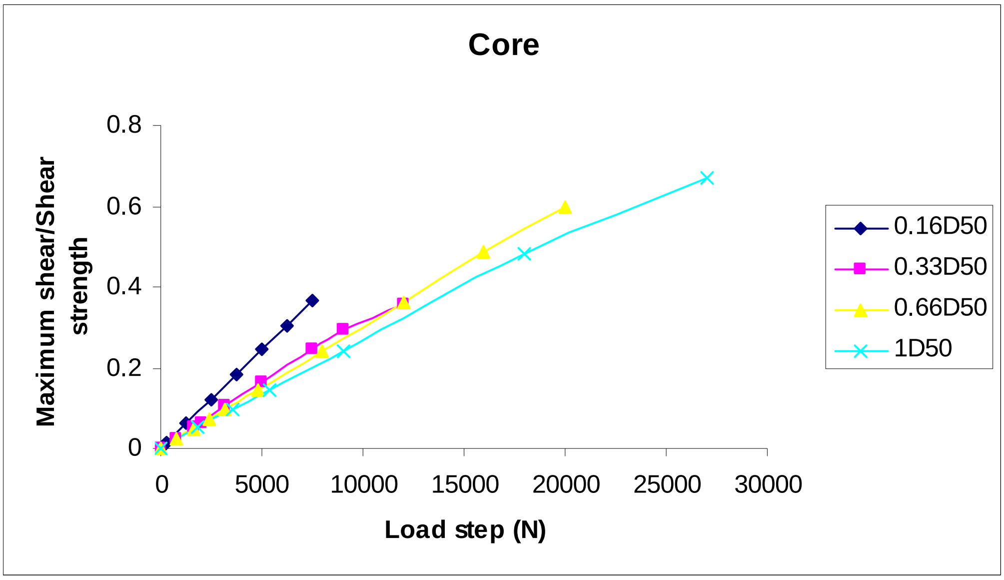

Figure A-3.47 Maximum core shear to shear strength versus load with variation of load size ratio at thickness 50mm and material D

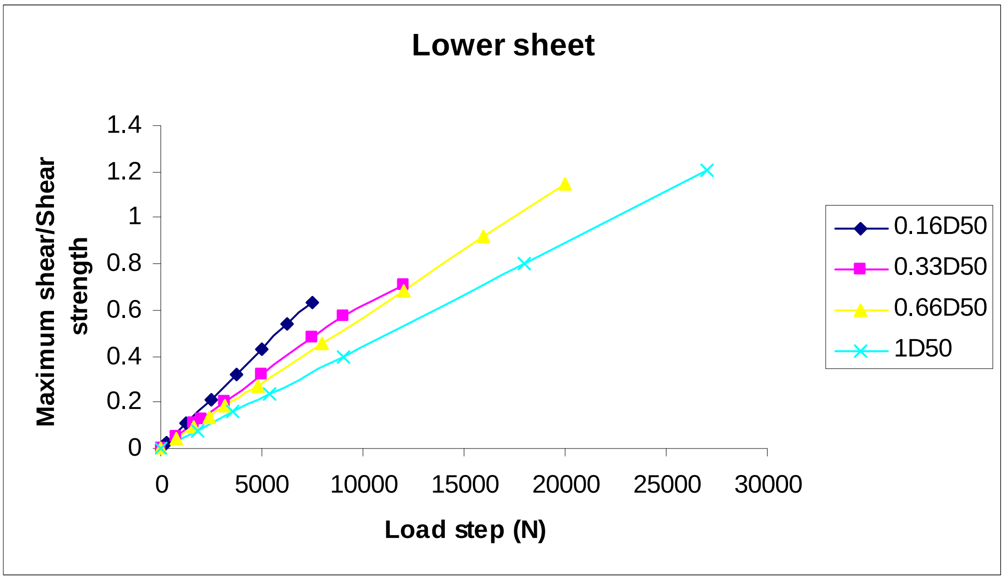

Figure A-3.48 Maximum lower sheet shear to shear strength versus load step with variation of load size ratio at thickness 50mm and material D

APPENDIX B

Tabulated results

Three main variables are investigated; core thickness, load-area-size and different core materials modulus. The following components are tabulated for each variation in the above parameters: maximum shear stress to shear strength ratio, core layer, and lower face sheet layer with load step in (kPa). Where the yellow color means that the core material is entering to the plastic range , the rose color means that the face sheet material is entering to the plastic range, the green color means that both core and sheet material are entering to the plastic range otherwise (no filling color) the core and sheets material are in the elastic range.

Table B-1.1. Maximum shear to shear strength ratio for core and lower sheet material at different load step for material A, load size ratio 0.16 with variation of thickness.

0.16A15		
loadstep(kPa)	TmaxC/Tyc	TmaxL/Tys
0	0	0
20	0.0662222	0.0239167
40	0.1324444	0.0488333
60	0.198	0.0746667
80	0.2622222	0.1016667
120	0.3888889	0.1566667
200	0.6222222	0.2683333
400	0.8311111	0.5741667
600	0.8444444	0.7783333

0.16A20		
loadstep(kPa)	TmaxC/Tyc	TmaxL/Tys
0	0	0
20	0.05155556	0.01833333
40	0.10311111	0.03725
60	0.15466667	0.05675
80	0.206	0.07675
120	0.30666667	0.11833333
200	0.50222222	0.205
500	0.83333333	0.5975
700	0.84666667	0.78333333

0.16A25		
loadstep(kPa)	TmaxC/Tyc	TmaxL/Tys
0	0	0
20	0.042222	0.01491667
40	0.084444	0.03016667
60	0.126667	0.04591667
80	0.168667	0.06191667
120	0.264444	0.095
200	0.417778	0.16416667
500	0.828889	0.45416667
700	0.842222	0.74833333

0.16A30		
loadstep(kPa)	TmaxC/Tyc	TmaxL/Tys
0	0	0
20	0.035556	0.01258333
40	0.071111	0.02541667
60	0.106667	0.03858333
80	0.142222	0.05191667
120	0.213111	0.07941667
200	0.353333	0.13666667
500	0.82	0.37
700	0.835556	0.63333333
900	0.848889	0.78416667

0.16A40		
loadstep(kPa)	TmaxC/Tyc	TmaxL/Tys
0	0	0
20	0.0268889	0.009583333
40	0.054	0.01925
60	0.0808889	0.029083333
80	0.1077778	0.039083333
120	0.1617778	0.059416667
200	0.2688889	0.101666667
500	0.66	0.273333333
700	0.8288889	0.405833333
900	0.8377778	0.6525
1000	0.8422222	0.750833333

0.16A50		
loadstep(kPa)	TmaxC/Tyc	TmaxL/Tys
0	0	0.00E+00
20	0.0226667	7.95E-03
40	0.0453333	1.59E-02
60	0.068	2.38E-02
80	0.0908889	3.18E-02
120	0.1364444	4.78E-02
200	0.2266667	7.97E-02
500	0.5644444	2.10E-01
700	0.7822222	3.03E-01
900	0.8288889	4.41E-01
1000	0.8333333	5.58E-01
1200	0.8444444	7.34E-01

Table B-1.2. Maximum shear to shear strength ratio for core and lower sheet material at different load step for material B, load size ratio 0.16 with variation of thickness.

0.16B15		
loadstep(kPa)	TmaxC/Tyc	TmaxL/Tys
0	0	0
20	0.0198125	0.0099167
40	0.0396875	0.03125
60	0.0595625	0.0470833
80	0.079375	0.0625
120	0.119375	0.0991667
300	0.2975	0.2466667
450	0.44375	0.3791667
600	0.568125	0.5166667
900	0.70625	0.8041667

0.16B20		
loadstep(kPa)	TmaxC/Tyc	TmaxL/Tys
0	0	0
20	0.01525	0.01183333
40	0.0305	0.02366667
60	0.0458125	0.03566667
80	0.0610625	0.04766667
120	0.091875	0.07191667
300	0.229375	0.18416667
450	0.34375	0.28166667
600	0.4575	0.38166667
900	0.64375	0.59833333

0.16B25		
loadstep(kPa)	TmaxC/Tyc	TmaxL/Tys
0	0	0
20	0.012375	0.00958333
40	0.02475	0.01916667
60	0.036875	0.02875
80	0.0495	0.03841667
120	0.074375	0.05791667
300	0.185625	0.1475
450	0.27875	0.22416667
750	0.464375	0.38416667
1000	0.59625	0.525
1200	0.6875	0.685

0.16B30		
loadstep(kPa)	TmaxC/Tyc	TmaxL/Tys
0	0	0
20	0.010375	0.00803333
40	0.020688	0.01608333
60	0.031063	0.02416667
80	0.041438	0.03225
120	0.062125	0.04858333
500	0.26	0.20833333
700	0.36375	0.29583333
1000	0.52	0.43083333
1200	0.603125	0.5275
1500	0.7	0.76833333

0.16B40		
loadstep(kPa)	TmaxC/Tyc	TmaxL/Tys
0	0	0
20	0.008	0.006091667
40	0.016	0.012166667
60	0.024	0.018333333
80	0.032	0.024416667
120	0.048	0.03675
500	0.200625	0.155833333
700	0.28125	0.220833333
1000	0.403125	0.319166667
1200	0.48375	0.386666667
1500	0.585625	0.4925
1800	0.68125	0.623333333
2000	0.7125	0.841666667

0.16B50		
loadstep(kPa)	TmaxC/Tyc	TmaxL/Tys
0	0	0
20	0.0066875	0.004858333
40	0.013375	0.00975
60	0.02	0.014583333
80	0.0266875	0.0195
120	0.0400625	0.02925
500	0.1675	0.123333333
700	0.235	0.174166667
1000	0.336875	0.251666667
1200	0.405	0.3
1500	0.5075	0.383333333
1800	0.5825	0.468333333
2000	0.6375	0.5325
2200	0.68125	0.608333333
2300	0.70625	0.691666667

Table B-1.3. Maximum shear to shear strength ratio for core and lower sheet material at different load step for material C, load size ratio 0.16 with variation of thickness.

0.16C15		
loadstep(kPa)	TmaxC/Tyc	TmaxL/Tys
0	0	0
20	0.0152857	0.0149167
40	0.0305238	0.03
60	0.0458095	0.0451667
100	0.0761905	0.0758333
150	0.1147619	0.115
400	0.3052381	0.3175
800	0.6	0.6533333

0.16C20		
loadstep(kPa)	TmaxC/Tyc	TmaxL/Tys
0	0	0
20	0.01171429	0.01133333
40	0.02347619	0.02275
60	0.03519048	0.03425
100	0.05857143	0.05733333
150	0.08809524	0.08666667
400	0.2352381	0.23666667
800	0.46904762	0.49
1000	0.58571429	0.62166667

0.16C25		
loadstep(kPa)	TmaxC/Tyc	TmaxL/Tys
0	0	0
20	0.009476	0.00916667
40	0.019	0.01841667
60	0.028524	0.02758333
100	0.047524	0.04616667
150	0.071429	0.0695
400	0.190476	0.18916667
800	0.380952	0.38833333
1000	0.47619	0.49166667
1200	0.571429	0.59666667

0.16C30		
loadstep(kPa)	TmaxC/Tyc	TmaxL/Tys
0	0	0
20	0.007952	0.00013917
40	0.015905	0.01541667
60	0.023857	0.04175
100	0.039762	0.03875
150	0.059524	0.05833333
400	0.159524	0.1575
1000	0.399048	0.40666667
1300	0.519048	0.53666667
1500	0.6	0.62416667
1800	0.719048	0.68083333

0.16C40		
loadstep(kPa)	TmaxC/Tyc	TmaxL/Tys
0	0	0
20	0.0060952	0.00585
40	0.0122381	0.011666667
60	0.0183333	0.017583333
100	0.0305714	0.029916667
150	0.0458571	0.044083333
400	0.122381	0.118333333
1000	0.307619	0.3025
1300	0.4004762	0.3975
1500	0.4628571	0.461666667
2000	0.6190476	0.625
2600	0.7952381	0.715833333

0.16C50		
loadstep(kPa)	TmaxC/Tyc	TmaxL/Tys
0	0	0
20	0.0050952	0.004675
40	0.0101429	0.009333333
60	0.0152381	0.014
100	0.0254286	0.023416667
150	0.0381429	0.035166667
400	0.1019048	0.094166667
1000	0.2561905	0.239166667
1500	0.3857143	0.363333333
2000	0.5142857	0.49
2500	0.647619	0.619166667
3000	0.7761905	0.670833333

Table B-1.4. Maximum shear to shear strength ratio for core and lower sheet material at different load step for material D, load size ratio 0.16 with variation of thickness.

0.16D15		
loadstep(kPa)	TmaxC/Tyc	TmaxL/Tys
0	0	0
20	0.0072889	0.0138333
40	0.0145556	0.0276667
60	0.0218444	0.0415833
80	0.0291111	0.0555833
120	0.0437778	0.0833333
300	0.1093333	0.2125
600	0.2186667	0.4358333
900	0.3266667	0.6466667

0.16D20		
loadstep(kPa)	TmaxC/Tyc	TmaxL/Tys
0	0	0
20	0.00553333	0.0105
40	0.01106667	0.021
60	0.01662222	0.0315
80	0.02215556	0.042
120	0.03333333	0.06316667
300	0.08311111	0.15916667
450	0.12488889	0.24083333
600	0.16644444	0.32416667
1000	0.27777778	0.55

0.16D25		
loadstep(kPa)	TmaxC/Tyc	TmaxL/Tys
0	0	0
20	0.004467	0.00841667
40	0.008911	0.01691667
60	0.013378	0.02533333
80	0.017844	0.03383333
120	0.026667	0.05075
300	0.066889	0.1275
450	0.100444	0.1925
1000	0.224444	0.43583333
1200	0.268889	0.52666667
1500	0.335556	0.64583333

0.16D30		
loadstep(kPa)	TmaxC/Tyc	TmaxL/Tys
0	0	0
20	0.003756	0.00706667
40	0.007511	0.01416667
60	0.011267	0.02125
80	0.015022	0.02833333
120	0.022444	0.0425
500	0.094	0.17916667
1000	0.188444	0.36166667
1500	0.282222	0.54916667
1800	0.34	0.64333333

0.16D40		
loadstep(kPa)	TmaxC/Tyc	TmaxL/Tys
0	0	0
20	0.0028889	0.005325
40	0.0035556	0.010666667
60	0.0086889	0.016
80	0.0115778	0.021333333
200	0.0288889	0.053333333
500	0.0724444	0.134166667
1000	0.1453333	0.27
1400	0.2037778	0.38
1800	0.2622222	0.491666667
2200	0.3222222	0.604166667
2600	0.38	0.66

0.16D50		
loadstep(kPa)	TmaxC/Tyc	TmaxL/Tys
0	0	0
20	0.0024222	0.004233333
40	0.0048222	0.0085
60	0.0072444	0.01275
80	0.0096444	0.016916667
120	0.0144889	0.025416667
500	0.0604444	0.106666667
1000	0.1211111	0.214166667
1500	0.1822222	0.3225
2000	0.2444444	0.431666667
2500	0.3044444	0.5425
3000	0.3666667	0.635833333

Table B-1.5. Maximum shear to shear strength ratio for core and lower sheet material at different load step for material A, load size ratio 0.33 with variation of thickness.

0.33A15		
loadstep(kPa)	TmaxC/Tyc	TmaxL/Tys
0	0	0
20	0.1435556	0.0639167
40	0.2844444	0.1291667
60	0.42	0.1941667
80	0.5466667	0.2583333
120	0.7733333	0.3841667
160	0.8266667	0.5008333
200	0.8333333	0.6041667
240	0.8377778	0.68

0.33A20		
loadstep(kPa)	TmaxC/Tyc	TmaxL/Tys
0	0	0
20	0.11044444	0.05033333
40	0.22044444	0.10166667
60	0.32888889	0.1525
80	0.43555556	0.20333333
120	0.63333333	0.30583333
160	0.81777778	0.40583333
200	0.82666667	0.50166667
240	0.83555556	0.59
280	0.84	0.68166667
320	0.84444444	0.73916667

0.33A25		
loadstep(kPa)	TmaxC/Tyc	TmaxL/Tys
0	0	0
20	0.089778	0.04325
40	0.179556	0.08666667
60	0.268889	0.13083333
80	0.357778	0.17416667
120	0.528889	0.2625
160	0.691111	0.35
200	0.82	0.43666667
240	0.831111	0.52
280	0.837778	0.6
320	0.844444	0.6825
380	0.851111	0.7525

0.33A30		
loadstep(kPa)	TmaxC/Tyc	TmaxL/Tys
0	0	0
20	0.075556	0.03891667
40	0.150889	0.07808333
60	0.226667	0.1175
100	0.375556	0.19583333
160	0.591111	0.31416667
220	0.797778	0.43166667
300	0.835556	0.58416667
380	0.848889	0.7225

0.33A40		
loadstep(kPa)	TmaxC/Tyc	TmaxL/Tys
0	0	0
20	0.0571111	0.034166667
40	0.1142222	0.068416667
60	0.1713333	0.1025
100	0.2844444	0.171666667
160	0.4533333	0.274166667
220	0.62	0.3775
300	0.82	0.513333333
400	0.8422222	0.680833333
600	0.8666667	1.016666667

0.33A50		
loadstep(kPa)	TmaxC/Tyc	TmaxL/Tys
0	0	0
20	0.0462222	0.031583333
40	0.0924444	0.06325
60	0.1397778	0.095
100	0.2311111	0.158333333
160	0.3688889	0.253333333
220	0.5066667	0.348333333
300	0.6866667	0.474166667
470	0.84	0.743333333
560	0.8711111	0.916666667

Table B-1.6. Maximum shear to shear strength ratio for core and lower sheet material at different load step for material B, load size ratio 0.33 with variation of thickness.

0.33B15		
loadstep(kPa)	TmaxC/Tyc	TmaxL/Tys
0	0	0
20	0.041625	0.0465
40	0.083125	0.0933333
80	0.166875	0.1875
120	0.249375	0.2825
240	0.48875	0.5666667
260	0.526875	0.6141667
280	0.555	0.6608333
300	0.58375	0.7066667

0.33B20		
loadstep(kPa)	TmaxC/Tyc	TmaxL/Tys
0	0	0
20	0.070625	0.03341667
40	0.06375	0.06891667
60	0.095625	0.10083333
120	0.19125	0.20166667
200	0.31875	0.33833333
240	0.381875	0.40666667
300	0.46875	0.51
360	0.556875	0.6125
400	0.60875	0.68083333

0.33B25		
loadstep(kPa)	TmaxC/Tyc	TmaxL/Tys
0	0	0
20	0.02575	0.02683333
40	0.0515	0.05366667
60	0.0775	0.08058333
120	0.155	0.16166667
240	0.309375	0.325
300	0.386875	0.4
350	0.450625	0.47583333
400	0.514375	0.545
450	0.565625	0.6125
500	0.621875	0.6825

0.33B30		
loadstep(kPa)	TmaxC/Tyc	TmaxL/Tys
0	0	0
40	0.0725	0.046
120	0.13	0.13833333
240	0.26	0.27833333
320	0.34625	0.37166667
500	0.539375	0.5825
550	0.580625	0.64166667
580	0.610625	0.6775
610	0.6375	0.71333333

0.33B40		
loadstep(kPa)	TmaxC/Tyc	TmaxL/Tys
0	0	0
40	0.07125	0.037916667
80	0.065625	0.075833333
120	0.09875	0.114166667
240	0.1975	0.228333333
280	0.230625	0.265833333
500	0.4125	0.476666667
700	0.56625	0.67
750	0.598125	0.72
800	0.64375	0.770833333

0.33B50		
loadstep(kPa)	TmaxC/Tyc	TmaxL/Tys
0	0	0
40	0.0290625	0.03375
80	0.058125	0.0675
120	0.0875	0.101666667
200	0.145625	0.169166667
360	0.2625	0.304166667
600	0.43875	0.5075
900	0.59	0.7725
1000	0.65	0.875

Table B-1.7. Maximum shear to shear strength ratio for core and lower sheet material at different load step for material C, load size ratio 0.33 with variation of thickness.

0.33C15		
loadstep(kPa)	TmaxC/Tyc	TmaxL/Tys
0	0	0
20	0.0319048	0.0466667
40	0.0638095	0.0933333
60	0.0957143	0.1408333
100	0.1595238	0.2358333
150	0.2390476	0.355
200	0.3171429	0.4741667
300	0.4671429	0.7116667
350	0.5380952	0.83
400	0.6095238	0.95

0.33C20		
loadstep(kPa)	TmaxC/Tyc	TmaxL/Tys
0	0	0
20	0.02438095	0.03283333
40	0.04857143	0.06575
60	0.07333333	0.09916667
100	0.12238095	0.165
150	0.18333333	0.24833333
250	0.3052381	0.42
400	0.48571429	0.66916667
500	0.6	0.84166667

0.33C25		
loadstep(kPa)	TmaxC/Ty	TmaxL/Tys
0	0	0
20	0.019714	0.02583333
40	0.039429	0.05175
60	0.059048	0.07775
100	0.098571	0.13
150	0.148095	0.195
250	0.247143	0.32666667
400	0.394762	0.525
500	0.490476	0.65833333
550	0.542857	0.725

0.33C30		
loadstep(kPa)	TmaxC/Ty	TmaxL/Tys
0	0	0
20	0.016524	0.02183333
40	0.033048	0.04375
60	0.049524	0.06566667
100	0.082857	0.10916667
200	0.165714	0.22
400	0.331429	0.44166667
600	0.495238	0.66583333
650	0.538095	0.72166667

0.33C40		
loadstep(kPa)	TmaxC/Tyc	TmaxL/Tys
0	0	0
20	0.0125238	0.017583333
60	0.037619	0.052833333
100	0.0628571	0.088333333
400	0.2519048	0.353333333
600	0.3785714	0.531666667
700	0.4414286	0.620833333
800	0.5047619	0.71
880	0.5571429	0.7825

0.33C50		
loadstep(kPa)	TmaxC/Tyc	TmaxL/Tys
0	0	0
20	0.0121905	0.015416667
60	0.0365238	0.046333333
100	0.0609524	0.077166667
400	0.2442857	0.309166667
700	0.4290476	0.541666667
900	0.552381	0.6975
1000	0.6138095	0.775833333

Table B-1.8. Maximum shear to shear strength ratio for core and lower sheet material at different load step for material D, load size ratio 0.33 with variation of thickness.

0.33D15		
loadstep(kPa)	TmaxC/Tyc	TmaxL/Tys
0	0	0
60	0.0622222	0.1475
120	0.1286667	0.2958333
200	0.2153333	0.495
240	0.26	0.5941667
360	0.3888889	0.8916667

0.33D20		
loadstep(kPa)	TmaxC/Tyc	TmaxL/Tys
0	0	0
60	0.04555556	0.09833333
120	0.07111111	0.1975
240	0.14288889	0.39833333
360	0.21533333	0.59916667
450	0.27111111	0.75083333
600	0.37333333	1.025
700	0.45555556	1.16666667

0.33D25		
loadstep(kPa)	TmaxC/Tyc	TmaxL/Tys
0	0	0
80	0.036222	0.09916667
120	0.056222	0.14916667
240	0.112667	0.29166667
280	0.131556	0.34916667
360	0.169556	0.45
450	0.212444	0.56333333
650	0.308889	0.8225

0.33D30		
loadstep(kPa)	TmaxC/Tyc	TmaxL/Tys
0	0	0
80	0.032667	0.08041667
160	0.065556	0.16083333
320	0.131556	0.32333333
360	0.148	0.36416667
450	0.185556	0.45583333
650	0.268889	0.66083333
750	0.311111	0.76666667

0.33D40		
loadstep(kPa)	TmaxC/Tyc	TmaxL/Tys
0	0	0
80	0.0273333	0.061333333
160	0.0546667	0.121666667
240	0.082	0.1825
320	0.1095556	0.244166667
450	0.1544444	0.343333333
650	0.2244444	0.4975
800	0.2755556	0.6125
900	0.3111111	0.69

0.33D50		
loadstep(kPa)	TmaxC/Tyc	TmaxL/Tys
0	0	0
80	0.0255556	0.051
160	0.0517778	0.106666667
200	0.0646667	0.1275
320	0.1037778	0.204166667
500	0.1622222	0.32
750	0.2444444	0.48
900	0.2933333	0.576666667
1200	0.3577778	0.705833333

Table B-1.9. Maximum shear to shear strength ratio for core and lower sheet material at different load step for material A, load size ratio 0.66 with variation of thickness.

0.66A15		
loadstep(kPa)	TmaxC/Tyc	TmaxL/Tys
0	0	0
20	0.3222222	0.2283333
40	0.6311111	0.4541667
60	0.8222222	0.6383333
80	0.84	0.7941667
90	0.8466667	0.9
100	0.8533333	1

0.66A20		
loadstep(kPa)	TmaxC/Tyc	TmaxL/Tys
0	0	0
20	0.24666667	0.18166667
40	0.48888889	0.365
60	0.72444444	0.54583333
80	0.82444444	0.675
90	0.83333333	0.7425
100	0.84	0.82916667
120	0.85333333	1.00833333

0.66A25		
loadstep(kPa)	TmaxC/Tyc	TmaxL/Tys
0	0	0
20	0.198222	0.1575
40	0.397778	0.31583333
60	0.613333	0.47333333
80	0.782222	0.62833333
90	0.82	0.69166667
100	0.828889	0.72666667
120	0.842222	0.875
140	0.853333	1.04166667

0.66A30		
loadstep(kPa)	TmaxC/Tyc	TmaxL/Tys
0	0	0
20	0.166	0.1425
40	0.333333	0.285
60	0.497778	0.42833333
80	0.662222	0.57
100	0.817778	0.71
120	0.84	0.79583333
140	0.842222	0.95
145	0.844444	0.99166667

0.66A40		
loadstep(kPa)	TmaxC/Tyc	TmaxL/Tys
0	0	0
20	0.1397778	0.125833333
40	0.2777778	0.251666667
60	0.42	0.3775
80	0.56	0.5025
100	0.6977778	0.626666667
120	0.8022222	0.755
140	0.8666667	0.9
160	0.8666667	1.016666667

0.66A50		
loadstep(kPa)	TmaxC/Tyc	TmaxL/Tys
0	0	0
20	0.142	0.1175
40	0.2844444	0.234166667
60	0.4266667	0.350833333
80	0.5688889	0.4675
100	0.7111111	0.5825
120	0.8044444	0.699166667
140	0.8666667	0.841666667
160	0.8688889	1.008333333
180	0.8711111	1.15

Table B-1.10. Maximum shear to shear strength ratio for core and lower sheet material at different load step for material B, load size ratio 0.66 with variation of thickness.

0.66B15		
loadstep(kPa)	TmaxC/Tyc	TmaxL/Tys
0	0	0
20	0.093125	0.1575
40	0.188125	0.3175
60	0.28375	0.4783333
80	0.379375	0.6391667
90	0.4275	0.7191667
100	0.475	0.7983333
120	0.569375	0.9583333
140	0.65625	1.1083333
160	0.7125	1.2166667

0.66B20		
loadstep(kPa)	TmaxC/Tyc	TmaxL/Tys
0	0	0
20	0.07375	0.115
40	0.148125	0.23166667
60	0.22375	0.34833333
80	0.29875	0.46583333
100	0.375625	0.58333333
120	0.451875	0.70166667
140	0.50625	0.81583333
160	0.56125	0.925
180	0.5975	1.025

0.66B25		
loadstep(kPa)	TmaxC/Tyc	TmaxL/Tys
0	0	0
20	0.059625	0.09333333
40	0.12125	0.1875
60	0.181875	0.2825
80	0.24375	0.3775
120	0.3675	0.56833333
160	0.47875	0.7575
200	0.5675	0.94166667
240	0.6375	1.10833333

0.66B30		
loadstep(kPa)	TmaxC/Tyc	TmaxL/Tys
0	0	0
20	0.060563	0.0815
40	0.12125	0.16333333
60	0.1825	0.245
80	0.24375	0.3275
120	0.366875	0.4925
160	0.49125	0.6575
200	0.58625	0.825
240	0.6375	0.99166667
270	0.66875	1.1

0.66B40		
loadstep(kPa)	TmaxC/Tyc	TmaxL/Tys
0	0	0
20	0.056	0.068416667
40	0.111875	0.136666667
60	0.168125	0.205833333
80	0.224375	0.274166667
120	0.336875	0.411666667
160	0.45	0.549166667
200	0.55375	0.69
240	0.5975	0.833333333
280	0.6375	1
320	0.68125	1.166666667

0.66B50		
loadstep(kPa)	TmaxC/Tyc	TmaxL/Tys
0	0	0
20	0.0564375	0.06175
40	0.113125	0.123333333
60	0.169375	0.185
80	0.22625	0.246666667
120	0.339375	0.37
160	0.453125	0.493333333
200	0.544375	0.619166667
240	0.58625	0.7525
280	0.64375	0.9
320	0.69375	1.066666667
360	0.73125	1.225

Table B-1.11. Maximum shear to shear strength ratio for core and lower sheet material at different load step for material C, load size ratio 0.66 with variation of thickness.

0.66C15		
loadstep(kPa)	TmaxC/Tyc	TmaxL/Tys
0	0	0
20	0.0742857	0.1566667
40	0.15	0.3158333
60	0.2261905	0.4758333
80	0.302381	0.6358333
120	0.4547619	0.95
160	0.6047619	1.2083333

0.66C20		
loadstep(kPa)	TmaxC/Tyc	TmaxL/Tys
0	0	0
20	0.06285714	0.1125
40	0.12666667	0.225
60	0.19047619	0.33916667
80	0.2552381	0.45333333
120	0.3847619	0.68333333
160	0.51428571	0.91666667
200	0.64285714	1.14166667

0.66C25		
loadstep(kPa)	TmaxC/Tyc	TmaxL/Tys
0	0	0
20	0.049524	0.09
40	0.099048	0.18
60	0.149048	0.27
80	0.199048	0.36083333
120	0.3	0.54333333
160	0.401429	0.72666667
180	0.452381	0.81916667
200	0.5	0.90833333
230	0.580952	1.04166667

0.66C30		
loadstep(kPa)	TmaxC/Tyc	TmaxL/Tys
0	0	0
20	0.04481	0.07675
40	0.089524	0.15333333
60	0.134762	0.23083333
80	0.18	0.30833333
120	0.26619	0.4625
140	0.316667	0.54166667
160	0.362381	0.61916667
200	0.45381	0.77583333
220	0.5	0.85833333
240	0.547619	0.93333333
280	0.638095	1.09166667

0.66C40		
loadstep(kPa)	TmaxC/Tyc	TmaxL/Tys
0	0	0
20	0.0439048	0.063083333
40	0.0880952	0.125833333
60	0.1319048	0.189166667
80	0.1761905	0.2525
120	0.2642857	0.379166667
160	0.3528571	0.505833333
200	0.4414286	0.633333333
300	0.6619048	0.95
350	0.7380952	1.116666667
400	0.8047619	1.25

0.66C50		
loadstep(kPa)	TmaxC/Tyc	TmaxL/Tys
0	0	0
20	0.0443333	0.056083333
40	0.0885714	0.1125
60	0.1333333	0.168333333
80	0.177619	0.224166667
120	0.2619048	0.336666667
160	0.3557143	0.449166667
200	0.4447619	0.560833333
300	0.6666667	0.841666667
360	0.7714286	1.016666667

Table B-1.12 .Maximum shear to shear strength ratio for core and lower sheet material at different load step for material D, load size ratio 0.66 with variation of thickness.

0.66D15		
loadstep(kPa)	TmaxC/Tyc	TmaxL/Tys
0	0	0
20	0.0657778	0.1608333
40	0.1322222	0.3233333
60	0.1993333	0.4858333
80	0.2666667	0.65
120	0.4022222	0.975
150	0.5022222	1.1583333

0.66D20		
loadstep(kPa)	TmaxC/Tyc	TmaxL/Tys
0	0	0
20	0.03844444	0.10916667
40	0.07688889	0.21916667
60	0.11555556	0.33
80	0.15444444	0.44083333
120	0.23333333	0.665
150	0.29111111	0.83333333
180	0.34888889	1
200	0.38888889	1.11666667

0.66D25		
loadstep(kPa)	TmaxC/Tyc	TmaxL/Tys
0	0	0
20	0.032222	0.08333333
40	0.068	0.1675
60	0.116222	0.25166667
80	0.129111	0.33583333
120	0.194222	0.50583333
200	0.324444	0.85
250	0.406667	1.06666667

0.66D30		
loadstep(kPa)	TmaxC/Tyc	TmaxL/Tys
0	0	0
20	0.028667	0.06866667
40	0.057333	0.1375
60	0.086222	0.20666667
80	0.115111	0.27583333
120	0.173111	0.415
200	0.288889	0.69416667
300	0.435556	1.05

0.66D40		
loadstep(kPa)	TmaxC/Tyc	TmaxL/Tys
0	0	0
20	0.0242222	0.053166667
40	0.0486667	0.106666667
60	0.0731111	0.16
80	0.0975556	0.213333333
120	0.146	0.32
200	0.2444444	0.534166667
300	0.3666667	0.803333333
400	0.4911111	1.075

0.66D50		
loadstep(kPa)	TmaxC/Tyc	TmaxL/Tys
0	0	0
20	0.024	0.045416667
40	0.048	0.090833333
60	0.0722222	0.136666667
80	0.0962222	0.181666667
120	0.1444444	0.2725
200	0.24	0.455
300	0.3622222	0.683333333
400	0.4844444	0.916666667
500	0.5955556	1.15

Table B-1.13. Maximum shear to shear strength ratio for core and lower sheet material at different load step for material A, load size ratio 1 with variation of thickness.

1A15		
loadstep(kPa)	TmaxC/Tyc	TmaxL/Tys
0	0	0
20	0.5155556	0.3891667
40	0.8311111	0.7925
50	0.8488889	1.0666667

1A20		
loadstep(kPa)	TmaxC/Tyc	TmaxL/Tys
0	0	0
20	0.39777778	0.31916667
40	0.79333333	0.63666667
60	0.84444444	1.075

1A25		
loadstep(kPa)	TmaxC/Tyc	TmaxL/Tys
0	0	0
20	0.328889	0.28083333
40	0.662222	0.56083333
60	0.822222	0.875
80	0.88	1.29166667

1A30		
loadstep(kPa)	TmaxC/Tyc	TmaxL/Tys
0	0	0
20	0.286667	0.2575
40	0.575556	0.51416667
60	0.822222	0.78083333
80	0.913333	1.175

1A40		
loadstep(kPa)	TmaxC/Tyc	TmaxL/Tys
0	0	0
20	0.2755556	0.2325
40	0.5488889	0.4625
60	0.7888889	0.6925
80	0.8622222	1.025

1A50		
loadstep(kPa)	TmaxC/Tyc	TmaxL/Tys
0	0	0
20	0.28	0.219166667
40	0.56	0.436666667
60	0.8066667	0.6525
80	0.8622222	0.95
100	0.8688889	1.241666667

Table B-1.14. Maximum shear to shear strength ratio for core and lower sheet material at different load step for material B, load size ratio 1 with variation of thickness.

1B15		
loadstep(kPa)	TmaxC/Tyc	TmaxL/Tys
0	0	0
20	0.164375	0.2508333
40	0.33125	0.5041667
60	0.49875	0.7583333
80	0.65625	1.0083333
90	0.70625	1.1166667

1B20		
loadstep(kPa)	TmaxC/Tyc	TmaxL/Tys
0	0	0
20	0.13125	0.19
40	0.263125	0.38083333
60	0.396875	0.57333333
80	0.51375	0.76333333
100	0.6	0.975
110	0.65	1.08333333

1B25		
loadstep(kPa)	TmaxC/Tyc	TmaxL/Tys
0	0	0
20	0.1075	0.15833333
40	0.215625	0.3175
60	0.325	0.4775
80	0.434375	0.6375
120	0.600625	0.96666667
160	0.70625	1.31666667

1B30		
loadstep(kPa)	TmaxC/Tyc	TmaxL/Tys
0	0	0
20	0.105625	0.14083333
40	0.21125	0.2825
60	0.3175	0.42416667
80	0.423125	0.56583333
100	0.520625	0.71
120	0.590625	0.85833333
130	0.62	0.94166667
150	0.675	1.11666667

1B40		
loadstep(kPa)	TmaxC/Tyc	TmaxL/Tys
0	0	0
20	0.105	0.1225
40	0.21	0.245
60	0.315625	0.3675
80	0.420625	0.489166667
100	0.513125	0.613333333
140	0.625	0.891666667
180	0.71875	1.225

1B50		
loadstep(kPa)	TmaxC/Tyc	TmaxL/Tys
0	0	0
20	0.11	0.113333333
40	0.22	0.225833333
60	0.33	0.338333333
80	0.44	0.450833333
120	0.58125	0.686666667
160	0.68125	0.975
200	0.725	1.341666667

Table B-1.15. Maximum shear to shear strength ratio for core and lower sheet material at different load step for material C, load size ratio 1 with variation of thickness.

1C15		
loadstep(kPa)	TmaxC/Tyc	TmaxL/Tys
0	0	0
20	0.13	0.245
40	0.2619048	0.49333333
60	0.3947619	0.74333333
80	0.5285714	0.99166667
100	0.6619048	1.16666667

1C20		
loadstep(kPa)	TmaxC/Tyc	TmaxL/Tys
0	0	0
20	0.10238095	0.18166667
40	0.20666667	0.36416667
60	0.31142857	0.54833333
80	0.41619048	0.7325
100	0.52380952	0.91666667
120	0.62857143	1.10833333
140	0.70952381	1.23333333

1C25		
loadstep(kPa)	TmaxC/Tyc	TmaxL/Tys
0	0	0
20	0.09714286	0.1491667
40	0.1952381	0.2991667
60	0.29333333	0.4491667
80	0.39190476	0.6008333
120	0.59047619	0.9
160	0.77619048	1.1833333

1C30		
loadstep(kPa)	TmaxC/Tyc	TmaxL/Tys
0	0	0
20	0.09047619	0.130833
40	0.17142857	0.261667
60	0.25714286	0.393333
80	0.34285714	0.525
120	0.51904762	0.7875
140	0.5952381	0.925
160	0.68095238	1.058333
175	0.74285714	1.158333

1C40		
loadstep(kPa)	TmaxC/Tyc	TmaxL/Tys
0	0	0
20	0.085238095	0.1116667
40	0.169047619	0.2225
60	0.254761905	0.3341667
80	0.33952381	0.4458333
120	0.50952381	0.6683333
160	0.680952381	0.8916667
180	0.742857143	1.0083333
200	0.79047619	1.1333333

1C50		
loadstep(kPa)	TmaxC/Tyc	TmaxL/Tys
0	0	0
20	0.086190476	0.1016667
40	0.171904762	0.2033333
60	0.258095238	0.305
80	0.344285714	0.4058333
120	0.514285714	0.6083333
160	0.685714286	0.81
200	0.804761905	1.025
250	0.876190476	1.2916667

Table B-1.16. Maximum shear to shear strength ratio for core and lower sheet material at different load step for material D, load size ratio 1 with variation of thickness.

1D15		
loadstep(kPa)	TmaxC/Tyc	TmaxL/Tys
0	0	0
20	0.084444444	0.2416667
40	0.170666667	0.485
60	0.257777778	0.7308333
80	0.344444444	0.975
100	0.431111111	1.1583333

1D20		
loadstep(kPa)	TmaxC/Tyc	TmaxL/Tys
0	0	0
20	0.061555556	0.16916667
40	0.123555556	0.3395
60	0.185777778	0.51083333
80	0.248888889	0.68333333
120	0.373333333	1.03333333
150	0.471111111	1.225

1D25		
loadstep(kPa)	TmaxC/Tyc	TmaxL/Tys
0	0	0
20	0.054222222	0.13333333
40	0.108666667	0.26666667
60	0.163333333	0.40083333
100	0.273333333	0.67083333
150	0.411111111	1.00833333
200	0.555555556	1.29166667

1D30		
loadstep(kPa)	TmaxC/Tyc	TmaxL/Tys
0	0	0
20	0.05	0.1125
40	0.1	0.225
60	0.150222222	0.3375
100	0.251111111	0.56416667
200	0.504444444	1.13333333
230	0.597777778	1.25833333

1D40		
loadstep(kPa)	TmaxC/Tyc	TmaxL/Tys
0	0	0
20	0.051333333	0.090833333
40	0.102666667	0.181666667
60	0.154	0.271666667
100	0.257777778	0.461666667
200	0.515555556	0.908333333
300	0.72	1.308333333

1D50		
loadstep(kPa)	TmaxC/Tyc	TmaxL/Tys
0	0	0
20	0.053777778	0.079833333
40	0.096222222	0.16
60	0.144222222	0.239166667
100	0.24	0.399166667
200	0.48	0.798333333
300	0.671111111	1.208333333

Appendix C: Close Form Solution Validation

C.1 Classical Sandwich Plate Theory

Consider a sandwich plate with dimension *a. b* as shown in Figure C.1. The positive senses for shear forces (*Qx*, *Qy*) acting on the panel are shown in Figure C.2. The shear forces have units of force per unit length.

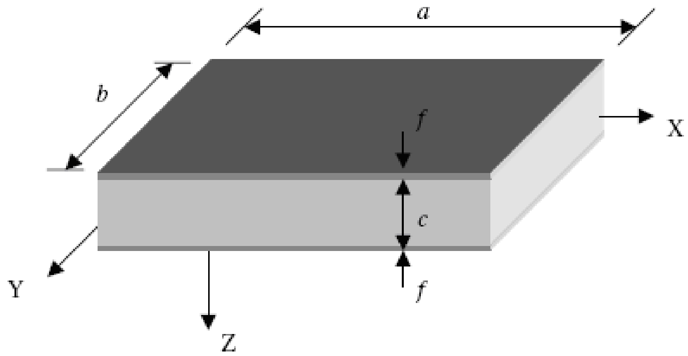

Figure C.1. Sandwich panel geometry

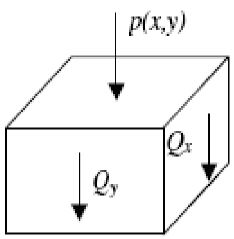

Figure C.2. Positive senses of forces

For sandwich plates that have a high overall length to thickness ratio, a small face sheet to overall thickness ratio, and a high face sheet to core mechanical properties ratio, the following assumptions are classically made:

1. Plane sections before deformation remain plane after deformation.

2. Transverse normal stiffness of core is infinite (i.e. no change in plate thickness).

3. Overall deflection is small compared to the thickness of the plate (i.e. no geometric non-

linearit4. Slopes of the plate are small enough such that $\tan[\frac{dw}{dx}] \cong \frac{dw}{dx}$

5. The core carries the entire shear load and the face sheets carry all bending load.

6. The total displacement of the sandwich plate is the result of bending and shear deformation.

7. The strains are small enough that the linear strain displacement relationship is valid, i.e. $\varepsilon_x = \frac{\partial u}{\partial x}$

8. The core and face sheets are perfectly bonded.

One of the assumptions in the classical sandwich plate theory is that the core carries the entire shear load. Therefore the shear load can also be expressed in terms of core shear rigidity and shear deflection:

$$Q_x = \tau_{xzc} c = G_{c0} c \gamma_{xzc} = S \frac{\partial w_s}{\partial x} \qquad \text{C.1}$$

$$Q_y = \tau_{yzc} c = G_{c0} c \gamma_{yzc} = S \frac{\partial w_s}{\partial y} \qquad \text{C.2}$$

The boundary conditions for a simply supported sandwich panel are shown in Figure C.3. The total deflection and the second derivative of the bending deflection should vanish along the edges of the simply supported plate as shown in the figure.

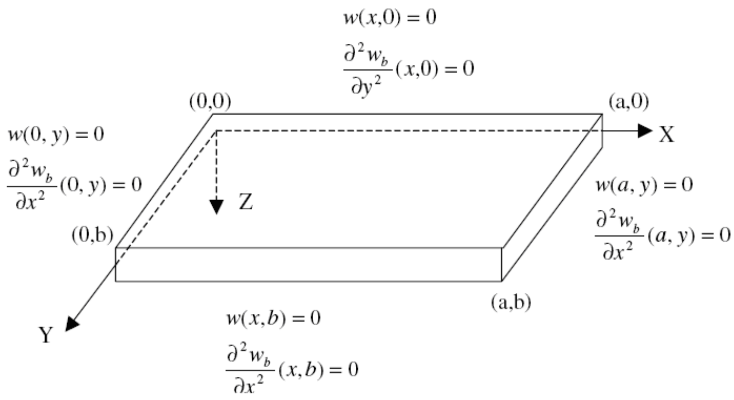

Figure C.3. Simply supported boundary condition for a sandwich panel

In order to find an expression that satisfies the simply supported boundary condition, a Fourier sine series solution, also called Navier's solution, is used. This solution automatically satisfies the expression of the bending deflection, shear deflection and the applied load terms within the simply supported panel under distributed load.

$$w_s(x,y) = \sum_m^{\infty} \sum_n^{\infty} r_{mn} \sin(\alpha x)\sin(\beta y) \qquad m,n = 1,2,3..... \qquad \text{...........C.3}$$

$$p(x,y) = \sum_m^{\infty} \sum_n^{\infty} p_{mn} \sin(\alpha x)\sin(\beta y) \qquad m,n = 1,2,3..... \qquad \text{............. C.4}$$

where $\alpha = \frac{m\pi}{a}$ and $\beta = \frac{n\pi}{b}$, r_{mn}, and p_{mn} are unknown coefficients and a, b are the length and width of the panel between the support.

The step pressure model assumes a uniform distributed load applied on the surface of the sandwich panel over a corresponding square effective area. Figure C.4 shows the schematic of the step pressure model.

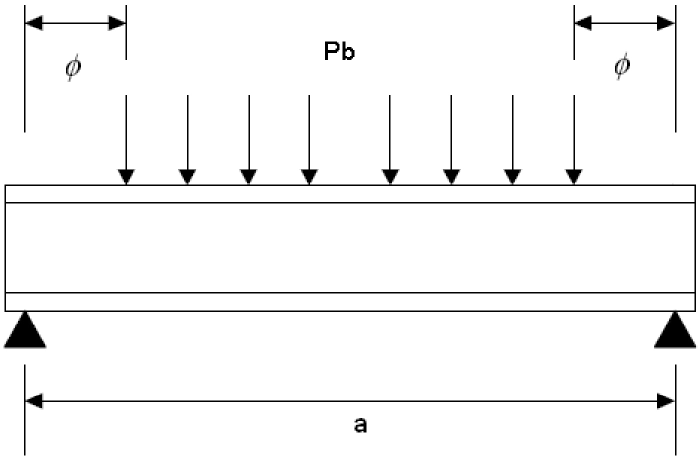

Figure C.4. Step pressure model on simply supported sandwich plate

This loading model can be represented mathematically as:

$$p(x,y) = \begin{cases} P_b & \phi \le x, y \le (a-\phi) \\ 0 & elsewhere \end{cases} \qquad \text{.......................... C.5}$$

The effective contact area, A_{eff} and the width of the unloaded region ϕ are given by the expressions:

$$\phi = \frac{1}{2}(a - \sqrt{A_{eff}}) \qquad \text{.......................................C.6}$$

With the step pressure model defined, r_{mn}, and p_{mn} can be determined by using equations C.3 and C.4

$$p_{mn} = \frac{16 p_b \cos(\frac{m\phi\pi}{a})\cos(\frac{m\phi\pi}{b})}{\pi^2 mn} \qquad m,n = 1,3,5.... \qquad \text{.........C.7}$$

$$r_{mn} = \frac{p_{mn}}{S(\alpha^2 + \beta^2)} \qquad m,n = 1,3,5.... \qquad \text{.........C.8}$$

From equations C.1, C.2 and C.3, the shear stress components of the can be represented as:

$$\tau_{xzc} = G_{c0}\frac{\partial w_s}{\partial x} = \sum_m^{\infty}\sum_n^{\infty} r_{mn}\cos(\alpha x)\sin(\beta y)(G_{c0}\alpha) \qquad \text{.........C.9}$$

$$\tau_{yzc} = G_{c0}\frac{\partial w_s}{\partial y} = \sum_m^{\infty}\sum_n^{\infty} r_{mn}\sin(\alpha x)\cos(\beta y)(G_{c0}\beta) \qquad \text{.........C.10}$$

In order to find the resultant shear load carried by the structure along any span pf the plate in the *X* and *Y*-axes, equations C.9 and C.10 are integrated with respect to their respective cross section areas. The results are:

$$Q_{xzc} = \int_0^c\int_0^b \tau_{xzc}\,dydz = \sum_m^{\infty}\sum_n^{\infty} r_{mn}\cos(\alpha x)(1-\cos(\beta y))(\frac{cG_{c0}\alpha}{\beta}) \qquad \text{.........C.11}$$

$$Q_{yzc} = \int_0^c\int_0^b \tau_{yzc}\,dydz = \sum_m^{\infty}\sum_n^{\infty} r_{mn}\cos(\beta y)(1-\cos(\alpha a))(\frac{cG_{c0}\beta}{\alpha}) \qquad \text{.........C.12}$$

These are the equations used to determine the behavior of the elastic sandwich plate in hydromat system.

C.2 Matlab Program for the Theoretical Plate Shear Distribution Calculation

```
% Calculate core shear distribution along the X-axis using classical sandwich plate theory

    % -----------------------------------------------------------------
    close all
    clear all
    clc
    Pb = 51700;                                          % pressure(pa)
    a = 0.60148;                                         % Length between support (X-axis)(m)
    b = 0.60148;                                         % Length between support (Y-axis)(m)
    ss = 49;                                             % Number of summations for Fourier Series
    Aeff = 0.18;                                         % Effective contact area(m^2)
    phi = 0.5*(a-(Aeff)^.5);                             % Length of non-contact area(m)
    c = 0.248;                                           %Core thickness (m)
    Gc0 = 14044943;                                      % Core shear modulus before yielding(pa)
    S = c*Gc0;                                           % Shear Stiffness
    for m = 1:2:ss
    for n = 1:2:ss
    % Pressure term (Equation C.7)
    Pmn(m,n) = (16*Pb*cos(m*phi*pi/a)*cos(n*phi*pi/b))/((pi^2)*m*n);

    % Constants used in double Fourier Series
    alpha(m) = m*pi/a;
    beta(n) = n*pi/b;
    % Constant used for shear deflection calculation (Equation C.8)
    rmn(m,n) = Pmn(m,n)/(S*(alpha(m)^2+beta(n)^2));
    % Total shear load at interested location (Equation C.12)
    to_add(m,n) = rmn(m,n)*Gc0*c*alpha(m)*(1-cos(beta(n)*b))*cos(alpha(m)*location)/beta(n);

           end
       end
    % coordinate. Result divided by two because only half span is considered
    result = sum(sum(to_add))/2;
    disp(result)
```

C.3 Total Shear Distribution

The classical sandwich plate theory is therefore used to compare and validate the numerically predicted shear distribution of the plate in the linear range. Comparison between the numerically determined shear distribution and the classical sandwich plate theory distribution was done at all load steps. It is assumed that is in the linear range the core carries the entire shear load. Results from equation C.12 are compared with the total resultant load in the global Y direction, $R_{TOT\ (Yg)}$, obtained numerically. Figures C.5 to C.7 show the total shear resultant comparisons between the numerical and theoretical models in the linear rang.

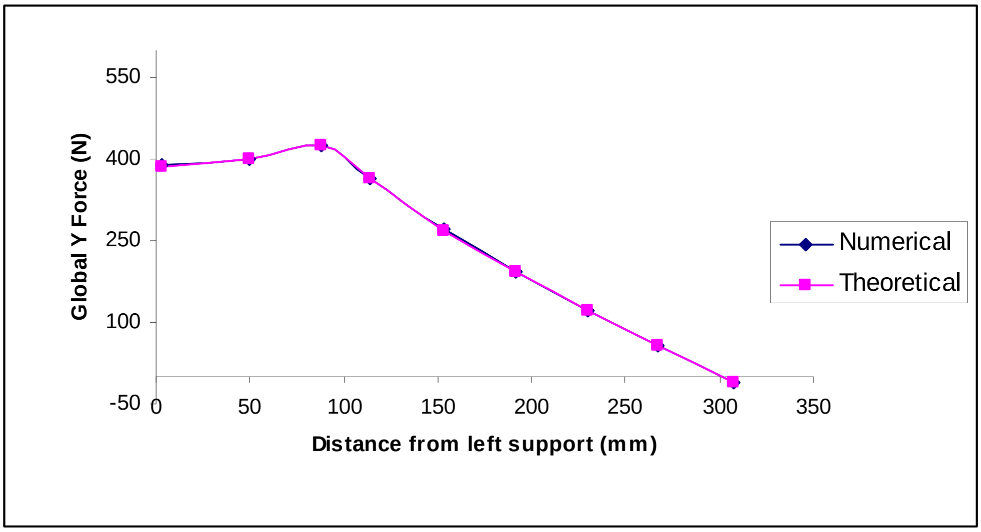

Figure C.5. Total plate shear distribution comparison along X-axis at 17.2 kPa

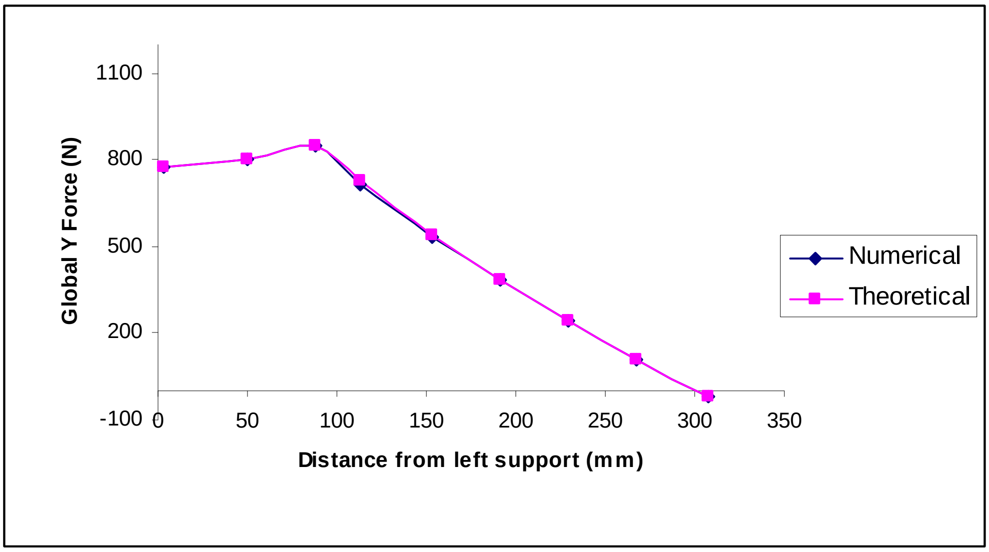

Figure C.6. Total plate shear distribution comparison along X-axis at 34.5 kPa

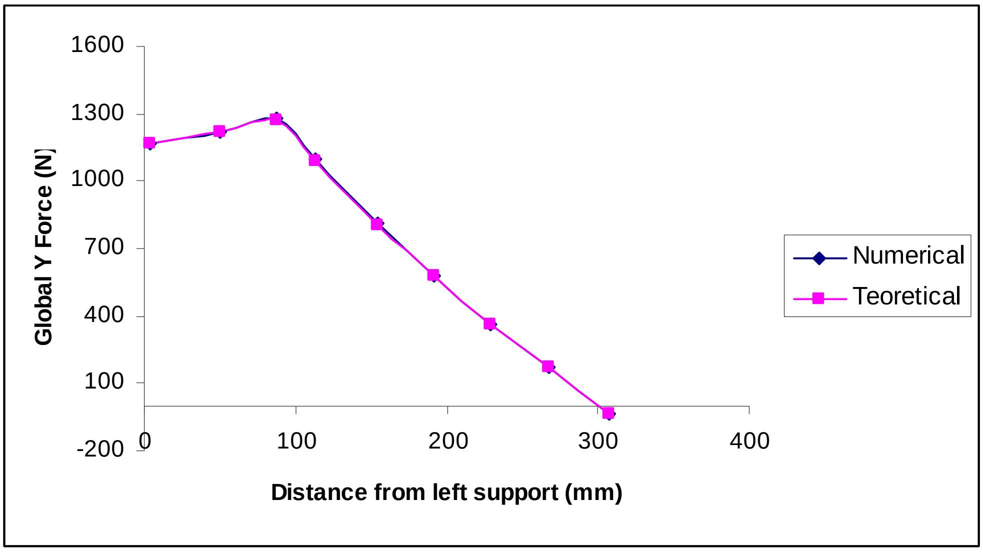

Figure C.7. Total plate shear distribution comparison along X-axis at 51.7 kPa

تصميم وأمثلة الصفائح المركبة في مرحلة ما بعد الخضوع

إعداد
حسين زعل محمد المعايطة

المشرف
الدكتور صالح العكور

ملخص

في هذا البحث تم تقديم تأثير سماكة الصفائح المركبة و تغير نوع المادة المستخدمة في صناعة قلب الصفيحة (Core material) أيضا تأثير تغير المساحة التي يؤثر بها الحمل الموزع (Distributed load) على الصفيحة باستعمال طريقة العنصر المحدود (Finite Element Method) .
أخذ البحث بالاعتبار وصول مادة القلب (Core material) إلى ما بعد مرحلة ما بعد الخضوع كما أخذ البحث بالاعتبار التأثير غير الخطي للشكل الهندسي (Non linear geometry).

تم تصديق و مقارنة نتائج العنصر المحدود (Finite Element Method) بتجارب مخبريه و تحليلية و نتائج من دراسات و أبحاث سابقه وكانت المشابهة متقاربة.

أعد في هذا البحث جداول و نتائج تفيد في أمثلة و تصميم الصفائح المركبة حتى لمرحلة ما بعد الخضوع تسهل و تفيد المهندس المصمم باختيار قياسات و توزيع الحمل و نوعية المادة المستخدمة في صناعة قلب الصفيحة بشكل أمثل حيث تستخدم هذه الصفائح في صناعة الهياكل الجوية و البحرية والبيوت المعدنية الجاهزة.